TURBULENCE IN RELATION TO THE PERFORMANCE OF HYDRAULIC FLOCCULATORS

by

JIE LIU

Doctor of Philosophy

School of Civil and Environmental Engineering
University of Edinburgh
1999

DECLARATION

This thesis is submitted to the University of Edinburgh for the degree of Doctor of Philosophy. The work described in this thesis was carried out by the candidate during the years 1996-1999 under the supervision of Gordon McConnachie, Dr. Robin Wardlaw and Dr. Martin Crapper. All the work was carried out in the Department of Civil and Environmental Engineering at the University of Edinburgh, Scotland, UK. The candidate declares that the thesis has been composed by himself and that the work described herein is his own unless otherwise stated in the text.

Jie Liu

ACKNOWLEDGEMENTS

First of all, the author would like to express his deep and sincere gratitude to his supervisor, Gordon McConnachie for his continuous supervision, guidance and assistance during the three years of this project. Also, the author is indebted to his second supervisor, Dr. Robin Wardlaw for his guidance and encouragement.

The author would like to especially thank to Dr. Martin Crapper for his great help in mathematical modelling and his friendship.

Thanks also go to Fabienee Kerbrate for help during the turbulence measurement and flocculation tests. I would also like to thank Jim Hutcheson for his supervision and concern for safety during the testing stage and Ian Fowler for his innovation and skill in preparing the flocculation and settling models for testing.

I am very grateful for the financial supports from the British Government and the University of Edinburgh through an ORS award and a studentship.

Thanks also go to my friends at the University of Edinburgh in particular, Kampanad Bhaktikul, Sharif Mohd, Dovoud Amadyar for their help in my study and many happy memories over the past years. I wish them and their families happy and safe futures.

Thanks are also due to my wife Yaqing Liu, my daughter Ouya Liu and my son James Zhonglun Liu for their love and understanding. Without them, I would not have finished my study. To them, I dedicate this thesis.

ABSTRACT

It is well known that turbulence can be used as a measure of the effectiveness of promoting flocculation, an extensively used and most important method of water treatment. Although the overall turbulence should be the integration of the turbulence intensity at each individual point in the flocculator rather than an average velocity gradient, the average velocity gradient has generally been employed as the turbulence parameter in assessing flocculation efficiency and designing the flocculation process as it can be evaluated relatively simply.

With the use of Computational Fluid Dynamics (CFD), this study was able to provide the value of turbulence at any point in a channel flocculator. Comparison between the model simulation and the experimental results obtained from Laser Doppler Anemometry (LDA) show that the model can reproduce the main features of flow in flocculators. The relationships between turbulence and velocity and the nominal velocity and the number of channels in a hydraulic flocculator, as found in this study, could substantially save the lead time and the costs of new flocculator designs. The effect of the geometry of the flocculator on flocculation efficiency was also studied.

A modified Argaman's equation (1968) is proposed to calculate the flocculation in relation to turbulence in an accurate and easy way based on the relationships mentioned above. Aggregation and breakup constants during flocculation were determined by experiments. Flocculation and settling performance under various flow rates, initial concentrations, retention times, coagulants, flocculator geometry and arrangements of settling were also investigated in the laboratory and the experimental results were used to verify the corresponding modelling.

The flocculation efficiency in terms of not only turbidity removal but floc size and floc density was investigated by means of a video imaging technique.

TABLE OF CONTENTS

LIST OF FIGURES

CHAPTER 2

CHAPTER 3

CHAPTER 4

CHAPTER 5

CHAPTER 6

LIST OF TABLES

NOTATION

The definitions of the symbols used in the thesis are given below in separate alphabetical lists of first Roman, then Greek characters. This is intended for reference and covers only the notation which is used repeatedly.

Roman characters

A	area (m^2)
C_d	drag coefficient (dimensionless)
C_μ	constant
f_d	Doppler shift frequency (Hz)
f_i	frequency of incident light (Hz)
f_s	scattered light frequency (Hz)
g	acceleration due to gravity (ms^{-2})
G	velocity gradient (s^{-1})
h	head loss (m)
H	water depth (m)
k	kinetic energy (m^2s^{-2})
K_a	aggregation constant (dimensionless)
K_b	breakup constant (s)
L	length in general (m)
n_0,n_1	concentration of primary particles at times t and 0 (NTU)
n_i,n_j, n_k	concentration of particles sizes of i, j and k (NTU)
P	height of weir (m)
Q	volumetric flow rate (m^3s^{-1})
t	time (s)
T	absolute temperature (^0K)
u,v,w	longitudinal, lateral and vertical velocity components (ms^{-1})
u', v', w'	velocity fluctuation in u, v and w velocities (ms^{-1})
W	power input per unit volume per unit time ($kgms^{-1}$)
X_L	shift distance in y direction (m)
X_T	corresponding shift distance of the tracker in y direction (m)
x, y, z	coordinates in three dimensions (m)

Greek characters

α	collision efficiency factor (dimensionless)
β	collision frequency function (m^3s^{-1})
α_v, α_k	velocity and kinetic energy related constants (dimensionless)
β_v	coefficient between the velocity and the number of channel
β_k	coefficient between the turbulence and the number of channel
d	floc diameter (m)
ε	floc porosity (dimensionless)
φ	floc solid volume fraction (dimensionless)
λ	wave length (m)
θ	Doppler angle (^{0})
ρ	density in general (kgm^{-3})
ρ_p, ρ_l	densities of particle and liquid (kgm^{-3})
τ	shear stress (Nm^{-2})
μ	dynamic viscosity ($kgm^{-1}s^{-1}$)
$\forall$	volume (m^{-3})
$\forall_i, \forall_j, \forall_k$	volumes of particles sizes of i, j, and k (m^{-3})

Chapter 1. Introduction

1.1 The need for further study of hydraulic flocculation

The most widely used equation describing turbulence intensity in respect of flocculation was developed by Camp and Stein (1943), $G=\sqrt{\frac{W}{\mu}}$, based on the relationship describing the aggregation of particles under the action of laminar shear proposed by Smoluchowski in 1917. G is called the root-mean-square (RMS) velocity gradient, W is the mean value of power input per unit volume per unit time, and μ is the dynamic viscosity of the stirred liquid. It is noted that Camp and Stein employed an RMS velocity gradient G representing the average of a number of local velocity gradients in any mixed reactor. Because it is possible to create the same G in a reactor using different types of stirrer in a mechanical flocculator (Lai, 1975), while the range of local G values varies considerably in each case, the application of G has been being criticised (Ives 1968, Lai 1975, Andreu-Villegas and Letterman 1976, Cleasby 1984, Clark 1985, McConnachie 1991). Although the previous investigators tried to compensate the use of averaged velocity gradient (G) by adopting some new terms they were still associated with G such as Gt, $G^n t$ and GtC, where n is a constant, C is the concentration of coagulant and t is the retention time.

Argaman (1968) developed a working equation for quantifying the relation between turbulence intensity and flocculation efficiency in a completely mixed mechanically stirred flocculator:

$$\frac{n_0}{n_1} = \frac{1 + K_a G t}{1 + K_b G^2 t} \qquad (1.1)$$

The rates of formation and break-up of flocs in terms of concentration of primary particles are given by the expressions $K_a Gt$ and $K_b G^2 t$. n_1 and n_0 are the concentrations of primary particles at times t and 0 and the ratio of n_0/n_1 represents the flocculation efficiency (Argaman, 1968). K_a and K_b are aggregation and breakup coefficients respectively. It should be noted that G is identically defined as the averaged velocity gradient rather than the integration of the local turbulence intensities and t is an averaged hydraulic retention time

rather than the real flocculation time for every individual unit in the flocculator. Therefore Argaman's equation is still a formula based on the average of turbulence and time while the fundamental discrete methodology was not addressed.

Since the average velocity gradient method is simple in calculation and is a relatively good fit in quantifying the flocculation efficiency in a mechanical flocculator, it has been used in engineering design as mentioned at the beginning of this section. However, there is no doubt a need of studying an accurate and easy approach in the calculation of turbulence in relation to flocculation not only in mechanical flocculation, which has been extensively studied, but also in hydraulic flocculation.

1.2 Purpose of this study

The basic aim of this study was to investigate the relationship between the rate of flocculation and the intensity of turbulence in hydraulic flocculators. Specifically, the study had the following objectives:

1. Laboratory investigation and mathematical simulation by Computational Fluid Dynamics (CFD) of turbulence and velocity in the horizontal flow hydraulic channel flocculators.

2. Revision of Argaman's (1968) equation applied to the calculation of the degree of flocculation and the development of an accurate and easy approach to calculating the degree of flocculation as a function of the hydrodynamic parameters (kinetic energy and velocity).

3. Laboratory study of flocculation performance and verification of the proposed analytical approach under various independent factors. Experimental study of floc characteristics, such as floc size, settling velocity and density.

4. Comparison of flocculent settling under different settling arrangements and investigation of the variation of settling performance with raw water turbidity, flow rate, settling time and location.

5. Development of design criteria and operational considerations for flocculation and settling processes.

1.3 Arrangement of the thesis

The thesis is organised into seven chapters which deal with the main body of the work, and two Appendices containing additional experimental data. A brief description of the content of each chapter is given below.

Chapter 1 is an introductory chapter. It generally puts forward the need for the current study and gives the aims of the study and the layout of the thesis.

Chapter 2 contains a review of the development of theories and techniques in the areas of flocculation, turbulence and settling relevant to the current study. It gives a background to the study and a reference to the rest of chapters.

Chapter 3 presents the laboratory investigation of turbulence in a single bend 180^0 channel. An experimental study of turbulence and velocity in the channel by means of Laser Doppler Anemometry (LDA) is described which established the distribution of the hydrodynamic characteristics throughout the channel and provided a basis to verify the model simulation by the Computational Fluid Dynamics (CFD) software, FLUENT.

Chapter 4 mainly concerns the computation of turbulence and velocity by FLUENT for the channel flocculators. The development and theoretical basis of turbulence modelling is given, the techniques of speeding up convergence are discussed. The model results are compared with laboratory data from Chapter 3. The relationships between velocity and turbulence and the nominal velocity and the number of channels in the flocculator are discussed.

Chapter 5 gives the details of the laboratory investigation of flocculation in hydraulic flocculators and floc settling performance under various flowrates, flocculation times, coagulants, raw water turbidities and arrangements of settling. Flocculation efficiency is presented not only in terms of turbidity but also floc density, and floc size and floc settling velocity measured by means of the video recording technique. The settling performance of floc against time and location is investigated. Flow characteristics in the flocculators and settling tanks are identified by a tracer study in order to utilise the appropriate equation(s) to calculate the flocculation efficiency in relation to turbulence in Chapter 6.

Chapter 6 describes a modified Argaman's (1968) flocculation vs turbulence equation by the author for application to the hydraulic flocculator. Based on the relationships found in Chapter 4, an accurate and simplified calculation approach in respect to the "point to point" method and the "average velocity gradient" method is presented. The aggregation and breakup constants during flocculation are determined and the effects of raw water turbidity, flocculation time, coagulant and the arrangement of settling are examined.

Chapter 7 completes the thesis by summarising the main conclusions of the previous six chapters and suggests some areas for further research.

Chapter 2. Theoretical background and literature review

2.1 Introduction

The review given in this chapter is not intended to be exhaustively comprehensive. Instead, a careful selection of the extensive literature relevant to this study is surveyed. It aims to give an introduction to relevant previous studies and to highlight the significant points that are referenced in the later chapters of this thesis.

The review consists of three main parts: theoretical basis of flocculation and the effect of turbulence on the degree of flocculation; experimental and mathematical techniques for measurement of floc size and density; and tube settling characteristics.

2.2 Theoretical basis of flocculation

In this section, the theoretical basis of flocculation is first discussed and the relation between flocculation and turbulence is described thereafter.

The completion of flocculation can be thought of as involving two steps, particle destabilisation and particle transport. The first step, destabilisation, is mainly the chemical process and the second is mainly the physical process (Amirtharajah and O'Melia, 1990).

2.2.1 Particle destabilisation

There are widely recognised four distinct mechanisms of particle destabilisation:

1. Compression of the double layer;
2. Adsorption and charge neutralisation;
3. Enmeshment in a precipitate or so called sweep flocculation; and
4. Adsorption and interparticle bridging.

In the first of these mechanisms, compression of the double layer, the ionic strength of the solution is increased. A higher ionic strength increases the availability of counterions to

surround the charged particle, so the volume or distance from the surface through which the diffuse layer extends is reduced. This reduction in the length of the diffuse layer tends to reduce the energy barrier (E_s) which must be overcome to allow particles to collide as shown in Figures 2.1 and 2.2. In order to do this, the electrostatic force must be reduced since attractive forces can not be increased because their nature is dictated by the form and structure of the colloid. According to the Schulze-Hardy rule, the higher the charge of the coagulant, the lesser the molar amount of it needed for destabilisation.

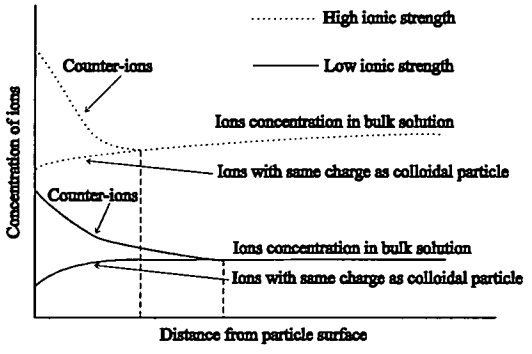

Figure 2.1 Compression of the diffuse layer

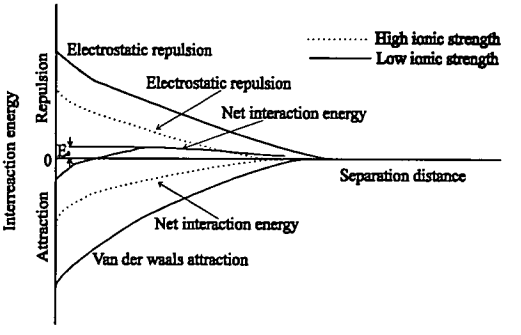

Figure 2.2 Reduction of energy barrier

The second mechanism, adsorption and charge neutralisation, occurs because of specific chemical interaction between the coagulant added and the surface of the particle. The driving force for such interaction is not electrostatic since further addition of coagulant beyond the dose needed for charge neutralisation will result in charge reversal and destabilised particles as shown in Figure 2.3. An important aspect of particle destabilisation by adsorption and charge neutralisation is that there is a correlation between the amount of coagulant dose required and the particle concentration, i.e. there is a stoichiometric effect of particle concentration as illustrated conceptually in Figure 2.4.

A corollary to this second mechanism is the patch model. In this view, complete charge neutralisation is not necessary for excellent destabilisation. Rather, once some positive charges (polymer molecules) are adsorbed on to the negatively charged particles in suspension, there are patches of positive charge (from the polymer) and patches of the raw negative charge on most particles. The positive patch of one can be attracted to the negative patch of another, resulting in destabilisation and attachment.

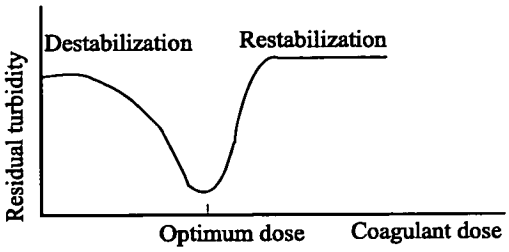

Figure 2.3 Coagulation via the mechanism of adsorption and charge neutralisation

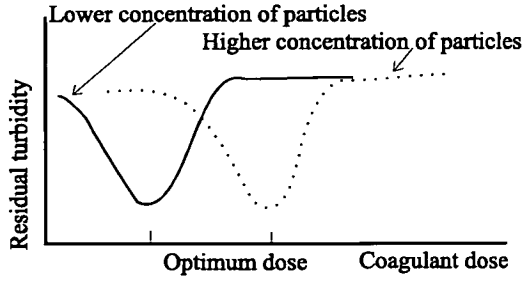

Figure 2.4 Stoichiometry between particle concentration and required dose of coagulant for destabilisation by adsorption and charge neutralisation

The third mechanism of destabilisation, enmeshment in a precipitate, occurs when a coagulant is added in such quantity that a precipitate occurs. In this mechanism, the particles originally in the water are caught within the framework of the precipitate as it is formed, or are captured by the large hydroxide flocs as they settle. Since the original particles present can serve as nuclei for the formation of the precipitate, there is, to a mild degree, an inverse stoichiometry, i.e. the more particles originally present, the less chemical necessary to achieve the desired level of particle capture. In sweep coagulation, the individual characteristics of the particles in suspension are obliterated within fraction of a second of adding the coagulant and the system becomes almost indistinguishable from coagulating metal hydroxide. An important function of the precipitated metal hydroxide is to provide a large number of particles and thereby improve coagulation kinetics very substantially (Packham and Sheiham, 1977).

Alum causes destabilisation in two ways: adsorption and charge neutralisation or enmeshment in a precipitate. The former is true because of the positively charged nature of the ions or polymers formed at pH values below the zero point of charge of the hydroxide precipitate. These positively charged ions can adsorb on to negatively charged particles and can cause neutralisation. The driving force for such adsorption is not charge but the surface-active nature of the molecules. Amirtharajah and Mills (1982) summarised results from a large number of jar tests reported in the literature on to a log concentration vs pH solubility diagrams for alum as shown in Figure 2.5. This Figure shows separate regions for effective

coagulation by each of the above three mechanisms for alum. It is shown that the dominant flocculation mechanism for alum is sweep flocculation at pH = 7, and alum dosage in the range of 25 to 80mg/l, the experimental condition of the flocculation tests of this study.

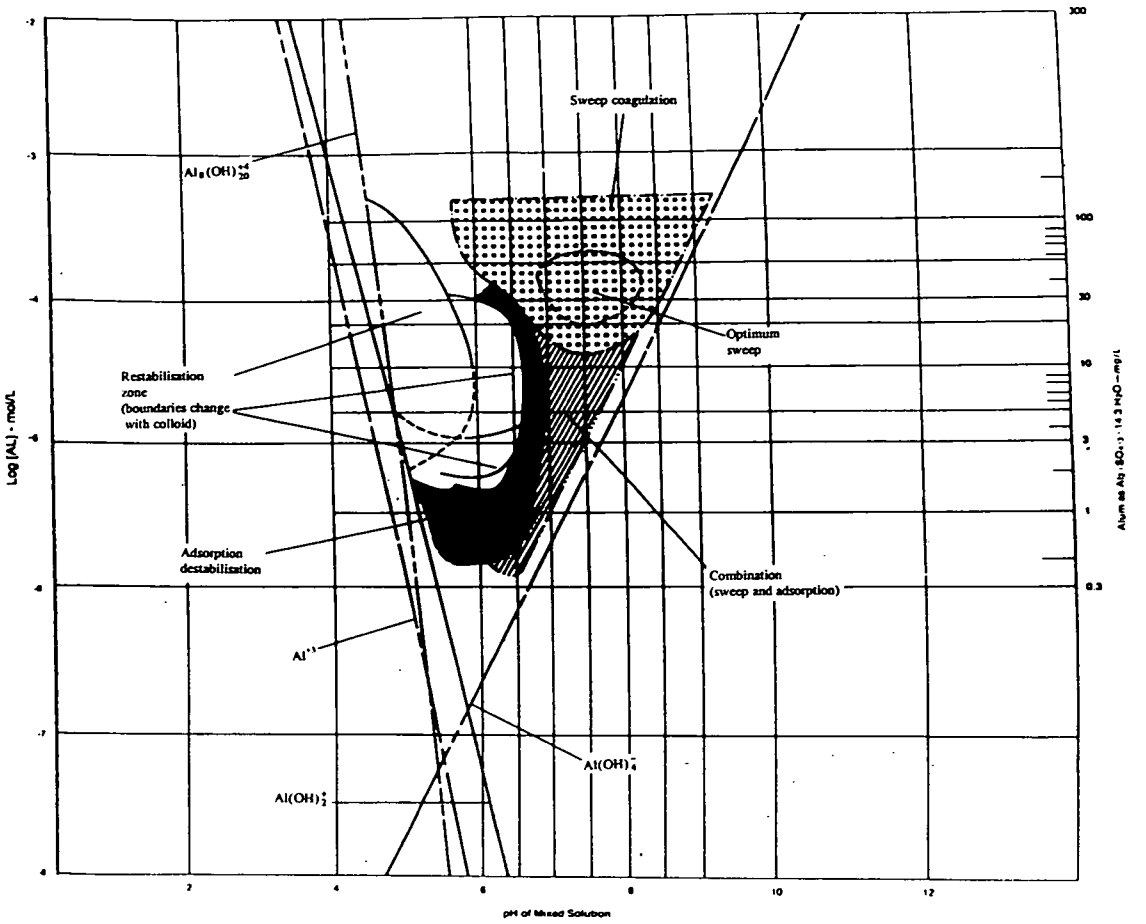

Figure 2.5 Dependence of floc formation with alum as coagulant on pH and alum dosage

Finally, the fourth mechanism of destabilisation is adsorption and interparticle bridging. This is particularly applicable to the use of synthetic organic polymers. In this mechanism, it is thought that the polymer attaches to the surface of two or more particles by some specific chemical interaction (not simply electrostatic) and forms a bridge between them. As an indication that attachment on to the surface is not simply electrostatic it is possible that polymers with the same charge as the particle surface can be effective in causing destabilisation by this mechanism. Here again, providing the proper dose is critical, since destabilisation is also possible by overdosing. According to the research of Gassenschmidt et al (1995), the flocculation with Moringa oleifera, a natural coagulant, follows the

combined mechanisms of patch charge and interparticle bridging. The description of Moringa oleifera is given in Chapter 5.

2.2.2 Particle transport

Smoluchowski first developed a model simulating the flocculation process in 1917 and almost all the subsequent developments of flocculation modelling have originated from this, aiming to modify each of the assumptions made by Smoluchowski.

Smoluchowski's assumptions:

- The collision efficiency factor, α, is unity for all collisions.
- Fluid motion undergoes laminar shear.
- The particles are monodispersed (i.e. all of the same size).
- No breakage of flocs occurs.
- All particles are spherical in shape and remain so after collision.
- Collisions involve only two particles.

The Smoluchowski's flocculation equation is given by Equation 2.1

- in symbols:

$$\frac{dn_k}{dt} = \frac{1}{2}\alpha \sum_{i+j=k} \beta\,(i,j)\, n_i n_j - \alpha n_k \sum_{\text{all } i} \beta\,(j,k)\, n_i \qquad (2.1)$$

- in words:

Rate of change with time of number concentration of particles of size k	=	Rate of growth of particles of size k by coagulation of smaller particles (the sum of whose volumes is size k)	−	Rate of loss of particles of size k by coagulation of a size k particle with any size particle

The first term on the right hand side expresses the gain of particles of size k by the collision and attachment of two smaller particles (sizes i and j whose total volume is that of size k; i.e. the "i+j=k" under the summation really means $\forall_i+\forall_j=\forall_k$, $\forall_i$, $\forall_j$, and $\forall_k$ are the volumes of the particle sizes of i, j, and k respectively), The second term describes the loss of particles of size k by coagulation of a size k particle with any other size particle to create a

particle larger than size k. In the equation, n_i, n_j and n_k are the number concentrations of sizes i, j and k respectively; α is a fraction ($0<\alpha<1$) which reflects the degree of destabilisation achieved and is called the destabilisation efficiency factor, β (i,j) is a collision frequency function which varies with the mechanism of interparticle collision and which expresses the frequency with which collisions will occur with the effect of concentration extracted. α represents the degree of the process of particle destabilisation, one of the two steps of completion of flocculation, whilst β accounts for the second step, particle transport.

The particle transport can be caused by Brownian motion, fluid shear or differential sedimentation. Smoluchowski developed the equations for the collision frequency function in 1917 for Brownian motion and fluid shear as Camp (1946) did for differential sedimentation as shown in Equations 2.2, 2.3 and 2.4.

$$\text{Brownian Motion: } \beta(i,j)=\frac{2kT}{3\mu}\left[\left(\frac{1}{\forall_i}\right)^{1/3}+\left(\frac{1}{\forall_j}\right)^{1/3}\right]\left[(\forall_i)^{1/3}+(\forall_j)^{1/3}\right] \tag{2.2}$$

$$\text{Fluid Shear: } \beta(i,j)=\frac{1}{\pi}\left[(\forall_i)^{1/3}+(\forall_j)^{1/3}\right]^3 G \tag{2.3}$$

$$\text{Differential Sedimentation: } \beta(i,j)=\left(\frac{6}{\pi}\right)^{1/3}\frac{g}{12\mu}(\rho_p-\rho_l)\left[(\forall_i)^{1/3}+(\forall_j)^{1/3}\right]^3\left|(\forall_i)^{1/3}-(\forall_i)^{1/3}\right| \tag{2.4}$$

-where k is Boltzman's constant, T is absolute temperature, μ is viscosity of the liquid, $\forall_i$ and $\forall_j$ are volumes of particle of size i and j respectively, G is velocity gradient, ρ_p, ρ_l are densities of particle and liquid respectively and g is the gravitational constant.

Direct conclusions can be summarised from equations 2.2, 2.3 and 2.4:

- Collision due to Brownian motion is directly proportional to water temperature and independent of fluid flow or gravity forces. Collisions between two small particles (less than 2μm) are dominated by Brownian motion, collision between large particles and particles considerably smaller are dominated by differential sedimentation, and collisions between particles of similar size (but greater than 1μm) are dominated by fluid shear (Wirojanagud, 1983).

- For differential sedimentation, the large particles settle at faster rates, overtake smaller particles during their settling, and form flocs with them. The greater the difference of the size of particles, the greater the collision by differential sedimentation. As the opportunity for collisions increases as the water depth increases, the effective water depth has an effect on the floc collision.

- Turbulence can induce collisions among particles and hence cause agglomeration. The particle transport is directly proportional to turbulence intensity quantified by velocity gradient based on Smoluchowski's assumption which ignores floc breakage. However the breakup of flocs happens especially when agitation is too vigorous and the generally accepted principal mechanisms (Argaman and Kaufman, 1970; Parker et al, 1972; Spielman, 1978; Glasgow and Hsw, 1982; Thomas et al, 1999) of disaggregation are surface erosion of primary particles from the floc and fracture of the floc to form smaller aggregates.

2.2.3 Turbulence in relation to flocculation

Treatment of water to remove fine suspended particles that do not readily settle out involves electrochemical destabilisation by coagulants followed by flocculation, the aggregation of particles by fluid agitation. This agitation must be of sufficient strength to overcome the effective repulsive force barrier between particles that remains after coagulation. Increasing mixing intensity will increase the frequency of contact between particles, but there will be an upper limit to the mixing intensity beyond which the flocs will begin to break up under high shear forces (McConnachie, 1991).

The turbulence motion created by agitation can be regarded as the superposition of eddies of ever-smaller size. Each size can be described in terms of a length scale representing the distance between two points in the fluid and a velocity scale or gradient representing the difference in velocity of the fluid at these point (Levich 1962). The length scale of turbulence can be crudely interpreted as the average size of turbulent eddies or the size of the packet of fluid within which high correlations of fluid velocity exist (Amirtharajah and O'Melia, 1990). Large eddies arise from the interaction of the mean flow within the boundary. These eddies have a macroscale and carry a large fraction of the turbulent energy of the system. The initial forces in the system transfer the energy via cascades from the

largest eddies to the smallest eddies where they are dissipated by viscous effects into heat. This cascade of energy destroys the original turbulence characteristics of the macroscale eddies that were related to system geometry, and the smallest eddies (microscale) are in a state of universal equilibrium. The length scale of the eddy where energy dissipation by viscous forces dominates is called the Kolmogorov microscale, defined as

$$\eta = \left(\frac{\nu^3}{\varepsilon} \right)^{1/4} \qquad (2.5)$$

in which ν is the kinematic viscosity and ε the rate of energy dissipation per unit mass. Amirtharajah and Tambo (1991) indicates that when the mean particle (or floc) size, is small compared to the Kolmogorov microscale, the rate of contact of particles of diameter d_1 with particles of diameter d_2 is expressed by

$$N(d_1, d_2) \propto n(d_1)n(d_2)\bar{d}^3\left(\frac{\varepsilon}{\nu}\right)^{1/2} \qquad \bar{d} << \eta \qquad (2.6)$$

in which $\bar{d} = (d_1 + d_2)/2$, $n(d_1)$ is the number concentration of particles of diameter d_1 and similarly $n(d_2)$for particles of diameter d_2; this shows $N \propto (\varepsilon/\nu)^{1/2}$ as the explicit dependence on ε and viscosity. When the mean particle sizes are larger than the Kolmogorov microscale, then

$$N(d_1, d_2) \propto \bar{d}^{7/3}\varepsilon^{1/3} \qquad \bar{d} > \eta \qquad (2.7)$$

in which it is evident that the rate of collisions responsible for floc growth is scales by $\varepsilon^{1/3}$ with no explicit dependence on the kinematic viscosity; this is because at these larger length scales, the turbulent motions are being dominated by fluid inertia as distinct from viscous forces. Between the regimes illustrated by equations 2.6 and 2.7, there also exist others in which the kinetic follow the same dependence on ε and ν as contained in equation 2.6 and 2.7, the precise from being ties to the ration $\bar{d}/\eta$ (Bache et al, 1996). Casson and Lawler (1990) concluded from their modelling simulation and experimental studies that in turbulent condition, collisions between particles are promoted by eddies of a size similar to those of the colliding particles. DeBoer et al (1989) studied the mechanism of coagulation by turbulence and concluded that the rate of growth for aggregates ranging from 1 to 20 microns is approximately proportional to the cube root of the average rate of shear in the tank. For particles of similar size the coagulation rate is approximately proportional to the square of the volume fraction of solids. Collisions between particles of widely different sizes were two orders of magnitude higher than predicted by theory. This phenomenon is

probably due to transport of small particles by eddies into a region of closed streamlines around the larger aggregates.

The difficulty of quantifying the range of eddy sizes and velocity gradients within a reactor has led to generalised expressions for orthokinetic flocculation. The first relationship describing the aggregation of particles under the action of laminar shear, developed by Smoluchowski in 1917, indicated that the rate of flocculation is directly proportional to the velocity gradient within the mixing chamber. However, as there is more than one velocity gradient in any mixed reactor, Camp and Stein (1943) related the root-mean-square (RMS) velocity gradient G_m to the mean value of work input per unit volume per unit time W as follows:

$$G_m = \sqrt{\frac{W}{\mu}} \tag{2.8}$$

-where μ is the dynamic viscosity of the stirred liquid. They also stated that under conditions of constant flow pattern, the velocity gradient G at a point and over a period of time is directly proportional to G_m. Thus

$$G = \sqrt{\frac{W}{\mu}} = \sqrt{\frac{P}{\mu \forall}} \tag{2.9}$$

in which P is total power input, $\forall$ is liquid volume and G becomes a mean value within the volume.

For the design of reactors for optimum flocculation, Camp (1955) suggested that the product Gt, where t is the retention time, should be used as the main parameter. However, criticism of this product has been made on the use of the RMS velocity gradient as a valid basis for the design of flocculation basins. Cleasby (1984) states the G_m is only valid for eddy sizes smaller than those necessary for flocculation in water and wastewater treatment. For practical purpose, he proposes the use of mean power input per unit mass to the two-third power instead of G_m and suggests that paddle configuration may have an effect on flocculation efficiency. Clark (1985) criticises the use of the terms absolute velocity gradient and RMS velocity gradient as used by Camp and Stein as they "essentially require that a 3-dimensional flow in general be represented by a single 2-dimensional flow" and proposes that they be replaced by characteristic velocity gradient and spatially averaged characteristic velocity gradient, respectively. Han and Lawler (1992) concluded that the importance of the velocity gradient (G) apparently has been overemphasised in the

traditional view of flocculation based on rectilinear models for collision frequency functions and the consideration of uniformly sized particles. It is possible to create the same mean G in a reactor using different types of stirrer (Lai 1975), while the range of local G in a reactor varies considerably in each case. This range stems from the spectrum of energy values within the turbulence field, normally expressed in terms of velocity fluctuations about the mean. For any configuration of fluid agitation, the mean value of the velocity fluctuation, $\overline{u'}$, will be zero and their RMS value $(\overline{u'^2})^{1/2}$ represents the intensity of turbulence (Amirtharajah and Trusler, 1986; Amirtharajah and O'Melia, 1990; McConnachie 1991).

Noticing the lack of expression of floc breakage in Smoluchowski's flocculation equation, Argaman (1968) developed the relationship between turbulence and flocculation in a mechanical flocculator by using $\overline{u'^2}$ as the turbulence parameter. He defined the rates of formation and break-up of flocs in terms of number concentration by $n_1 K_a \frac{\overline{u'^2}}{K_p}$ and $n_0 K_b \left(\frac{\overline{u'^2}}{K_p}\right)^2$, where n_1 and n_0 are the number concentrations of primary particles at times t and 0 and K_a and K_b are the aggregation and breakup constants respectively, K_p is the stirrer performance coefficient for a mechanical flocculator and has a particular value for a specific flocculator, and $\overline{u'^2}$ is the square of the averaged flow velocity fluctuation in a flocculator. For a completely stirred tank reactor (CSTR) with a retention time t, the relation between the ratio of primary particles in influent to effluent $(\frac{n_1}{n_0})$ with turbulence, quantified by flow velocity fluctuation can be established using the continuity equation as follows:

Descriptive mass balance equation is

accumulation = inflow ± utilisation or generation,

$$\forall \frac{dn_1}{dt} = Qn_0 - Qn_1 + \forall \left[-n_1 K_a \frac{\overline{u'^2}}{K_p} + n_0 K_b \left(\frac{\overline{u'^2}}{K_p}\right)^2 \right] \qquad (2.10)$$

-where $\forall$ is the volume of the reactor and Q is the flow rate passing through the reactor.

Detention time: $t = \frac{\forall}{Q}$ (2.11)

therefore,

$$\frac{dn_1}{dt} = \frac{1}{t}(n_0 - n_1) - n_1 K_a \frac{\overline{u'^2}}{K_p} + n_0 K_b \left(\frac{\overline{u'^2}}{K_p}\right)^2 \quad (2.12)$$

$$\frac{dn_1}{dt} = n_1\left(-\frac{1}{t} - K_a \frac{\overline{u'^2}}{K_p}\right) + n_0\left(\frac{1}{t} + K_b \left(\frac{\overline{u'^2}}{K_p}\right)^2\right) \quad (2.13)$$

For steady-state conditions $\frac{dn_1}{dt} = 0$, therefore,

$$0 = \frac{1}{t}(n_0 - n_1) - n_1 K_a \frac{\overline{u'^2}}{K_p} + n_0 K_b \left(\frac{\overline{u'^2}}{K_p}\right)^2 \quad (2.14)$$

Rearranging,

$$n_1\left(1 + K_a \frac{\overline{u'^2}}{K_p} t\right) = n_0\left(1 + K_b \left(\frac{\overline{u'^2}}{K_p}\right)^2 t\right) \quad (2.15)$$

therefore,

$$\frac{n_1}{n_0} = \frac{1 + K_b \left(\frac{\overline{u'^2}}{K_p}\right)^2 t}{1 + K_a \frac{\overline{u'^2}}{K_p} t} \quad (2.16)$$

For the variation of particle concentration with turbulence in a plug flow reactor at steady state with a detention time t, the mathematical solution is identical to that of a batch reactor. Hence,

$$\frac{dn_1}{dt} = -n_1 K_a \frac{\overline{u'^2}}{K_p} + n_0 K_b \left(\frac{\overline{u'^2}}{K_p}\right)^2 \quad (2.17)$$

Separating variables and integrating,

$$\int_{n_0}^{n_1} \frac{dn_1}{-n_1 K_a \frac{\overline{u'^2}}{K_p} + n_0 K_b \left(\frac{\overline{u'^2}}{K_p}\right)^2} = \int_0^t dt \quad (2.18)$$

$$-\frac{1}{K_a\frac{\overline{u'^2}}{K_p}}\ln\left(-n_1K_a\frac{\overline{u'^2}}{K_p}+n_0K_b\left(\frac{\overline{u'^2}}{K_p}\right)^2\right)\Bigg|_{n_0}^{n_1}=t\Big|_0^t \tag{2.19}$$

$$-\frac{1}{K_a\left(\frac{\overline{u'^2}}{K_p}\right)}\ln\frac{-n_1K_a\left(\frac{\overline{u'^2}}{K_p}\right)+n_0K_b\left(\frac{\overline{u'^2}}{K_p}\right)^2}{-n_0K_a\left(\frac{\overline{u'^2}}{K_p}\right)+n_0K_b\left(\frac{\overline{u'^2}}{K_p}\right)^2}=t \tag{2.20}$$

$$\frac{n_1}{n_0}=\frac{K_b}{K_a}\frac{\overline{u'^2}}{K_p}+(1-\frac{K_b}{K_a}\frac{\overline{u'^2}}{K_p})e^{-K_a\frac{\overline{u'^2}}{K_p}t} \tag{2.21}$$

According to Argaman (1968) $\overline{u'^2}$ can be expressed by the ratio between the average value of G and K_p in a mechanical flocculator:

$$G=\overline{u'^2}/K_p \tag{2.22}$$

Therefore, Argaman's flocculation equation for a complete mixing flow and a plug flow can be expressed by Equations 2.18 and 2.19 respectively, which are commonly used design equations (Amirtharajah and O'Melia, 1990).

$$\frac{n_1}{n_0}=\frac{1+K_bG^2t}{1+K_aGt} \tag{2.23}$$

$$\frac{n_1}{n_0}=\frac{K_b}{K_a}G+(1-\frac{K_b}{K_a}G)e^{-K_aGt} \tag{2.24}$$

However, it should be noted that the G used in Argaman's equation is the averaged velocity gradient rather than the integration of the square of the individual velocity fluctuation (u'^2) and t is the averaged hydraulic retention time rather than the real flocculation time for each individual unit in the flocculator. Although the previous investigators (Ives 1968, Lai 1975, Andreu-Villegas and Letterman 1976, Cleasby 1984, Clark 1985, McConnachie 1991) tried to compensate for the use of averaged velocity gradient (G) by adopting some new terms

still associated with the G such as Gt, $G^n t$ and GtC, where n is a constant, C is the concentration of coagulant and t is the average retention time, they still kept using the average concept whilst the fundamental discrete methodology was not addressed.

2.3 Determination of floc characteristics

Floc characteristics, such as floc size, floc density and floc strength are important parameters in assessing flocculation and settling performance. According to the research of Treeweek and Morgan (1980), turbidity measurement alone is not adequate to evaluate the effectiveness of the flocculation process and there is no simple, direct relationship between the characteristics of flocs and turbidity. Kavanaugh, et al (1978) recommended that both turbidity and particle size distribution measurements be used for accurate process control and monitoring of solid/liquid separation processes.

There is very little fundamental understanding of the factors affecting the strength of aggregates or their mode of breakage under stress, and most work has been of an empirical nature (Thamos, 1999). It is generally accepted (Muhle, 1993) that the breakage mechanism in turbulent flow depends upon a floc's size relative to the Kolmogorov miroscale. For flocs smaller than the Kolmogorov microscale, viscous forces predominate and erode the surface of the floc. On the other hand, for flocs larger than the Kolmogorov microscale, deformation or fracture may occur as a result of fluctuating dynamic pressure. These ideas imply that floc strength is proportional to floc size. However, recent experimental work by Yeung and Pelton (1996) has suggested that rather than strength being related to floc size, it is related to floc compactness and they found that more compact flocs were more likely to undergo erosions whereas less compact flocs were more likely to undergo fracture. Floc strength is not given in detail here since it is not the main interest of this study, references can be found from the works of Tambo and Hozumi (1979a) and Bache et al (1991).

2.3.1 Measurement of floc size and settling velocity

The main techniques for measurement of floc size can be mainly categorised into the following four methods: microscopy, electrical sensing zone, probe and sensor techniques, and video recording and photographing.

In earlier times, optical and electron microscopy might be the only available methods for determining particle size (Wirojanagud, 1983). It is capable of measuring the sizes of particles in the colloidal range (1nm-1μm) and the optical microscope remains the essential technique for instrument calibration and determination of particle shapes. However, microscopy techniques are time consuming in terms of sample preparation and measurement and is potentially inaccurate because of errors caused by handling and judgement errors in estimating particle sizes.

An electrical sensing zone method has been developed to measure particle size distributions, especially for the particulates of dimension greater than 1 μm. This technique requires significantly less time than the microscopy method. The total time required for particle size distribution measurement is only a few minutes, depending on the size range of the distribution. The Coulter counter is one such particle counting apparatus allowing for the rapid and accurate measurement of particles on a volume basis over a large size spectrum. Several investigators (Lawler 1979, Strickland 1982, and Wirojanagud 1983) applied the electronic particle counting techniques for particle size distribution measurement and concluded that this technique is only capable of detecting relatively small variation in particle size distributions and is in need of improvement. Measurement of particle size with this technique is limited due to particle clogging of the sensor orifice and particle break-up. Electronic noise and coincident pulse are also problems in using the Coulter instrument.

Sharma et al (1994) used a Partech 100 particle size analyser for the determination of particle size. The analyser was equipped with a 2.54 cm diameter sealed probe that contained both a laser source and detector. The particle size analysis was taken every 42 seconds. A floc sensor for measuring floc size developed by Kurotani et al (1995) is capable of carrying out on-line, real-time measurement of the mean particle size of fine flocs.

A CCTV camera was used by Bache et al (1991) for the monitoring of floc sizes and settling velocity. The images on a video recording were digitised and analysed using a computer. The video recording technique was also utilised by many other investigators (Tambo and Watanabe 1979, Kusuda et al 1981, and Adachi and Tanaka 1997). This typically involves taking a small sample from a flocculation vessel and transferring it to a settling column for direct observation (Kimpel et al, 1986). Floc size can be measured from an enlarged recorded picture and floc settling velocity determined by timing a specific travelling

distance, such as 5cm used by Tambo and Watanabe (1979), of an individual floc. A related problem is that it is usually easiest to observe settling flocs close to the wall of a transparent column and hydrodynamic interaction with the wall can give a significantly lower settling rate than for isolated flocs. In addition, it is important for control of the floc temperature since serious errors resulted from small temperature differences between the floc and the liquid in the settling tube.

The video recording technique was chosen in this study as it can record floc size and settling velocity simultaneously and, is relatively easy to operate.

2.3.2 Measurement of floc density

Lagvankar (1968) developed an experimental technique of floc density measurement based on the simple principle that if the mass density of a floc particle is equal to the mass density of the solution in which it is suspended, it will not sink or rise. Standard density solutions were prepared by dissolving different known weights of sucrose at 20^0C. Individual flocs were pipetted out carefully from the flocculating suspension and placed in a slightly coloured mother liquor layered over a solution of known density. A needle was then used to push the floc carefully through the interface between the density solution and the mother liquor.

Once a floc is placed in a density solution, it can not be retrieved usefully. Another floc must be selected, and a new density solution tried. In the case of very small flocs, where settling velocities were too small even in the mother liquor, the error caused by mass transfer diffusion in the period required to make one density measurement could be serious. Hence, it is essential for the density measurements by this kind of technique that the floc size is 0.2 mm^2 and larger (Lagvankar and Gemmell, 1968).

Knocke et al (1993) improved the above approach by using a density gradient column, containing a solution or suspension of material with increasing concentration down the column. Flocs are introduced and, in principle should settle to an equilibrium position in the column, where their density is equal to the local density of the liquid. The procedure can be made more rapid by employing a centrifuge, instead of gravity settling. However there is a major difficulty caused by diffusion of solutes such as sucrose as this can be quite rapid and reliable floc density measurements would be very difficult to make.

It is noticed that the experimental method of directly measuring floc density is time consuming, uncertain in accuracy and difficult under realistic condition. So many researchers have attempted to indirectly obtain floc density by measuring floc size and floc settling velocity and studying the relationship between floc density and floc size.

2.3.3 Calculation of floc density

The general approach by many investigators for indirectly determining floc density is by recording the floc settling time for a specific distance, calculating floc settling velocity and measuring floc dimensions from an enlarged photograph. The floc density is then calculated using a modified Stokes' velocity. To satisfy the use of Stokes' velocity formula, it is essential for the measurement of floc settling velocity in such a settling column containing a very dilute floc solution that floc settles independently.

Stokes' law is based on spherical particle but because aggregates are not usually spherical, expressions for the drag coefficient of spheres need to be modified (Tambo and Watanabe, 1979). The sphericity of flocs was assumed by them to be around 0.8 and, for low values of the Reynolds number, the drag coefficient is given approximately by $C_d \approx 45/Re$.

Fair, Geyer and Okun (1968) found from their experiments that floc density can be estimated from the settling velocity of floc with $\frac{24}{Re} + \frac{3}{Re^{0.5}} + 0.34$ as the drag coefficient (C_d) corresponding to that from a spherical particle and 1.1 as correction factor due to deformation. Floc diameter decreases as mixing intensity increases and an aggregate, consisting of a greater number of primary particles is less dense with floc settling velocity proportional to the n th power of the floc diameter. n ranged from 0.8 to 1.6 in their study. The exponent n decreases with the increase in the ratio of concentration of a coagulant to that of suspended solids and in the ratio of rapid mixing intensity to slow mixing intensity as long as these ratios are less than 10. Beyond this value, the floc settling velocity-diameter relationship becomes independent of the ratio of rapid mixing intensity to slow mixing intensity.

Kimpel (1984) calculated floc density using a modified Stokes' settling formula according to Reynolds number. He followed the approach suggested by Concha and Almendra (1979)

that drag coefficient (C_d) equals 0.28 $(1+\frac{9.06}{Re^{0.5}})^2$ for Reynolds number in the range of 0.01 to 2.

Prior to the introduction of the relation between floc size and density, a number of definitions used in previous studies of the relation are now given:

A general relationship between floc porosity, ε, and the floc solid volume fraction, φ, can be written as

$$1-\varepsilon = \forall_s/\forall_f = \varphi \qquad (2.25)$$

-where $\forall_s$ and $\forall_f$ are the solid volume and the total floc volume respectively. The floc solid volume fraction, φ, can be related to the floc buoyant density, $\Delta\rho_f = \rho_f - \rho_l$ by knowing

$$\rho_f = \rho_s\varphi + \rho_l(1-\varphi) \qquad (2.26)$$

-where ρ_f , ρ_s, and ρ_l are the densities of floc, solid and liquid, respectively, and by defining floc and solid buoyant densities as

$$\Delta\rho_f = \rho_f - \rho_l \qquad (2.27)$$

$$\Delta\rho_p = \rho_p - \rho_l \qquad (2.28)$$

Substitution of Equations 2.24 and 2.25 into 2.23 then yields

$$1-\varepsilon = \varphi = \Delta\rho_f/\Delta\rho_p \qquad (2.29)$$

-where $\Delta\rho_f/\Delta\rho_p$ is the relative buoyant density.

Lagvankar and Gemmell (1968) performed density measurements on an agglomerated suspension of ferric-hydroxide, formed by adding $Fe_2(SO_4)_3$ to simulate natural water at a selected optimal pH of 6.8. Their results indicated that the rate of density decrease for floc diameter (d) larger than 1400 micrometers was substantially less than for those smaller than

1400 micrometers. The results from each of these two regions were fitted, using least squares, to give the following power laws:

$$\Delta\rho_f = 0.50\, d^{-0.70} \qquad 1400 \geq d \geq 500\mu m \tag{2.30}$$

$$\Delta\rho_f = 0.03\, d^{-0.32} \qquad d \geq 1400\ \mu m \tag{2.31}$$

Matsumoto and Mori (1975) determined the buoyant density of bentonite coagulated with alum ($Al_2(SO_4)_3 18H_2O$). The relationship between floc size and settling velocity was first determined by allowing a sample of flocs to settling in a tank, and measuring the time required for a specified floc to settle some distance. Floc size was determined using a photographic technique. After determination of the size-settling velocity relationship, the total weight of flocs with diameter d, and total number of flocs N, were obtained by simultaneous use of a photo extinction method and a sedimentation balance. The buoyant density was then determined by knowing the total weight and the total volume of equally sized flocs. Results of this study were expressed by the following power function:

$$\Delta\rho_f = 2.34 d^{-0.94} \qquad 100 \geq d \geq 2500\mu m \tag{2.32}$$

Tambo and Watanabe (1979) used video recording techniques to directly measure individual floc settling rates and sizes under a variety of conditions and hence, with appropriate assumptions, derived the floc density. The equipment used consisted of a floc chamber and a quiescent settling tube which was connected to the bottom of the flocculator. The floc was introduced through a sliding trap entrance at the top of the settling tube. The time required for the floc to settle a distance of 5cm was measured, and a photograph of the settling aggregate was taken. The diameter was later measured from an enlarged photograph. The floc density was then calculated using modified Stokes' velocity. Several different system variables were investigated including pH, agitation intensity, raw water alkalinity, and the ratio of aluminium ions to suspended particles concentration, referred to as the ALT ratio. It was concluded that none of the above variables significantly influenced the density-size relationship, except for the ALT ratio. A typical relationship describing the floc buoyant density as a function of size was expressed as

$$\Delta\rho_f = 23 d^{-1.32} \qquad 3000 \geq d \geq 500\mu m \tag{2.33}$$

Dirican (1981) determined the density of individual TiO_2 flocs through direct measurement of floc size and the corresponding settling velocities. The flocs were allowed to settle in a tank while a super-eight mm camera filmed their movement. The effects of mixing time, impeller speed, and solids concentration were investigated. It was concluded that none of these variables had any significant effect on floc density, and all measurements were combined and fitted to the following power law.

$$\Delta\rho_f = 51.43\, d^{-0.915} \qquad (2.34)$$

Klimpel and Hogg (1986) found that floc density generally decreases with increasing floc size. The experimental data were fitted to an empirical model which was used in statistical testing for significant differences between measured floc density-size relationships in different systems. The effects of flocculation system variables such as agitation intensity, polymer concentration, mixing time, solids concentration, and primary particle size on resultant floc structures were presented and discussed and are summarised as follows:

- The effect of polymer dosage on floc porosity is insignificant while floc size is strongly affected by polymer type and dosage, therefore average floc density may be a function of these variables.

- The density of large flocs generally increase slightly with excessive mixing beyond polymer addition and with high shear rates. However, this is accompanied by a significant decrease in the maximum floc size.

- Floc density generally appears to increase with increasing solids concentration.

- Differences in primary solid particle size demonstrate the most significant changes between density-size relationships and, for any given floc size, floc density increases with increasing initial particle size.

Based on these results, a simple multistage model was postulated.

Bache et al (1991) found that pH is one of the critical parameters controlling the floc size. The effective density was gauged from knowledge of the floc velocity and size and was shown to be sensitive to coagulant. They recommended that an effective diameter, d, should

be used for specifying floc size. Experiments showed trends between floc size and effective density, ρ_e, in response to the coagulant dose at a fixed pH. Trend lines are conveniently represented by the empirical expression, $\rho_e = Ad^{-m}$, where, A and m are coefficients dependent on the concentration.

Gregory (1997) pointed out that flocs are not usually spherical and expressions for the drag coefficient of spheres need to be modified by an empirical factor 0.8. Chellam and Wiesmer (1993) stated that the porosity of aggregates results in a decreased drag compared with that for an impermeable sphere of the same size and density and that the effect becomes very significant for high porosities (fractal dimension less than about 2). This means that flocs would settle faster than solid objects of the same size and density. However, the effect in practice can be considered negligible (Klimpel et al. 1986) by using proper settling experimental methodology, such as judicious choice of the flocs to be measured to have shape as close to spheres as possible.

2.4 The effect of water temperature and pH on flocculation

The effect of temperature on flocculation is still a controversial topic. Chojnacki's studies (1968) on the coagulation of river water using alum showed that the dose decreased with increasing temperature. On the basis of jar tests, Hudson and Wagner (1981) reported that floc formation takes longer at low temperatures. Morris and Knocke (1984) have shown that temperature has a great impact on coagulation with alum. In some typical tests, residual turbidities increased from 0.5 to 0.8 NTU at 25 and 5^0C, to 2.4 NTU at 1^0C with alum as a coagulant at dosages greater than 10mg/l. Amirtharajah and O'Melia (1990) thought water temperature has a significant influence on flocculation. Flocculation performance is generally better at higher temperature than that of lower temperature. When temperature is too low, even if dosage is increased, the formation of flocs is very slow and its structure is loose. The following are the reasons for the decreased efficiency caused by low temperature:

1. The hydrolysis reaction of the coagulant is a heat-absorption process. Low temperature slows the rates of hydrolysis and precipitation of the coagulant. The hydrolysis process of alum is extremely slow when temperature is below 5^0C;

2. An increase of viscosity due to lower temperature reduces the turbulence intensity and also particle settling velocity;

3. A decrease of Brownian motion diminishes the chance for the aggregation of flocs.

However, Velz (1934) observed that if the pH is held constant, the minimum alum dose to achieve good colour removal increases, as the temperature increases. Similar features were reported in Dolejs' work (1984). Leipold (1934) who used alum to flocculate a turbid water at pH 8 (the sweep floc range) and led to the comment that cold temperature had no preventative or retarding effect on alum floc formation. Camp et al (1940) were more specific and stated that changes in temperature have no measurable effect on the time of floc formation, if coagulation takes place at the optimum pH. Bache et al (1996) pointed out that it is not always clear whether low temperature is a manifestation of slower floc formation, weaker flocs, or perhaps arising from incorrect pH adjustment-particularly if one accepts the statement of Camp et al (1940) noted above. Perhaps the most important conclusion of practical value when using metallic inorganic coagulants such as alum, is the necessity of adjusting the pH in response to changes in temperature. When the pH is properly adjusted, Bache's analysis (1996) suggests that the coagulation and flocculation processes are largely unaffected by temperature.

The predominance of a particular hydrolysis species of an inorganic coagulant during destabilisation is very largely dependent on the pH value (Argaman 1968). For a particular colloidal suspension, it is logical to consider that there exists a particular hydrolysis species most effective for destabilisation and the adjustment of pH to a range where the most effective hydrolysis species of the coagulant is formed is shown to be very essential in producing optimum coagulation.

Amirtharajah and Mills (1982) thought that pH and dosage are two parameters influencing the mechanism of alum flocculation (see Figure 2.5). For the pH of 6.8 to 8.2 and alum dosage of 25 to 80mg/l as the experimental conditions in this study, alum coagulation lies in the zone of sweep coagulation.

Gassenschmidt et al (1995) found that the main flocculent protein of Moringa oleifera was comparable to that of a synthetic polymer, such as polyacrylamide, and that the flocculation

follows the combined mechanism of charge and interparticle bridging. It is indicated that the effect of pH is not so significant for the flocculation with Moringa oleifera as coagulant since Bratby (1980) found that interparticle bridging dominant flocculation is insensitive to the change of pH.

2.5 Tube settling

In flocculent settling, particles grow by flocculation and therefore the settling velocity is not constant but increases over time (or across the length of the tank). The theoretical trajectory of a particle is no longer a straight line as that in discrete settling, but a curved one. This variation of settling velocity means that depth and detention time become important design variables, as well as the surface area. The amount of flocculation should be directly proportional to the retention period and to the depth of the tank (Camp, 1946).

In response to the shallow depth clarification theory (Camp, 1946), tube settling tank has been developed and has grown rapidly in recent years with a need for space conservation and compact (Willis, 1978). Willis (1978) stated there are three basic requirements essential for successful performance of tube settles.

1. There must be laminar (or viscous) flow conditions within the tubes at the maximum flow rate required. Laminar flow is essential so that each slowly settling floc particles within a tube maintains a steady descent to the collecting surface of the tube and is not intermittently swept upward by turbulent currents within the tube. To ensure a laminar flow state, Reynolds number must be less than 2000 and in most tube settling tank designs it is less than 400.

2. The residence time within each tube must be ample so that a floc particle entering at the extreme upper edge of the tube will have sufficient time to settle to the collecting surface a vertical distance below. The residence time T_{tube} is equal to the length of the tube L (see Figure 2.6.) divided by linear flow rate v_{tube}. As the flow velocity at the tube entrance approximates to an uniform distribution (Willis, 1978; Fadel and Baumann, 1990), the volume flow per tube, q, equals the total flow of tubes, Q, divided by the number of tubes, N. The linear flow rate equals q divided by the cross-sectional area of a tube A_{tube}. θ is the angle of the tube to the bottom of the settling tank. 60 degree tube angle minimises the tendency of the stream to flush out settled sludge in the direction of flow. With the 60

degree tubes, the continuous self-flushing sludge removal avoids the build-up problem within the tubes and also avoids the design requirement for back-flushing. If the diameter of the tube is D, the maximum particle-settling or drop distance H_{tube} is

$$H_{tube} = D/\cos\theta \qquad (2.35)$$

3. The velocity of flow through the tubes must not exceed a critical maximum that would cause the settled sludge to lose stability and be swept out of the tube in the direction of normal flow. The maximum value, $GPM/A_F = 2.5$, where GPM is the total flow in gallons per minute and A_F is horizontal face area of the tubes in square feet (Willis, 1978). This criterion limits the sweep-out action to reasonable bound.

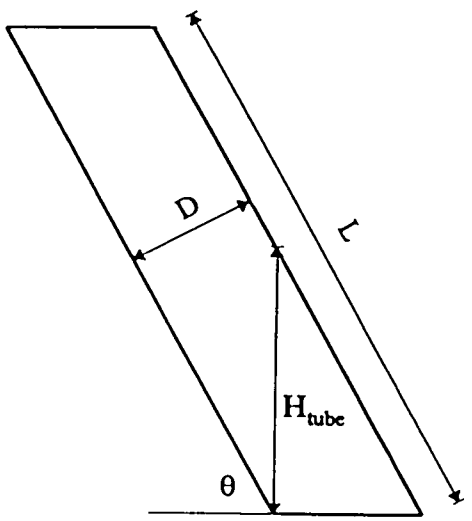

Figure 2.6 Single tube dimensions

Fadel and Baumann (1990) summarised the factors affecting tube settling tank performance on the basis of computer solutions of the Fadel model (1985):

Whilst the conditions of flow velocity, degree of tube inclination, and temperature remain constants, smaller diameter tubes provide better performance. Degrees of tube inclination in the range of $5\text{-}20^0$ have little influence on the required tube length. However, the model indicates that the tube length required increases significantly at angles of 20^0 or more. Increasing particle settling velocity has a significant effect on reducing the required length of tube for particle removal. Temperature affects both fluid viscosity and particle settling velocity, however, the total effects of temperatures between 10 to 27^0C are relatively insignificant.

2.6 Conclusions

A review has been given of both the experimental and theoretical techniques used to study flocculation and settling. These previous studies can be summarised:

1. Average velocity gradient, G, can not accurately represent the local variations of turbulence in a flocculator. The square of the velocity fluctuation, u'^2, is a well defined property of the of turbulence.

2. Averaged hydraulic retention time rather than the real flocculation time has been used for evaluating flocculation performance whilst the fundamental discrete methodology was not addressed.

3. A video recording technique can be used for measuring floc size and floc settling velocity. Floc density is mainly determined by substituting the measured floc size and settling velocity into a modified Stokes' settling formula.

4. For successful performance of tube settling tank, Reynolds number must be less than 2000. The angle of the tube to the bottom of the tank is recommeded as 60 degree, which minimises the tendency of the stream to flush out settled sludge in the direction of flow and avoids the sludge build-up problem within the tubes.

Chapter 3. Laboratory investigation of turbulence in a channel flocculator

3.1 INTRODUCTION

This chapter describes the investigation of turbulence and velocity throughout a channel flocculator under two different flowrates with the measurements used to verify the results of numerical modelling which will be discussed in Chapter 4. It was expected to identify the velocity profile 100mm downstream of the baffles in the first channel, an important boundary condition of the modelling simulation, and assess its effect on the distribution of turbulence and velocity within the channel. The two main instruments, Laser Doppler Anemometry and STREAMFLO meter, which were used in measuring velocity and turbulence are discussed in section 3.2.

The experiment was carried out in a single 180^0 bend horizontal flow channel with two legs each 150mm wide, 2800mm effective length and 200mm effective depth with 8mm dividing wall (see Figures 3.1.1 and 3.1.2). The dividing wall was constructed in perspex and the gap between the dividing wall and the end wall was 150mm. There were 500mm long perspex walls on both sides of the channel extending from the end wall which allowed the laser beam to pass through. Most of the measurements were taken in this working area. The rest of the channel was made of wood.

Measurements were taken at 5 levels and 6 positions across the channel and 6 distances from the end wall as shown in Figure 3.2. The measuring points were not evenly distributed in the three dimensions to allow some concentration at the locations where high gradients were expected, such as the area near the bend, water surface and the walls. The arrangement was also considered to fit with the output location of the modelling simulation.

The experimental procedure is described in section 3.3. Section 3.4 gives the experimental results, discussion and an assessment of experimental error. Conclusions of this chapter are found in section 3.5.

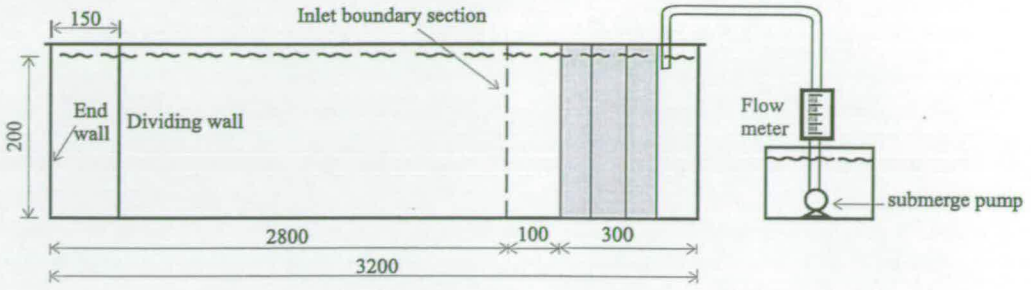

A-A SECTION

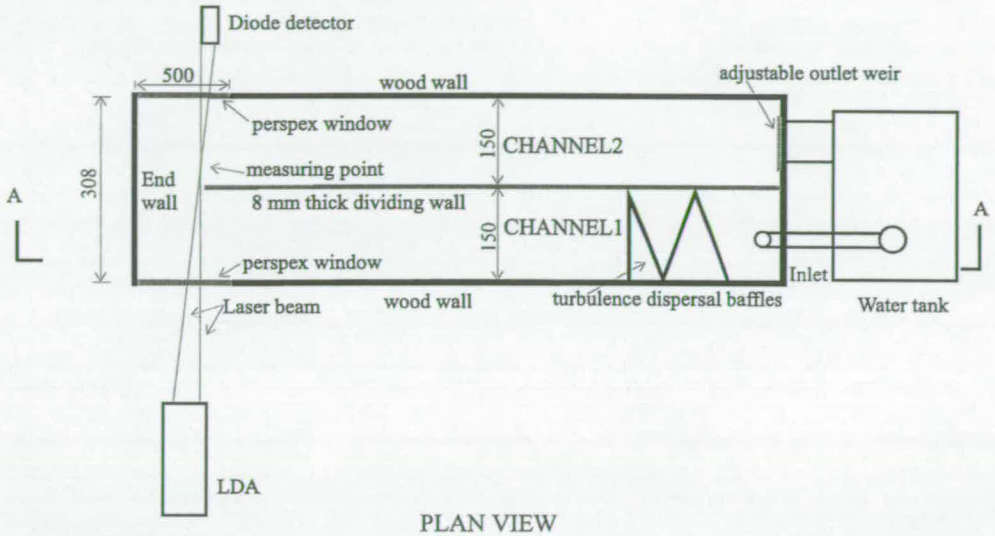

PLAN VIEW

Figure 3.1.1 Layout of the channel, LDA and auxiliary devices (dimension shown in mm, not to scale)

Figure 3.1.2 LDA and the channel flocculator in position

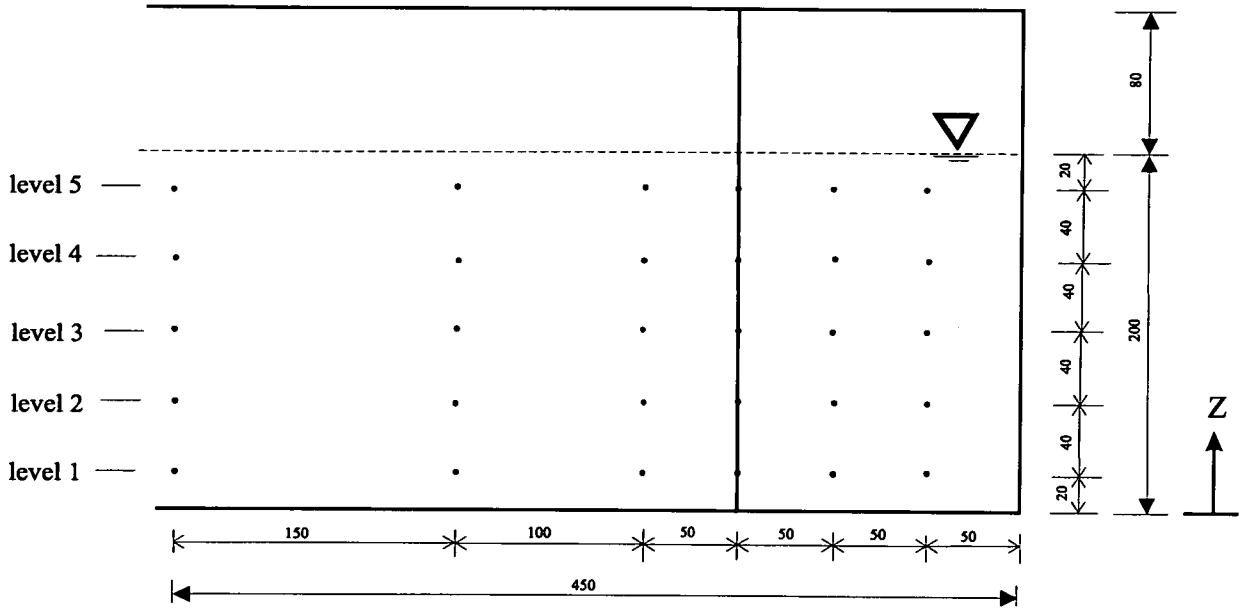

Elevation

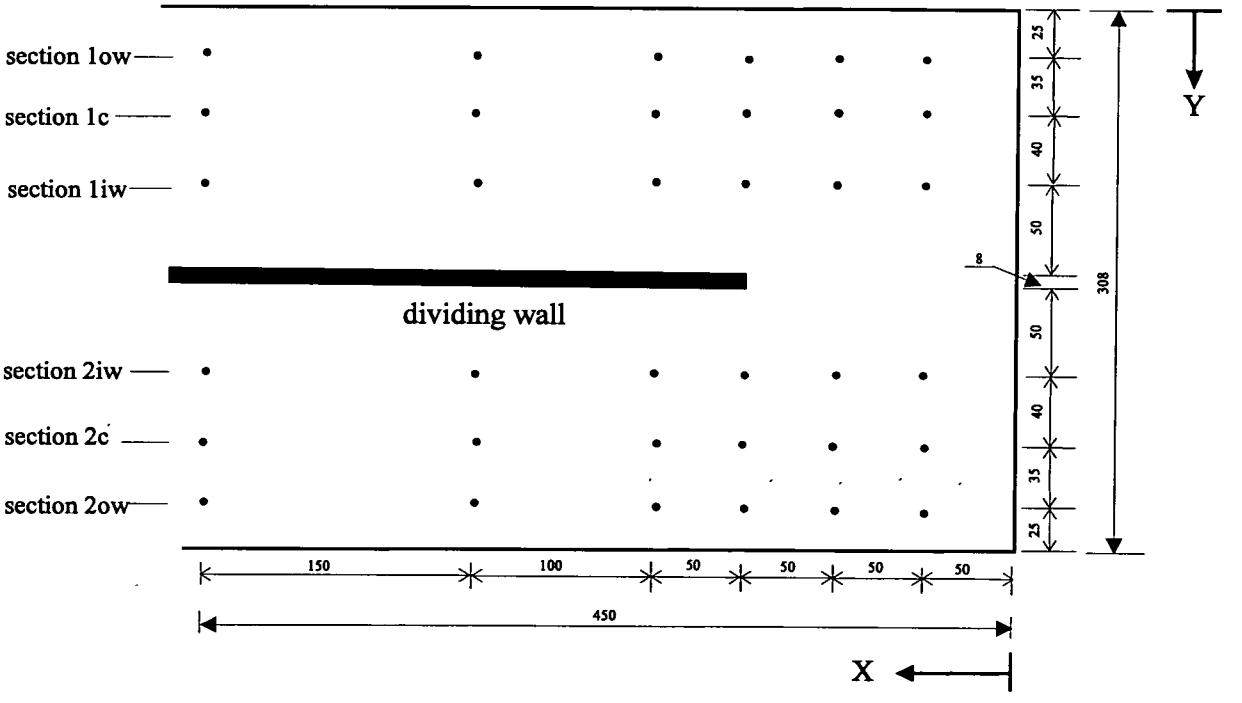

Plan

Figure 3.2 Arrangement of measuring points (Dimension shown in mm, Points where LDA value can be derived:•)

3.2 EXPERIMENTAL INSTRUMENTATION AND AUXILIARY DEVICES

The following paragraphs describe the two main instruments, Laser Doppler Anemometer which was used to measure water velocity and turbulence and the STREAMFLO meter which was used to measure water velocity and some auxiliary devices during the investigation of the flow characteristics within the channel flocculator.

3.2.1 Laser Doppler Anemometry (LDA)

The most notable advantage of LDA is the non-contact probing, that does not disturb the fluid motion by any probe (such as hot-film Anemometry) while readings are being taken, which is particularly important in situations such as described here where velocities are low. The anemometer has excellent spatial resolution characteristics. Another important feature of the anemometer is the calibration-free output voltage, which is linearly related to the flow velocity. Full detailed introduction can be found in the manufacturer's manuals (DISA Laser Doppler 1983). A general discussion on the principles and operational procedures of the LDA system used in the channel is expressed in this section.

3.2.1.1 Principles of the LDA system

The Laser Doppler Anemometer uses the Doppler shift of light scattered by moving particles to determine particle velocity and thus find the fluid flow velocity. The general equation expressing the Doppler shift, f_d, in the frequency of the scattered light as a linear function of flow velocity is:

$$f_d = f_s - f_i = \frac{2U}{\lambda} \sin(\theta/2) \qquad (3.1)$$

-where f_s is the frequency of scattered light, f_i the frequency of incident light, U flow velocity, θ the angle between incident and scattered beam and λ the wavelength of incident light. For the system used in this study, the monochromatic coherent light was a class 3B monochrome red Helium-Neon laser beam, $\lambda = 632.8 \times 10^{-9}$ m, $\theta = 11.48^0$.

Equipment for LDA velocity measurements mainly consists of the laser, LDA optics which includes a beam splitter and lens, a diode detector, a frequency tracker, a frequency shifter, an oscilloscope and a control computer (see Figure 3.3). The laser beam was split into two coherent beams of light using the beam splitter. The lens then caused these two beams to

intersect at a single point, the measuring point. The two beams formed a pattern of interference fringes. Particles in the flow cross these fringes, scattering light as they do so, the frequency of the scattered light corresponding to the speed of the particles as they cross the fringes. Particles contained in tap water are assumed to move at the same speed as adjacent fluid (DISA Laser Doppler 1983) and their passage through the measuring point is shown by a Doppler burst on the oscilloscope. Fluid velocity can therefore be taken to be equal to the measured particle's velocity. The scattered light is gathered by the diode detector, which generates output signals by means of a photoelectric cell and is connected to the oscilloscope displaying the frequency of the particles passing through the laser's interference pattern. These signals are fed into the frequency shifter, which applies a known shift to the LDA frequencies so that Doppler Shift frequencies due to forward and reverse flows can be separated. The channel's shifted frequency is then fed to a frequency tracker, which tracks the most powerful frequency at any given instant and gives an analogue output corresponding to the Doppler shift frequency plus the applied shift for the given channel. The analogue signals corresponding to the velocity components measured were collected using the atTRACKtion data acquisition system (atTRACKtion Technical reference manual, 1989) to digital conversion board and software mounted on an IBM compatible 486DX-OP-WBP. Measurements were collected using a digitising frequency of 1000Hz. A measurement consists of 4096 samples and the value of the measured parameters, such as velocities in this study, were the average of 20 measurements at a same point, so the completion of the LDA measurements for a parameter at a specific point took 82 seconds. The choice of this frequency was based on its steadier LDA readings than those with higher frequencies, such as 2000, 3000, 4000 and 8000 and its quicker and comparable reading compared with those with lower frequencies, such as 500, 250, 150 and 65Hz.

3.2.1.2 Operation of the LDA system

The set-up of the LDA system as used on the channel is shown in Figures 3.1.1 and 3.1.2. The laser and transmission optics were mounted on a horizontal steel rail and a vertical screw, allowing the point of measurement to be placed at most locations within the working section of the channel. The diode detector was mounted on a separate rail and screw system usually on the other side of the channel. Points could be positioned to ±0.1mm.

LDA is able to provide the readings of velocity, velocity fluctuation, turbulence intensity of the fluid and the skewness and flatness of velocity fluctuations relative to the root mean

square value. The readings were obtained by placing the measuring point at the first measuring location, focusing the collection optics until a locked-on signal could be obtained and clear Doppler bursts registered on the oscilloscope, collecting a sample using the atTRACKtion data acquisition system and then moving the beam intersection to the next location and repeating the process. A single point measurement typically resulted from 20 times averaging of 4096 readings.

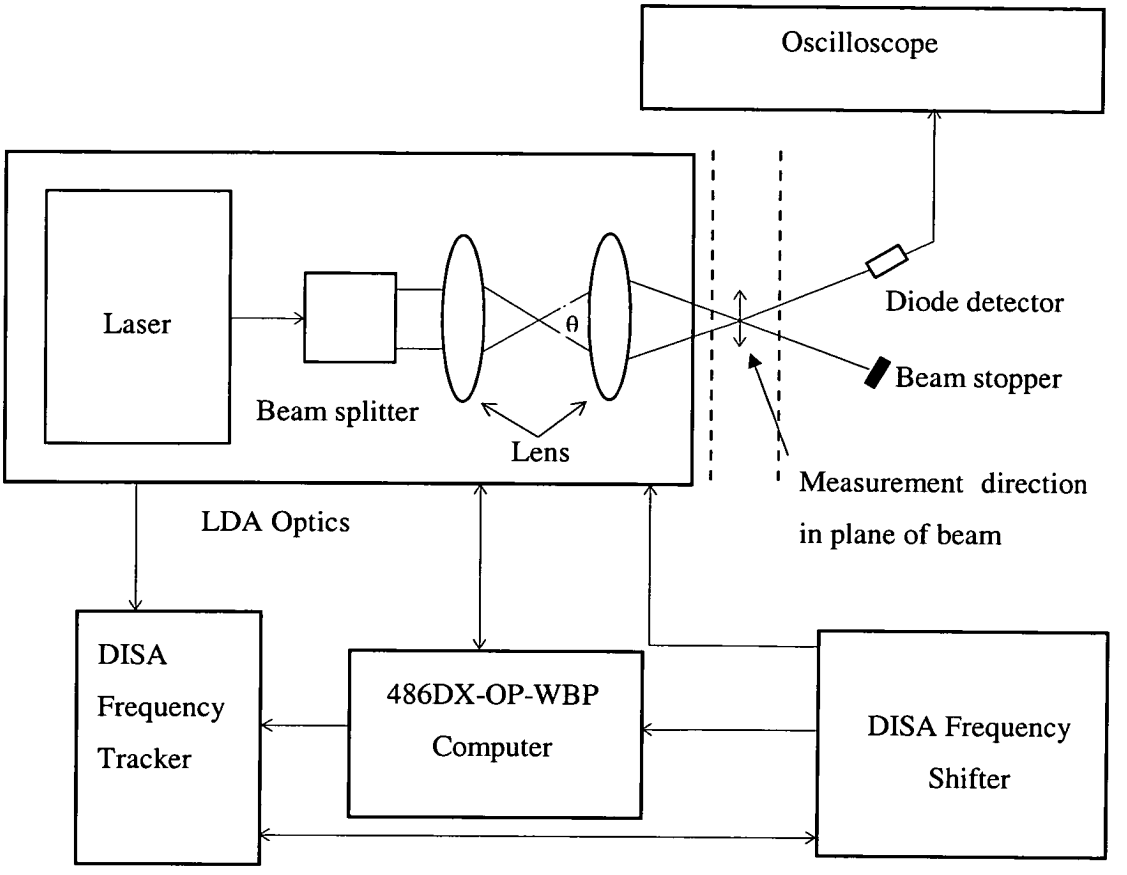

Figure 3.3 Arrangement of LDA system

The one-channel LDA system used here can resolve only one component of the parameters (such as turbulence shear stress u'u' and velocity u) in a plane at right angles to the average path of its two beams as shown in Figure 3.3. The vertical components of the shear stress and velocity were able to be measured by turning the lens 90^0 and repeating the same measuring procedures as for the measurement of u'u'and u. The measurement of the

transversal component was not so straight forward and is discussed in Section 3.4.3. Since the laser beam is deflected by the perspex, the shift distance of the laser beam in the y direction (X_L) is not exactly the same as the movement of the tracker in the same direction (X_T). A series set of data was measured and a correlationship was found:

$X_L = 0.06942X_T - 0.0708$ (cm) as shown in Figure 3.4.

As this correlationship has some error ($R^2 = 0.995$), the final adjustment of the absolute position of the measuring location was also checked using a ruler.

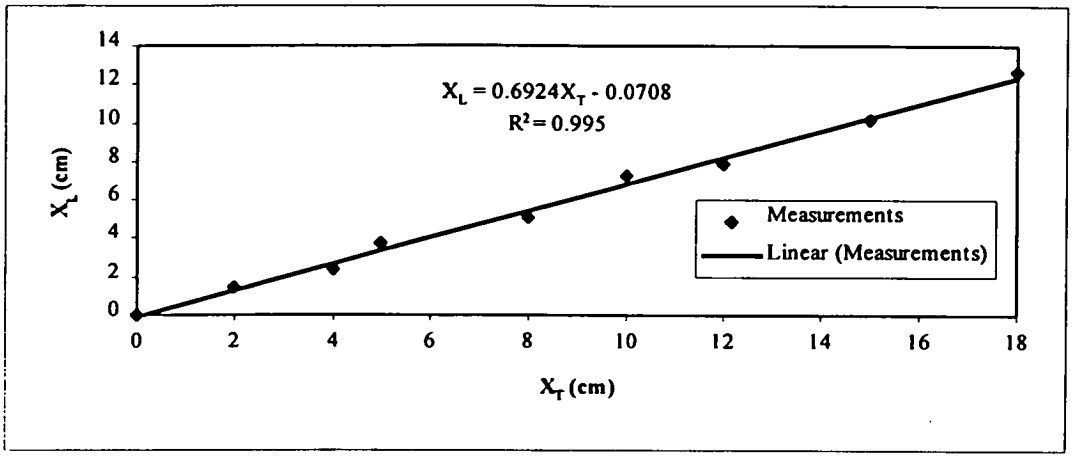

Figure 3.4 Correlation of X_L and X_T

3.2.2 STREAMFLO velocity meter

Since the LDA system could be used only in the working section of the channel where the clear walls allowed the passage of laser light, it was necessary to use an alternative instrument to obtain velocity measurements at other locations in the channel such as at the entrance to the effective channel length. The instrument chosen for this purpose was the STREAMFLO meter (Figure 3.5). Its results were also used to compare with the readings of LDA and the output of numerical modelling. A brief explanation of the principles of the velocity meter is given in the following paragraphs and a detailed introduction can be obtained from the manufacturer's manuals (STREAMFLO velocity meter 400).

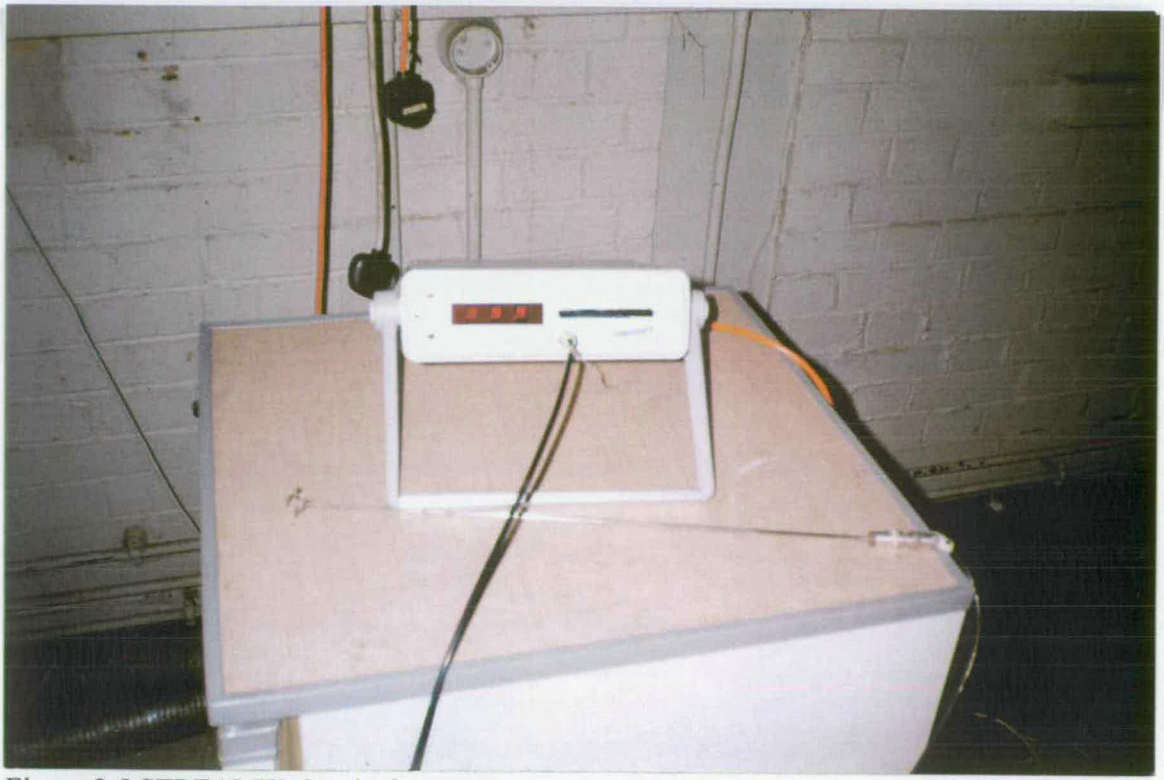

Figure 3.5 STREAMFLO velocity meter

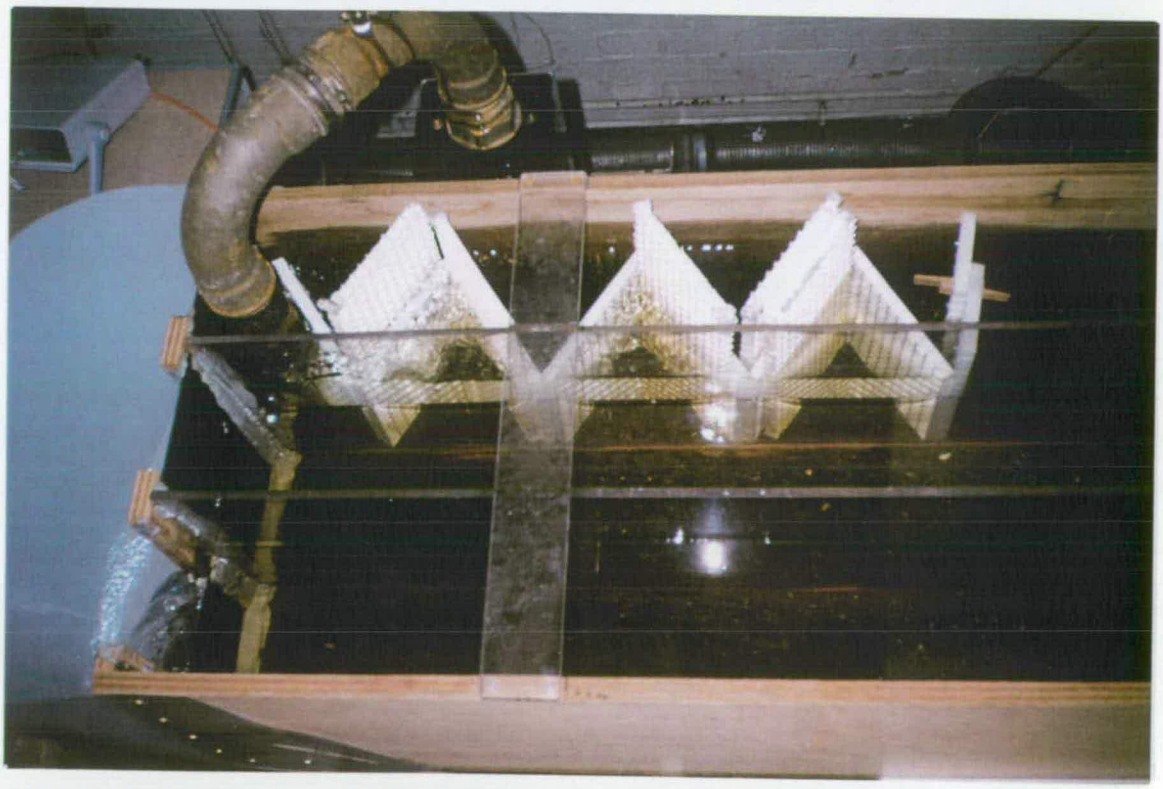

Figure 3.6 Arrangement of baffles located near the inlet pipe

The STREAMFLO miniature current velocity meter system is designed for measuring very low velocities (2.5 to 150cm/sec) of conducting fluids, usually water, in open channel with accuracy of ±5% for the velocity range of 0.025 to 0.075m/s, and ±2% for the velocity of 0.075 to 0.15m/s.

The velocity meter consists of three main parts: a measuring head, a stainless steel tube containing an insulated gold wire terminated 1.0mm away from the measuring head, and an electronic measuring unit.

The measuring head with a cage approximately 15mm diameter enables readings to be taken in confined spaces. The measuring head is composed of a five bladed rotor mounted on a hard stainless steel spindle. The spindle terminates in a fine burnished conical pivot which runs in jewel bearings mounted in an open frame. Frictional torque is thus extremely low and results in a linear output over a wide range of velocities. The pivot and jewels are shrouded to reduce the possibility of fouling. An occasional brief wash in a 30:1 Hydrochloric Acid solution is recommended to remove deposits of grease and film. The head is attached to the end of the stainless steel tube, and is connected to the measuring unit via a co-axial cable.

When the rotor is immersed in a fluid, the passage of the rotor blades past the gold wire tip slightly varies the measurable impedance between the tip and the tube. This variation is used to modulate a 15kHz carrier signal generated within the indicating instrument which in turn is applied to the electronic detector circuits. Automatic compensation is made for change in liquid conductivity and following amplification and filtering of the carrier frequency a square wave signal is obtained. In the analogue indicator this is used to drive a diode pump integrator hence obtaining a current signal proportional to the velocity. In the digital indicator the pulses are counted over a known time period to obtain a digital reading.

3.2.3 The auxiliary devices

The auxiliary devices needed for measurement of velocity and turbulence are shown in Figure 3.1.1 and included a water recycling tank of approximately 180 litres with a submerge pump for lifting water to the channel and a flow meter (0 to 200 litre/min) to check that the flow rate of water was constant at the designed values.

3.3 EXPERIMENTAL PROCEDURE

Prior to the formal start of the measurement, all facilities were cleaned to minimise the disturbance from impurities in the water to the measurement by LDA and the velocity meter.

The recycling tank was filled with tap water at a temperature of 20 ± 1^0C. While setting up the LDA and the STREAMFLO meter, the pump was left running for about 20 minutes to steady the flow status in the channel and to allow the flow meter to settle to the designed flowrate. Initially two LDA readings of velocity and turbulence shear stress for a specific point within the channel were taken at a time interval of about 5 minutes. When the two readings were comparable, it was assumed that the steady-state condition was reached. General measurements were then commenced.

To minimise the influence of the initial turbulence caused by the water discharging into the channel on the distribution and magnitude of the turbulence and the velocity throughout the channels, plastic baffles were located near the inlet pipe. The baffles were 10mm thick with the grid wall 1.5mm wide and openings 12.5mm x 12.5mm. The arrangement of baffles can be seen in Figure 3.6. The effects of the baffles on the magnitude and distribution of velocities and turbulence in the channel are discussed in section 3.4.1.

The water surface in the channel was controlled by a rectangular outlet weir. The height of the outlet weir was varied with flow rates and an estimation of weir height came from the following equation (Webber, 1968):

$$(H - P)^{1.5} = \frac{3Q}{2\sqrt{2g}C_d L} - 0.0012 \qquad (3.2)$$

-where $C_d = 0.602 + 0.083\frac{H-P}{P}$, P is the height of the weir, H the water depth in the channel, Q the flowrate, L the channel width, g the gravity acceleration, C_d a coefficient of discharge. Final adjustment of P was made to set H = 200mm.

Two nominal flowrates, 180 l/min and 90 l/min, were used in the investigation, these corresponding to the nominal velocities of 0.1m/s and 0.05m/s. These two velocities cover most of the velocities tested in the flocculation and settling experiments in Chapter 5 and provide a suitable retention time for the flocculation and settling.

As shown in Figure 3.2, turbulence and velocity profiles were measured by the LDA system at 25mm, 60mm and 100mm from the outside wall. Each profile consisted of measurements at 20mm above the bed, then at nominal vertical intervals of 40mm intervals to the surface. The STREAMFLO meter was used for the measuring of velocity at the entrance to the effective channel length, where the LDA system could not be applied. Another purpose of its use is to provide additional readings for the LDA measurement zone, which was associated with the measurement from the LDA to verify the modelling output. Table 3.1 shows a good comparability between the measured results from the LDA and the STREAMFLO meter with a maximum difference in u-velocity of about 5%.

Table 3.1 Comparison of measured u-velocity from the LDA and the STREAMFLO meter under the nominal velocity of 0.1m/s.

Location (mm)	u-velocity (m/s)	
	LDA	STREAMFLO meter
x=450, y=60, z=60	6.00E-2	6.31E-2
x=450, y=248, z=60	-7.31E-2	-7.01E-2
x=450, y=60, z=100	9.79E-2	9.37E-2
x=450, y=248, z=100	-9.16E-2	-9.12E-2
x=450, y=60, z=140	1.02E-1	9.89E-2
x=450, y=248, z=140	-1.02E-1	-1.06E-1

3.4 EXPERIMENTAL RESULTS AND DISCUSSION

It is noted that the experimental study and the numerical modelling of the flow in the channel flocculator were carried out simultaneously. This allowed determination of all necessary data from experiment for the input to the modelling simulation whilst the experiment was being undertaken and at the same time feed back the benefits from the modelling study to the experimental investigation in order to minimise the demand from the experiment.

In all the tests described in the following paragraphs, a consistent coordinate system was used in the channel, measuring x longitudinally along the length of the channel, with x = 0 at the end wall, y laterally across the width of the channel from inlet to outlet and z vertically upwards from the bed (see Figure 3.2). The three dimensional velocities in x, y and z directions are represented by u, v and w respectively. The longitudinal velocity, u, was set positive along the main flow direction in channel 1 and so became negative in channel 2,

whilst the transversal velocity, v, was set positive in the y direction and the vertical velocity, w, positive in the z direction.

3.4.1 Velocities at the inlet section to the channel

Steady measurements were obtained 100mm downstream from the plastic baffles, so the inlet boundary section was set 2800mm from the end wall (shown in Figure 3.1.1). The velocity profiles measured by the STREAMFLO meter provided input for the modelling study of the flow in the flocculator.

The measurements for the inlet velocity profiles were taken at heights of 20mm, and then at intervals of 40mm up to 180mm above the channel bed. The locations of measurement and the measurement results are listed in Table 3.2. Transverse and vertical velocities were too low to be detected by the STREAMFLO meter at the entrance section and the corresponding modelled values are given in the table. It is shown that the magnitudes of these modelled data were less than the meter's lowest detectable velocity of 0.025m/s.

Table 3.2 Locations and measurements of the inlet velocity profiles (* indicates modelling value)

Location (mm) x = 2800		Nominal velocity of 0.1m/s			Nominal velocity of 0.05m/s		
		u (m/s)	v* (m/s)	w* (m/s)	u (m/s)	v* (m/s)	w* (m/s)
y = 40	z = 20	0.093	1.30E-3	2.12E-4	0.036	6.18E-4	1.90E-4
	z = 60	0.106	4.10E-4	3.49E-4	0.045	1.95E-4	3.75E-4
	z = 100	0.116	-9.99E-4	-8.80E-5	0.050	-4.76E-4	2.50E-4
	z = 140	0.120	-4.94E-4	-9.25E-4	0.052	-2.35E-4	-8.22E-5
	z = 180	0.122	1.91E-3	-7.00E-4	0.046	9.09E-4	-1.46E-4
y = 60	z = 20	0.095	1.38E-3	-6.54E-5	0.043	6.56E-4	-3.11E-5
	z = 60	0.108	5.35E-4	1.10E-4	0.049	2.55E-4	5.24E-5
	z = 100	0.119	-3.11E-4	-2.37E-4	0.053	-1.48E-4	-1.13E-4
	z = 140	0.125	7.76E-6	-1.17E-3	0.057	3.70E-6	-5.58E-4
	z = 180	0.126	1.21E-3	-7.59E-4	0.056	5.75E-4	-3.62E-4
y = 100	z = 20	0.089	1.31E-4	3.99E-4	0.040	6.23E-4	1.01E-4
	z = 60	0.106	1.37E-4	7.88E-4	0.048	6.51E-5	1.66E-4
	z = 100	0.118	1.78E-4	5.24E-4	0.054	8.46E-5	-4.19E-5
	z = 140	0.122	3.60E-4	-1.73E-4	0.056	1.71E-4	-4.40E-4
	z = 180	0.121	-2.63E-4	-3.08E-4	0.056	-1.25E-4	-3.33E-4

The u-velocity profiles at the inlet section are shown in Figures 3.7.1 and 3.7.2. The longitudinal velocity at the entrance increases monotonically from the channel bed and is quite close to a logarithmic profile from 20 to 180mm above the bed. The variation of its magnitude across the channel gives the maximum value around the centre line as would be expected in a straight channel.

To test the effectiveness of the baffles, longitudinal velocity, u, and kinetic energy at six points were measured by LDA with and without the baffles at x = 450mm in channel 1 and channel 2. The results are listed in Table 3.3 and clearly show that there is no significant difference between the two sets of data indicating that the initial turbulence has little effect on the distribution and magnitude of turbulence and velocity beyond a certain distance. These are confirmed by the modelling study, and the effecting distance of the initial turbulence is discussed in Chapter 4.

Table 3.3 Comparison of u-velocity and kinetic energy with and without baffles under the nominal velocity of 0.1m/s.

Location	u-velocity (m/s)		Kinetic energy (m^2/s^2)	
(mm)	With baffles	Without baffles	With baffles	Without baffles
x=450, y=60, z=60	6.00E-2	6.04E-2	2.39E-4	2.34E-4
x=450, y=248, z=60	-7.31E-2	-7.31E-2	9.55E-5	9.55E-5
x=450, y=60, z=100	9.79E-2	9.87E-2	2.19E-4	2.21E-4
x=450, y=248, z=100	-9.16E-2	-9.14E-2	5.85E-5	5.85E-5
x=450, y=60, z=140	1.02E-1	1.07E-1	1.36E-4	1.43E-4
x=450, y=248, z=140	-1.02E-1	-1.02E-1	3.20E-5	3.21E-5

3.4.2 Velocities and turbulence in the measured sections

Three dimensional velocities (u, v, and w) and the turbulence shear stresses ($u'u', v'v', w'w'$) under the nominal velocity of 0.1m/s measured by LDA are listed in Tables A1.1 to A1.5 in Appendix A and examples shown in Figures 3.8.1 to 3.12.4.

Variations of u, v and w at three different channel heights (level 1, level 3 and level 5) are shown in Figures 3.8.1 to 3.8.6. The absolute value of the longitudinal velocity, u, gradually decreases approaching the bend and continuously increases from the end wall, quickly

reaching a steady value 200mm away from the end wall in the second channel, whilst the value of the transversal and vertical velocities go through an opposite process.

From the full set of tabled results, the magnitudes of the longitudinal velocities at the level near the channel bottom in channel 1 are generally 1.1 to 1.6 times of those at the middle level and 1.0 to 2.7 times of those at the level near the surface where the lowest values occur. In channel 2, the lowest magnitude of u velocity was at the level 1. A similar phenomenon was found by Crapper (1995) and is partly due to the redistribution of flow as it passes along the straight channel section, and partly to backing up effects from the bend. The variation trends of the velocities of v and w remained essentially same for the different levels.

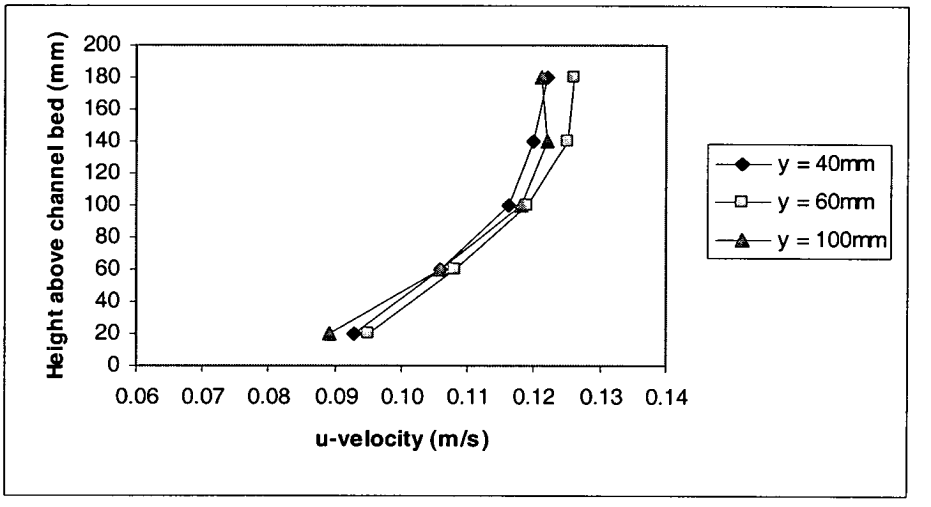

Figure 3.7.1 u-velocity at x=2800mm for nominal velocity of 0.1m/s

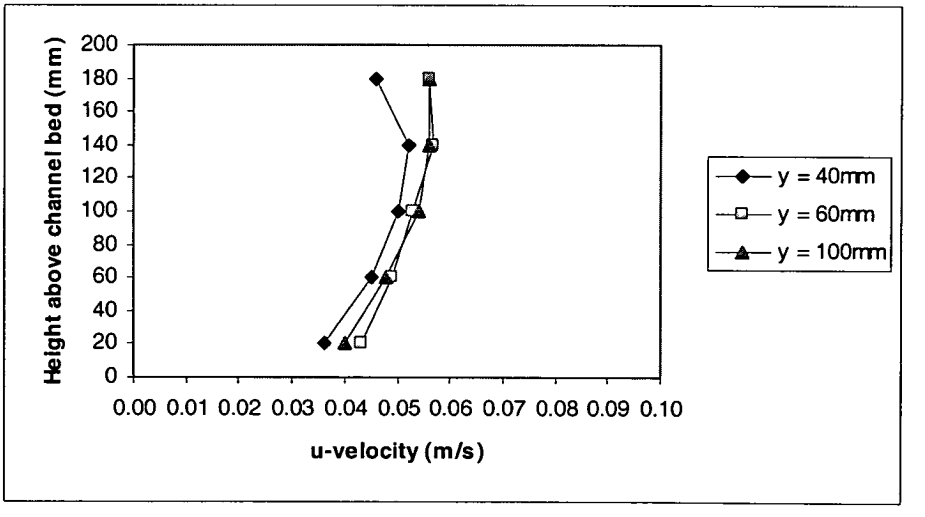

Figure 3.7.2 u-velocity at x=2800mm for nominal velocity of 0.05m/s

Figures 3.9.1 to 3.9.6 exhibit how the velocities vary with the width of the channel at the region near the bend. In channel 1, the maximum u-velocity is generally at the outside wall. In channel 2, as shown in Figure 3.9.4 the maximum magnitude of the u-velocity is closer to the inside wall. The v-velocity has a similar variation trend to that of the u-velocity. The vertical velocity, w, varies slightly with the width of the channel and goes to zero at x=200mm.

The turbulence information derived from the LDA measurements is the temporal means of the products of u'u', v'v' and w'w', where the prime indicates a turbulent fluctuation of the corresponding mean velocity. As discussed in Chapter 2, kinetic energy (k) as the sum of the three products is one of the most useful turbulence parameter in assessing the turbulence in relation to flocculation, therefore the kinetic energy was calculated by the following equation and listed in Tables A1.1 to A2.5 in Appendix A.

$$k = 0.5\,(u'u' + v'v' + w'w') \tag{3.3}$$

There is a general trend that the kinetic energy decreases from x=0.45m towards the end wall in the first channel due to the backup effect of the bend and decreases from the end wall towards the outlet in the second channel as shown in Figures 3.10.1 to 3.11.2. The minimum magnitude of kinetic energy lies at the level near the water surface as shown in the Figures 3.10.1 and 3.10.2. There is no obvious variation trend of the kinetic energy with the channel width as can be seen in Figures 3.11.1 and 3.11.2.

Volume weighted average values of six elevational points and three transversal points of longitudinal velocity (u) and kinetic energy under nominal velocity of 0.05 and 0.1m/s are compared in Figures 3.12.1 to 3.12.4. The choice of kinetic energy and u-velocity is based on the two most essential parameters in assessing turbulence in relation to flocculation as discussed in Chapter 2 and will be mentioned in Chapter 4. The choice of u-velocity is also because the LDA readings of the u-velocity are much more steady and reliable than the other velocity components, with a relative error of the v-velocity and w-velocity up to 11 times that of the relative error of the corresponding u-velocity at the same measuring point as shown in Tables A3.1 to A4.5 in Appendix A.

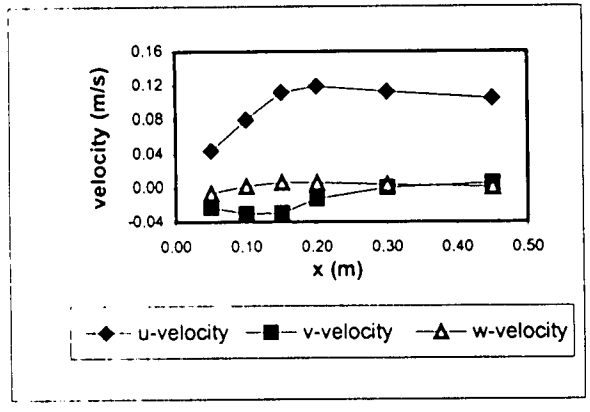

Figure 3.8.1 Velocity variation vs x coordinate (Level 1, Section 1c)

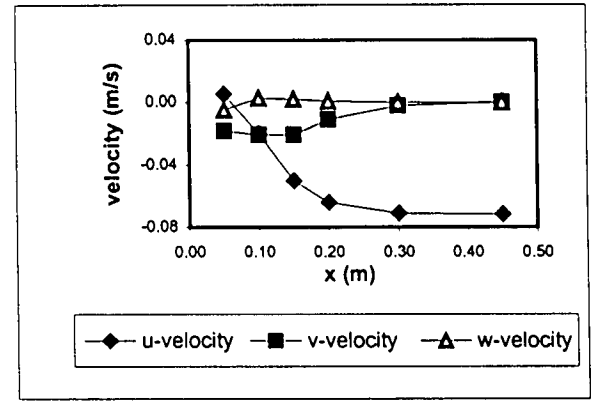

Figure 3.8.2 Velocity variation vs x coordinate (Level 1, Section 2c)

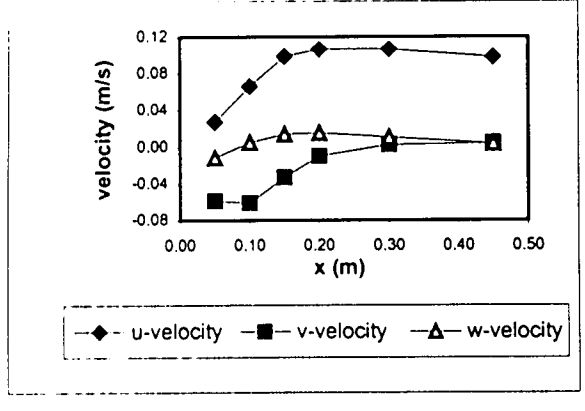

Figure 3.8.3 Velocity variation vs x coordinate (Level 3, Section 1c)

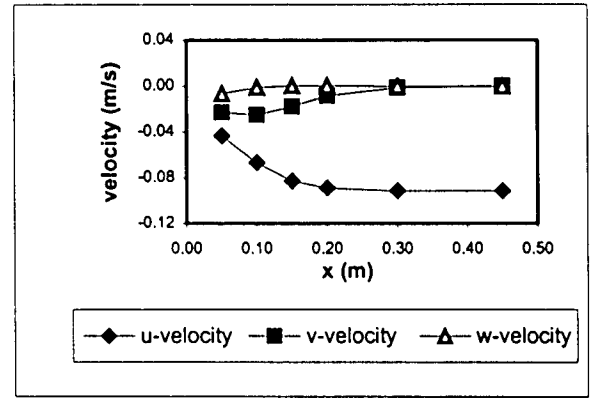

Figure 3.8.4 Velocity variation vs x coordinate (Level 3, Section 2c)

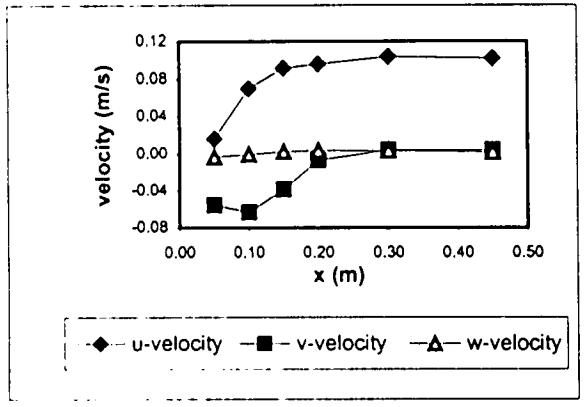

Figure 3.8.5 Velocity variation vs x coordinate (Level 5, Section 1c)

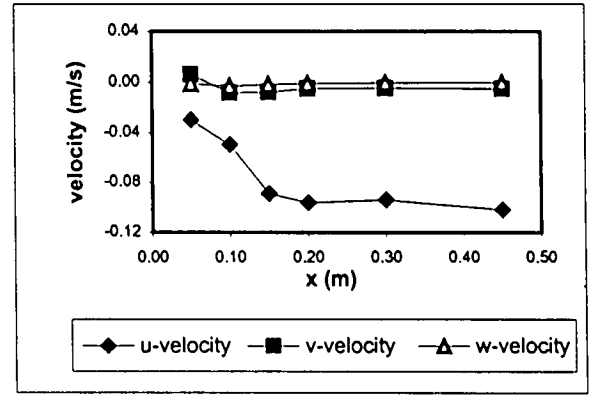

Figure 3.8.6 Velocity variation vs x coordinate (Level 5, Section 2c)

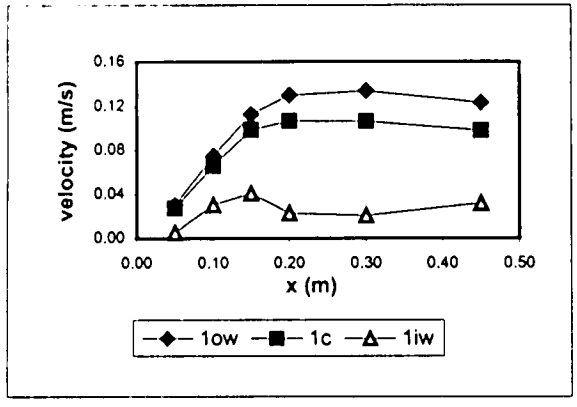

Figure 3.9.1 u-Velocity variation vs x coordinate (Level 3, channel 1)

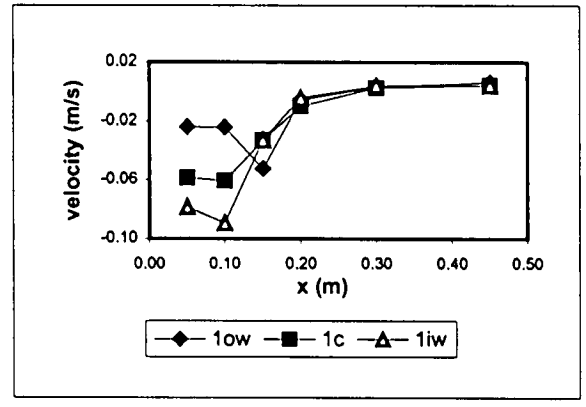

Figure 3.9.2 v-Velocity variation vs x coordinate (Level 3, channel 1)

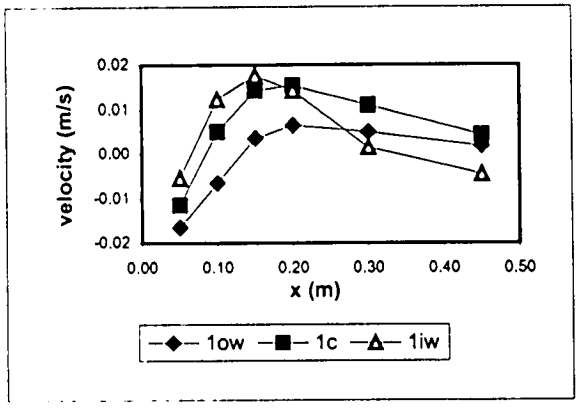

Figure 3.9.3 w-Velocity variation vs x coordinate (Level 3, channel 1)

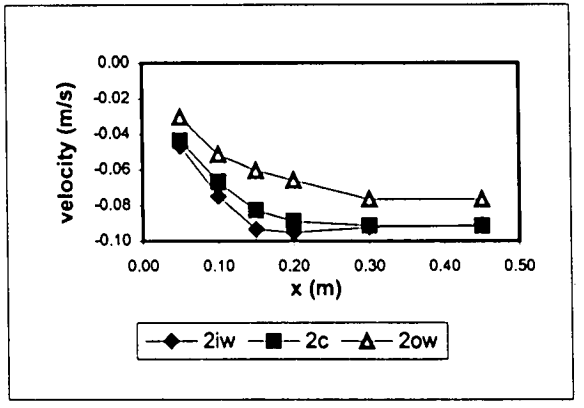

Figure 3.9.4 u-Velocity variation vs x coordinate (Level 3, channel 2)

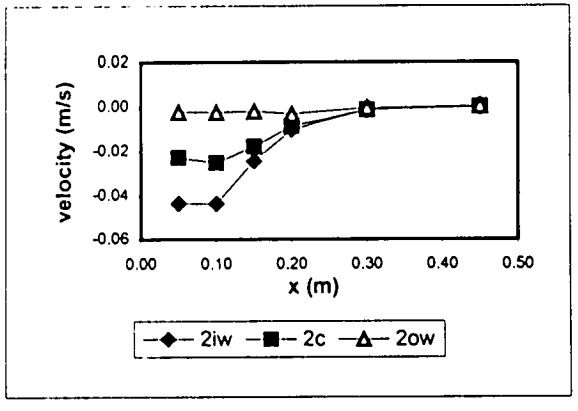

Figure 3.9.5 v-Velocity variation vs x coordinate (Level 3, channel 2)

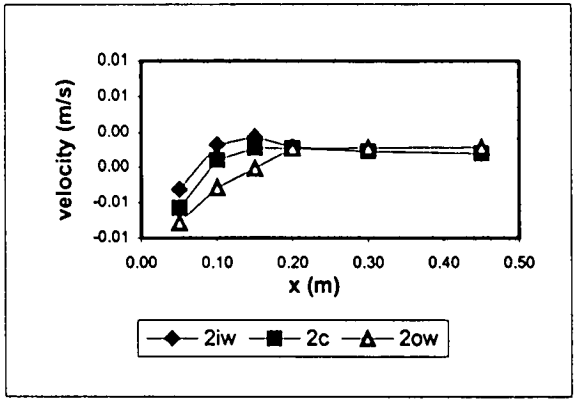

Figure 3.9.6 w-Velocity variation vs x coordinate (Level 3, channel 2)

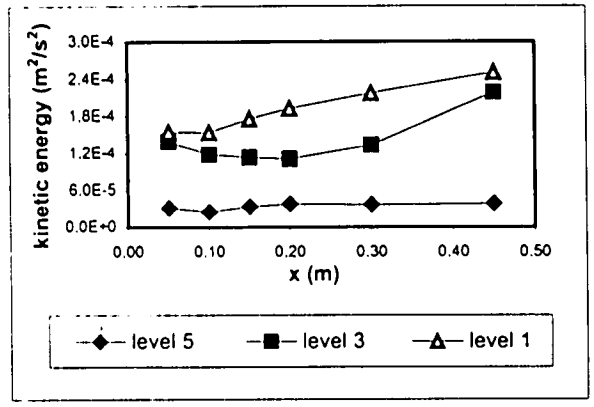

Figure 3.10.1 Kinetic energy at various levels (Channel 1)

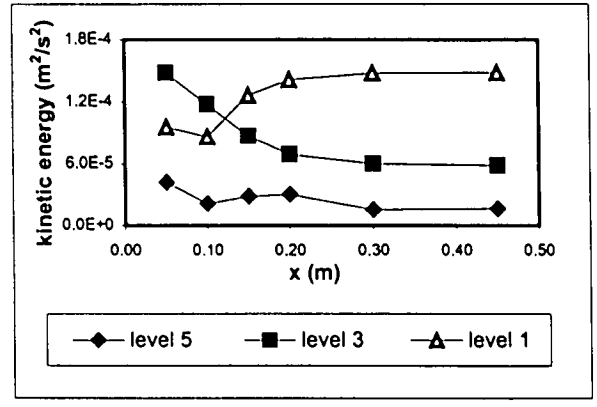

Figure 3.10.2 Kinetic energy at various levels (Channel 2)

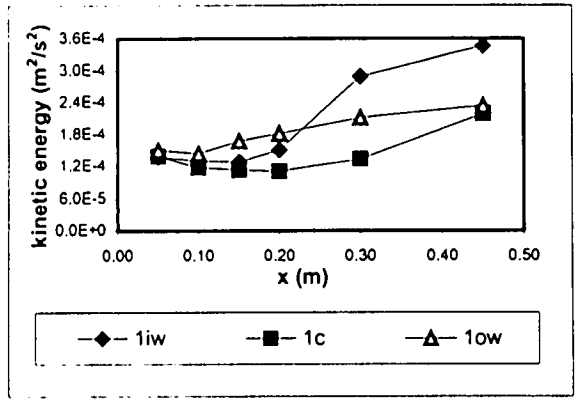

Figure 3.11.1 Kinetic energy across channel width (Level 3,channel 1)

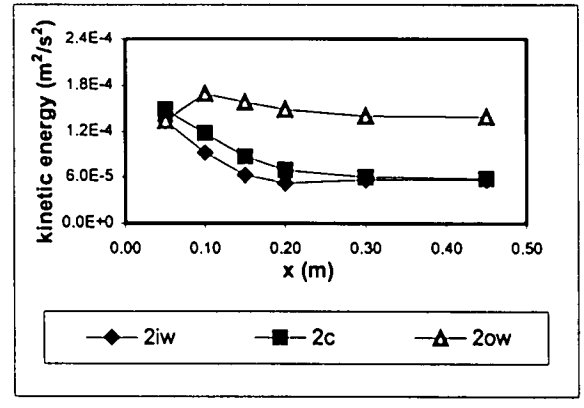

Figure 3.11.2 Kinetic energy across channel width (Level 3, channel 2)

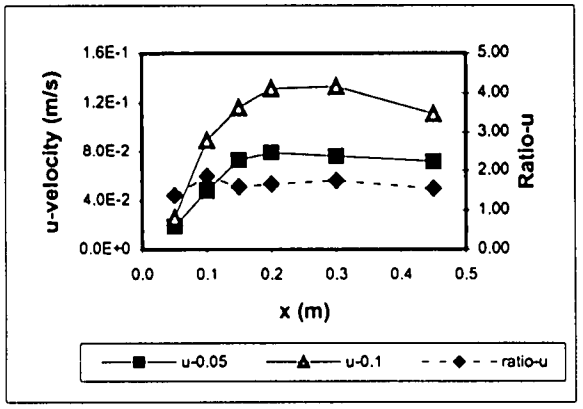

Figure 3.12.1 Comparison of u-velocity in 1st channel under nominal velocity of 0.05 and 0.1m/s

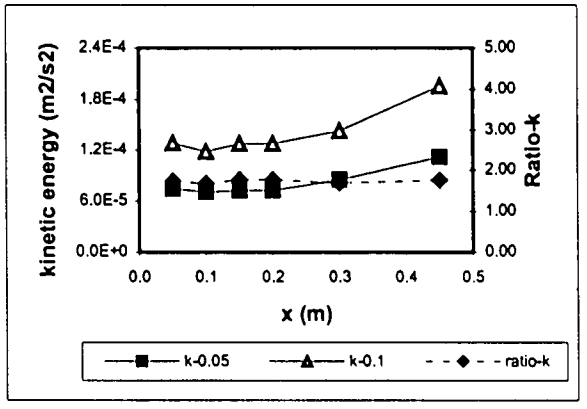

Figure 3.12.2 Comparison of kinetic energy in 1st channel under nominal velocity of 0.05 and 0.1m/s

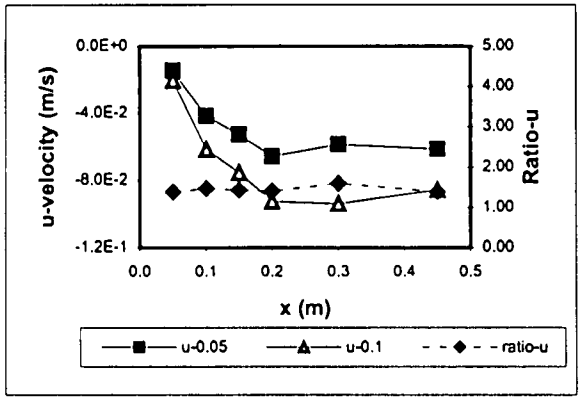

Figure 3.12.3 Comparison of u-velocity in 2nd channel under nominal velocity of 0.05 and 0.1m/s

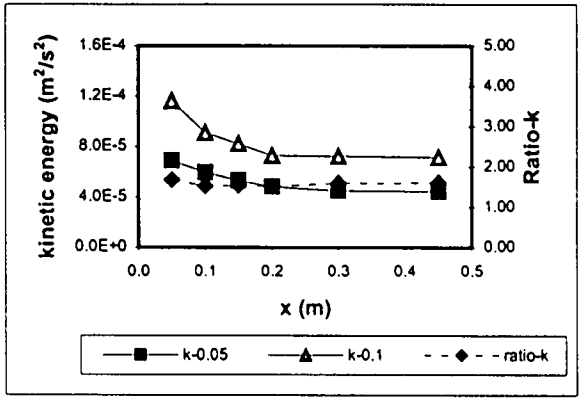

Figure 3.12.4 Comparison of kinetic energy in 2nd channel under nominal velocity of 0.05 and 0.1m/s

There is an obvious trend that the u-velocity and the kinetic energy of the nominal velocity of 0.1m/s are greater than that of the nominal velocity of 0.05m/s for all the cases as shown in the Figures 3.12.1 to 3.12.4. Crapper (1995) found there was a tendency for values of Reynolds stress to be higher as the incoming velocity increases. However, there is no literature available for quantifying the relationships between velocity and kinetic energy in the channels and the nominal velocities. It was attempted to establish such a correlation by calculating the ratios of velocity and kinetic energy from the measurements of LDA for the nominal velocities of 0.05 and 0.1m/s. Ratio-u in the Figures 3.12.1 and 3.12.3 represents the u-velocity ratio of nominal velocity of 0.1m/s to that of nominal velocity of 0.05m/s. The corresponding kinetic energy ratio is labelled as Ratio-k in the Figures 3.12.2 and 3.12.4. The calculated ratios shown in these Figures are very stable, which indicates that the magnitudes of the velocity and the kinetic energy are directly proportional to the corresponding nominal velocity. The mathematical modelling study in Chapter 4 confirms this finding.

3.4.3 Measurement of transversal velocity and turbulence by LDA

Quantifying the transversal velocity and turbulence is an important step for identifying the variation of the three dimensional velocities and turbulence shear stresses in the channel, for example to demonstrate the existence of secondary flow (Henderson, 1960 and Rosovskii, 1965), especially for the region near the bend. However, for measurements in this direction with the usual LDA set up the laser beam would have to travel about 3m before reaching the diode detector resulting in a very weak signal.

To overcome this a 1.2 x 2.4 cm high grade mirror was placed at an angle of about 45^0 to the incoming laser beam, 5cm beyond the measuring point in order to deflect the beam 90^0 to its original direction ensuring a short path to the diode detector (see Figure 3.13). A clear signal was exhibited on the oscilloscope.

To test the effect of the mirror on the flow status (turbulence and velocity are the most important parameters) and the accuracy of this approach, u-velocity and turbulence shear stress u'u' were measured with and without the mirror. The results are listed in Table 3.3 showing that the two sets of data are essentially the same with maximum difference in velocity of about 3% and in shear stress 2%.

Table 3.3 Comparison of u-velocity and turbulence shear stress (u'u') with and without mirror for the nominal velocity of 0.1m/s.

Location (mm)	u-velocity (m/s)		Turbulence shear stress (u'u') (m^2/s^2)	
	With mirror	Without mirror	With mirror	Without mirror
x=100, y=60, z=100	6.60E-2	6.61E-2	8.58E-5	8.58E-5
x=100, y=248, z=100	-6.68E-2	-6.68E-2	1.20E-4	1.22E-4
x=200, y=60, z=60	7.02E-2	7.00E-2	1.21E-4	1.21E-4
x=200, y=248, z=60	-8.50E-2	-8.54E-2	1.14E-4	1.12E-4
x=200, y=60, z=100	1.03E-1	1.06E-1	8.08E-5	8.08E-5
x=200, y=248, z=100	-8.88E-2	-8.89E-2	6.39E-5	6.39E-5

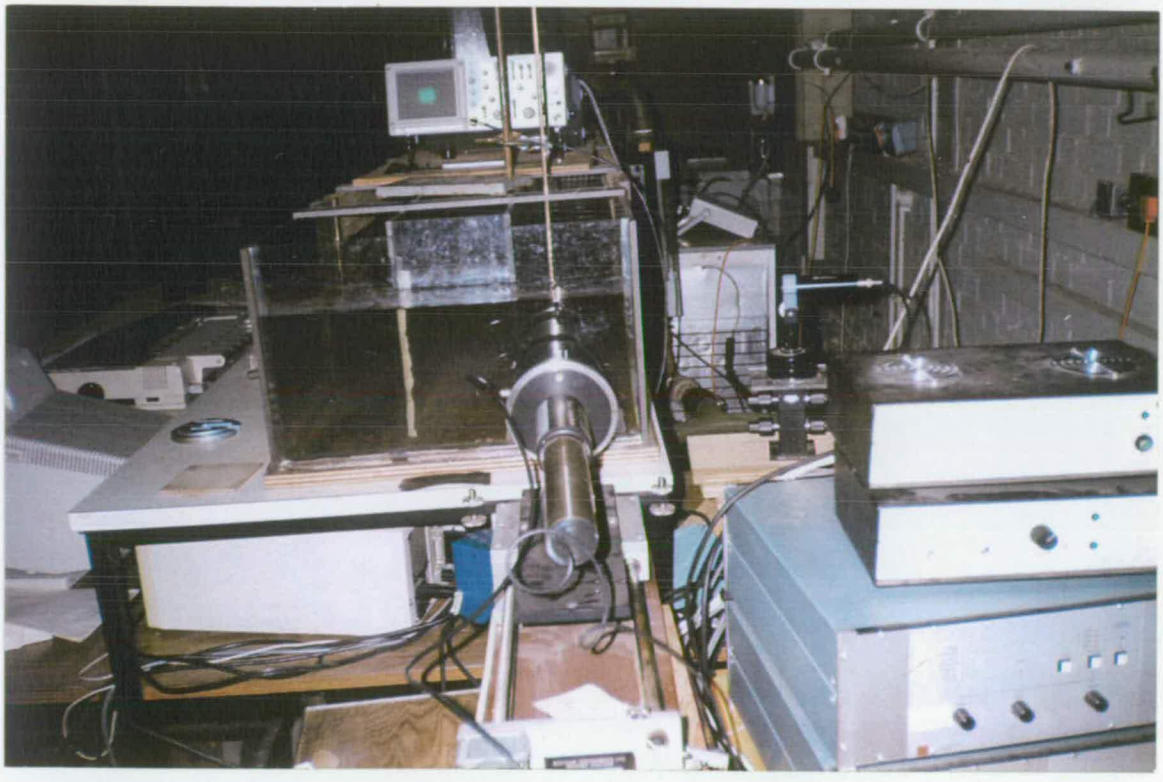

Figure 3.13 Arrangement of LDA system for the measurement in transversal direction

3.4.4 Assessment of experimental error

Experimental error was assessed for directly measured parameters, such as the three component velocities, u, v and w, and the velocity fluctuations, u', v', and w', and indirectly measured parameters, such as Reynolds stresses, u'u', v'v' and w'w' and kinetic

energy, k. The velocity measurements at x = 2800mm by the STREAMFLO meter had an accuracy of ±2% to ±5% according to its specification. The value of directly measured parameters measured by the LDA was the average of 20 readings at a same point. The overall mean values of the velocities and kinetic energy are listed in the Tables A1.1 to A2.5 in Appendix A. The arithmetic mean difference, Δx, between the individual measurement, x_i, and the average value, $\bar{x}$, is represented by the following equations:

$$\Delta x = \frac{\sum_{i=1}^{n} |x_i - \bar{x}|}{n} \tag{3.4}$$

$$\bar{x} = \frac{1}{n} \sum_{i=1}^{n} x_i \tag{3.5}$$

The variabilities of the measurements in terms of standard deviation (SD) and relative error (RE) to the arithmetic mean of the measured parameters were calculated for the 36 locations on each of the five levels within the channel and for all 180 locations throughout the channel flocculator for two nominal flow velocities of 0.05 and 0.1m/s (see Tables A3..1 to 4.5 in Appendix A).

$$SD = \left[\frac{\sum (x_i - \bar{x})^2}{(n-1)} \right]^{\frac{1}{2}} \tag{3.6}$$

$$RE = \frac{SD}{N} \% \tag{3.7}$$

-where, n=20, is the number of measurements. N is the arithmetic mean of the measured parameters. SD is thus a measure of the homogeneity of the velocity and turbulence fields and RE is a percentage of variation to the mean value.

The absolute and relative error of indirectly measured parameters were calculated as the function of errors of directly measured parameters as follow (Li, 1988):

$$SD = \sqrt{\left(\frac{\partial f}{\partial x_1}\right)^2 SD_{x1}^2 + \left(\frac{\partial f}{\partial x_2}\right)^2 SD_{x2}^2 + \ldots\ldots + \left(\frac{\partial f}{\partial x_n}\right)^2 SD_{xn}^2} \tag{3.8}$$

-where SD is the standard deviation of the indirectly measured parameter, SD_{x1}, SD_{x2}.....SD_{xn} are the standard deviations of directly measured parameters of x_1, x_2.....x_n. For example, the standard deviation of Reynolds stress, u'u':

$$SD_{u'u'} = \sqrt{(2u')^2 SD_{u'}^2} = 2u'SD_{u'} \tag{3.9}$$

The standard deviations of Reynolds stresses, v'v', and w'w', can therefore be calculated as follows:

$$SD_{v'v'} = 2v'SD_{v'} \tag{3.10}$$

$$SD_{w'w'} = 2w'SD_{w'} \tag{3.11}$$

For the kinetic energy, $k = \frac{1}{2}(u'u'+v'v'+w'w')$, its standard deviation can be expressed in terms of the standard deviations of Reynolds stresses in the following Equation 3.12 and the standard deviation of velocity fluctuations in Equation 3.13 according to Equation 3.8:

$$SD_k = \sqrt{\left(\frac{1}{2}\right)^2 SD_{u'u'}^2 + \left(\frac{1}{2}\right)^2 SD_{v'v'}^2 + \left(\frac{1}{2}\right)^2 SD_{w'w'}^2} = \frac{1}{2}\sqrt{SD_{u'u'}^2 + SD_{v'v'}^2 + SD_{w'w'}^2} \tag{3.12}$$

$$SD_k = \sqrt{(u'SD_{u'})^2 + (v'SD_{v'})^2 + (w'SD_{w'})^2} \tag{3.13}$$

Equation 3.7 was applied to the calculation of the relative error of indirectly measured parameters, such as kinetic energy. The standard deviation of directly and indirectly measured parameters and their corresponding relative errors are listed in the Tables A3.1 to A4.5 in Appendix A.

For the nominal velocity of 0.1m/s, the arithmetic mean relative error of u-velocity is 11.2% with a maximum of 26.8% and minimum of 2.9%. The relative error of the u-velocity gradually decreases, in general, as the x coordinate increases, i.e. with the increase of magnitude of the u-velocity. This agrees with the expectation that the longitudinal velocity becomes steadier as the flow moves away from the bend. In contrast the relative error of the v and w velocities generally go through a "U" shape as x increase. It can be explained that the higher relative errors of vertical and transversal velocities in the region near (5cm) the end wall are due to the effect of the wall, whilst the higher relative error at the location away from the bend (x=30cm and x=45cm) may result from the relatively lower magnitude of the mean of v and w velocities. The u-velocity is more steady and reliable than the other velocity components, with a relative error of the v-velocity and w-velocity up to 11 times that of the corresponding u-velocity at the same measuring point as shown in Tables A4.1 to

A4.5 in Appendix A. The standard deviations and relative errors of kinetic energy as a function of the velocity fluctuations are very steady as shown in the tables. The arithmetic mean relative error is about 12% and generally decreases as x increases.

Comparison of the relative errors for the nominal velocity of 0.05 and 0.1m/s shows that the u-velocity and kinetic energy for the velocity of 0.05m/s are not so steady as that of the velocity of 0.1m/s with up to 4.2 times and 2.7 times relative errors respectively. There is no clear trend of variation of the errors for the vertical and transversal velocities for these two nominal velocities. The arithmetic mean errors of u-velocity and kinetic energy are 16.3% and 16.5% respectively for the nominal velocity of 0.5m/s.

It can be concluded that the measurements of velocity and turbulence are quite steady and reliable according to the above discussions, especially for the longitudinal velocity and kinetic energy which are the two most useful parameters in this study.

3.5 CONCLUSIONS

The main conclusions drawn from the laboratory investigation of the flow in the channel are summarised as follows:

1. The longitudinal flow velocity at the inlet end of the effective channel length exhibits a logarithmic profile from the channel bottom to the water surface. The magnitude of transversal and vertical velocity components were too low to be measured by mini velocity meter.

2. The absolute value of the longitudinal velocity gradually decreases approaching the bend in channel 1 and continuously increases from the end wall and reaches a steady value after about 50mm away from the bend in channel 2, whilst the value of the transversal and vertical velocities go through an opposite process. The magnitudes of the longitudinal velocities at the level near the channel bottom in channel 1 are generally 1.1 to 1.6 times of those at the middle level and 1.0 to 2.7 times of those at the level near the surface where the lowest values occur. In channel 2, the lowest magnitude of u velocity was at the level 1. This is partly due to the redistribution of flow as it passes along the straight channel section, and partly to backing up effects from the bend. The variation trends of the velocities of v and w remained essentially the same for the different levels.

3. Velocities vary across the width of the channel. Due to the influence of the channel bend, in the first channel the maximum longitudinal velocity, u, is generally at the outside wall of the channel but in the second channel it is closer to the inside wall of the channel. Transversal velocity, v, has a similar variation trend as that of u-velocity. The vertical velocity, w, has a slight variation with the width of the channel and goes to zero 50mm downstream from the bend.

4. There is a general trend that the turbulence kinetic energy decreases from about x=0.45m towards the end wall in the channel 1 due to the backup effect of the bend and decreases from the end wall towards the outlet in the channel 2. The minimum magnitude of kinetic energy lies at the level near the water surface. There is no obvious variation trend of the kinetic energy with the channel width.

5. There is an obvious trend that the u-velocity and the kinetic energy of the nominal velocity of 0.1m/s are greater than those of the nominal velocity of 0.05m/s at all points. The experimental results show that the magnitudes of the velocity and the kinetic energy are directly proportional to the corresponding nominal velocity.

6. Assessment of measurement errors shows that the measurements of velocity and turbulence are quite steady and reliable, especially for the longitudinal velocity and kinetic energy under different nominal velocities.

7. The use of a high grade mirror to deflect the measurement laser beam gives no effective change to recorded values of velocity or kinetic energy.

Chapter 4. Computation of turbulence and velocity in channel flocculators

4.1 Introduction

It should be appreciated that the computer simulation of the flow in the channels and the experimental phase of this study were carried out simultaneously. It enabled simultaneously using the experimental results to verify the performance of the simulation and using the verified computer model of flows within the flocculator to exhibit a much fuller picture of the flow regime in the channel than could be obtained from experimental data alone. With the verified model, it becomes possible to determine, for example, velocities and Reynolds shear stresses at any location within the channel's working section under a wide range of conditions, on the basis of limited and not easily obtained experimental data, such as water surface velocities. It also gives a more comprehensive understanding and quantification of the features of flow regime in the channels. With the help of the computer model, it was possible to complete the computation of the flow characteristics for up to 85 channels in this study within a few days, which would take very much longer to finish by experiment. The relationship between turbulence and velocity and the nominal mean velocities and the number of channels computed by the model could substantially save the lead time and the costs of new flocculator designs.

In this chapter the development and theoretical basis of turbulence modelling including the setup of the model pre-processor (domain, grid, boundary conditions etc.) and solver are given, followed by the techniques of speeding up convergence. Comparison between the modelled results and experimental data is presented in section 4.6, and the modelling application to the specific channels in section 4.7. Conclusions are given in section 4.8.

4.2 Modelling flow in channel by CFD

Computational Fluid Dynamics (CFD) codes are constructed around the numerical algorithms that can tackle fluid flow problems. Its commercial packages, such as PHOENICS, FLOW3D and FLUENT have been proved to be able to simulate a wide variety

of two and three dimensional fluid flow problems in channels using Navier-Stokes equations.

Graham et al (1992) used FLOW3D and Petersen and Krishnappan (1994) used PHOENICS to simulate the turbulence in annular flumes by solving k-ε model. In their studies, a symmetrical boundary was set which simplified the problems into two dimensions. The modelled results were in good agreement with the experimental output. It was concluded that the CFD models of the experimental facilities provided a sound basis for an accurate and comprehensive interpretation of the result of flow in the channels. Crapper (1995) applied FLUENT to model the flow in a channel bend by employing Reynolds stress model. The comparison of the modelling and experimental results showed that the use of the FLUENT package enabled the convenient setup and execution of a three-dimensional mathematical model study of fluid flows in the channels. The FLUENT model of the channels was capable of producing results giving a good fit to experimentally determined flow velocities and turbulence.

Considering the accuracy and availability of the CFD commercial package in modelling of the flow in channels, it was appropriate to use such a facility to model the flow in the channels. Such an approach enables the author to concentrate attention on the modelling aspects of the particular case under consideration without having to concern with the development of a working solution to the Navier-Stokes equations since it was provided by the CFD packages. The FLUENT package from FLUENT Incorporated of Lebanon, New Hampshire (FLUENT Incorporated 1993) was applied in the simulation of the flow within the channels of this study. This was chosen in preference to other CFD programmes because it was readily available at the University of Edinburgh as well as being much more user friendly than other CFD packages (Steven, 1990).

4.2.1 Computation of open channel flow

Hafez (1995) used the finite element method to solve the Reynolds equations of motion and continuity to predict three-dimensional velocity and boundary shear distributions in open straight channels. The k-ε model was applied to model turbulent stresses in terms of the mean velocities and turbulent viscosity. However, the standard k-ε model can only be applied in the high Reynolds number region of the flow and its use is limited to simple

turbulent flows. The more comprehensive multi-equation Reynolds stress model performs significantly better in calculation of mean flow properties and all Reynolds stresses for complex flows including wall jets, asymmetric channel and non-circular duct flows and curved flows (Chen and Guo, 1991; Yang, 1995).

Bernard (1986) observed that all of the k-ε closure approaches fail to account for the large peak k value in the wall region that is evident in the experimental data. It was shown that this defect may be attributed to a fundamental inconsistency in the commonly used model for the pressure diffusion term in the k equation near the boundary. Zhang's experiment (1993) showed that log-law velocity profile model can be simulated for both smooth and rough wall surfaces in a rectangular channel. The predicted turbulent kinetic energy and dissipation rate agree reasonably with the experimental data.

De Vriend (1977) started to use two-dimensional, depth averaged results to assume a logarithmic distribution of vertical velocities. Leschziner and Rodi (1979) developed this approach to three dimensional problems. Younus and Chaudhry (1994) applied this method to compute free-surface unsteady flow in a straight rectangular channel.

Lane and Richards (1998) solved the depth-averaged form of the Navier-Stokes equations for open channel flow incorporating the simulation of the free surface by means of a 'rigid lid' or horizontal fixed boundary at which vertical, but not horizontal velocities, were set to zero (Leschziner and Rodi 1979). Some corrections were made by Lane and Richards due to the fact that water which in reality would rise up above the level of the rigid lid is assumed by the model to be hydrodynamically passive to fit with field measurement. Both Mendis (1987) and Crapper (1995) used the assumption of the rigid lid to represent the free surface by employing the CFD package PHOENICS and FLUENT respectively. Their models simulated pretty well the main characteristics of flow in channels.

4.2.2 Theoretical basis of FLUENT

The FLUENT package is a general computer programme for modelling fluid flow, heat transfer, chemical reaction as well as the basic laminar and turbulent flow of water. In this section, only the basic equations and solution features are outlined and the specific options

used in this investigation are discussed. For a full discussion of the package's capabilities refer to the FLUENT user's guide (FLUENT Incorporated 1993).

4.2.2.1 Basic equations

FLUENT models the wide range of phenomena by solving the conservation equations for mass, momentum and energy using a control volume based finite difference method. Navier-Stokes equations are the basic equations of motion used in FLUENT.
The continuity equation is:

$$\frac{\partial \rho}{\partial t} + \frac{\partial (\rho u_i)}{\partial x_i} = 0 \qquad (4.1)$$

whilst conservation of momentum in the ith direction is described by

$$\frac{\partial}{\partial t}(\rho u_i) + \frac{\partial}{\partial x_j}(\rho u_i u_j) = \frac{\partial \tau_{ij}}{\partial x_j} - \frac{\partial p}{\partial x_i} + \rho g_i + F_i \qquad (4.2)$$

In the above equations, ρ is the fluid density, x_i, x_j and u_i, u_j the distances and velocities in the ith and jth directions, p the fluid pressure and g_i and F_i the acceleration due to gravity and external body forces in the ith direction. τ_{ij} is the shear stress tensor.

The source/sink terms are not included in either of Equations 4.1 and 4.2 because of the conservation of both mass and momentum of the water flow in the investigated channels. In addition, the FLUENT software does not consider any sourcing or sinking of mass and momentum due to exchange with another phase, for example due to combustion or chemical reactions. However, these features were not relevant to the author's application of the software.

There are two basic turbulence closure models, k-ε model and Reynolds stress equation model (RSM), available in FLUENT. The k-ε model is a semi-empirical model that has been demonstrated to provide engineering accuracy in a wide variety of turbulent flows including flows with planar shear layers such as jet-flows and duct flows. However, the k-ε model includes an isotropic description of the turbulence, and is thus not well suited to prediction of highly non-isotropic turbulence such as that which arises in swirling flows.

Several major drawbacks of the k-ε model emerge when it is attempted to predict flows with complex strain fields or significant forces. Under such conditions the individual Reynolds stresses are poorly represented by k-ε model even if the turbulent kinetic energy is computed to reasonable accuracy. It is potentially the most general of all classical turbulence models, with only initial and/or boundary conditions required. It is very accurate for the calculation of mean flow properties and all Reynolds stresses for many simple and more complex flows including wall jets, asymmetric channel and non-circular duct flows and curved flows.

The RSM is a second-order closure model which creates a high degree of tight coupling between the momentum equations and the turbulent stresses in the flow, and thus can be more prone to stability and convergence difficulties than the standard k-ε model. Nevertheless, its output can be directly compared with velocity fluctuations from experiment. Therefore, the Reynolds Stress Model was chosen for the study described in this thesis.

The Reynolds Stress modelling strategy originates from Launder's work (1975) evaluating turbulent shear stresses using a time averaged method, with closure of the equations being achieved by relating time averaged turbulent shear stresses to mean flow properties. The time averaged shear stress can be expressed as

$$\overline{u_i' u_j'} = -\tau_{ij} / \rho \qquad (4.3)$$

The simultaneous velocity at a point can be expressed as the sum of the mean velocity and fluctuating components.

$$u_i = \overline{u_i} + u' \qquad (4.4)$$

-where the u' represents the turbulent fluctuation of a mean flow property and the $\overline{u_i}$ a temporal average over a time scale sufficiently long to encompass many turbulent fluctuations of the quantity they enclose. Equation 4.4 can be substituted into the momentum equation 4.2 without affecting any of the other terms but to replace all the u_i parameters by their temporal means $\overline{u_i}$. The correlation $\overline{u_i' u_j'}$ in Equation 4.3 has six unique terms which in the Reynolds stress model are evaluated in terms of mean flow properties by solving Equation 4.5.

$$\frac{\partial}{\partial t}\left(\overline{u'_i\,u'_j}\right)+\overline{u_k}\frac{\partial}{\partial x_k}\left(u'_i\,u'_j\right)=\frac{\partial}{\partial x_k}\left(\frac{\mu_t}{\sigma_k}\frac{\partial\overline{u'_i\,u'_j}}{\partial x_k}\right)+P_{ij}+\Phi_{ij}-\varepsilon_{ij}+R_{ij} \quad (4.5)$$

-where σ_k is an empirical Prandtl number governing the diffusion of turbulent kinetic energy, P_{ij} is the stress production rate, Φ_{ij} is a source/sink due to the pressure/strain correlation, ε_{ij} is the viscous dissipation and R_{ij} is the rotation term.

The turbulent eddy viscosity μ_t is computed from

$$\mu_t=\rho C_\mu\frac{k^2}{\varepsilon} \quad (4.6)$$

-where C_μ is a constant and k is the turbulent kinetic energy derived from Equation 4.7

$$k=\frac{1}{2}(u'_i\,u'_i+u'_j\,u'_j+u'_k\,u'_k) \quad (4.7)$$

-where u'_i, u'_j, and u'_k are the three dimensional velocity fluctuations. The parameter ε in equation 4.6 represents isotropic viscous dissipation, and is determined by means of a number of empirically based assumptions. In Equation 4.5, the production term P_{ij} is computed directly, without the use of any assumptions:

$$P_{ij}=-\left(\overline{u'_iu'_k}\frac{\partial u_j}{\partial x_k}+\overline{u'_ju'_k}\frac{\partial u_i}{\partial x_k}\right) \quad (4.8)$$

However, Φ_{ij}, ε_{ij} and R_{ij} are variously derived according to the modelling assumptions inherent in the Reynolds stress model.

4.2.2.2 Control volume based finite difference method used by FLUENT

After selecting the mathematical model, the control volume based finite difference method (Patankar, 1980) was used in FLUENT to approximate the differential equations by a system of algebraic equations for the variables, such as velocity, pressure and turbulent properties for each discrete control volume. The control volume was used for integration of the mass and momentum conservation equations and the values of all the variables such as velocity, pressure and turbulent properties are stored at the control volume cell centre. The control volume is illustrated schematically in Figure 4.1.

The Power Law Scheme is provided by default in FLUENT to interpolate the properties at cell faces. It was used in the current study. Properties of the power law differencing scheme are similar to those of the hybrid scheme and it provided sufficiently accurate and adequately rapid solutions for the channels. Various high order differencing schemes such as QUICK were also provided in FLUENT, however, none was used in this study to avoid utilising the necessary additional computing resources.

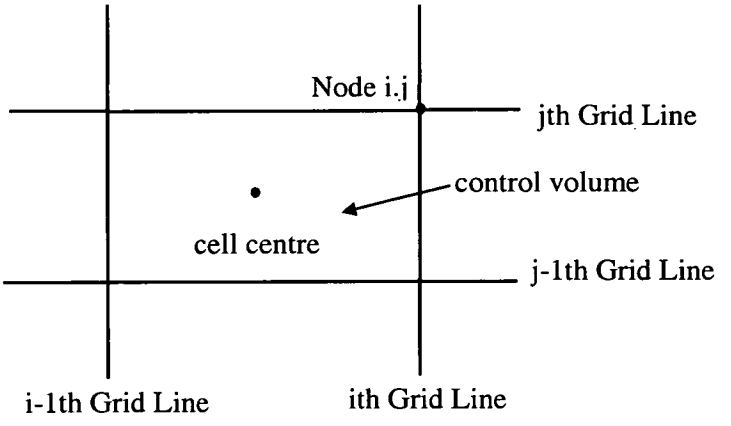

Figure 4.1 Control volume storage scheme

The face value of a variable ϕ is interpolated by the Power Law Scheme using an exact solution to an one-dimensional convection-diffusion equation:

$$\frac{\partial}{\partial x}(\rho u \phi) = \frac{\partial}{\partial x}\Gamma\frac{\partial \phi}{\partial x} \tag{4.9}$$

in which the density ρ, velocity u and the diffusivity parameter Γ are assumed to be constant over the interval ∂x. With the boundary conditions: $\phi_0 = \phi|_{x=0}$, $\phi_L = \phi|_{x=L}$, this equation can be integrated to give the solution:

$$\frac{\phi(x) - \phi_0}{\phi_L - \phi_0} = \frac{e^{\left(P_e \frac{x}{L}\right)} - 1}{e^{(P_e)} - 1} \tag{4.10}$$

where $P_e = \frac{\rho u L}{\Gamma}$ is the Peclet number. The Peclet number governs the relative importance of convection and diffusion.

In the case of small velocity (u≈0) or large diffusivity Γ, the Peclet number tends to zero and convection can be neglected; the solution is then linear in x. When the Peclet number is large, ϕ grows slowly with x and then suddenly rises to ϕ_L over a short distance close to x=L (See Figure 4.2). The sudden change in the gradient of ϕ provides a severe test of the discretization method.

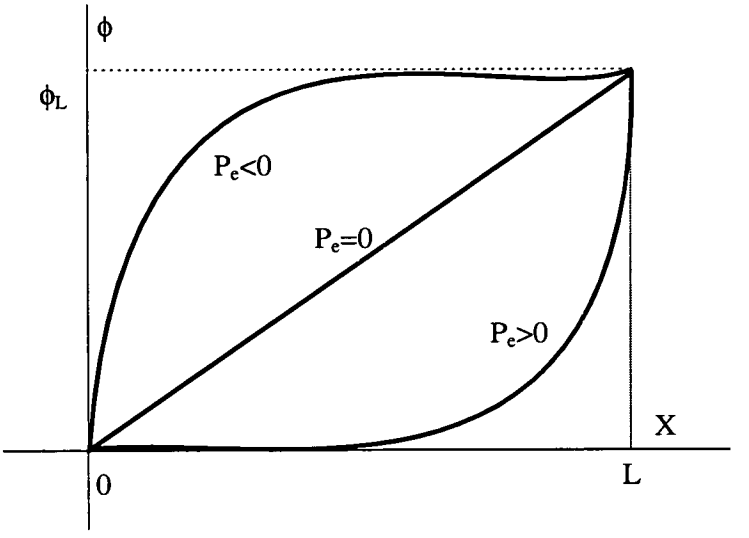

Figure 4.2 Variation of variable ϕ with Peclet number

4.2.2.3 Solution for pressure-velocity coupling

FLUENT uses the SIMPLE family of algorithms to iterate the solution to the momentum, mass and continuity equations. The basic approach is to use the relationship between velocity and pressure corrections in order to recast the continuity equation in terms of pressure correction calculation. It is carried out interactively and progressed line by line across the finite difference grid to achieve an acceptable residual for all points in the model domain. Compared with the simultaneous solution of the equation across the full flow field, the line by line method is much more efficient in terms of the use of computer resources.

The basic iterative solution procedure is illustrated below by consideration of an one dimensional momentum equation. The discretised one dimensional momentum equation developed can be written as follows:

$$C_p u_p = \sum_{NB} C_{NB} u_{NB} + (p_W - p_E)A + S \qquad (4.11)$$

Here C_p is the finite difference coefficient for the convection and C_{NB} for diffusion. u_p and u_{NB} are the local velocity and neighbour velocity values, and p_E and p_w are the "east" and "west" face pressures acting across the momentum control volume, A is the area of the control volume, S is the local strain rate in the fluid.

The guessed velocity field, u* is initially calculated by the substitution of a guessed pressure field, p*, into Equation 4.11. The actual velocity and pressure fields are now related to the guessed fields according to Equations 4.12.1 and 4.12.2.

$$p = p^* + p' \tag{4.12.1}$$

$$u = u^* + u' \tag{4.12.2}$$

-where p', u' are pressure correction and velocity correction. A momentum balance equation in terms of the velocity and pressure corrections u' and p' can be found by substitution of Equations 4.12.1 and 4.12.2 into 4.11 as follows:

$$u' = \frac{1}{A_p}(p'_W - p'_E)A \tag{4.13}$$

Using the similar process of generating u' based on the continuity equation, the pressure correction p' can be calculated from the continuity equation in terms of pressure correction. The mass balance:

$$-(\rho A)_w \left(\frac{1}{A_p}\right)_w (p'_W - p'_P) = 0 \tag{4.14}$$

Equation 4.14 can now be solved to give the correction for the pressure field, which is then used in Equation 4.13 to determine the velocity correction. In this way the whole flow field can ultimately be solved.

4.3 Model domain and grid setup

Three test units were to be modelled in this section. The first was a 150mm wide channel with a single 180^0 bend channel as mentioned in Chapter 3. The comparison between LDA and FLUENT results for this case is given in section 4.6 of this Chapter to verify the validity

of FLUENT's simulation in the channel flow. The second was a horizontal flow flocculator of up to 85 channels in series each 45mm wide, 1215mm long, with 200 mm water depth at the head of the first channel and 8 mm dividing walls giving an effective total flow length of about 103m. The flocculator was adjustable in longitudinal slope. The actual number of the channels used was dependent on the various flowrates and retention times. The third was a flocculator with adjustable slope but with 22 channels in series each 150mm wide, 1215mm long with 200 mm water depth at the head of the first channel and 8 mm dividing walls with an effective total flow length of about 26.7m. To simplify description, the first case is called "150mm wide channel", the second "45mm wide channel" and the third "150mm wide tilted channel" in this thesis.

4.3.1 Grid generation and model domain

For the "150mm wide channel", curvilinear body-fitted coordinates were used to conform to the physical geometry of the channels. To minimise the number of cells while maintaining a sufficient degree of accuracy in the solution, a non-uniform distributed grid was set. In the non-uniform grids, the grid spacing was reduced in regions near the channel bend where high gradients were expected and increased elsewhere where the flow was relatively uniform. To modify Argaman's equation (mentioned in Chapter 2) and apply it to the calculation of turbulence in relation to flocculation, it was essential to figure out the turbulence quantified by kinetic energy and longitudinal velocity at each point throughout the channel. Each leg of the 150mm wide single bend channel was geometrically symmetrical but not hydrodynamically similar, therefore simulation must be made in three dimensions for both legs. This has obvious implications in terms of the number of computational nodes to be included in the simulation and the corresponding demand on computer time. Therefore, in order to keep such demands to a minimum without losing so much information as to render the simulation valueless, it was tested to establish a suitable number of grids.

For the "45mm wide channel" and the"150mm wide tilted channel", Cartesian coordinates and a uniform distributed grid were used to make use of the main frame of FLUENT and simplify the procedure of grid generation. Because the rectangular shape of channel approximated to the Cartesian coordinates, there would not be significant difference caused due to the different coordinate system set from the curvilinear body-fitted coordinates.

The model domain plan size and shape were fixed according to the actual dimensions of the three cases of channels. The vertical dimension for each grid represented the water depth and the vertical dimension of the first section of the grid was set at 200mm for all three test units. The number of channels to be used is dependent on the flow rate and retention time, so that the last channel's water depth varies and was directly measured from experiment (see details in Chapter 5).

The FLUENT CFD model's logical coordinates were set to match the physical coordinates in order to give an obvious view of the variation of hydrodynamic parameters with the geometry of the channel. The model's longitudinal, x-axis was taken to represent a line passing along the straight working section, the lateral or y-axis was taken as being from the first channel to the last, whilst the vertical direction was from the flume base upwards. The model domain and corresponding coordinates for the "150mm wide channel" and the "45mm wide channel" and the "150mm wide tilted channel" are shown in plan in Figures 4.3, 4.4.1 and 4.4.3. A picture of the "45mm wide channel" flocculator is given in Figure 4.4.2.

4.3.2 Grid size

Setting of grid size is an important task in the numerical simulation by finite difference, since too large size of grid results in grid dependent solution, while too small size costs great computational resources.

In this study, a number of trial runs of FLUENT was carried out in order to derive a grid-independent solution of sufficient detail for the simulation of flows in both "150mm wide (as well as 150mm wide tilted) channel" and "45 mm wide channel". Evenly spaced grids of both nominal 100mm and 50mm cell size were initially tested for the "150mm wide channel". Considerable variation was found in the model results obtained for these two sizes of grid. It was noted that gradients of flow parameters in the lateral (Y) and vertical (Z) direction were much greater than that in the longitudinal (X) direction, except near the bend region.

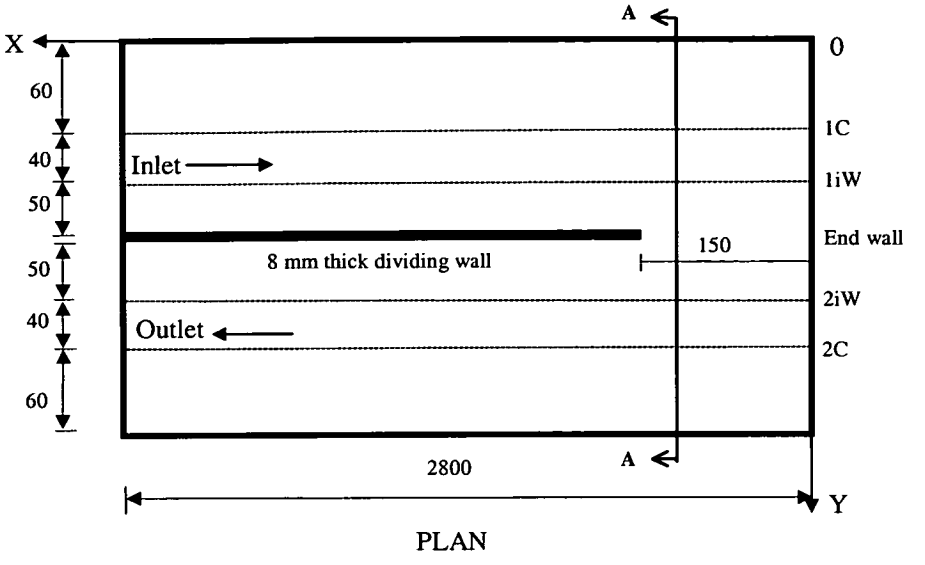

PLAN

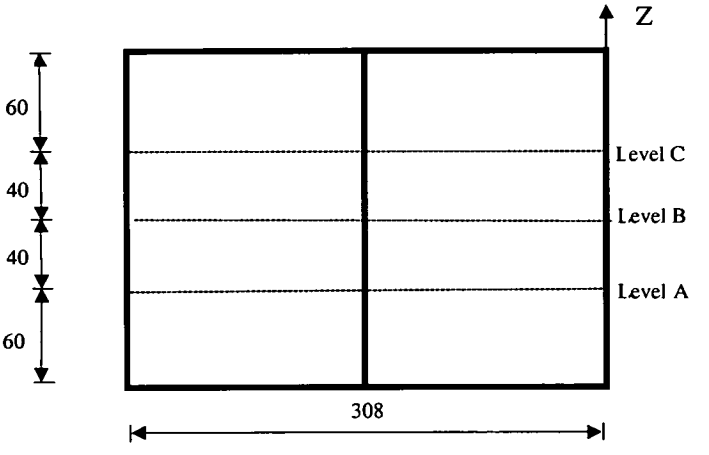

SECTIONAL ELEVATION AA

Figure 4.3 Model domain and coordinates for 150mm wide channel: Dimensions shown in mm, Not to scale

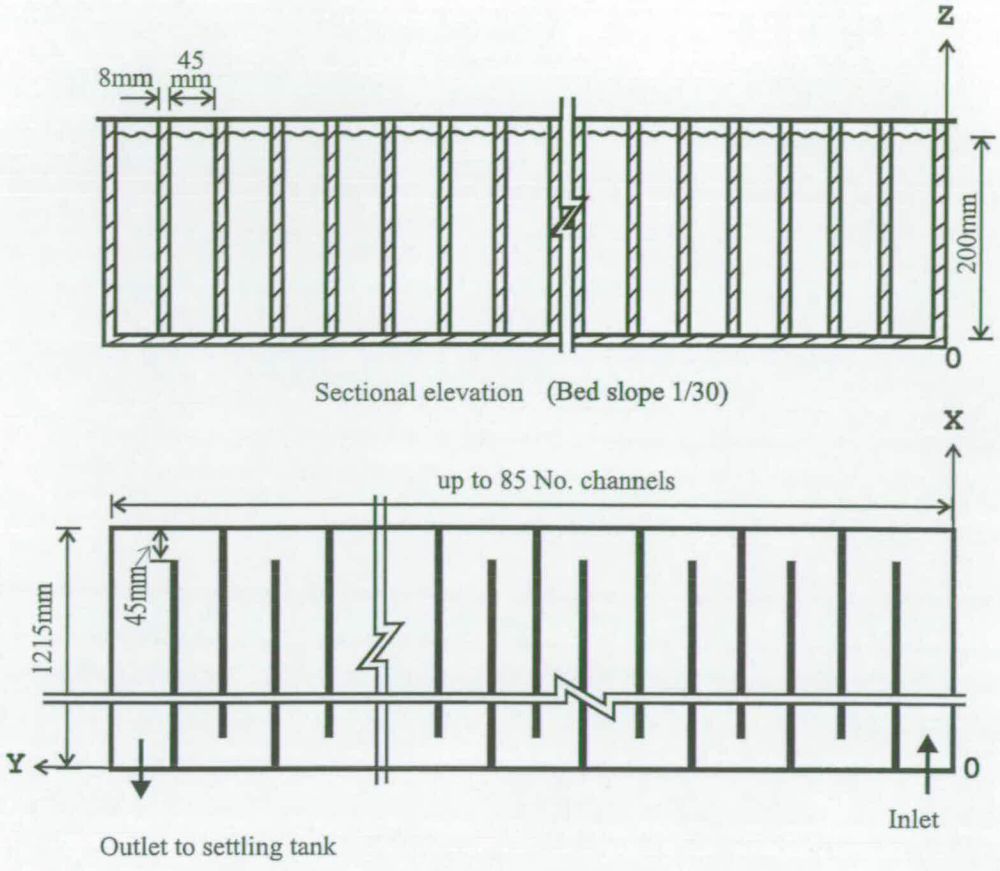

Figure 4.4.1 Model domain and coordinate system for 45mm wide channel: not to scale

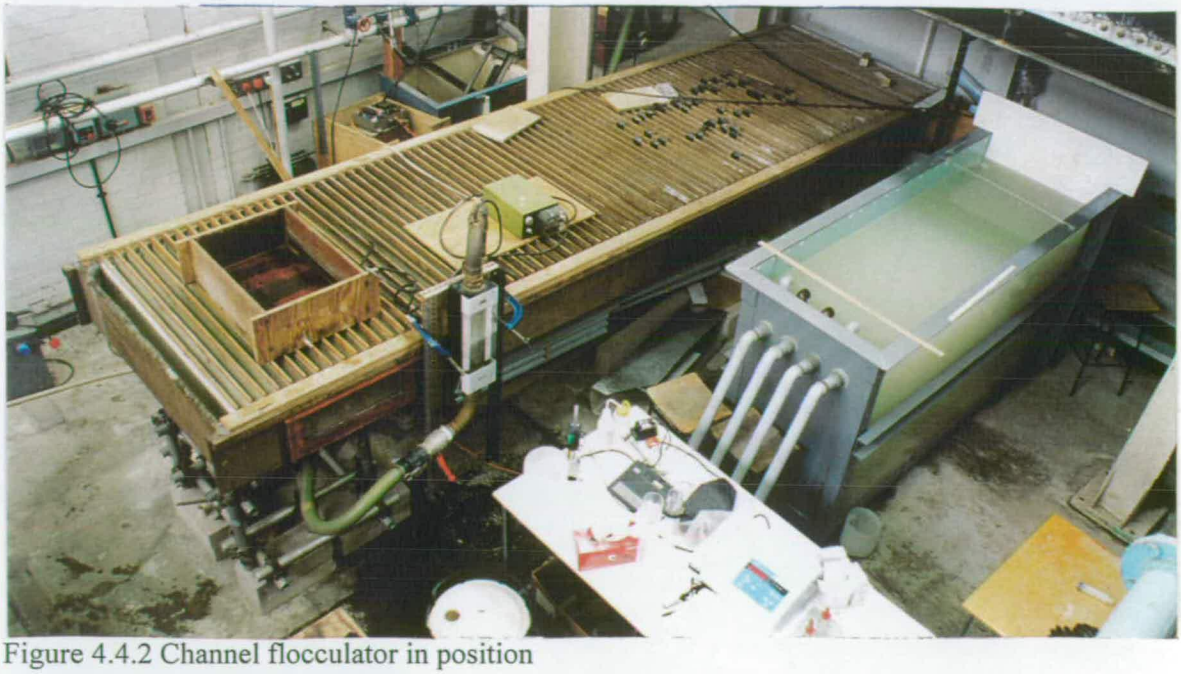

Figure 4.4.2 Channel flocculator in position

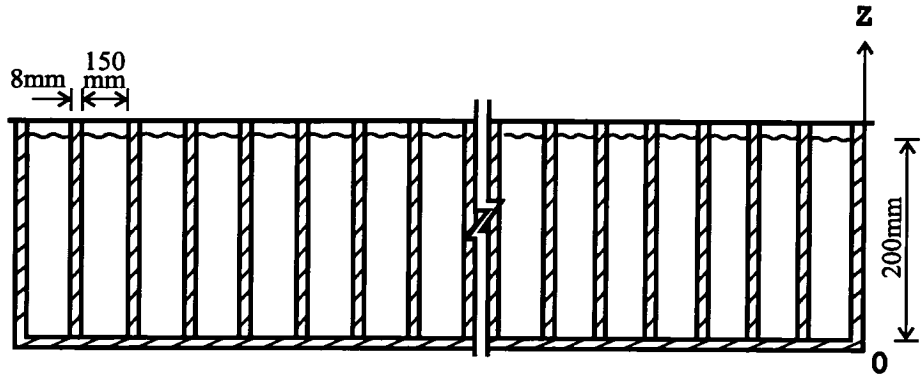

Sectional elevation (Bed slope 1/80)

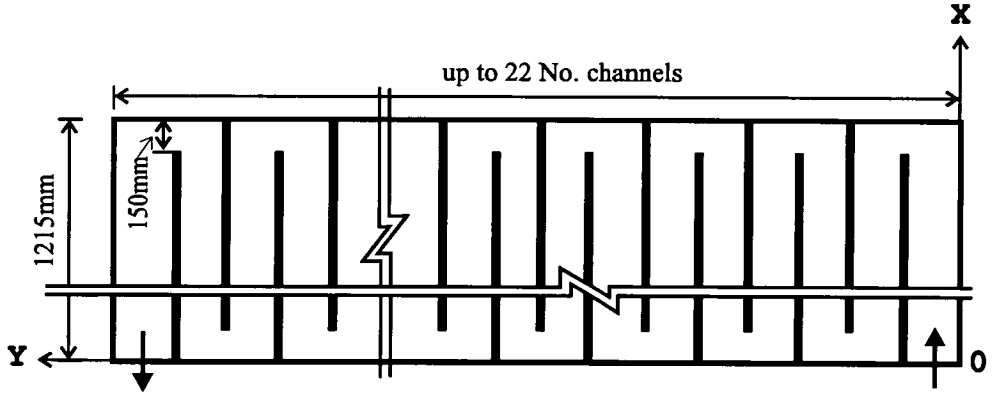

Plan view

Figure 4.4.3 Model domain and coordinate system for 150mm wide tilted channel (not to scale)

In respect of the relative importance of the x cells near the bend and the y and z grid sizes and considering the fit of the locations of model output with the arrangement of the measuring points mentioned in Chapter 3, it was determined to decrease y cell size in the channel to 25mm and z cell size to 40mm whilst the x cell size varied from approximately 10mm near the end wall to approximately 100 mm at their furthest points from the wall. This resulted in a maximum cell aspect ratio of 10:1 by utilising the Body Fitted Coordinate for establishing an uneven grid, so as to concentrate grid lines near the turning bend where gradients in flow parameters were at a maximum.

The new grids were found to perform satisfactorily, converging to a solution in 533 iterations. In order, therefore, to determine whether the solution achieved was grid-dependent, the y and z cell sizes were reduced by halves and the test simulation was rerun. This time convergence was achieved in 1582 iterations. The simulation results from the two grids were found to be identical, and it was therefore concluded that the uneven grid with the larger cell sizes was sufficient to achieve a grid-dependent solution for the flow in the "150mm wide channel". Applying the same approach to the "45 mm wide channel", however, the main frame of FLUENT was utilised for primarily establishing an uniformly distributed grid to simplify the very time consuming procedures of grid generation for up to 85 channels. Since the channel bed was adjustable for creating various bed slops and the water surface was varied from channel to channel, so the z cell and its size were varied accordingly whilst x and y cell size were densified near the bend and the wall. The size of x grid was set from 22.5mm near the bend and 45mm at the furthest points from the bend. The size of y grid was set from 9mm near the wall and 18mm at the furthest points from the wall. The model domain of the "45mm wide channel" was vertically divided into 13 levels, the detailed settings for nominal velocities of 0.1 and 0.05m/s are given in Figures 4.5.1 and 4.5.2. It should be noted that the grid size used in the "150mm wide tilted channel" was exactly the same as that used for the "150mm wide channel". The x and y grid size settings for the "45mm wide channel" are the same for all the nominal velocities, 0.035 to 0.1m/s, used in the flocculation test in Chapter 5, however the setting of water surface by z grid was varied according to the measured head loss caused by different flow velocities. Because of the little difference in water level of the flows corresponding to the nominal velocities of 0.05 and 0.075 m/s in a set of ten "45mm wide channels", the grid setting for the velocity of 0.05m/s was also used for the velocity of 0.075m/s.

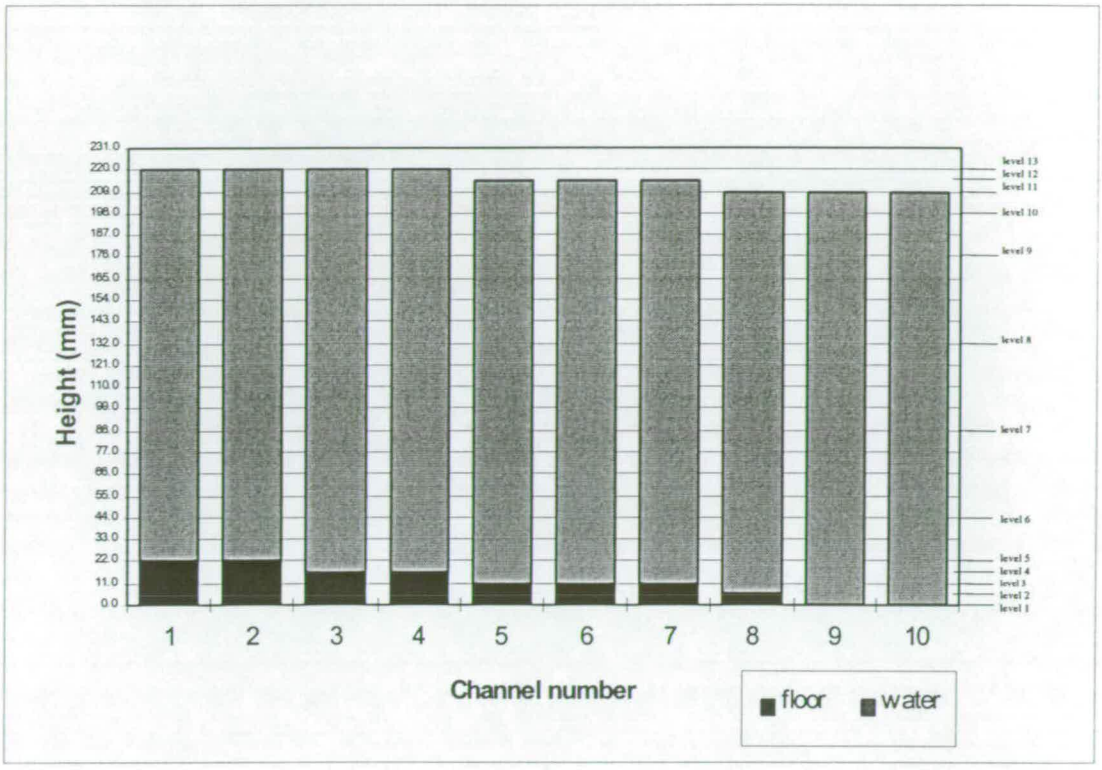

Figure 4.5.1 Model levels and height of floor and water for nominal velocity of 0.1m/s

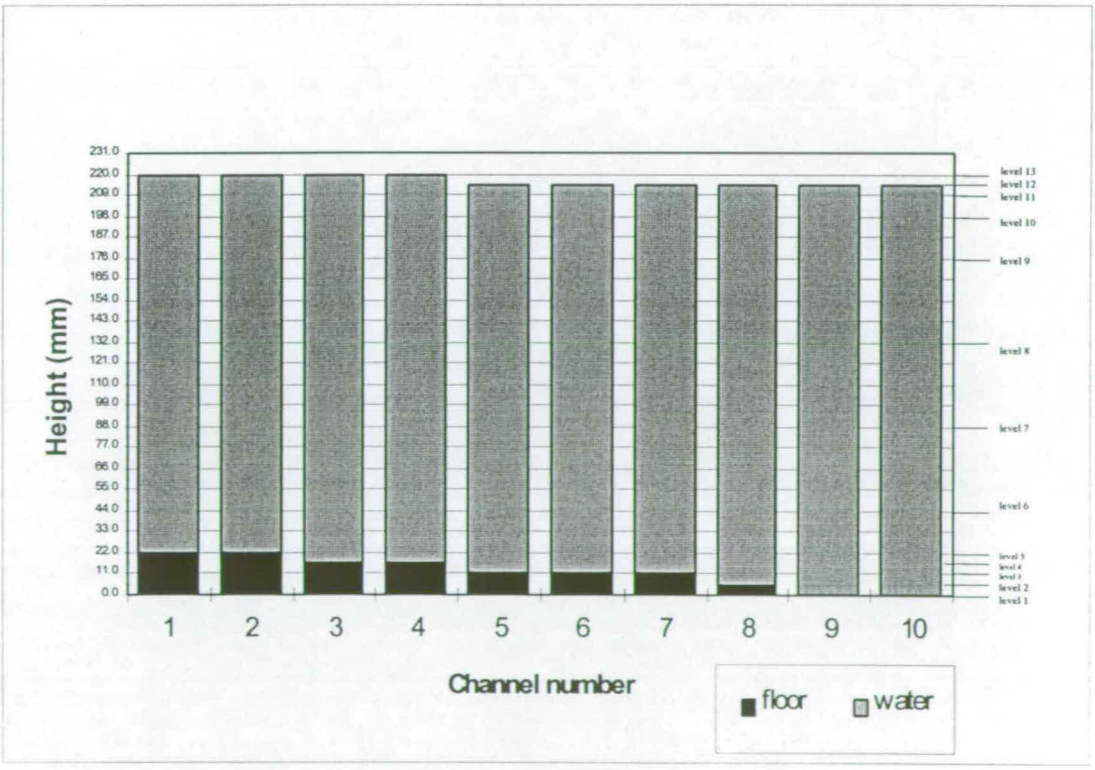

Figure 4.5.2 Model levels and height of floor and water for nominal velocity of 0.05m/s

4.4 Boundary conditions

Correct and complete definition of the boundary conditions is essential to produce an acceptable solution. However, the required values of parameters are sometimes practically unreliable or even unknown. In this section, the approximation of the inlet boundary is discussed. The effect of the lateral and vertical velocities and turbulence characteristics at the inlet as well as the length of channel on the magnitude and distribution of velocities and turbulence in the channels are considered. By means of the method of custom wall, it became possible to simulate the free surface using the closure CFD package FLUENT.

4.4.1 Setup for boundary conditions

It is appropriate where the exit flow is close to a fully developed condition, that the outlet boundary condition assumes a zero normal gradient condition for all variables. For this reason, the outlet boundary should be as far downstream of the region of interest as possible to avoid the occurrence of error propagating upstream. Here, 10m, 5m and 2.8m were chosen as the channel lengths for the "150mm wide channel" and the "150mm wide tilted channel" and 10m, 5m and 1.215m for the "45mm wide channel" to establish the shortest length for each case which gives the length-independent solution and which provides sufficient detail for the simulation of flows, at the same time preventing the need for complex and resource-demanding customisations of the FLUENT software. The 2.8m is the effective length of the "150mm wide channel" and 1.215m is the real length of the "45mm wide channel" and the "150mm wide tilted channel" (See Figures 4.3, 4.4.1 and 4.4.3). The 5m and 10m were chosen as trials to extend the channel length.

The comparisons (kinetic energy is taken as an example in Figures 4.6.1 to 4.7.3) exhibited that there was little difference caused by the three chosen channel lengths for a nominal velocity of 0.1m/s. Therefore the 2.8m and 1.215m were adopted as the standard lengths for the applications of the FLUENT software for the cases in the current study. In the figures here and afterwards, tot-i represents the volume weighted average of kinetic energy in the first leg of 150mm wide channels whilst tot-o represents the average in the second leg.

At the inlet boundary, all quantities have to be prescribed. The longitudinal u-velocities were directly specified based on experimental data and input in the form of a vertical (i.e. z-direction) profile of velocities at each y-grid location. The input velocities were obtained

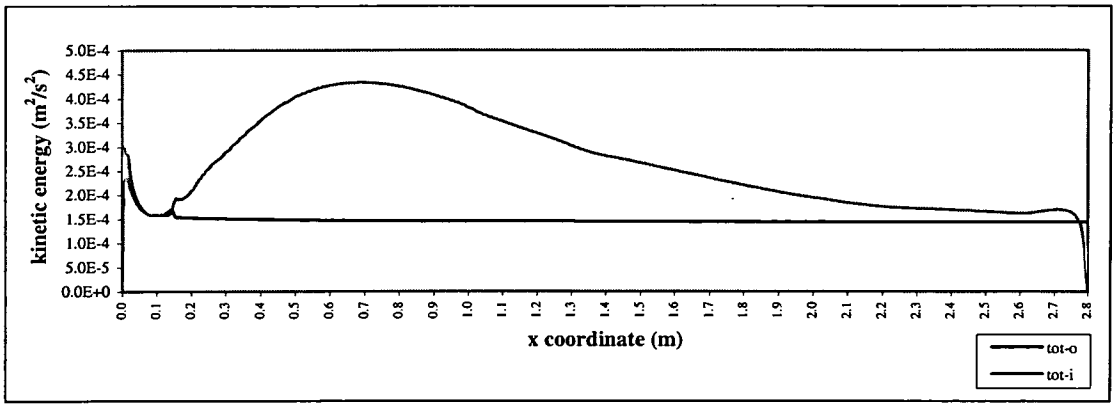

Figure 4.6.1 Kinetic energy vs x coordinate in 2.8m long 150 mm wide channel

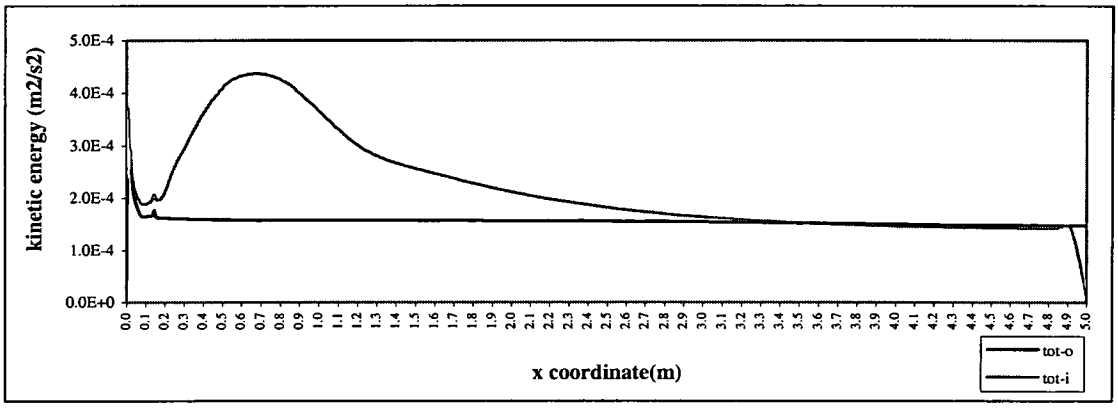

Figure 4.6.2 Kinetic energy vs x coordinate in 5m long 150 mm wide channel

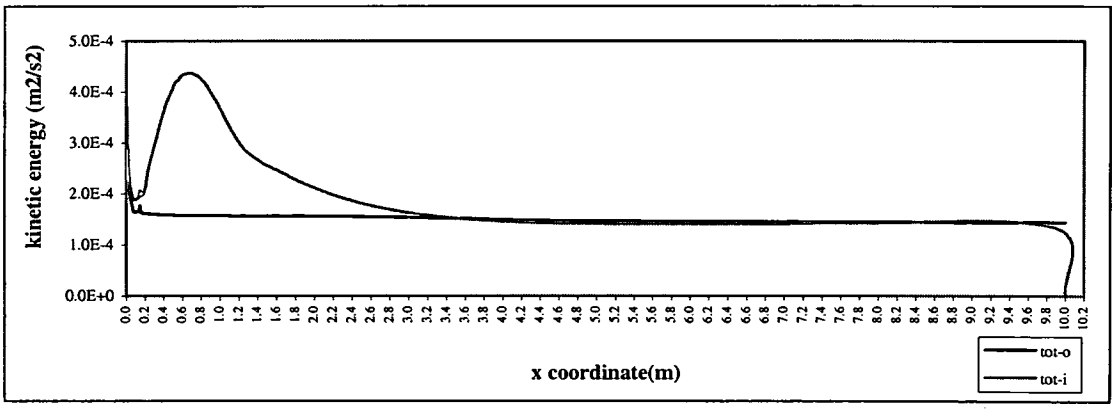

Figure 4.6.3 Kinetic energy vs x coordinate in 10m long 150 mm wide channel

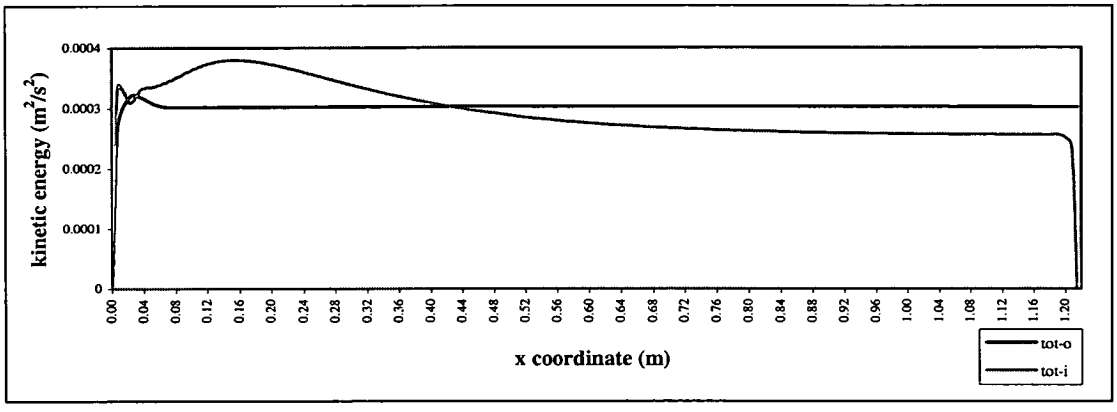

Figure 4.7.1 Kinetic energy vs x coordinate in 1.215m long 45 mm wide channel

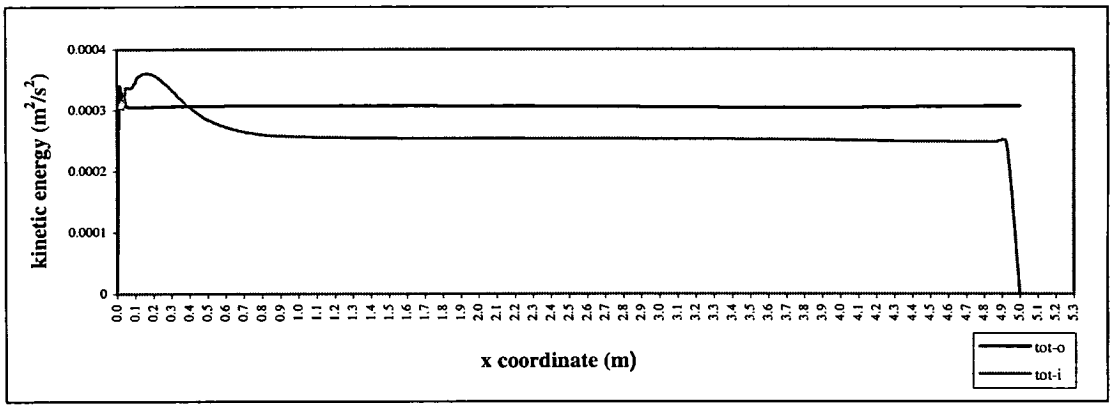

Figure 4.7.2 Kinetic energy vs x coordinate in 5m long 45 mm wide channel

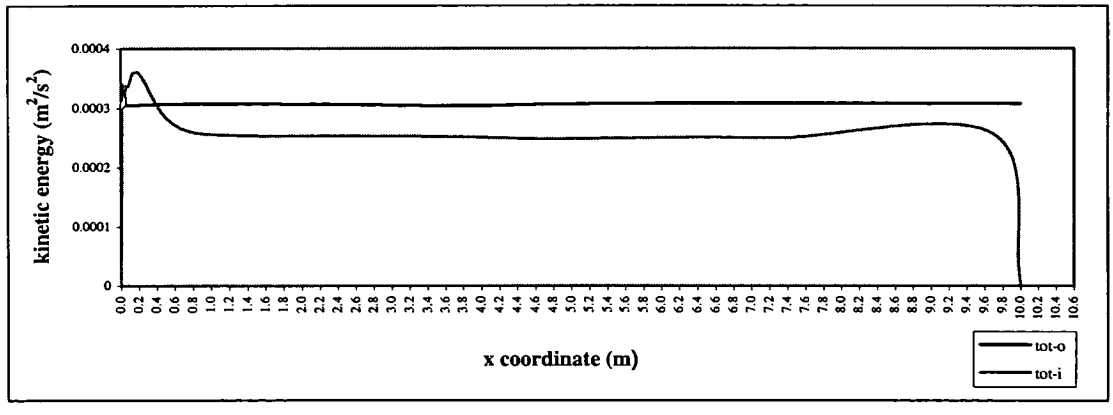

Figure 4.7.3 Kinetic energy vs x coordinate in 10m long 45 mm wide channel

from the STREAMFLO readings included in Table 3.2. The input profiles were determined by plotting the lateral FLUENT grid locations to scale, and then superimposing upon them plots of measured velocity. The required velocity profile at each y-grid location could then be determined by interpolation from the measured data. However no information with regard to lateral or vertical velocities at the input section to the modelled domain was available, since the value of these parameters was too low to be detected by the STREAMFLO meter. It was therefore assumed that lateral and vertical velocities at the input section of the model domain were zero. In addition to flow velocities, it was necessary to specify turbulence characteristics at the input section to the model domain which were impossible to measure by means of LDA at the inlet region where the wooden side wall did not allow the laser beam to pass through. The effect of lateral and vertical velocities and turbulence characteristics on the magnitude and distribution of velocities and turbulence in the channels are discussed in the following section. It was concluded that the assumption of zero input of lateral and vertical velocities and turbulence quantified by kinetic energy would make no significant difference to the quality of the FLUENT simulation of flows in the channel.

As for the setting of the outlet, it is beneficial to move the inlet boundary as far from the region of interest (the area near the bend) as possible if conditions at the inlet are not well known. Since the velocity and other variables are given, all the associated fluxes can be calculated. The diffusive fluxes are usually not known, but they can be approximated using known boundary values of the variables and one-side finite difference approximations for the gradients. As mentioned in the setup of outlet boundary, the 2.8m and 1.215m were chosen for both inlet and outlet channels for the 150mm wide, 150mm wide tilted and 45mm wide channels.

In many application areas the solution domain changes in time due to the movement of boundaries. In free surface flows the movement should be calculated as part of the solution. Flows with free surfaces are a difficult class of flows due to moving boundaries. The free surface can be expressed as a single valued function (Casulli, 1998):

$$z = f(x, y, t) \tag{4.15}$$

Where z represents the vertical depth of the free surface, x and y are the horizontal locations, t is the time. The position of the boundary is known only at the start, its position later having to be determined as part of the solution. The closure CFD package, FLUENT,

cannot simulate a free surface directly. This problem was solved by assuming the free water surface in the channel as a specific custom wall boundary condition at the top of the cells, while the velocity normal to the surface, w, was constrained to be zero; u, v velocities and the pressure were determined in the normal way from the solution of the model equations. Non-zero surface pressures resulting from this process were then taken as indicative of changes in surface level such as those due to superelevation of the flow passing round the channel bend. This is the so called rigid lid method, which was recommended by Leschziner and Rodi (1979).

At the impermeable wall boundaries, such as the base, sides and the dividing baffle of the channels, all three velocity components were set to zero. The wall shear stresses within the log-law region in the wall boundary were computed via the log-law function: (see FLUENT user's guide, 1993)

$$\frac{u_p}{u^*} = \frac{1}{\kappa}\ln\left(Ey^+\right) - \Delta B(K_s^+) \qquad (4.16)$$

-where u* is the friction velocity $\sqrt{\frac{\tau_w}{\rho}}$, u_p the near wall velocity, κ is Von Karmans' constant (0.42), E is the log-law constant set by default to 9.8 for a smooth wall, K_s^+ is the function of average wall roughness height and ΔB the amount by which the rough wall velocity profile shifts downward. For a smooth wall condition, such as the wooden channel in this investigation, the last term of Equation 4.16 can be ignored. The dimensionless distance factor from the wall, y^+ can be calculated by Equation 4.17 by the assumption of equilibrium between production and dissipation of kinetic energy in the boundary layer: (see FLUENT user's guide, 1993)

$$y^+ = \frac{\rho k_p^{\frac{1}{2}} C_\mu^{\frac{1}{4}} \Delta y}{\mu} \qquad (4.17)$$

-where k_p is the near wall turbulence kinetic energy, C_μ is an empirical constant (0.98), μ is the fluid viscosity, Δy is the distance to the wall.

The near wall value of the turbulence kinetic energy, k_p, is computed via the solution of the full transport equation (see FLUENT user's guide), with the generation term containing the

wall shear stress (equation 4.16) and a zero gradient assumed for k_p at the wall whilst the turbulent dissipation ε is calculated by FLUENT from the known k_p by using an empirically based formulation as follows:

$$\varepsilon = \frac{C_\mu^{\frac{3}{4}} \rho k_p^{\frac{1}{2}} y^+}{\rho u^*} \tag{4.18}$$

4.4.2 Effect of turbulence and velocities at inlet on the magnitude and distribution of velocities and turbulence in the channels

The effect of initial turbulence and velocity on the distribution of velocity and turbulence kinetic energy in the channel was studied. Various initial conditions were tested at the same u-velocity profile but at different initial turbulence levels, v-velocity and w-velocity for the 10m long 150mm wide single bend channel and the 1.215m long 45mm wide single bend channel. U-velocity was assumed to be uniformly profiled and v-velocity and w-velocity uniformly profiled equalling 1/10 of the corresponding u-velocity, since there was no evidence from the experimental study to suggest that the lateral and vertical velocities were likely to be greater than 10% of the longitudinal velocity in the inlet area. The input data are tabulated in Table 4.1.

Table 4.1 Input for the test of effect of initial velocity and turbulence

channel	test no.	u (m/s)	v (m/s)	w (m/s)	u'u' (m^2/s^2)	v'v' (m^2/s^2)	w'w' (m^2/s^2)	kinetic energy (m^2/s^2)
10m long	1	0.2	0	0	0	0	0	0
150mm	2	0.2	0.02	0.02	1.2E-4	1.2E-4	1.2E-4	1.8E-4
wide	3	0.2	0	0	2.5E-3	0	0	1.25E-3
1.215m long	4	0.1	0	0	0	0	0	0
45mm wide	5	0.1	0.01	0.01	3.5E-3	0	0	1.75E-3

It is shown in Figures 4.8.1 to 4.9.2 that the turbulence quantified by the kinetic energy in the channel was essentially the same in value and position for the tests of 1, 2, 3 and 4, 5. The initial turbulence does have various impacts on the region near the inlet depending on the difference in kinetic energy between the initial input and the main stream, however, its influence was limited to the first 10 cm along the channel. Therefore, the input of initial

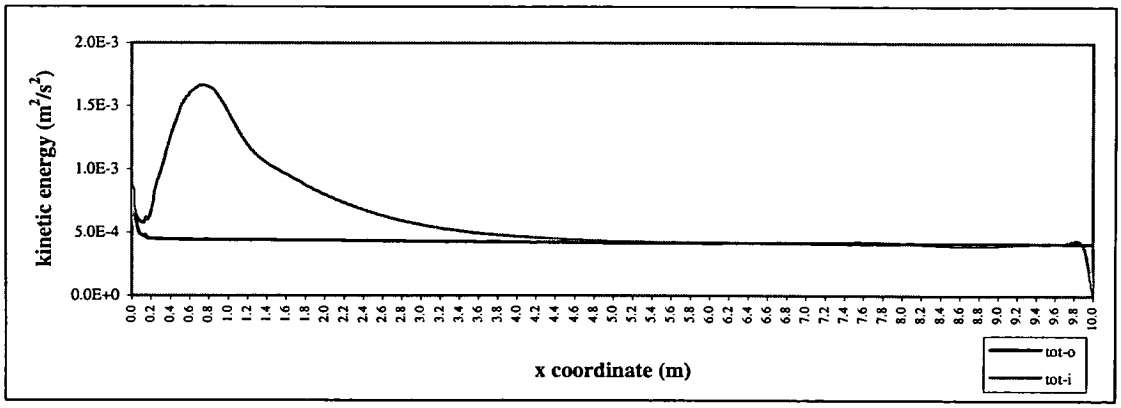

Figure 4.8.1 Kinetic energy vs x coordinate when initial turbulence kinetic energy equals zero (test 1)

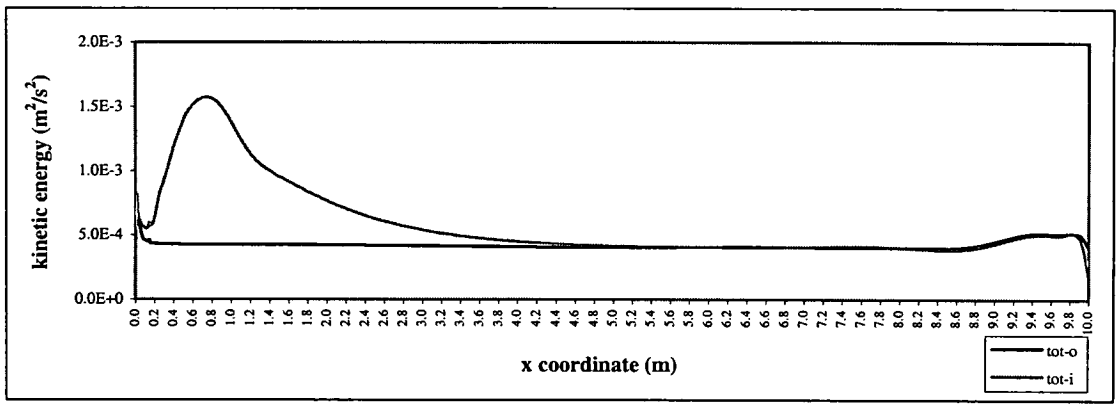

Figure 4.8.2 Kinetic energy vs x coordinate when initial turbulence kinetic energy equals 1.80E-4 m^2/s^2 (test 2)

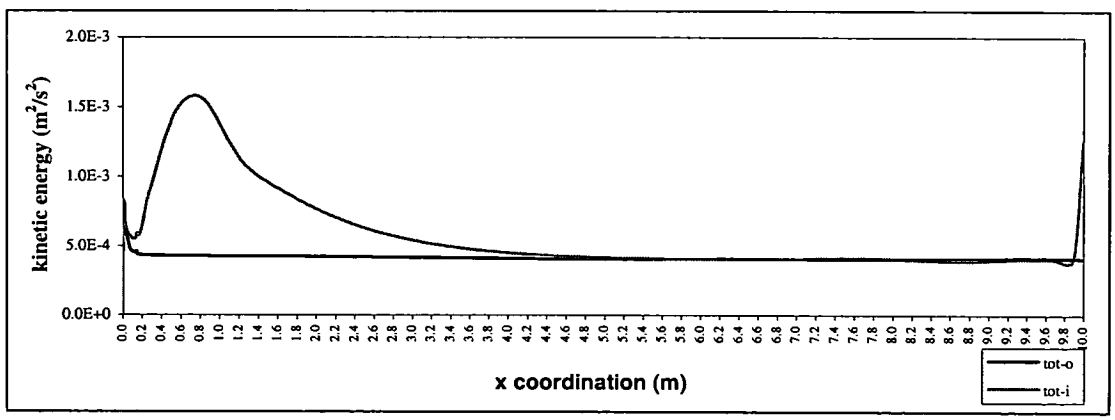

Figure 4.8.3 Kinetic energy vs x coordinate when initial turbulence kinetic energy equals 1.25E-3 m^2/s^2 (test 3)

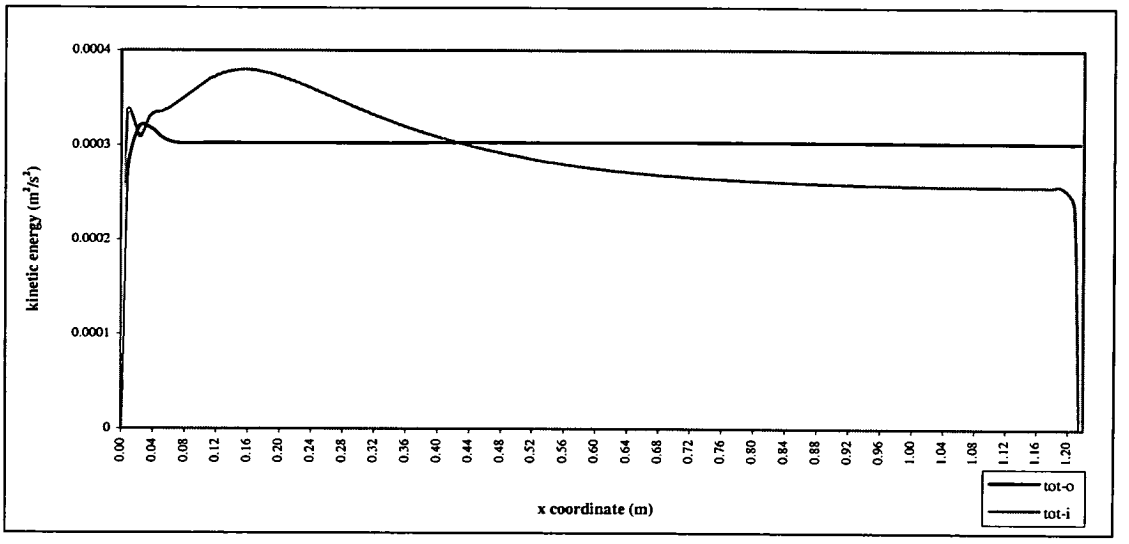

Figure 4.9.1 Kinetic energy vs x coordinate when initial turbulence kinetic energy equals zero (test 4)

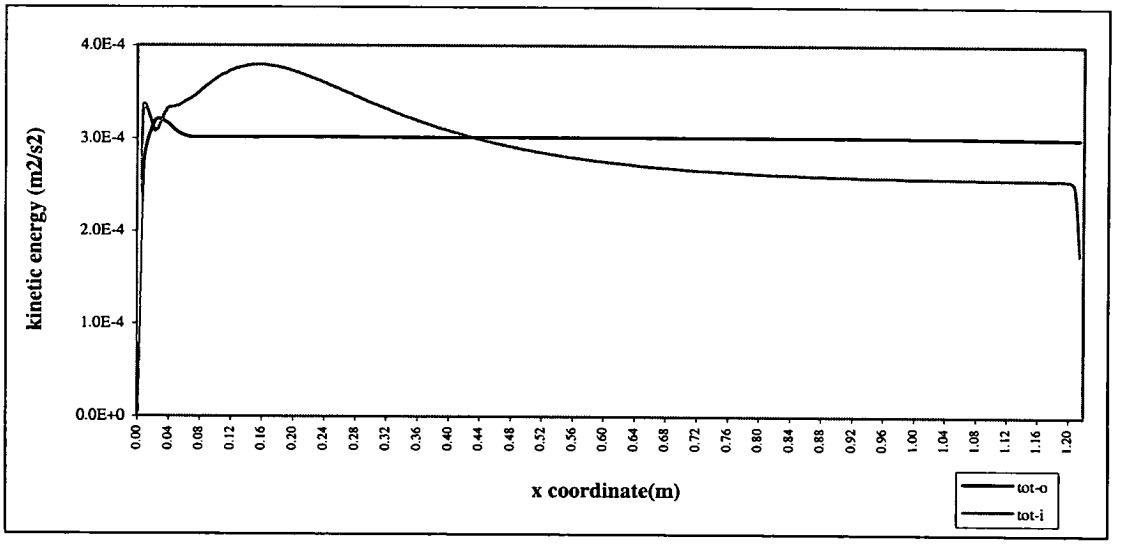

Figure 4.9.2 Kinetic energy vs x coordinate when initial turbulence kinetic energy equals 1.75E-3 m^2/s^2 (test 5)

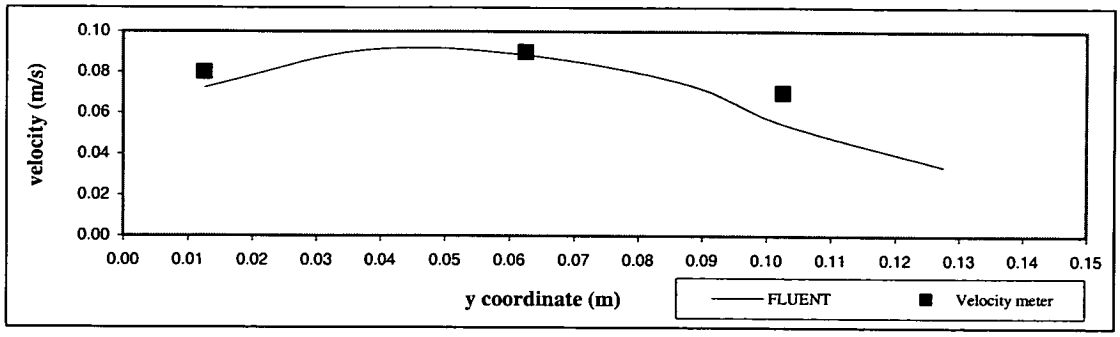

Figure 4.10.1 U-velocity: comparison between velocity meter readings and FLUENT results (x=1.0m, z=20mm, nominal velocity of 0.1m/s)

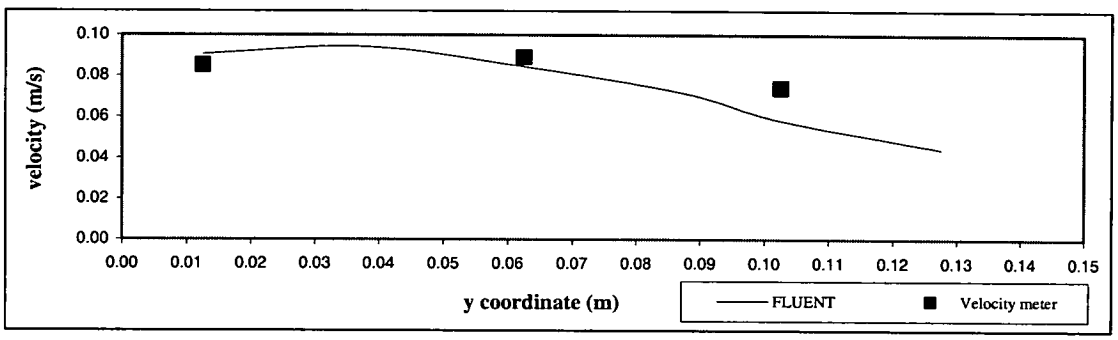

Figure 4.10.2 U-velocity: comparison between velocity meter readings and FLUENT results (x=1.0m, z=60mm, nominal velocity of 0.1m/s)

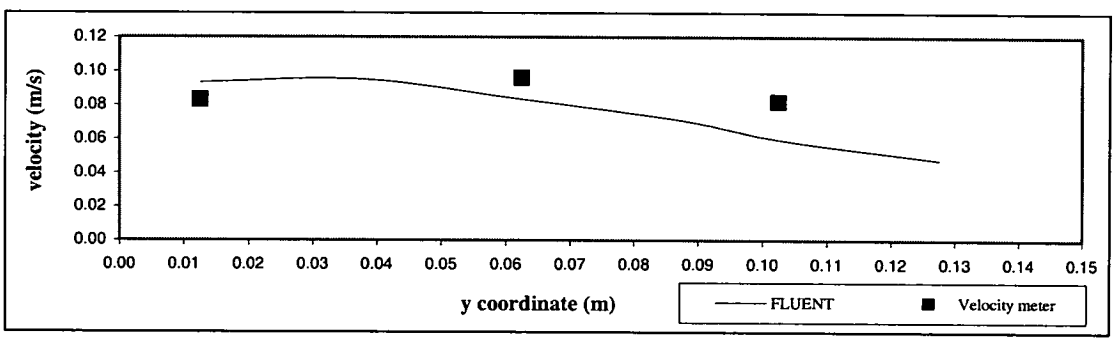

Figure 4.10.3 U-velocity: comparison between velocity meter readings and FLUENT results (x=1.0m, z=100mm, nominal velocity of 0.1m/s)

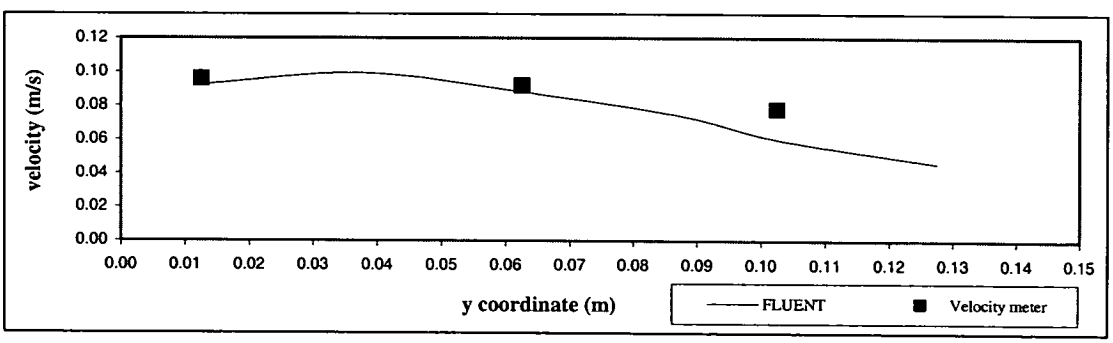

Figure 4.10.4 U-velocity: comparison between velocity meter readings and FLUENT results (x=1.0m, z=140mm, nominal velocity of 0.1m/s)

hydrodynamic conditions (such as kinetic energy, energy dissipation, Reynolds shear stress and three dimensional velocities) to FLUENT could be simplified to an input of u-velocity alone without subsequently causing any significant error. Comparison of measured velocity by STREAMFLO meter and measured turbulence and velocity by LDA with the simulation by FLUENT as shown in Figures 4.10.1 to 4.10.4 and Figures 4.11.1 to 4.29.4 indicate that the above simplification is acceptable.

4.5 Speeding up techniques

Solution convergence can be hindered by a number of factors. Large numbers of computational cells and complex physics are often a cause. Judicious setup of under-relaxation factors and an appropriate selection of the solution method are the basic two approaches to enhance convergence and are discussed in the following sections 4.5.1 and 4.5.2.

4.5.1 The setup of under-relaxation

Because of the non-linearity of the equation set being solved by FLUENT, it is not generally possible to obtain a solution by fully substituting the improved values for each variable which have been generated by the approximate solution of the finite difference equation. Convergence can be achieved, however, by underrelaxation which reduces the change in each variable produced during each iteration. In a simple form, the new value of the variable ϕP at node P depends upon the old value ϕP_{old} , the computed change in ϕP, ΔP, and the underrelaxation factor α, as follows:

$$\phi P = \phi P_{old} + \alpha \Delta P \quad , \tag{4.19}$$

In FLUENT the default underrelaxation parameters for all variables except the velocities are set to low values in order to ensure convergence in the largest possible number of cases. Unfortunately this may not give rise to the fastest rate of convergence, and an improvement can often be obtained by a judicious increase in one or more of these parameters.

A correct choice of underrelaxation factor α is essential for cost-effective simulations. Too large a value of α may lead to oscillatory or even divergent iterative solutions and a value which is too small will cause extremely slow convergence. Unfortunately, the optimum

values of under-relaxation factors are flow dependent and must be sought on a case-by-case basis. The choice of underrelaxation parameters is largely a matter of experience and is highly dependent on the flow configuration being modelled. It is a good practice to begin a calculation using the default setting by FLUENT. If the solution appears stable after initial calculations, it may be decided to increase the underrelaxation parameters to enhance the solution convergence. For flows without complex chemistry, thermal gradients or multiphase interactions, a suggested trial set of values might be 0.7 for velocity components, 0.6 for pressure correction and 0.4 for other variables. Typically, an increase in the underrelaxation factors brings about a slight increase in the residuals, but these increases usually disappear as the solution progresses. If the residuals jump by a few orders of magnitude, it should be decided to halt the calculation and return to the original settings.

In this study, a series of trials was run to find the appropriate underrelaxation factors for different components under various conditions. For the 150mm wide channel, α was given 0.7 for velocity and pressure components, 0.4 for Reynolds stresses, body force and viscosity and eddy dissipation. This resulted in 520 iterations for convergence compared with over 1000 iterations to convergence under the default underrelaxation factors. For a set of ten 45mm wide channels, α was given 0.6 for Reynolds stress w'w', velocity and pressure components, 0.4 for Reynolds stresses u'u', u'v', u'w', v'v', body force, viscosity and eddy dissipation, and 0.9 for Reynolds stress v'w'. This resulted in 1800 iterations for convergence compared with over 8000 iterations which failed to reach convergence under the default underrelaxation factors. The basis of choosing the above under-relaxation factors is to judiciously increase the under-relaxation factor(s) for the slowest convergencing parameter(s). It is totally a trial and error experience.

4.5.2 The choice of multigrid acceleration

Two solution methods, a line-by-line solver and a multigrid solver, are provided by FLUENT. The line by line solution technique is known as the line-Gauss-Siedel (LGS) method, in which unknown values on neighbouring lines are left explicit during the solution process, which reduces local errors with relative ease. That is, the effect of the solution on one line is communicated to adjacent lines relatively quickly. However, the line-by-line solver is less effective at reducing long-wavelength errors which exist over a large number of control volumes. Thus, global corrections to the solution across a large number of control

volumes occur slowly, over many iterations, when the line-by-line solver is used. Multigrid provides a remedy for this weakness of the line solver by deriving global corrections which are based on a control volume balance over a large number of cells.

It is recommended to apply the multigrid method when large cell aspect ratios exist in the finite difference grid and when rapidly varying or non-isotropic transport properties occur in the domain. Multigrid can accelerate the convergence of such problems by enforcing a global balance over large regions of the grid, in effect smoothing the non-isotropy that exists on the local scale.

In most cases, multigrid should be applied to the pressure-correction equation and scalar equations, which could reduce the number of iterations required to converge it. Applying multigrid to momentum or source-dominated scalar equations, on the other hand, provides little if any benefit (Source dominated scalars include the turbulence parameters and enthalpy or chemical species in reacting flows). Such equations tend to be dominated by local conditions and the line-by line solver is good at reducing these local errors. In fact, convergence may be hindered by applying multigrid to such equations as the global corrections may introduce significant local errors that are difficult to remove. In this study, the multigrid method solver was employed only for the calculation of pressure and the line-by-line method was used for the rest of the parameters.

The default multigrid parameter setting (residual reduction parameter, β=0.7 and termination criteria, α=0.1) in general, provides good performance in many problems. However, this performance should be checked by calculating one or more global interpolations using the multigrid monitors, and then making any adjustments to the parameters as indicated by the monitor to improve performance.

Other techniques used for improving the convergence rate are controlling the sweep direction and optimising the number of sweeps on the individual Reynolds stresses and/or on the momentum and turbulence dissipation equations for difficult and large problems. In this study, the sweep direction was kept in the x direction, the solver marching direction was in the z direction and the default numbers (5 for the pressure and 1 for the rest of the parameters) were used for all the cases.

4.6 Comparison between model results and experimental data

Comparisons between experimental data of velocity and turbulence and modelling results of the "150mm wide channel" under two nominal velocities (v) of 0.05 and 0.1m/s are shown in Figures 4.11.1 to 4.29.4. The locations and levels referred to are shown in Figure 4.3. The experimental results were obtained using the LDA system and were discussed independently in Chapter 3. Comparison of longitudinal velocity (u-velocity) at the distance 60mm from the outside wall of the two channels (vertical sections 1c and 2c) and 50mm from the inside wall (vertical sections 1iw and 2iw) at three levels of A, B and C are given in Figures 4.11.1 to 4.16.4. The direction of longitudinal velocity, u, was set positive along the flow direction in the first channel and opposite to the x coordinate, whilst the traversal velocity, v, was set positive along the direction from the first channel to the second channel and vertical velocity, w, was set positive along the direction from the bottom to the top of the channels. Comparisons of transversal (v-velocity) and vertical velocity (w-velocity) are given for the centre of the channels at level B for 0.1m/s (Figures 4.17.1 to 4.18.2). Modelled results agreed very well with measured data in longitudinal velocities (u-velocity), fairly well in transversal (v-velocity) and vertical velocity (w-velocity). It might be due to the comparatively smaller velocity in the above two directions which cause relatively larger error in measurement. According to the error assessment described in Chapter 3, the relative error (RE) value of v-velocity and w-velocity are up to 11 times that of the RE of the corresponding u-velocity at the same point. It is noticed that the modelled three dimensional velocities compare well with the experimental results in the locations near the centre of the channel width and the middle of the channel height, but there is a comparatively poor fit in the locations near the water surface, channel bottom and the walls (Figures 4.11.1 to 4.18.2). The modelling assumptions of free surface and near wall equations plus the greater likelihood of experimental errors in these locations may be the reasons. The difference is greatest near the water surface; however, there is also a relatively larger error in the modelled results near the bed and wall, up to 9.3 times that of the relative error of the averaged experimental measured velocity compared with that of modelled velocity in the main body of the channels, due to the above assumptions.

FLUENT simulation results for the nominal velocities of 0.1m/s and 0.05m/s (Figure 4.11.1 to 4.16.4) show that there is a very good qualitative fit with the experimentally determined longitudinal velocities and the basic shape of the LDA velocity profiles are well reproduced by the CFD software. Simulation for the velocity of 0.05m/s is not quite so good, however

as that for velocity of 0.1m/s. This may be due to the larger possibility of experimental error when the velocity is relatively lower. It is identified by the larger REs for the lower velocity of 0.05m/s which are up to 4.2 and 2.8 times that of the REs for the velocity of 0.1m/s in u-velocity and kinetic energy respectively.

Figures 4.19.1 to 4.23.2 show the turbulence shear stresses u'u', v'v' and w'w' determined from the LDA measurements against those output directly from FLUENT's Reynolds stress turbulence model. As for the comparison given to velocity, the comparison of u'u' is for the centre of two channels (sections 1c and 2c) and near the inside wall (sections 1iw and 2iw) at three levels, A, B and C. Comparison of v'v' and w'w' are given for the centre line of channels at section B. Poorer agreements occur near the walls, water surface and bottom, but the modelled Reynolds stress values are still of the same order of magnitude as the experimental data and match the experimental variation trend.

Comparison of turbulence shear stresses and kinetic energy (k) quantified as the turbulence intensity with the experimental results presented in Chapter 3 is shown in Figures 4.19.1 to 4.29.4. Although there is some difference between the modelled and the experimental results in turbulence shear stresses u'u', v'v' and w'w', modelled kinetic energy as a sum of the above shear stresses agrees very well with experimental data. In the longitudinal direction the kinetic energy increases as the flow moves towards the bend and reaches its maximum around 0.5m from the end wall and decreases till very near the end wall (about 5cm from the wall) where it has a jump again. The peak value and its location may result from the backup effect of the bend. In the vertical direction, the highest turbulence occurs in the middle of the water depth in the channels, decreasing towards the bottom and reaching its lowest near the water surface.

In view of the above discussions, it may be concluded that the FLUENT CFD model study of the channel flows yield very similar results to the experimental data, and in the case of the mean longitudinal flows give a very good fit to the measured data. Therefore, it may be concluded that the FLUENT results so far obtained exhibit sufficient similarities with measured data to enable their use in determining a range of flow properties such as velocities and kinetic energy.

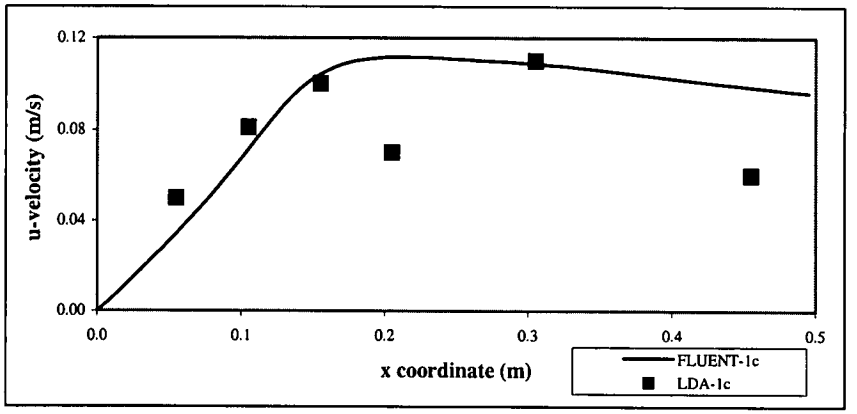

Figure 4.11.1 U-velocity: comparison between LDA with FLUENT results (Level A, section 1c, V=0.1m/s)

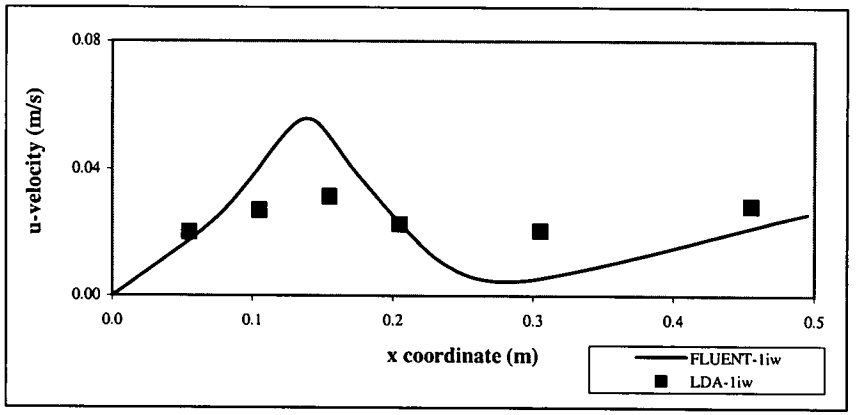

Figure 4.11.2 U-velocity: comparison between LDA with FLUENT results (Level A, section 1iw, V=0.1m/s)

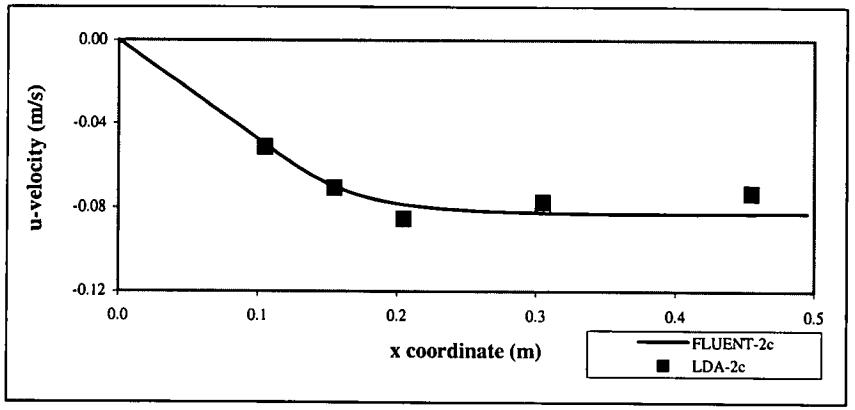

Figure 4.11.3 U-velocity: comparison between LDA with FLUENT results (Level A, section 2c, V=0.1m/s)

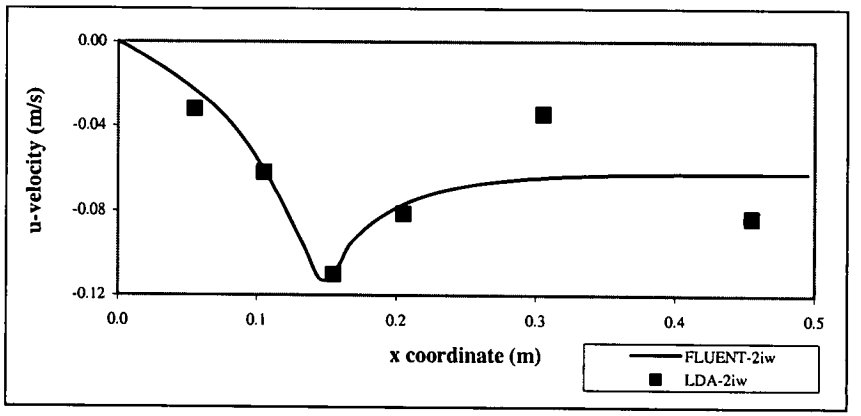

Figure 4.11.4 U-velocity: comparison between LDA with FLUENT results (Level A, section 2iw, V=0.1m/s)

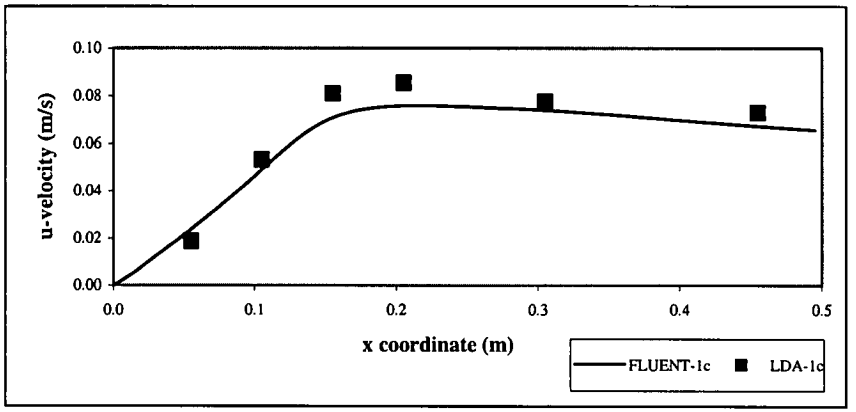

Figure 4.12.1 U-velocity: comparison between LDA with FLUENT results (Level A, section 1c, V=0.05m/s)

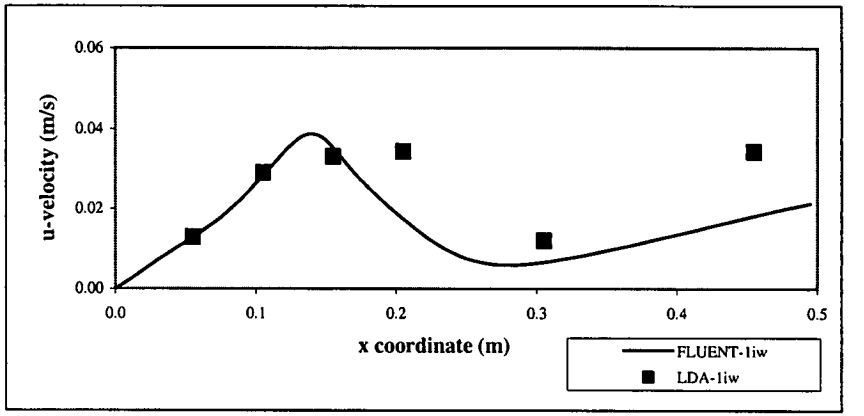

Figure 4.12.2 U-velocity: comparison between LDA with FLUENT results (Level A, section 1iw, V=0.05m/s)

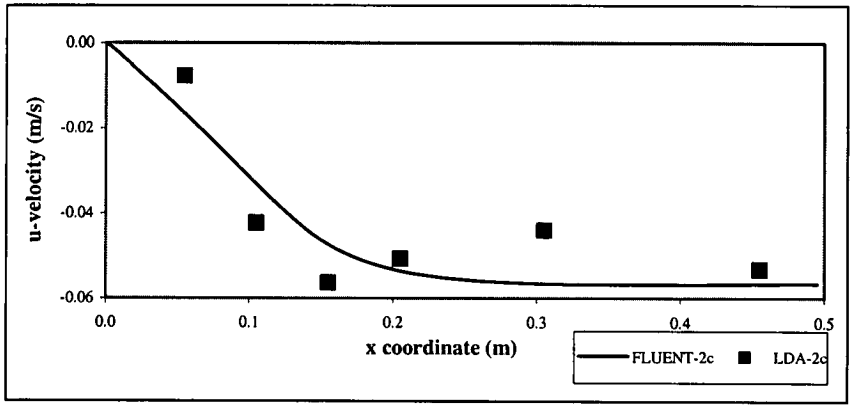

Figure 4.12.3 U-velocity: comparison between LDA with FLUENT results (Level A, section 2c, V=0.05m/s)

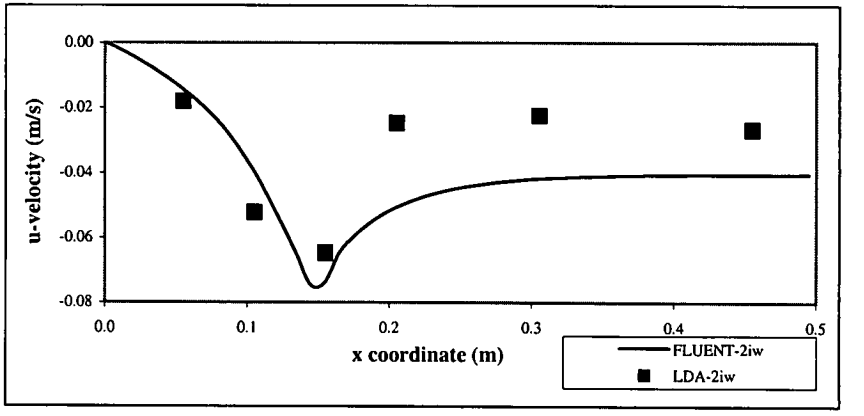

Figure 4.12.4 U-velocity: comparison between LDA with FLUENT results (Level A, section 2iw, V=0.05m/s)

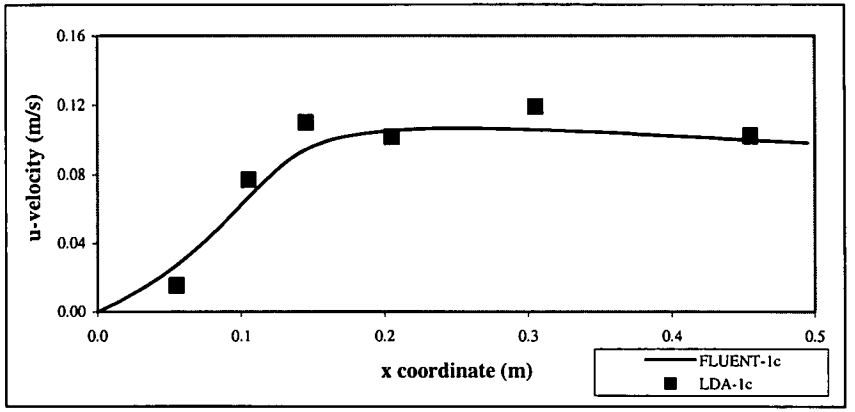

Figure 4.13.1 U-velocity: comparison between LDA with FLUENT results (Level B, section 1c, V=0.1m/s)

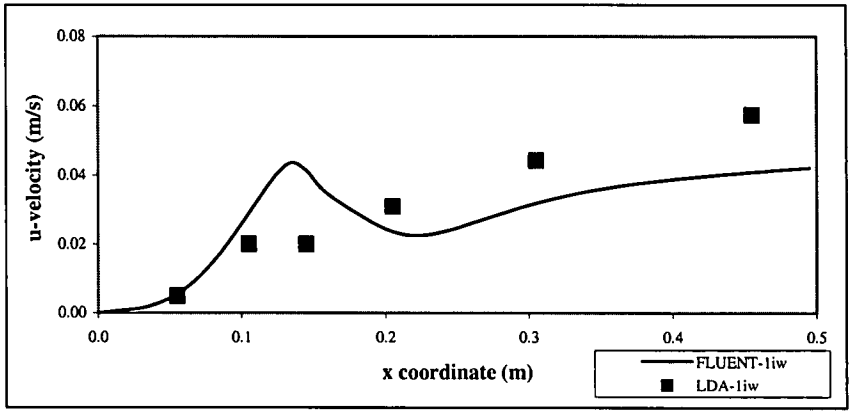

Figure 4.13.2 U-velocity: comparison between LDA with FLUENT results (Level B, section 1iw, V=0.1m/s)

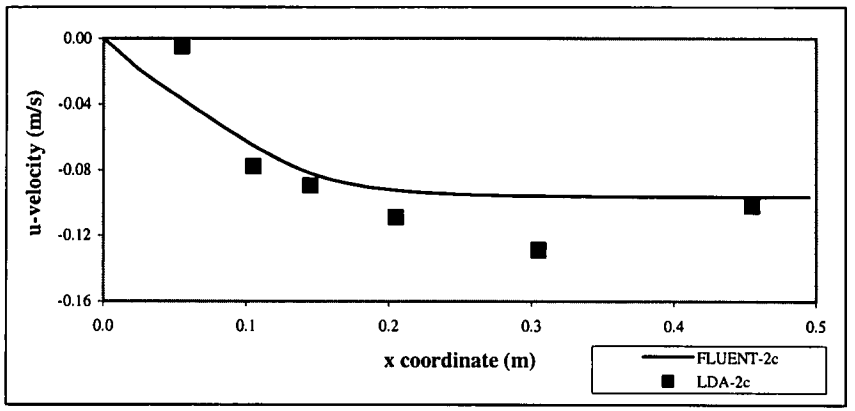

Figure 4.13.3 U-velocity: comparison between LDA with FLUENT results (Level B, section 2c, V=0.1m/s)

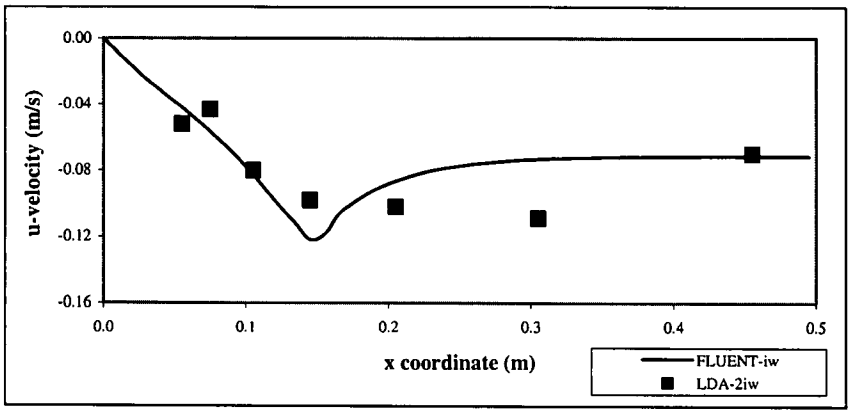

Figure 4.13.4 U-velocity: comparison between LDA with FLUENT results (Level B, section 2iw, V=0.1m/s)

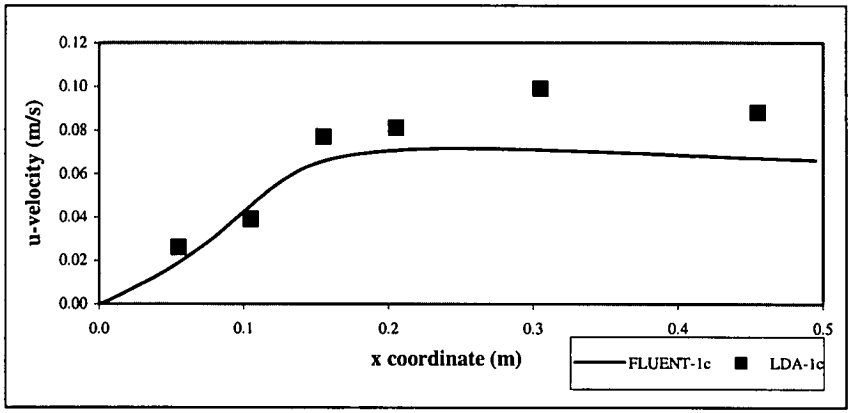

Figure 4.14.1 U-velocity: comparison between LDA with FLUENT results (Level B, section 1c, V=0.05m/s)

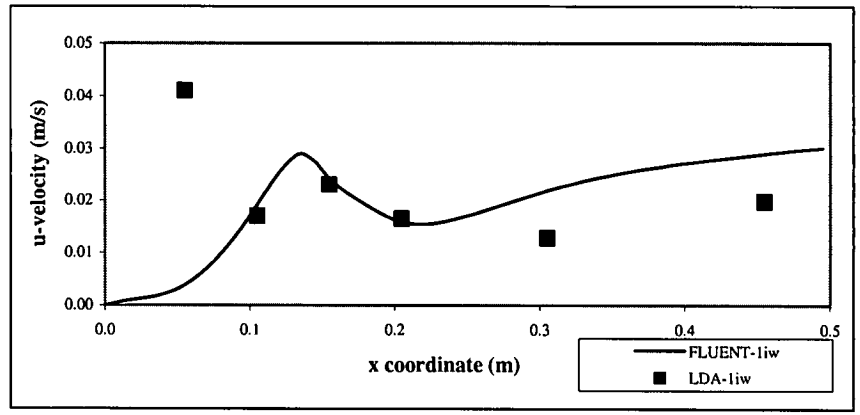

Figure 4.14.2 U-velocity: comparison between LDA with FLUENT results (Level B, section 1iw, V=0.05m/s)

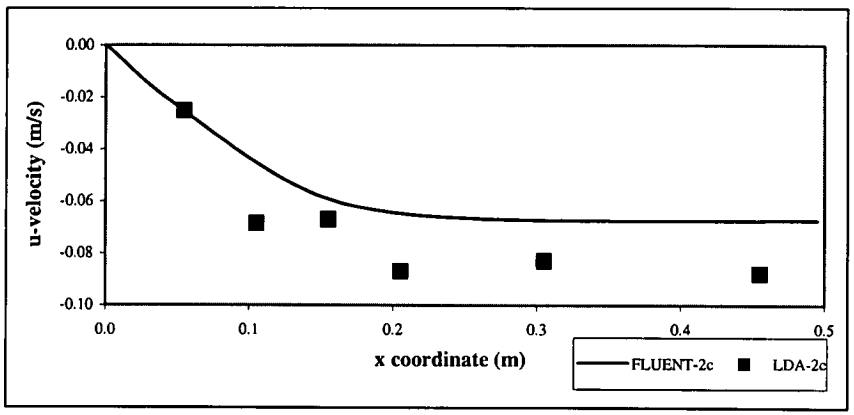

Figure 4.14.3 U-velocity: comparison between LDA with FLUENT results (Level B, section 2c, V=0.05m/s)

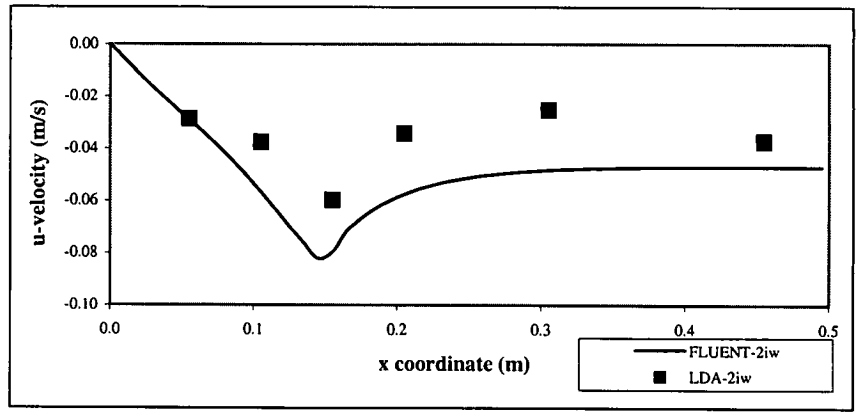

Figure 4.14.4 U-velocity: comparison between LDA with FLUENT results (Level B, section 2iw, V=0.05m/s)

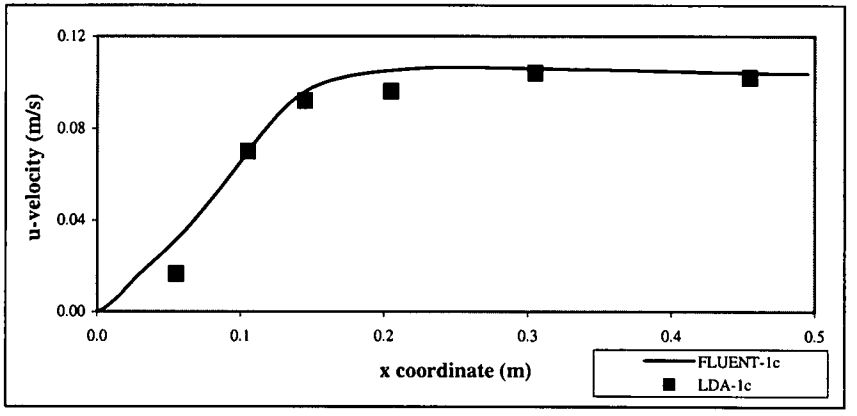

Figure 4.15.1 U-velocity: comparison between LDA with FLUENT results (Level C, section 1c, V=0.1m/s)

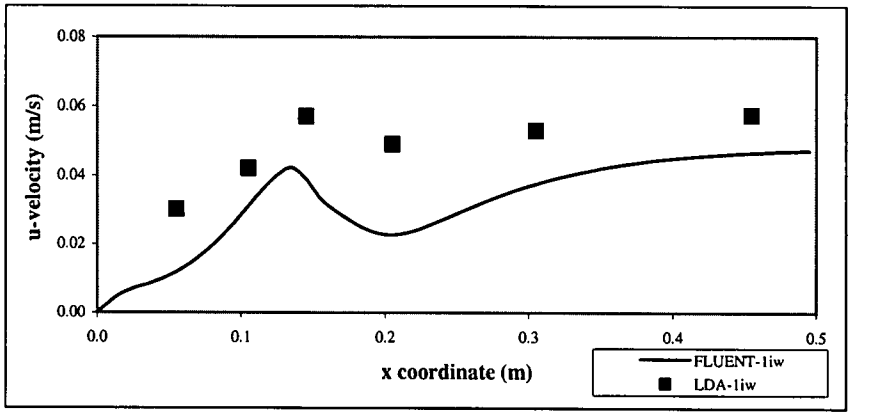

Figure 4.15.2 U-velocity: comparison between LDA with FLUENT results (Level C, section 1iw, V=0.1m/s)

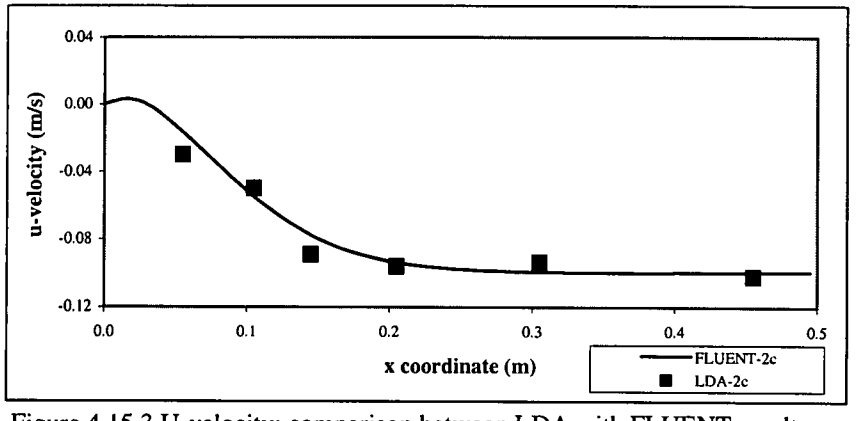

Figure 4.15.3 U-velocity: comparison between LDA with FLUENT results (Level C, section 2c, V=0.1m/s)

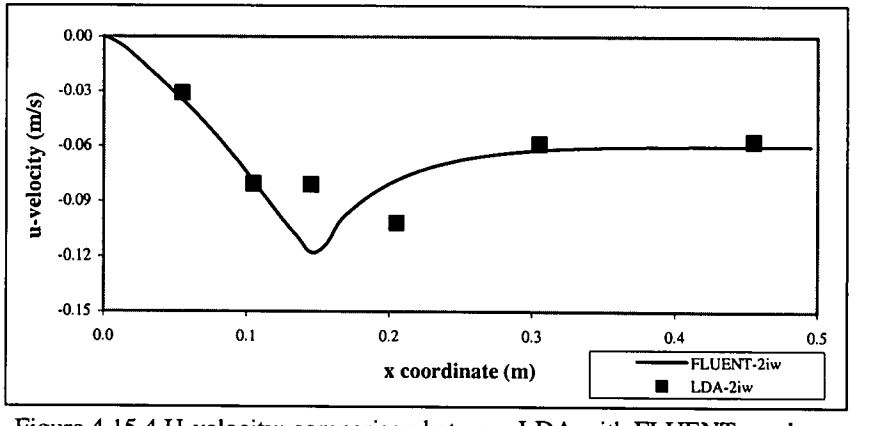

Figure 4.15.4 U-velocity: comparison between LDA with FLUENT results (Level C, section 2iw, V=0.1m/s)

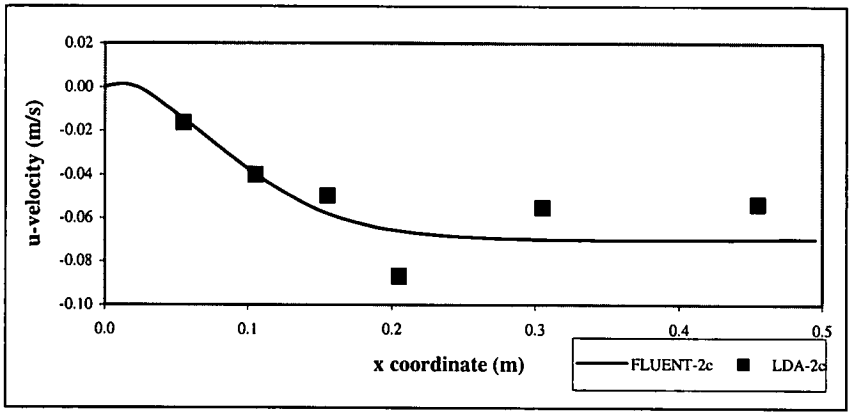

Figure 4.16.1 U-velocity: comparison between LDA with FLUENT results (Level C, section 1c, V=0.05m/s)

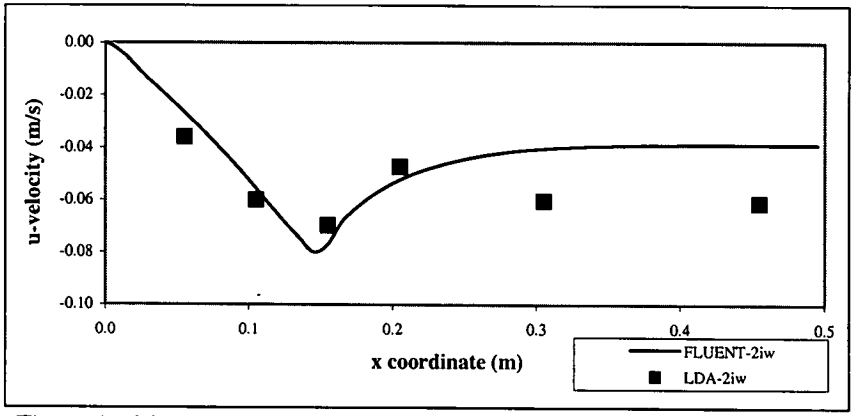

Figure 4.16.2 U-velocity: comparison between LDA with FLUENT results (Level C, section 1iw, V=0.05m/s)

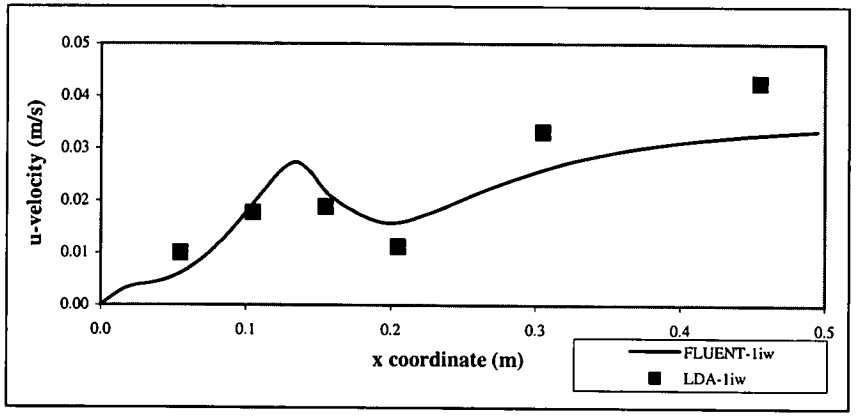

Figure 4.16.3 U-velocity: comparison between LDA with FLUENT results (Level C, section 2c, V=0.05m/s)

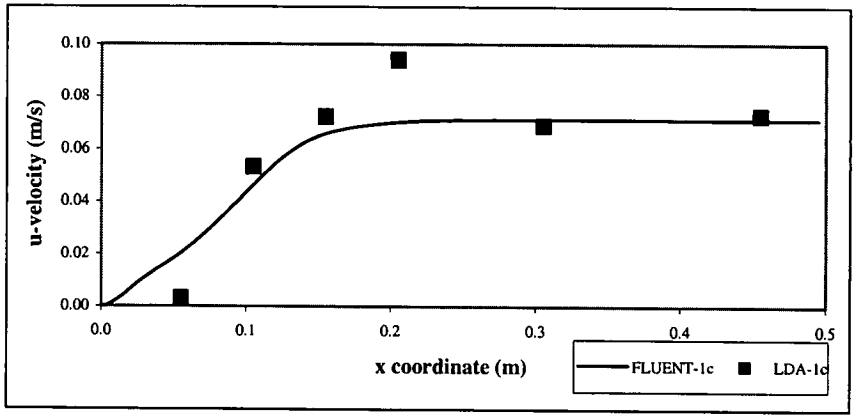

Figure 4.16.4 U-velocity: comparison between LDA with FLUENT results (Level C, section 2iw, V=0.05m/s)

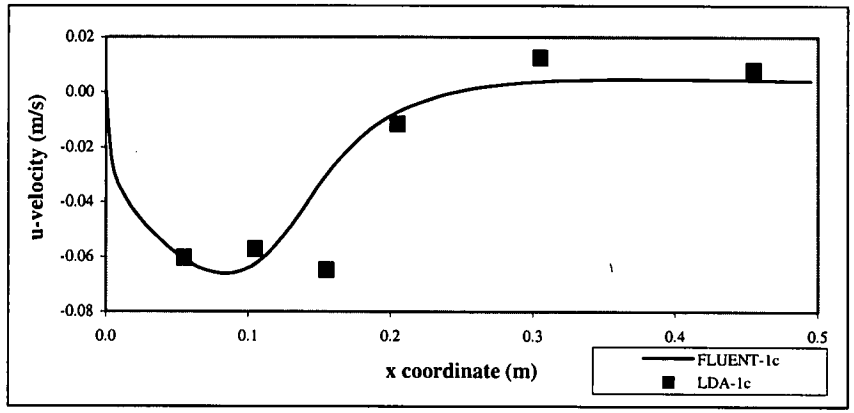

Figure 4.17.1 V-velocity: comparison between LDA with FLUENT results (Level B, section 1c, V=0.1m/s)

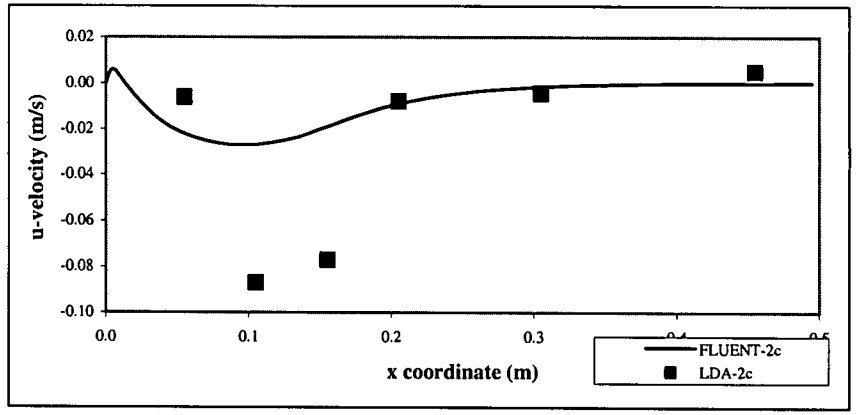

Figure 4.17.2 V-velocity: comparison between LDA with FLUENT results (Level B, section 2c, V=0.1m/s)

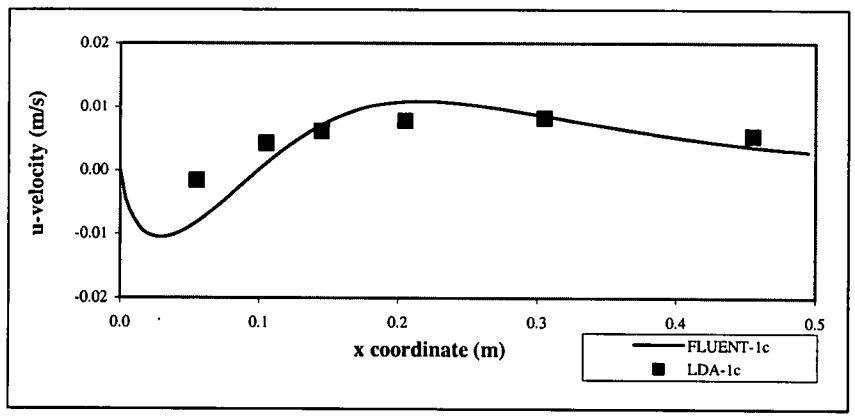

Figure 4.18.1 W-velocity: comparison between LDA with FLUENT results (Level B, section 1c, V=0.1m/s)

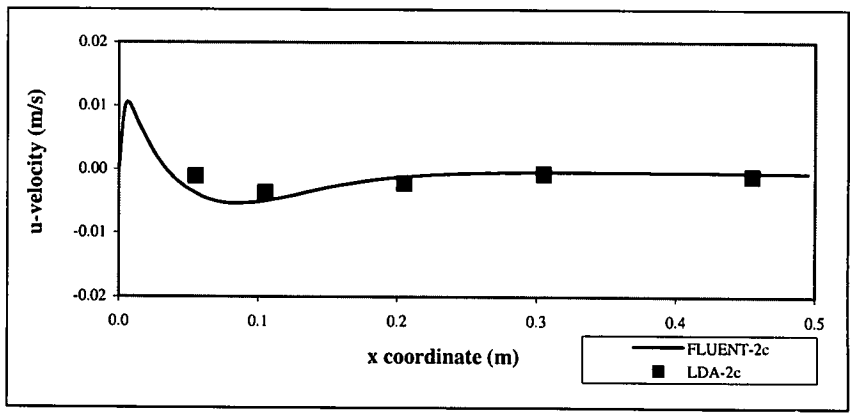

Figure 4.18.2 W-velocity: comparison between LDA with FLUENT results (Level B, section 2c, V=0.1m/s)

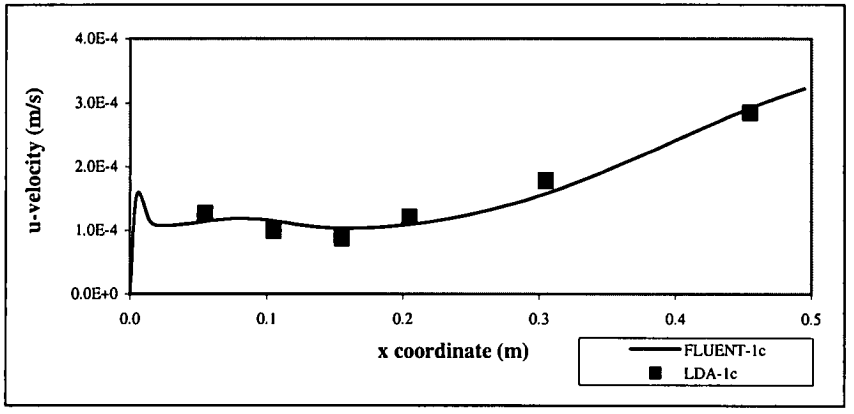

Figure 4.19.1 Shear stress u'u': comparison between LDA with FLUENT results (Level A, section 1c, V=0.1m/s)

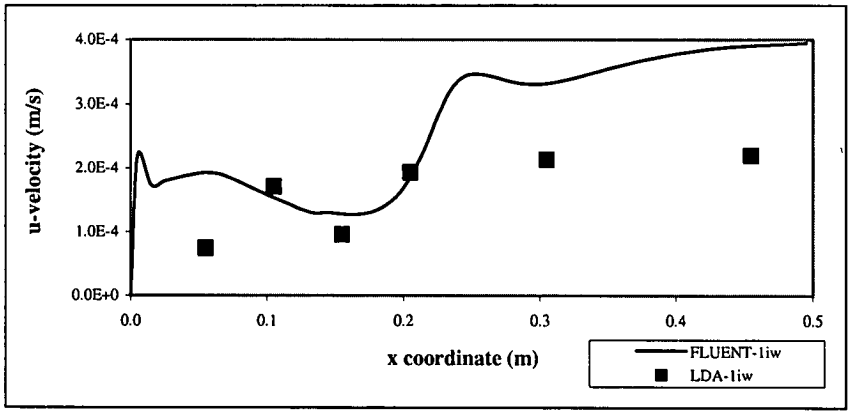

Figure 4.19.2 Shear stress u'u': comparison between LDA with FLUENT results (Level A, section 1iw, V=0.1m/s)

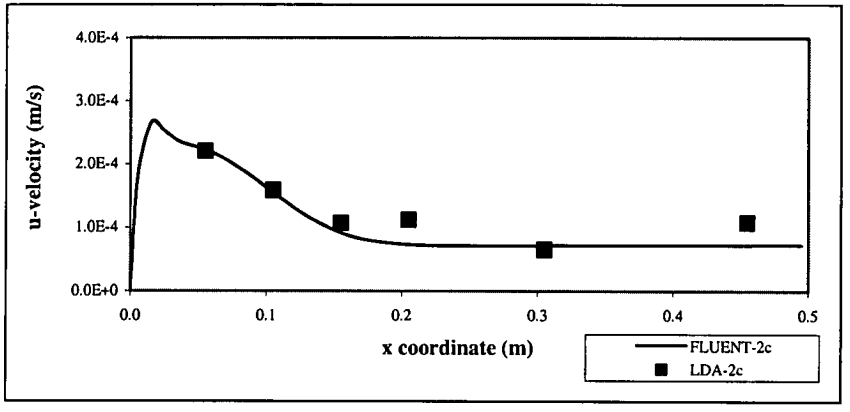

Figure 4.19.3 Shear stress u'u': comparison between LDA with FLUENT results (Level A, section 2c, V=0.1m/s)

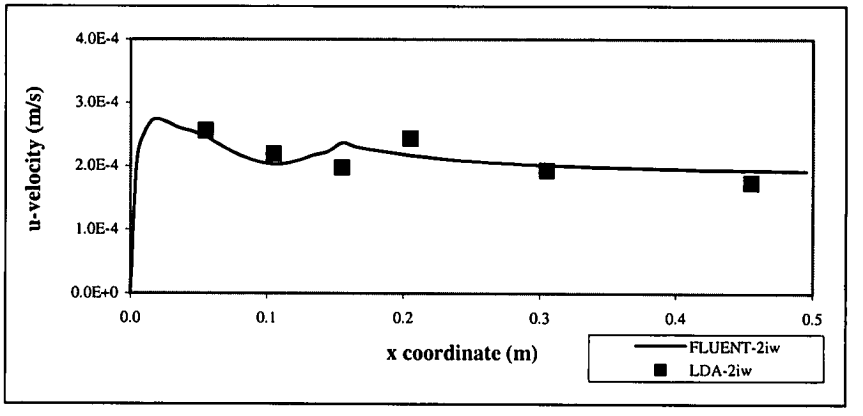

Figure 4.19.4 Shear stress u'u': comparison between LDA with FLUENT results (Level A, section 2iw, V=0.1m/s)

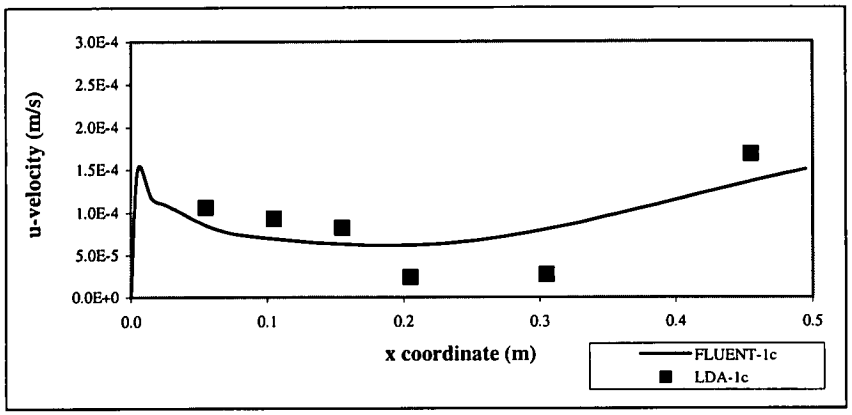

Figure 4.20.1 Shear stress u'u': comparison between LDA with FLUENT results (Level B, section 1c, V=0.1m/s)

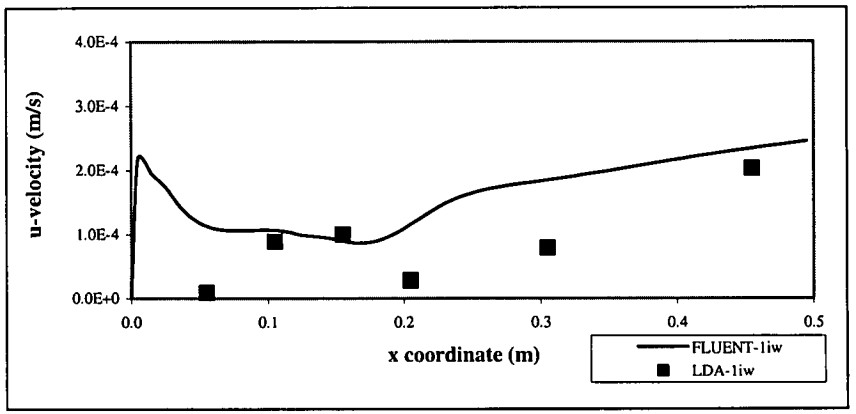

Figure 4.20.2 Shear stress u'u': comparison between LDA with FLUENT results (Level B, section 1iw, V=0.1m/s)

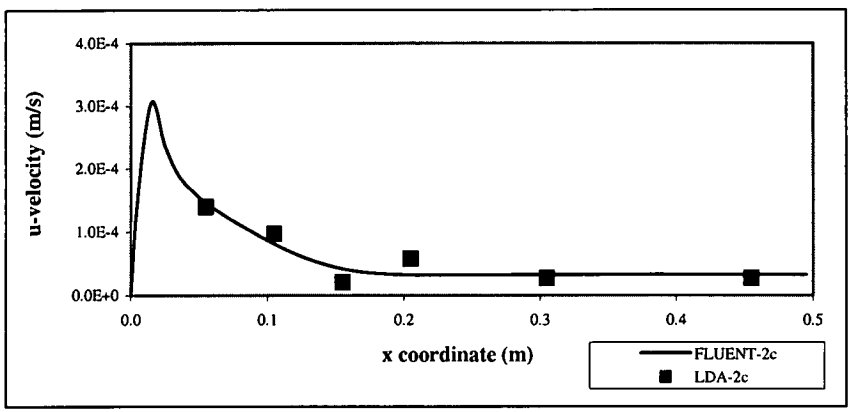

Figure 4.20.3 Shear stress u'u': comparison between LDA with FLUENT results (Level B, section 2c, V=0.1m/s)

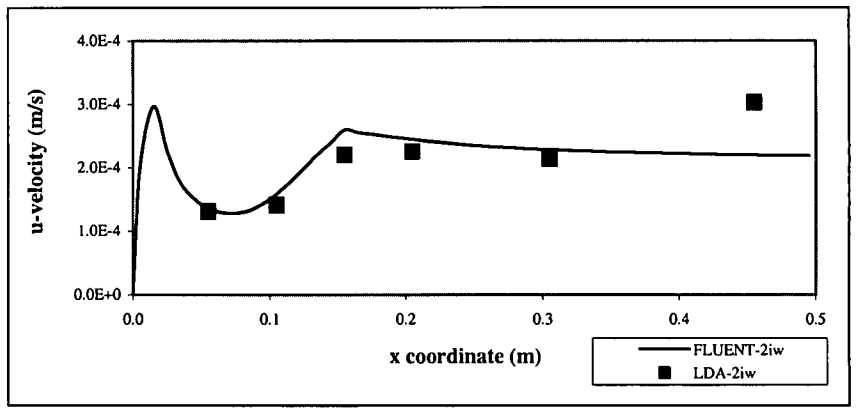

Figure 4.20.4 Shear stress u'u': comparison between LDA with FLUENT results (Level B, section 2iw, V=0.1m/s)

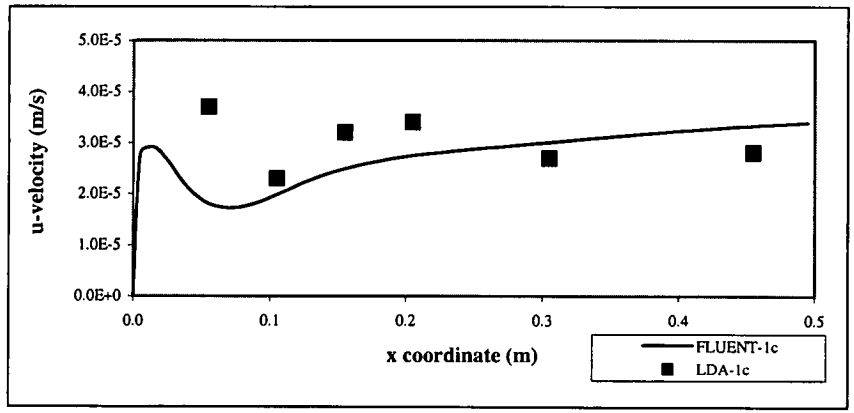

Figure 4.21.1 Shear stress u'u': comparison between LDA with FLUENT results (Level C, section 1c, V=0.1m/s)

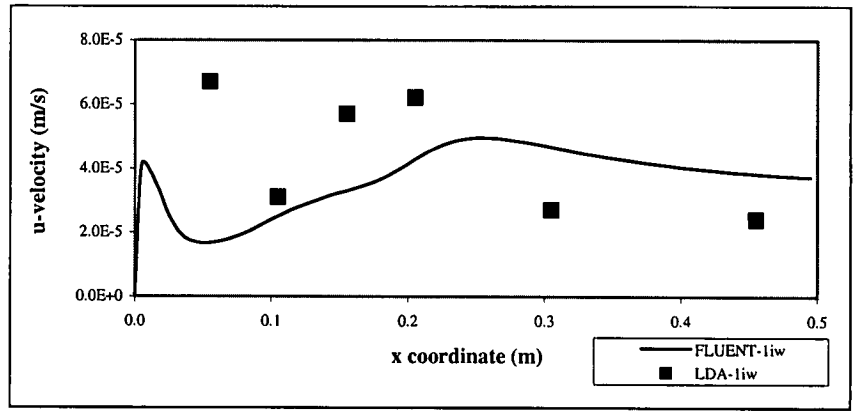

Figure 4.21.2 Shear stress u'u': comparison between LDA with FLUENT results (Level C, section 1iw, V=0.1m/s)

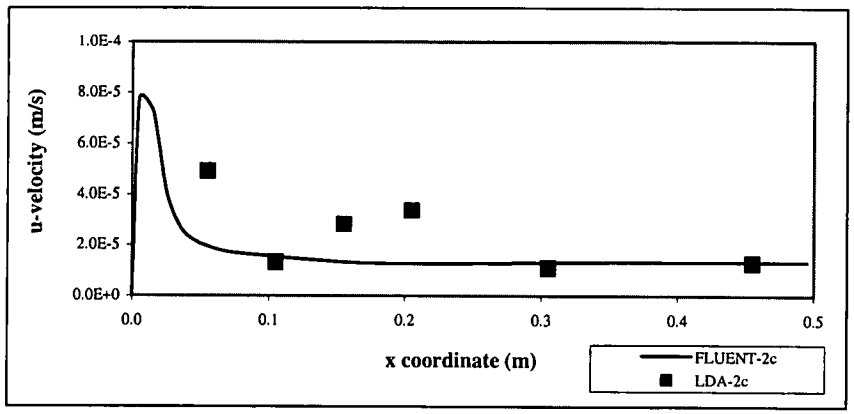

Figure 4.21.3 Shear stress u'u': comparison between LDA with FLUENT results (Level C, section 2c, V=0.1m/s)

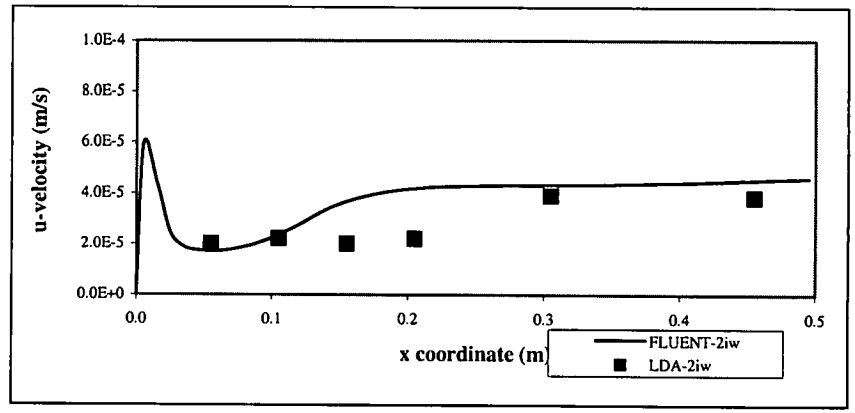

Figure 4.21.4 Shear stress u'u': comparison between LDA with FLUENT results (Level C, section 2iw, V=0.1m/s)

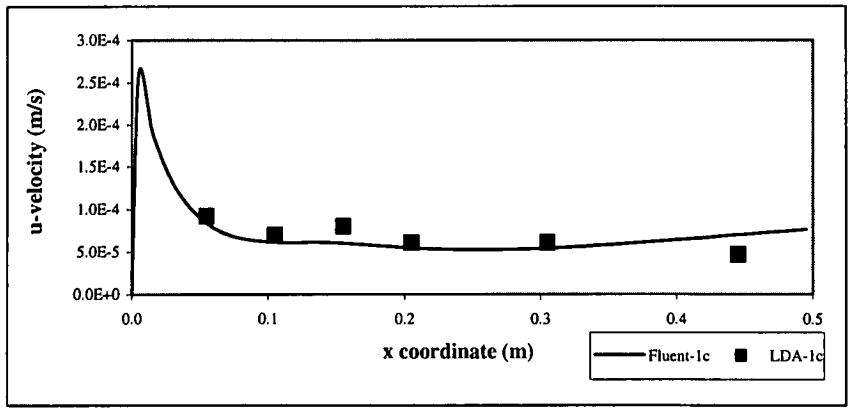

Figure 4.22.1 Shear stress v'v': comparison between LDA with FLUENT results (Level B, section 1c, V=0.1m/s)

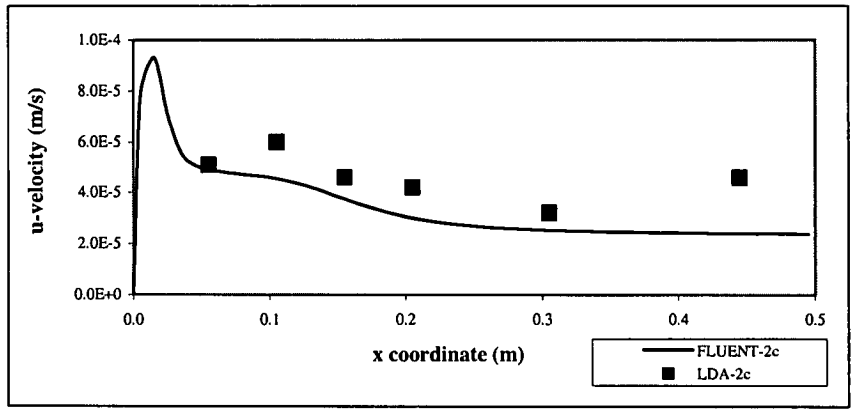

Figure 4.22.2 Shear stress v'v': comparison between LDA with FLUENT results (Level B, section 2c, V=0.1m/s)

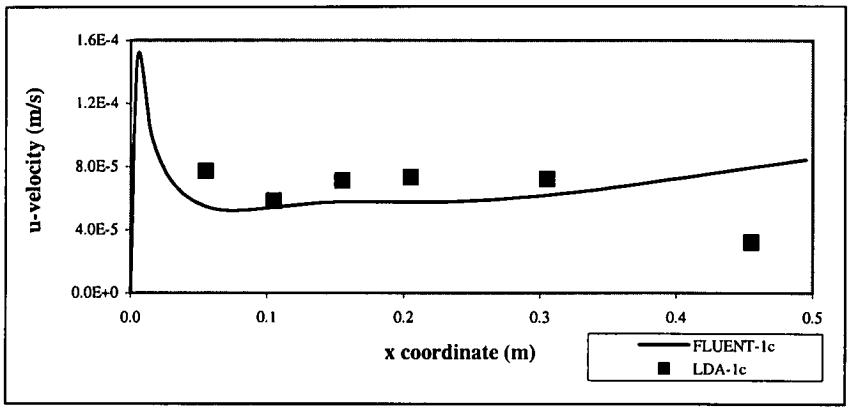

Figure 4.23.1 Shear stress w'w': comparison between LDA with FLUENT results (Level B, section 1c, V=0.1m/s)

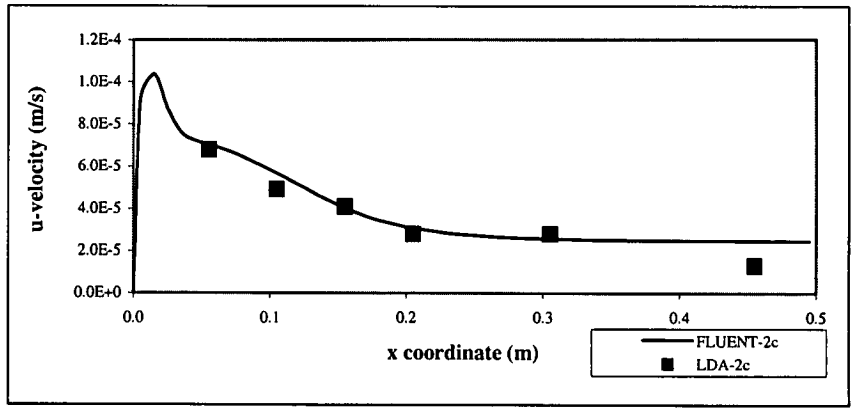

Figure 4.23.2 Shear stress w'w': comparison between LDA with FLUENT results (Level B, section 2c, V=0.1m/s)

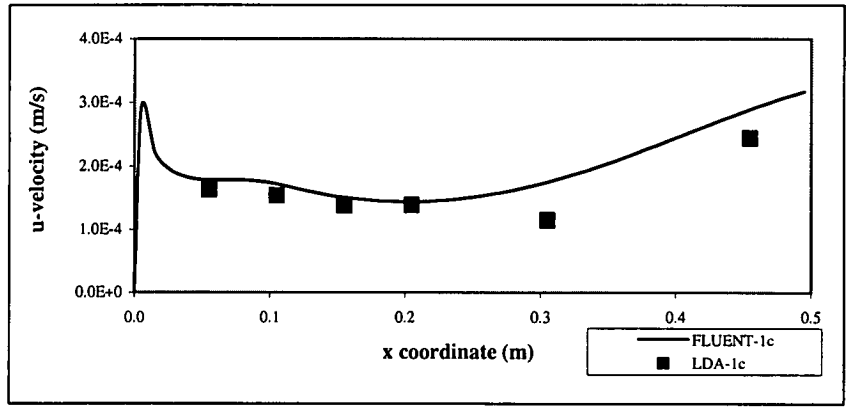

Figure 4.24.1 Kinetic energy: comparison between LDA with FLUENT results (Level A, section 1c, V=0.1m/s)

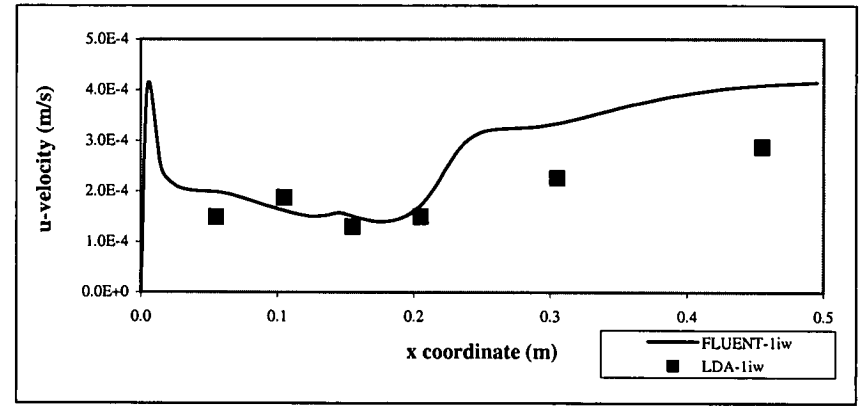

Figure 4.24.2 Kinetic energy: comparison between LDA with FLUENT results (Level A, section 1iw, V=0.1m/s)

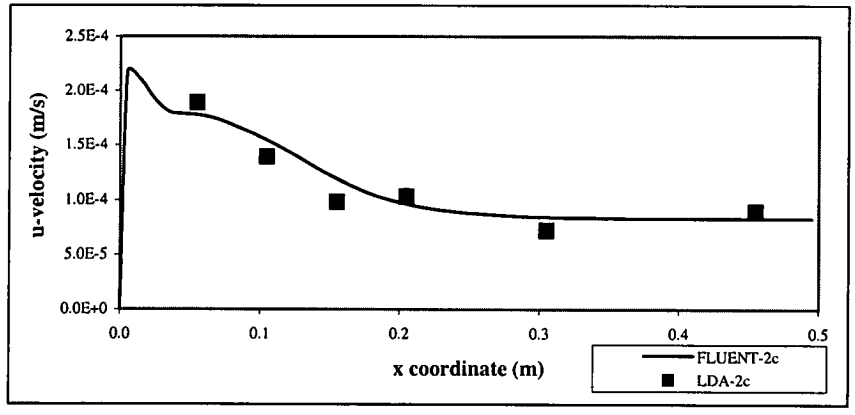

Figure 4.24.3 Kinetic energy: comparison between LDA with FLUENT results (Level A, section 2c, V=0.1m/s)

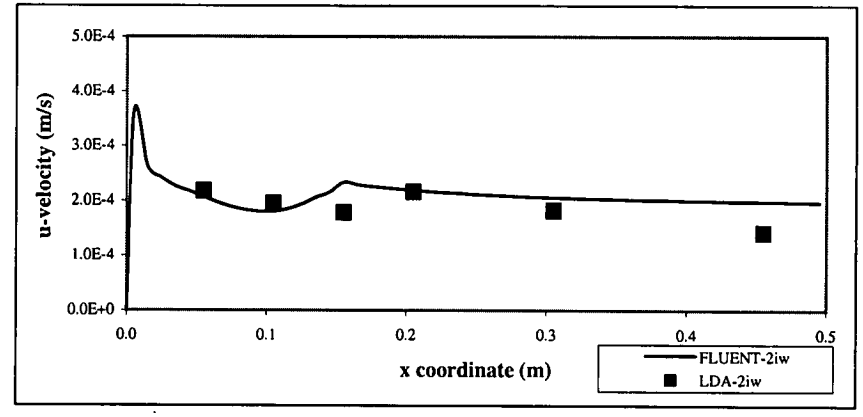

Figure 4.24.4 Kinetic energy: comparison between LDA with FLUENT results (Level A, section 2iw, V=0.1m/s)

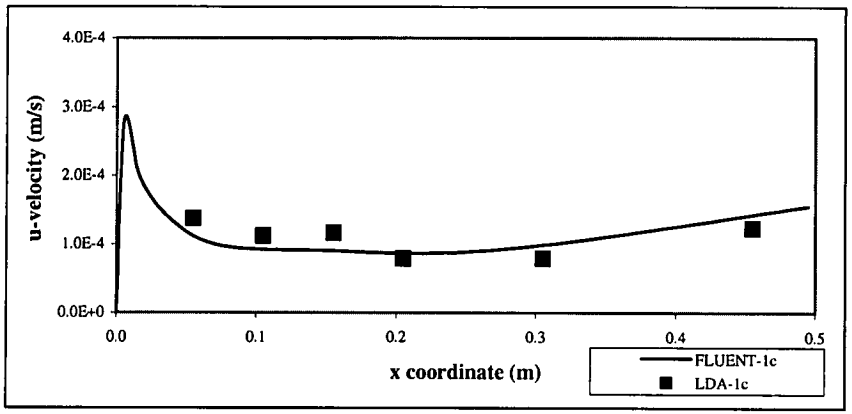

Figure 4.25.1 Kinetic energy: comparison between LDA with FLUENT results (Level B, section 1c, V=0.1m/s)

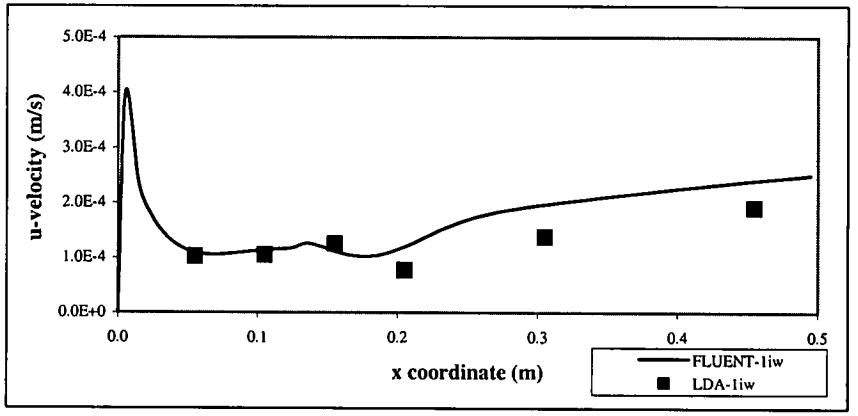

Figure 4.25.2 Kinetic energy: comparison between LDA with FLUENT results (Level B, section 1iw, V=0.1m/s)

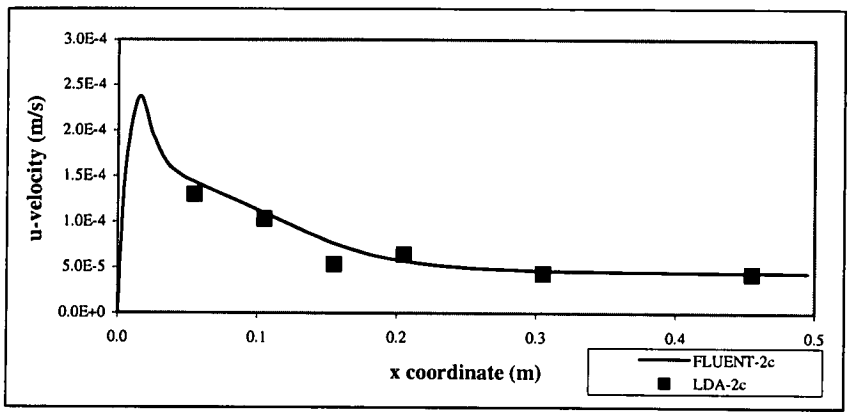

Figure 4.25.3 Kinetic energy: comparison between LDA with FLUENT results (Level B, section 2c, V=0.1m/s)

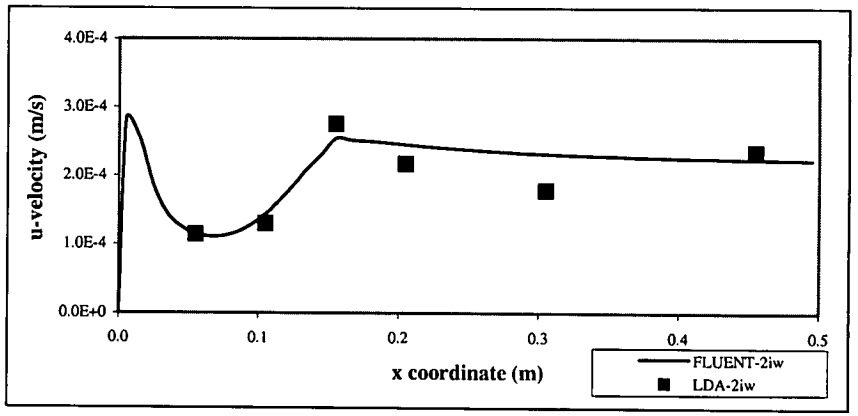

Figure 4.25.4 Kinetic energy: comparison between LDA with FLUENT results (Level B, section 2iw, V=0.1m/s)

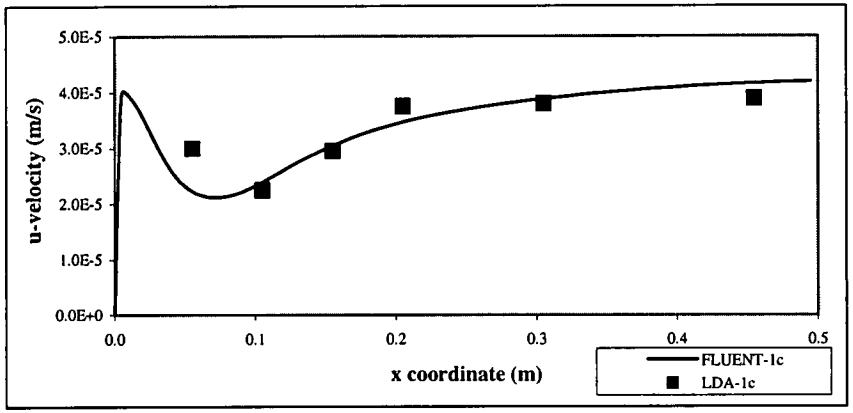

Figure 4.26.1 Kinetic energy: comparison between LDA with FLUENT results (Level C, section 1c, V=0.1m/s)

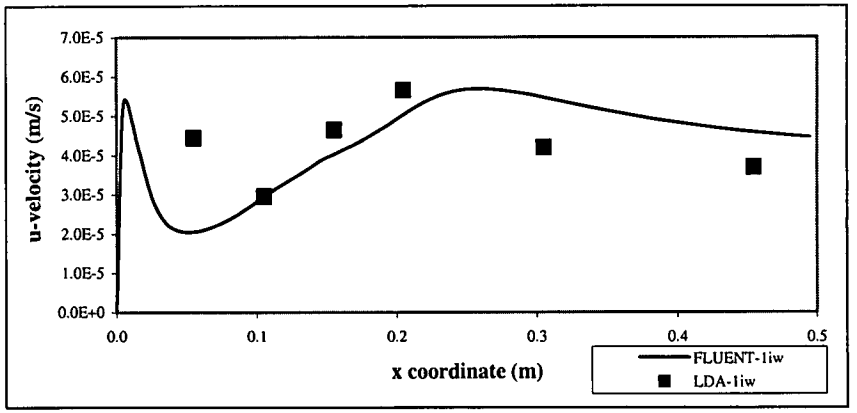

Figure 4.26.2 Kinetic energy: comparison between LDA with FLUENT results (Level C, section 1iw, V=0.1m/s)

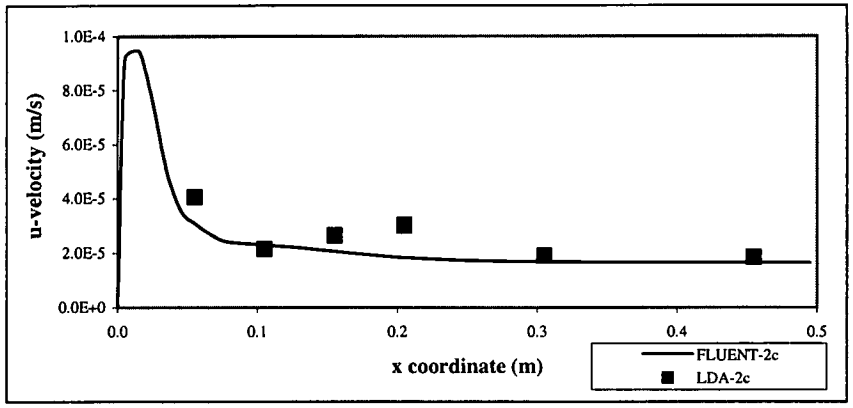

Figure 4.26.3 Kinetic energy: comparison between LDA with FLUENT results (Level C, section 2c, V=0.1m/s)

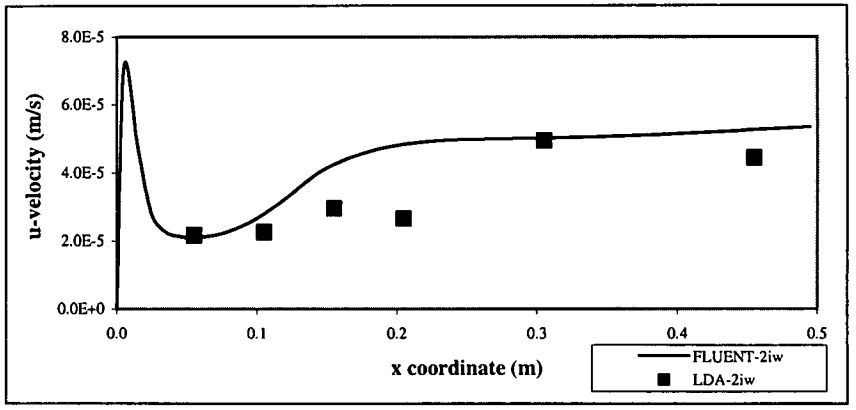

Figure 4.26.4 Kinetic energy: comparison between LDA with FLUENT results (Level C, section 2iw, V=0.1m/s)

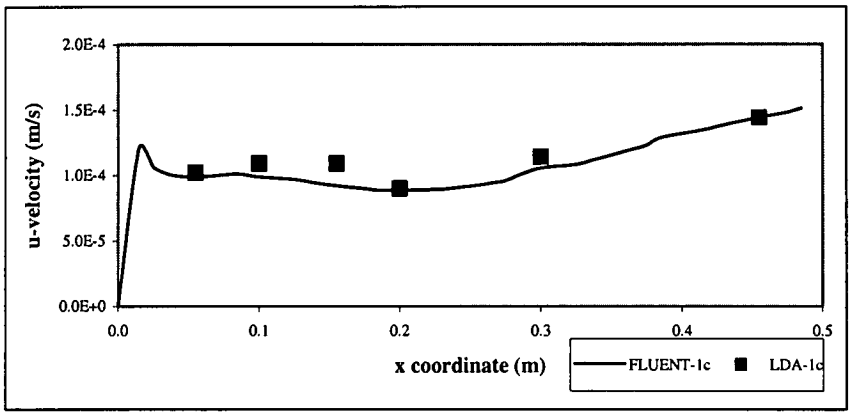

Figure 4.27.1 Kinetic energy: comparison between LDA with FLUENT results (Level A, section 1c, V=0.05m/s)

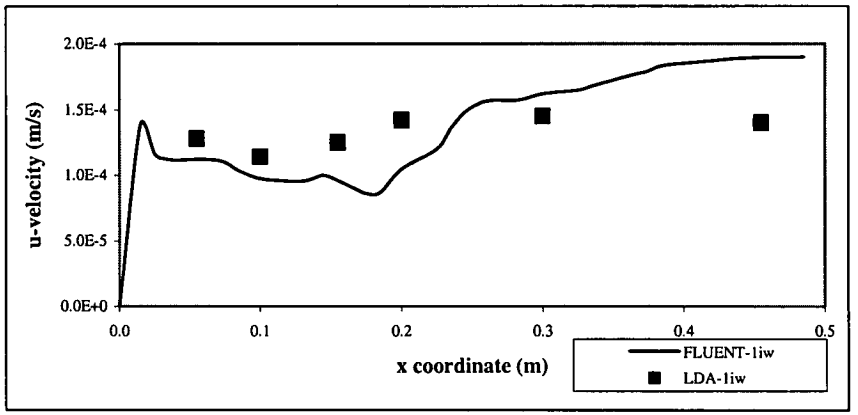

Figure 4.27.2 Kinetic energy: comparison between LDA with FLUENT results (Level A, section 1iw, V=0.05m/s)

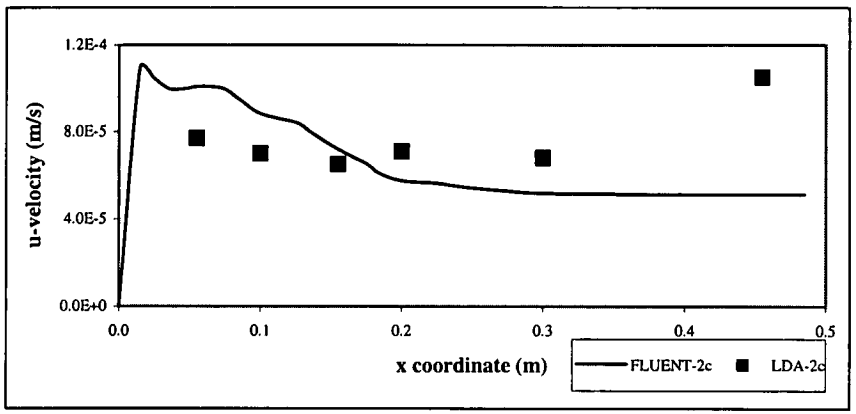

Figure 4.27.3 Kinetic energy: comparison between LDA with FLUENT results (Level A, section 2c, V=0.05m/s)

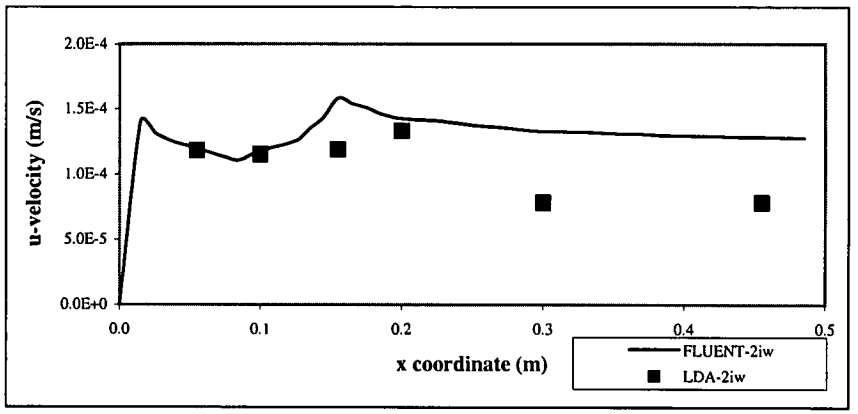

Figure 4.27.4 Kinetic energy: comparison between LDA with FLUENT results (Level A, section 2iw, V=0.05m/s)

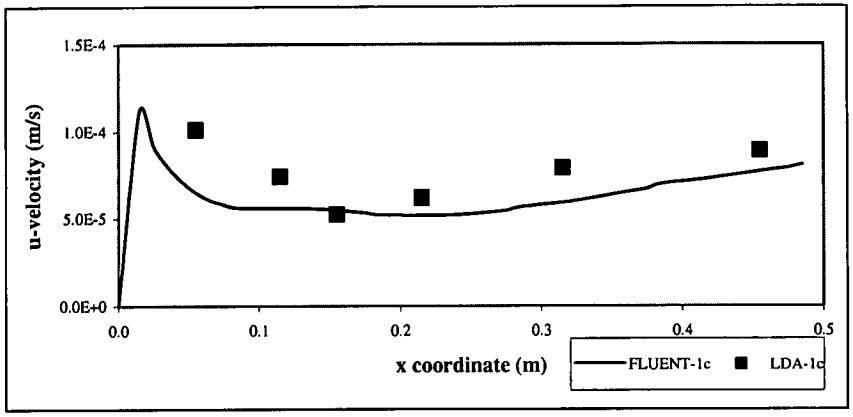

Figure 4.28.1 Kinetic energy: comparison between LDA with FLUENT results (Level B, section 1c, V=0.05m/s)

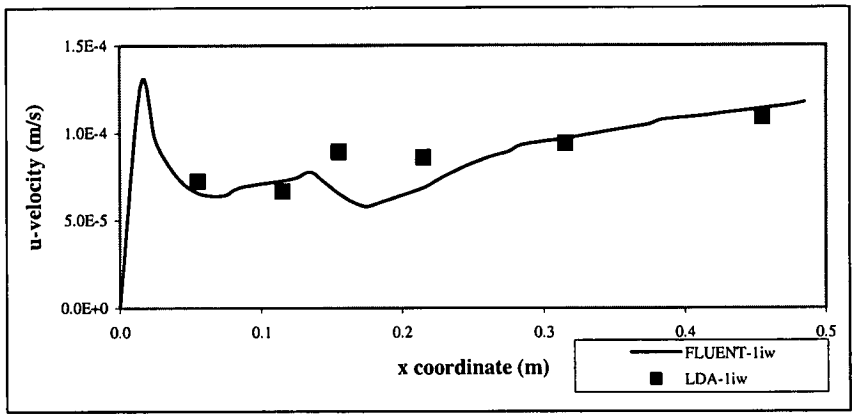

Figure 4.28.2 Kinetic energy: comparison between LDA with FLUENT results (Level B, section 1iw, V=0.05m/s)

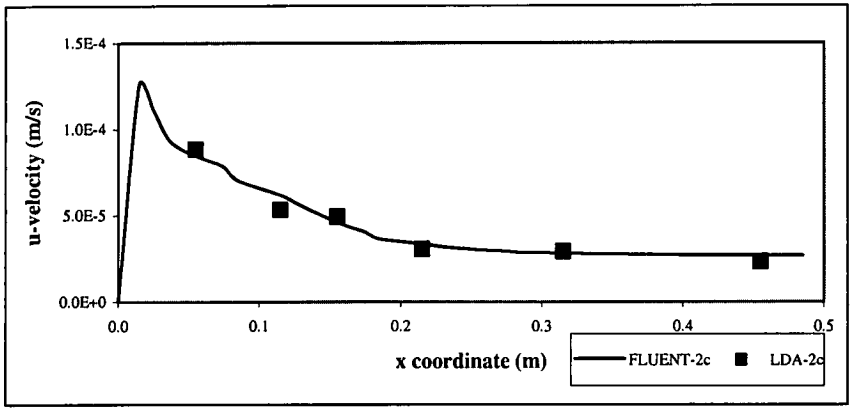

Figure 4.28.3 Kinetic energy: comparison between LDA with FLUENT results (Level B, section 2c, V=0.05m/s)

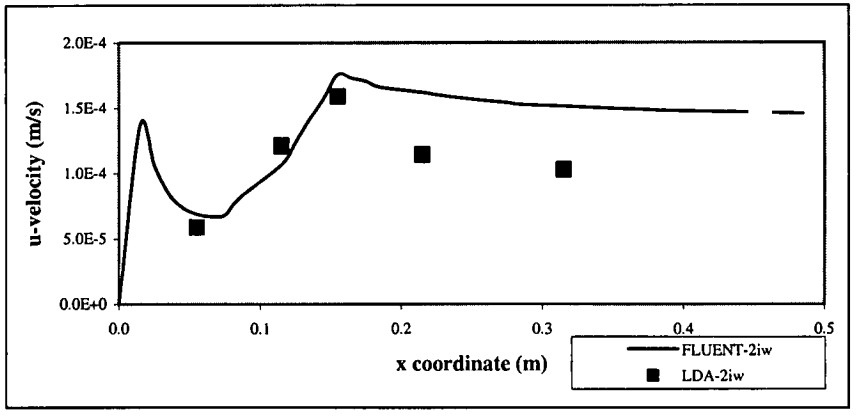

Figure 4.28.4 Kinetic energy: comparison between LDA with FLUENT results (Level B, section 2iw, V=0.05m/s)

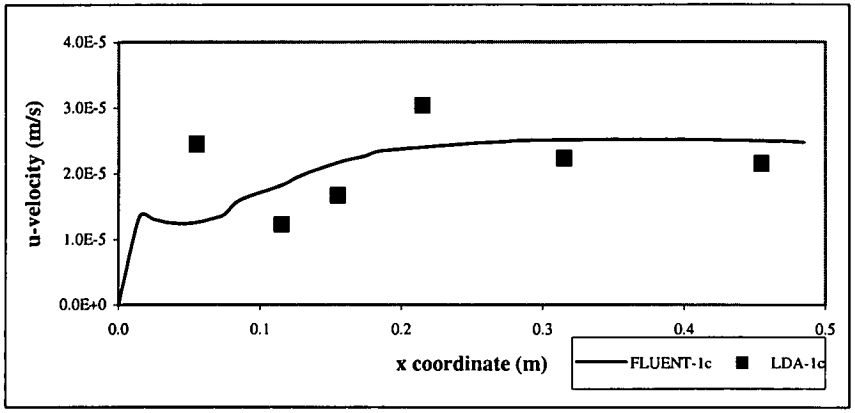

Figure 4.29.1 Kinetic energy: comparison between LDA with FLUENT results (Level C, section 1c, V=0.05m/s)

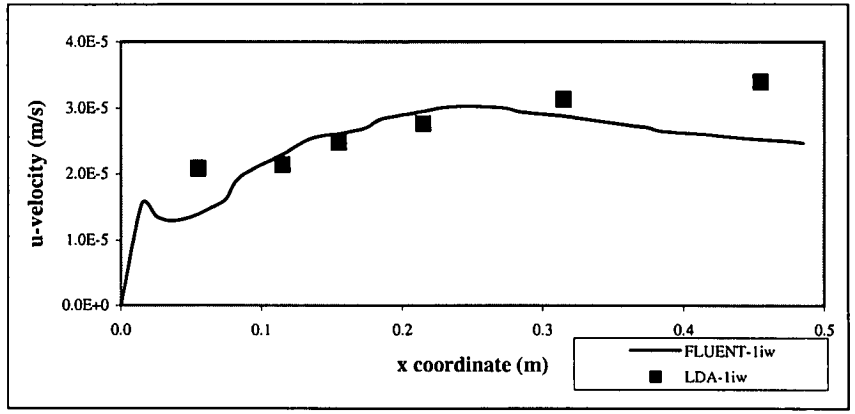

Figure 4.29.2 Kinetic energy: comparison between LDA with FLUENT results (Level C, section 1iw, V=0.05m/s)

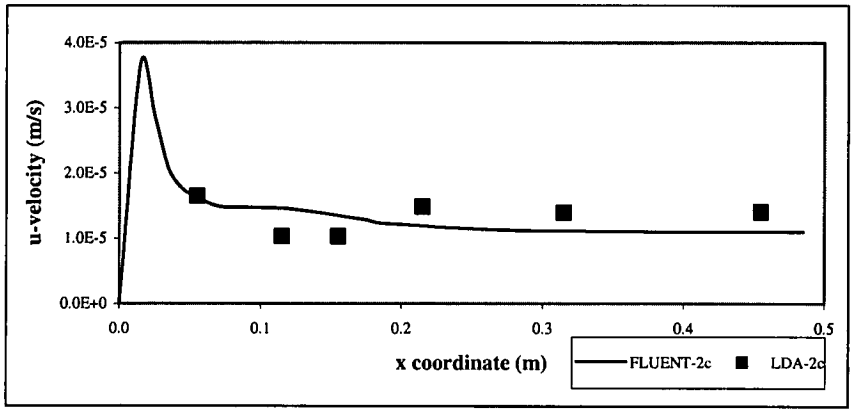

Figure 4.29.3 Kinetic energy: comparison between LDA with FLUENT results (Level C, section 2c, V=0.05m/s)

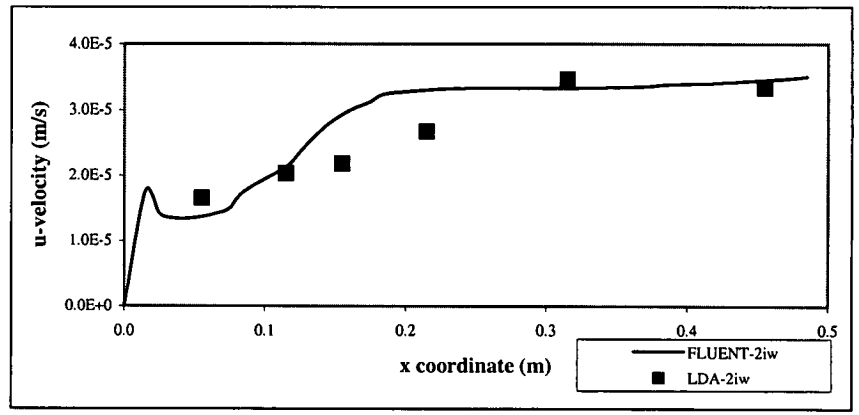

Figure 4.29.4 Kinetic energy: comparison between LDA with FLUENT results (Level C, section 2iw, V=0.05m/s)

4.7 Application to 45mm wide channel flocculator

On the basis of the good fit between the model simulation and the experimental results measured by LDA in the "150mm wide channel", the model application to the 45mm wide channel flocculator for the nominal velocity between 0.035m/s to 0.1m/s, which was mainly used in the flocculation investigation described in Chapter 5, is discussed in this section.

4.7.1 Relationship between turbulence and velocity and the nominal mean velocities

Kinetic energy and velocity for nominal incoming velocities of 0.1, 0.075, 0.065, 0.06, 0.05 and 0.035m/s were firstly computed for a 1.215m long 45mm wide single bend flat channel. The kinetic energy ratios, such as $k_{0.05}/k_{0.035}$, $k_{0.06}/k_{0.035}$, $k_{0.075}/k_{0.035}$, and velocity ratios, such as $v_{0.05}/v_{0.035}$, $v_{0.06}/v_{0.035}$, $v_{0.075}/v_{0.035}$ for the various nominal velocities were calculated. As it was found from the experimental investigation (see Chapter 3), Tables 4.2 and 4.3 show that the kinetic energy and velocity are approximately directly proportional to the nominal velocities. Thus,

$$k_i/k_j \approx \alpha_k V_i/V_j \tag{4.19}$$

$$v_i/v_j \approx \alpha_v V_i/V_j \tag{4.20}$$

-where k_i and k_j are the kinetic energies at the same geometry point in the channels under mean velocities V_i and V_j, v_i and v_j are the instantaneous velocities at the same geometry point in the channels under mean velocities V_i and V_j, α_k and α_v are defined as kinetic energy related constants and velocity related constants, both being subject to the specific setting of the channel. For the 45mm wide flat channel, α_k ranged from 0.95 to 1.16 with a volume weighted average of around 1.03; α_v ranged form 0.974 to 0.991 with a volume weighted average of around 0.99. The x and y coordinates in Tables 4.2 to 4.8 are the same as the settings in the section 4.3.1.

Then the computation was applied to three consecutive sets of ten 45mm wide channels with a bed slope of 1/30 for two different velocity profiles of nominal mean velocity equalling 0.075 and 0.05m/s, for example. The kinetic energy ratio, $k_{0.075}/k_{0.05}$, and the velocity ratio, $v_{0.075}/v_{0.035}$, are tabulated in the Tables 4.4 and 4.5. The ratios 2 to 13 in Tables 4.4 and 4.5 are the width weighted average ratios of kinetic energy between the two different nominal

velocities of 0.075 and 0.05m/s at levels 2 to 13. Here, the level is the same as the setting in section 4.3.2. An approximate relation was found that:

$$k_i/k_j \approx v_i/v_j \approx \alpha_v V_i/V_j \approx \alpha_k V_i/V_j \qquad (4.21)$$

Here, $\alpha_v = \alpha_k = 1.05$. Therefore, knowing the magnitude of kinetic energy and the direction and value of velocity in a specific geometry for one initial velocity profile, the kinetic energy and velocity for any given incoming velocity can be calculated.

Table 4.2. Ratio of kinetic energy to corresponding nominal velocity

Location	y(cm)	Kinetic energy ratio $k_{0.05}/k_{0.035}$	Nominal velocity ratio 0.05/0.035	α_k	Kinetic energy ratio $k_{0.06}/k_{0.035}$	Nominal velocity ratio 0.06/0.035	α_k	Kinetic energy ratio $k_{0.075}/k_{0.035}$	Nominal velocity ratio 0.075/0.035	α_k
	9.0	1.456	1.43	1.019	1.764	1.71	1.032	2.225	2.14	1.038
x=1.02m	7.7	1.420	1.43	0.994	1.704	1.71	0.994	2.134	2.14	0.996
Height	6.3	1.444	1.43	1.011	1.743	1.71	1.019	2.193	2.14	1.023
Weighted	3.6	1.422	1.43	0.996	1.698	1.71	0.988	2.099	2.14	0.980
Average	2.3	1.412	1.43	0.988	1.677	1.71	0.974	2.059	2.14	0.961
	0.9	1.458	1.43	1.021	1.771	1.71	1.039	2.253	2.14	1.052
	9.0	1.467	1.43	1.027	1.784	1.71	1.040	2.264	2.14	1.056
x=0.5m	7.7	1.451	1.43	1.016	1.760	1.71	1.027	2.233	2.14	1.042
Height	6.3	1.423	1.43	0.996	1.704	1.71	0.994	2.122	2.14	0.990
Weighted	3.6	1.498	1.43	1.048	1.839	1.71	1.073	2.361	2.14	1.102
Average	2.3	1.518	1.43	1.063	1.877	1.71	1.095	2.430	2.14	1.134
	0.9	1.419	1.43	0.993	1.692	1.71	0.987	2.094	2.14	0.977
	9.0	1.461	1.43	1.023	1.773	1.71	1.034	2.243	2.14	1.047
x=0.1m	7.7	1.417	1.43	0.992	1.696	1.71	0.989	2.117	2.14	0.988
Height	6.3	1.441	1.43	1.009	1.737	1.71	1.013	2.181	2.14	1.018
Weighted	3.6	1.504	1.43	1.053	1.859	1.71	1.084	2.409	2.14	1.124
Average	2.3	1.576	1.43	1.103	1.990	1.71	1.161	2.646	2.14	1.235
	0.9	1.463	1.43	1.024	1.767	1.71	1.031	2.213	2.14	1.033
	9.0	1.460	1.43	1.022	1.771	1.71	1.033	2.240	2.14	1.045
x=0.05m	7.7	1.417	1.43	0.992	1.697	1.71	0.990	2.120	2.14	0.989
Height	6.3	1.443	1.43	1.010	1.740	1.71	1.015	2.186	2.14	1.020
Weighted	3.6	1.389	1.43	0.972	1.644	1.71	0.959	2.035	2.14	0.950
Average	2.3	1.411	1.43	0.988	1.712	1.71	0.998	2.239	2.14	1.045
	0.9	1.519	1.43	1.063	1.890	1.71	1.102	2.476	2.14	1.155
Volume Weighted Average α_k				1.02			1.03			1.04
		α_k=1.03								

Table 4.3 Ratio of u-velocity to corresponding nominal velocity

Location	Velocity ratio $v_{0.05}/v_{0.035}$	Nominal velocity ratio 0.05/0.035	α_v	Velocity ratio $v_{0.06}/v_{0.035}$	Nominal velocity ratio 0.06/0.035	α_v	Velocity ratio $v_{0.075}/v_{0.035}$	Nominal velocity ratio 0.075/0.035	α_v
x=1.02m, Height & Width Weighted Average	1.416	1.43	0.991	1.699	1.71	0.991	2.124	2.14	0.991
x=0.5m, Height & Width Weighted Average	1.416	1.43	0.991	1.685	1.71	0.983	2.087	2.14	0.974
x=0.1m, Height & Width Weighted Average	1.416	1.43	0.991	1.700	1.71	0.991	2.125	2.14	0.991
x=0.05m, Height & Width Weighted Average	1.405	1.43	0.983	1.686	1.71	0.983	2.089	2.14	0.975
Volume Weighted Average α_v	1.413		0.989	1.692		0.987	2.106		0.983
	α_v=**0.99**								

4.7.2 Relationship between turbulence and velocity and the number of channels

To simplify the calculation of kinetic energy and velocity required to figure out the effect of turbulence on flocculation efficiency, nine successive sets of ten 45mm wide channels rather than one set of eighty-five 45mm wide channels were simulated by FLUENT. The primary task was to find out relations between the consecutive 10 channels in the value of kinetic energy and velocity. Therefore, the very time-consuming calculation of 85 channels can be converted to the relatively easy calculation of 10 channels. The eventual aim was to expose the relation between any two channels in the flocculator in terms of kinetic energy and velocity.

To achieve the above tasks, three sets of 10 channels with nominal incoming velocities of 0.05m/s and 0.1m/s were used. Height weighted average kinetic energy and velocities were calculated for each channel along the channel length at 13 levels. The setting of the levels was described in section 4.3.2. The ratios of the values at the corresponding points in two sets of consecutive 10 channels were computed and are shown in Tables 4.6 to 4.9. "RatioAB-C" in the column 1 of the tables indicates which pair of 10 channel sets are being considered for corresponding points and the water level at which values of velocity and kinetic energy are computed i.e. A equals 1 and 2, B equals A+1, and C equals 2 to 13.

It was found that there is a generally constant ratio between the different two sets of 10 channels in each level.

$$k_1/k_{11}= k_2/k_{12} = k_3/k_{13}=... = k_{10}/k_{20} = k_{11}/k_{21}= k_{12}/k_{22} = ... = k_{20}/k_{30} =\beta_k \quad (4.22)$$

$$v_1/v_{11}= v_2/v_{12} = v_3/v_{13}=... = v_{10}/v_{20} = v_{11}/v_{21}= v_{12}/v_{22} = ... = v_{20}/v_{30} =\beta_v \quad (4.23)$$

Where, k_1 is the kinetic energy at a point in the first channel, k_{11} is the kinetic energy at the corresponding point in the eleventh channel, and so on. v_1 is the u-velocity at a point in the first channel, v_{11} is the u-velocity at the corresponding point in the eleventh channel, and so on. β_k and β_v are defined as the kinetic energy coefficient and the velocity coefficient, both being subject to the specific geometry of the channel and the flow characteristics. For nominal velocity equal to 0.05m/s, the ratio of kinetic energy was mainly in the range of 1.20 to 1.27. The ratio of velocity was generally in this range as well. The volume weighted average ratio was 1.22 for both velocity and kinetic energy. For nominal velocity equal to 0.1m/s, the ratio of kinetic energy was largely between 1.05 to 1.07. Again, the ratio of velocity was 1.05 to 1.07, in general, as well. The volume weighted average ratio was 1.05 for both kinetic energy and velocity.

Next task was to find the relations of kinetic energy and velocity for any two number of channels in a set of ten channels. It was noted that the hydrodynamic characteristics are similar for any two odd and/or even channels in the successive channels. Therefore, the same approach as calculating the ratios for two different sets of 10 channels as above to the calculation of the ratios for two odd and/or even channels within one set of 10 channels was used. This gave a similar relation to that for different sets of 10 channels but different values of the ratios. Tables 4.10 and 4.11 list the ratios of kinetic energy (β_k) and velocity (β_v) for the nominal velocity of 0.05m/s. Using the same approach in calculating the ratios for nominal velocities of 0.035, 0.06, 0.065, 0.075 and 0.1m/s, which were also employed in the flocculation test in this study, it was found that the value of β_k is identical to the value of β_v for any value of this nominal velocity range. Hence, the relationships between velocity and kinetic energy and the number of channels in the hydraulic flocculator can be expressed as follow:

$$u_i/u_{i+2} = \beta_v= k_i/k_{i+2} = \beta_k= \beta \quad (4.24)$$

Table 4.4 Kinetic energy ratios for nominal velocities of 0.075 and 0.05m/s ($k_{0.075}/k_{0.05}$)

x(mm)	11.25	33.75	67.50	112.50	157.50	202.50	247.50	292.50	337.50	382.50	427.50	472.50	517.50	562.50	607.50	652.50	697.50	742.50	787.50	832.50	877.50	922.50	967.50	1012.50	1057.50	1102.50	1147.50	1192.50	1203.75
ratio2	1.78	1.72	1.76	1.88	1.93	1.93	1.89	1.85	1.81	1.79	1.76	1.75	1.73	1.72	1.72	1.71	1.71	1.70	1.70	1.69	1.69	1.68	1.68	1.68	1.67	1.68	1.64	1.68	1.74
ratio3	1.58	1.61	1.64	1.72	1.79	1.82	1.82	1.80	1.78	1.76	1.74	1.72	1.70	1.69	1.68	1.68	1.67	1.66	1.66	1.65	1.65	1.64	1.64	1.64	1.63	1.62	1.60	1.67	1.58
ratio4	1.62	1.62	1.66	1.77	1.86	1.89	1.87	1.83	1.78	1.75	1.73	1.72	1.71	1.71	1.70	1.69	1.69	1.68	1.68	1.67	1.67	1.66	1.66	1.65	1.65	1.65	1.63	1.67	1.65
ratio5	1.63	1.61	1.65	1.78	1.87	1.87	1.83	1.80	1.77	1.75	1.74	1.73	1.72	1.71	1.71	1.70	1.69	1.69	1.68	1.68	1.67	1.67	1.66	1.66	1.65	1.65	1.62	1.66	1.61
ratio6	1.55	1.57	1.56	1.59	1.62	1.65	1.67	1.68	1.68	1.68	1.68	1.67	1.67	1.66	1.65	1.64	1.64	1.63	1.62	1.62	1.61	1.61	1.60	1.60	1.59	1.59	1.57	1.62	1.59
ratio7	1.55	1.56	1.55	1.57	1.58	1.59	1.59	1.59	1.59	1.58	1.58	1.57	1.57	1.56	1.56	1.56	1.55	1.55	1.55	1.55	1.54	1.54	1.54	1.54	1.54	1.54	1.52	1.56	1.55
ratio8	1.53	1.55	1.54	1.56	1.58	1.59	1.59	1.59	1.58	1.57	1.56	1.55	1.54	1.53	1.53	1.52	1.52	1.52	1.52	1.51	1.51	1.51	1.51	1.51	1.51	1.51	1.50	1.54	1.53
ratio9	1.52	1.53	1.53	1.56	1.59	1.60	1.60	1.59	1.58	1.57	1.56	1.55	1.54	1.53	1.52	1.52	1.51	1.51	1.51	1.50	1.50	1.50	1.50	1.50	1.50	1.50	1.49	1.53	1.52
ratio10	1.50	1.53	1.54	1.57	1.59	1.60	1.59	1.59	1.58	1.57	1.56	1.55	1.54	1.54	1.53	1.53	1.52	1.52	1.52	1.52	1.52	1.52	1.52	1.52	1.52	1.52	1.51	1.55	1.53
ratio11	1.51	1.56	1.57	1.59	1.61	1.62	1.62	1.61	1.60	1.60	1.59	1.58	1.58	1.57	1.57	1.56	1.56	1.56	1.55	1.55	1.55	1.55	1.55	1.55	1.55	1.55	1.54	1.53	1.50
ratio12	1.54	1.57	1.56	1.56	1.57	1.57	1.57	1.56	1.56	1.55	1.54	1.53	1.52	1.52	1.51	1.51	1.51	1.50	1.50	1.50	1.50	1.49	1.49	1.49	1.49	1.49	1.47	1.47	1.47
ratio13	1.46	1.46	1.44	1.45	1.46	1.46	1.46	1.46	1.46	1.46	1.47	1.47	1.47	1.48	1.48	1.49	1.49	1.50	1.50	1.51	1.51	1.51	1.51	1.50	1.48	1.46	1.46	1.48	1.44
Height weighted average ($k_{0.075}/k_{0.05}$)	1.55	1.57	1.57	1.60	1.62	1.63	1.64	1.63	1.62	1.61	1.60	1.59	1.59	1.58	1.58	1.57	1.57	1.56	1.56	1.56	1.56	1.55	1.55	1.55	1.55	1.55	1.54	1.57	1.56
0.075/0.05	1.50	1.50	1.50	1.50	1.50	1.50	1.50	1.50	1.50	1.50	1.50	1.50	1.50	1.50	1.50	1.50	1.50	1.50	1.50	1.50	1.50	1.50	1.50	1.50	1.50	1.50	1.50	1.50	1.50
Volume Weighted	1.04	1.05	1.05	1.07	1.08	1.09	1.09	1.09	1.08	1.07	1.07	1.06	1.06	1.05	1.05	1.05	1.04	1.04	1.04	1.04	1.04	1.04	1.04	1.03	1.03	1.03	1.02	1.05	1.04
α_k	$\alpha_k = 1.05$																												

Table 4.5 Velocity ratios for nominal velocities of 0.075 and 0.05m/s ($v_{0.075}/v_{0.05}$)

x(mm)	11.25	33.75	67.50	112.50	157.50	202.50	247.50	292.50	337.50	382.50	427.50	472.50	517.50	562.50	607.50	652.50	697.50	742.50	787.50	832.50	877.50	922.50	967.50	1012.50	1057.50	1102.50	1147.50	1192.50	1203.75
ratio2	1.68	1.63	1.66	1.79	1.89	1.89	1.79	1.78	1.78	1.68	1.68	1.67	1.67	1.67	1.67	1.67	1.67	1.67	1.67	1.57	1.57	1.57	1.57	1.57	1.57	1.57	1.56	1.57	1.57
ratio3	1.58	1.61	1.64	1.67	1.68	1.78	1.78	1.78	1.78	1.68	1.67	1.67	1.67	1.57	1.57	1.57	1.57	1.57	1.55	1.57	1.56	1.56	1.56	1.56	1.56	1.56	1.56	1.57	1.56
ratio4	1.56	1.56	1.57	1.68	1.58	1.79	1.79	1.78	1.68	1.68	1.67	1.67	1.67	1.67	1.67	1.67	1.67	1.67	1.67	1.67	1.67	1.67	1.67	1.67	1.67	1.66	1.66	1.67	1.66
ratio5	1.66	1.56	1.56	1.57	1.68	1.68	1.68	1.68	1.68	1.68	1.67	1.67	1.67	1.67	1.67	1.67	1.57	1.57	1.57	1.57	1.57	1.57	1.57	1.57	1.57	1.57	1.56	1.57	1.56
ratio6	1.55	1.57	1.56	1.59	1.62	1.65	1.67	1.66	1.67	1.67	1.67	1.67	1.67	1.66	1.65	1.64	1.64	1.63	1.62	1.62	1.61	1.61	1.60	1.60	1.59	1.59	1.57	1.62	1.59
ratio7	1.52	1.53	1.53	1.56	1.59	1.60	1.60	1.59	1.58	1.57	1.56	1.55	1.54	1.53	1.53	1.52	1.52	1.52	1.52	1.51	1.51	1.51	1.51	1.51	1.51	1.51	1.50	1.54	1.53
ratio8	1.55	1.56	1.55	1.57	1.58	1.59	1.59	1.59	1.59	1.58	1.58	1.57	1.57	1.56	1.56	1.56	1.55	1.55	1.55	1.55	1.54	1.54	1.54	1.54	1.54	1.54	1.52	1.56	1.55
ratio9	1.53	1.55	1.54	1.56	1.58	1.59	1.59	1.59	1.58	1.57	1.56	1.55	1.54	1.53	1.52	1.52	1.51	1.51	1.51	1.50	1.50	1.50	1.50	1.50	1.50	1.50	1.49	1.53	1.52
ratio10	1.51	1.53	1.55	1.55	1.55	1.59	1.57	1.57	1.56	1.56	1.56	1.55	1.54	1.54	1.53	1.53	1.53	1.53	1.53	1.53	1.53	1.53	1.53	1.53	1.53	1.53	1.53	1.55	1.53
ratio11	1.51	1.56	1.57	1.58	1.58	1.58	1.60	1.60	1.59	1.59	1.59	1.57	1.57	1.57	1.57	1.56	1.56	1.56	1.56	1.56	1.56	1.56	1.56	1.56	1.56	1.56	1.54	1.53	1.50
ratio12	1.55	1.57	1.57	1.56	1.57	1.58	1.58	1.56	1.56	1.55	1.54	1.52	1.52	1.52	1.51	1.51	1.51	1.51	1.51	1.50	1.50	1.49	1.49	1.49	1.49	1.49	1.47	1.48	1.48
ratio13	1.47	1.47	1.47	1.45	1.46	1.46	1.45	1.45	1.46	1.46	1.47	1.45	1.47	1.48	1.48	1.49	1.49	1.50	1.50	1.50	1.51	1.51	1.51	1.47	1.48	1.44	1.44	1.47	1.44
Height weighted average (v_{ave}/v_{ave})	1.55	1.57	1.56	1.59	1.60	1.62	1.62	1.62	1.61	1.60	1.60	1.59	1.58	1.58	1.57	1.57	1.56	1.56	1.56	1.55	1.55	1.55	1.55	1.55	1.55	1.55	1.54	1.57	1.56
0.075/0.05	1.50	1.50	1.50	1.50	1.50	1.50	1.50	1.50	1.50	1.50	1.50	1.50	1.50	1.50	1.50	1.50	1.50	1.50	1.50	1.50	1.50	1.50	1.50	1.50	1.50	1.50	1.50	1.50	1.50
Volume Weighted α_v	1.03	1.05	1.04	1.06	1.07	1.08	1.08	1.08	1.07	1.07	1.07	1.06	1.06	1.05	1.05	1.05	1.04	1.04	1.04	1.04	1.04	1.03	1.03	1.03	1.03	1.03	1.02	1.05	1.04
	$\alpha_v = 1.05$																												

Table 4.6 Summary of velocity ratio of first, second and third 10 channels when initial incoming velocity equals 0.05m/s

x (mm)	11.25	33.75	67.50	112.50	157.50	202.50	247.50	292.50	337.50	382.50	427.50	472.50	517.50	562.50	607.50	652.50	697.50	742.50	787.50	832.50	877.50	922.50	967.50	1012.50	1057.50	1102.50	1147.50	1192.50	1203.75
Ratio12-2	1.290	1.283	1.295	1.326	1.328	1.316	1.302	1.290	1.281	1.274	1.268	1.264	1.261	1.259	1.257	1.255	1.253	1.251	1.250	1.248	1.247	1.246	1.245	1.244	1.244	1.246	1.241	1.128	1.399
Ratio23-2	1.313	1.302	1.311	1.337	1.331	1.316	1.302	1.291	1.283	1.276	1.271	1.267	1.265	1.262	1.260	1.258	1.256	1.255	1.253	1.251	1.250	1.249	1.248	1.248	1.248	1.251	1.249	1.140	1.449
Ratio12-3	1.222	1.226	1.235	1.249	1.256	1.254	1.249	1.242	1.235	1.229	1.225	1.221	1.218	1.216	1.214	1.212	1.211	1.209	1.208	1.206	1.205	1.204	1.203	1.202	1.202	1.201	1.201	1.184	0.965
Ratio23-3	1.233	1.236	1.245	1.257	1.260	1.256	1.248	1.241	1.234	1.228	1.224	1.221	1.218	1.216	1.214	1.212	1.211	1.209	1.208	1.206	1.205	1.204	1.203	1.203	1.203	1.203	1.204	1.183	0.965
Ratio12-4	1.256	1.253	1.266	1.298	1.312	1.304	1.285	1.268	1.258	1.253	1.250	1.249	1.247	1.246	1.244	1.242	1.241	1.239	1.237	1.236	1.234	1.233	1.232	1.231	1.231	1.232	1.230	1.159	1.315
Ratio23-4	1.274	1.269	1.281	1.311	1.317	1.301	1.281	1.268	1.260	1.257	1.254	1.253	1.251	1.249	1.247	1.245	1.243	1.241	1.239	1.238	1.237	1.235	1.234	1.234	1.234	1.236	1.235	1.163	1.343
Ratio12-5	1.213	1.217	1.228	1.246	1.253	1.249	1.240	1.233	1.228	1.225	1.223	1.222	1.220	1.219	1.217	1.215	1.214	1.212	1.211	1.209	1.208	1.207	1.206	1.205	1.205	1.203	1.205	1.206	1.157
Ratio23-5	1.224	1.227	1.238	1.254	1.257	1.250	1.241	1.234	1.230	1.228	1.226	1.224	1.222	1.220	1.218	1.216	1.215	1.213	1.211	1.210	1.209	1.208	1.207	1.206	1.206	1.206	1.207	1.205	1.127
Ratio12-6	1.201	1.200	1.201	1.207	1.212	1.216	1.219	1.220	1.220	1.220	1.219	1.217	1.216	1.214	1.212	1.211	1.209	1.208	1.206	1.205	1.204	1.203	1.202	1.201	1.200	1.199	1.200	1.204	1.210
Ratio23-6	1.208	1.206	1.208	1.214	1.220	1.224	1.226	1.226	1.225	1.224	1.222	1.220	1.218	1.217	1.215	1.213	1.211	1.210	1.209	1.207	1.206	1.205	1.204	1.204	1.203	1.203	1.204	1.208	1.213
Ratio12-7	1.200	1.196	1.194	1.193	1.194	1.195	1.196	1.197	1.198	1.199	1.200	1.200	1.201	1.201	1.202	1.202	1.202	1.202	1.202	1.202	1.202	1.202	1.201	1.201	1.201	1.201	1.200	1.201	1.204
Ratio23-7	1.207	1.202	1.200	1.200	1.201	1.202	1.204	1.205	1.206	1.206	1.207	1.207	1.208	1.208	1.208	1.208	1.208	1.208	1.208	1.208	1.208	1.207	1.207	1.207	1.207	1.207	1.206	1.207	1.211
Ratio12-8	1.199	1.195	1.193	1.192	1.191	1.191	1.192	1.192	1.192	1.192	1.192	1.193	1.193	1.193	1.194	1.194	1.194	1.194	1.195	1.195	1.195	1.196	1.196	1.196	1.196	1.196	1.196	1.196	1.197
Ratio23-8	1.206	1.202	1.199	1.198	1.198	1.198	1.199	1.199	1.199	1.199	1.200	1.200	1.200	1.201	1.201	1.201	1.202	1.202	1.202	1.203	1.203	1.203	1.204	1.204	1.204	1.204	1.204	1.204	1.206
Ratio12-9	1.199	1.196	1.194	1.192	1.191	1.191	1.190	1.190	1.190	1.190	1.190	1.190	1.190	1.190	1.191	1.191	1.191	1.191	1.192	1.192	1.193	1.193	1.193	1.194	1.194	1.194	1.194	1.194	1.193
Ratio23-9	1.207	1.203	1.200	1.198	1.197	1.197	1.197	1.197	1.197	1.197	1.197	1.197	1.197	1.198	1.198	1.198	1.199	1.199	1.200	1.200	1.200	1.201	1.201	1.201	1.202	1.202	1.202	1.202	1.203
Ratio12-10	1.202	1.198	1.195	1.194	1.193	1.193	1.192	1.192	1.192	1.193	1.193	1.193	1.194	1.194	1.194	1.195	1.195	1.195	1.196	1.196	1.196	1.197	1.197	1.197	1.197	1.197	1.197	1.197	1.199
Ratio23-10	1.209	1.205	1.201	1.200	1.199	1.199	1.199	1.199	1.199	1.199	1.200	1.200	1.201	1.201	1.201	1.202	1.202	1.203	1.203	1.203	1.203	1.204	1.204	1.204	1.204	1.204	1.204	1.204	1.206
Ratio12-11	1.198	1.198	1.199	1.199	1.199	1.200	1.200	1.200	1.200	1.200	1.200	1.200	1.200	1.200	1.200	1.200	1.200	1.200	1.200	1.200	1.200	1.199	1.199	1.199	1.199	1.199	1.201	1.205	1.211
Ratio23-11	1.206	1.205	1.205	1.206	1.206	1.206	1.206	1.207	1.207	1.207	1.207	1.207	1.207	1.206	1.206	1.206	1.206	1.206	1.206	1.206	1.205	1.205	1.205	1.205	1.205	1.205	1.207	1.210	1.215
Ratio12-12	1.206	1.205	1.204	1.204	1.204	1.204	1.204	1.204	1.204	1.204	1.204	1.204	1.203	1.203	1.203	1.202	1.202	1.202	1.201	1.201	1.201	1.200	1.200	1.200	1.199	1.200	1.204	1.215	1.209
Ratio23-12	1.214	1.213	1.211	1.210	1.211	1.211	1.211	1.211	1.211	1.210	1.210	1.210	1.209	1.209	1.208	1.208	1.207	1.207	1.207	1.206	1.206	1.206	1.205	1.205	1.204	1.205	1.209	1.216	1.221
Ratio12-13	1.209	1.209	1.208	1.208	1.209	1.209	1.208	1.208	1.208	1.207	1.207	1.206	1.205	1.205	1.204	1.204	1.203	1.202	1.202	1.202	1.201	1.201	1.200	1.200	1.199	1.200	1.205	1.219	1.212
Ratio23-13	1.214	1.213	1.211	1.210	1.211	1.211	1.211	1.211	1.211	1.211	1.210	1.210	1.209	1.209	1.208	1.208	1.208	1.207	1.207	1.206	1.206	1.206	1.205	1.205	1.204	1.205	1.209	1.216	1.222
Height weighted average 12	1.21	1.21	1.21	1.21	1.21	1.21	1.21	1.21	1.21	1.21	1.21	1.21	1.21	1.21	1.21	1.21	1.21	1.21	1.21	1.21	1.21	1.21	1.21	1.21	1.21	1.21	1.21	1.21	1.21
Height weighted average 23	1.22	1.22	1.22	1.22	1.22	1.22	1.22	1.22	1.22	1.22	1.22	1.22	1.22	1.22	1.22	1.22	1.22	1.22	1.22	1.22	1.22	1.22	1.22	1.22	1.22	1.22	1.22	1.22	1.22
Volume Weighted β_v	$\beta_v = 1.22$																												

Table 4.7 Summary of kinetic energy ratio of first, second and third 10 channels when initial incoming velocity equals 0.05m/s

x(mm)	11.25	33.75	67.50	112.50	157.50	202.50	247.50	292.50	337.50	382.50	427.50	472.50	517.50	562.50	607.50	652.50	697.50	742.50	787.50	832.50	877.50	922.50	967.50	1012.50	1057.50	1102.50	1147.50	1192.50	1203.75
Ratio12-2	1.302	1.282	1.295	1.328	1.332	1.320	1.306	1.294	1.284	1.277	1.271	1.266	1.263	1.260	1.258	1.257	1.255	1.253	1.251	1.250	1.248	1.247	1.246	1.245	1.245	1.247	1.241	1.256	1.289
Ratio23-2	1.321	1.301	1.312	1.340	1.335	1.321	1.306	1.295	1.286	1.278	1.273	1.269	1.266	1.264	1.262	1.259	1.257	1.256	1.254	1.252	1.251	1.250	1.249	1.248	1.248	1.251	1.249	1.266	1.307
Ratio12-3	1.237	1.242	1.252	1.279	1.294	1.296	1.290	1.282	1.273	1.266	1.260	1.255	1.251	1.248	1.245	1.243	1.241	1.239	1.237	1.235	1.233	1.232	1.230	1.229	1.228	1.227	1.223	1.241	1.231
Ratio23-3	1.254	1.256	1.266	1.293	1.302	1.300	1.292	1.282	1.273	1.266	1.260	1.256	1.252	1.249	1.246	1.244	1.242	1.240	1.238	1.236	1.234	1.233	1.232	1.231	1.230	1.230	1.227	1.245	1.244
Ratio12-4	1.246	1.244	1.261	1.295	1.313	1.311	1.297	1.282	1.272	1.266	1.262	1.258	1.256	1.254	1.251	1.249	1.247	1.245	1.243	1.241	1.239	1.238	1.237	1.236	1.235	1.235	1.232	1.250	1.252
Ratio23-4	1.261	1.260	1.276	1.309	1.320	1.310	1.294	1.282	1.273	1.268	1.264	1.261	1.258	1.256	1.253	1.251	1.248	1.246	1.244	1.243	1.241	1.240	1.238	1.238	1.238	1.239	1.237	1.258	1.266
Ratio12-5	1.221	1.225	1.237	1.269	1.290	1.291	1.282	1.271	1.262	1.257	1.253	1.251	1.248	1.246	1.243	1.241	1.239	1.237	1.235	1.233	1.231	1.229	1.228	1.227	1.226	1.225	1.220	1.238	1.222
Ratio23-5	1.234	1.238	1.252	1.284	1.298	1.293	1.281	1.271	1.264	1.259	1.256	1.253	1.250	1.247	1.244	1.242	1.240	1.238	1.236	1.234	1.232	1.231	1.229	1.228	1.228	1.227	1.223	1.242	1.234
Ratio12-6	1.210	1.216	1.215	1.228	1.239	1.247	1.251	1.252	1.252	1.250	1.247	1.244	1.241	1.238	1.235	1.232	1.230	1.228	1.226	1.224	1.222	1.221	1.219	1.218	1.217	1.216	1.211	1.230	1.222
Ratio23-6	1.217	1.223	1.224	1.238	1.248	1.255	1.258	1.258	1.256	1.252	1.249	1.245	1.242	1.239	1.236	1.233	1.231	1.229	1.227	1.225	1.223	1.222	1.221	1.220	1.219	1.218	1.214	1.235	1.229
Ratio12-7	1.210	1.215	1.210	1.215	1.219	1.222	1.222	1.221	1.219	1.218	1.216	1.215	1.213	1.212	1.211	1.211	1.200	1.199	1.199	1.199	1.199	1.199	1.199	1.199	1.199	1.199	1.195	1.210	1.208
Ratio23-7	1.216	1.221	1.216	1.222	1.226	1.227	1.227	1.226	1.224	1.223	1.221	1.220	1.219	1.218	1.217	1.216	1.216	1.215	1.214	1.214	1.213	1.213	1.212	1.212	1.211	1.211	1.206	1.223	1.220
Ratio12-8	1.207	1.211	1.208	1.215	1.219	1.221	1.220	1.217	1.214	1.211	1.208	1.206	1.204	1.203	1.201	1.200	1.201	1.201	1.201	1.200	1.200	1.200	1.200	1.201	1.201	1.201	1.198	1.212	1.205
Ratio23-8	1.214	1.218	1.215	1.221	1.225	1.225	1.224	1.221	1.218	1.215	1.213	1.211	1.209	1.208	1.207	1.207	1.206	1.206	1.206	1.206	1.206	1.206	1.206	1.206	1.206	1.207	1.203	1.218	1.217
Ratio12-9	1.202	1.207	1.207	1.215	1.220	1.222	1.220	1.217	1.213	1.210	1.207	1.204	1.202	1.200	1.198	1.197	1.197	1.196	1.196	1.196	1.196	1.196	1.196	1.196	1.196	1.197	1.193	1.207	1.205
Ratio23-9	1.210	1.216	1.214	1.222	1.226	1.226	1.224	1.220	1.217	1.213	1.210	1.208	1.206	1.205	1.204	1.203	1.203	1.203	1.203	1.203	1.203	1.203	1.203	1.204	1.204	1.205	1.201	1.216	1.214
Ratio12-10	1.198	1.208	1.209	1.217	1.221	1.222	1.220	1.217	1.214	1.211	1.208	1.206	1.204	1.203	1.202	1.201	1.201	1.200	1.200	1.200	1.200	1.200	1.200	1.200	1.200	1.201	1.198	1.212	1.204
Ratio23-10	1.205	1.216	1.216	1.223	1.227	1.227	1.224	1.221	1.218	1.215	1.213	1.211	1.210	1.209	1.208	1.208	1.208	1.207	1.207	1.207	1.207	1.207	1.208	1.208	1.208	1.208	1.205	1.220	1.212
Ratio12-11	1.203	1.218	1.217	1.224	1.228	1.230	1.229	1.227	1.224	1.221	1.219	1.217	1.216	1.214	1.213	1.212	1.211	1.211	1.210	1.210	1.209	1.209	1.209	1.208	1.208	1.208	1.205	1.208	1.197
Ratio23-11	1.211	1.227	1.225	1.232	1.236	1.236	1.234	1.232	1.229	1.227	1.225	1.223	1.221	1.220	1.219	1.218	1.217	1.217	1.216	1.216	1.215	1.215	1.215	1.215	1.214	1.214	1.212	1.214	1.203
Ratio12-12	1.208	1.217	1.213	1.214	1.215	1.215	1.214	1.211	1.208	1.205	1.203	1.200	1.198	1.197	1.195	1.194	1.193	1.192	1.192	1.191	1.191	1.190	1.190	1.189	1.189	1.189	1.182	1.184	1.185
Ratio23-12	1.214	1.224	1.219	1.220	1.221	1.220	1.218	1.215	1.212	1.209	1.206	1.204	1.203	1.201	1.200	1.199	1.198	1.197	1.197	1.196	1.196	1.195	1.195	1.194	1.194	1.194	1.187	1.191	1.192
Ratio12-13	1.176	1.189	1.179	1.181	1.187	1.192	1.194	1.195	1.194	1.193	1.192	1.190	1.189	1.188	1.187	1.186	1.185	1.185	1.184	1.184	1.183	1.183	1.182	1.182	1.182	1.180	1.174	1.184	1.186
Ratio23-13	1.184	1.194	1.184	1.187	1.194	1.198	1.200	1.201	1.200	1.198	1.197	1.195	1.194	1.193	1.192	1.191	1.191	1.190	1.189	1.189	1.188	1.188	1.188	1.187	1.187	1.185	1.180	1.192	1.193
Height weighted average12	1.22	1.23	1.22	1.23	1.24	1.24	1.24	1.24	1.24	1.23	1.23	1.23	1.23	1.22	1.22	1.22	1.22	1.22	1.22	1.22	1.22	1.22	1.22	1.22	1.22	1.22	1.21	1.23	1.22
Height weighted average 23	1.23	1.23	1.23	1.24	1.25	1.25	1.25	1.24	1.24	1.24	1.23	1.23	1.23	1.23	1.23	1.23	1.23	1.23	1.22	1.22	1.22	1.22	1.22	1.22	1.22	1.22	1.22	1.23	1.23
Volume weighted β_v	$\beta_v = 1.22$																												

Table 4.8 Summary of kinetic energy ratio of first, second and third 10 channels when initial incoming velocity equals 0.1m/s

x (mm)	11.25	33.75	67.50	112.50	157.50	202.50	247.50	292.50	337.50	382.50	427.50	472.50	517.50	562.50	607.50	652.50	697.50	742.50	787.50	832.50	877.50	922.50	967.50	1012.50	1057.50	1102.50	1147.50	1192.50	1203.75
Ratio12-2	1.062	1.058	1.060	1.068	1.075	1.079	1.081	1.081	1.079	1.076	1.074	1.072	1.070	1.068	1.067	1.066	1.065	1.064	1.064	1.064	1.064	1.064	1.064	1.064	1.064	1.064	1.060	1.060	1.060
Ratio23-2	1.064	1.060	1.064	1.072	1.079	1.083	1.085	1.084	1.081	1.078	1.075	1.073	1.071	1.070	1.069	1.068	1.068	1.067	1.067	1.067	1.067	1.067	1.067	1.067	1.067	1.066	1.063	1.063	1.063
Ratio12-3	1.049	1.052	1.053	1.058	1.064	1.069	1.073	1.075	1.075	1.074	1.073	1.072	1.070	1.069	1.067	1.066	1.065	1.064	1.064	1.063	1.063	1.063	1.063	1.062	1.062	1.062	1.061	1.065	1.054
Ratio23-3	1.051	1.054	1.055	1.061	1.068	1.073	1.076	1.078	1.078	1.076	1.075	1.073	1.072	1.070	1.069	1.068	1.067	1.067	1.066	1.066	1.066	1.065	1.065	1.065	1.065	1.064	1.063	1.068	1.056
Ratio12-4	1.054	1.053	1.055	1.062	1.069	1.075	1.079	1.080	1.079	1.076	1.073	1.070	1.069	1.068	1.067	1.066	1.065	1.065	1.064	1.064	1.064	1.064	1.063	1.063	1.063	1.063	1.062	1.063	1.058
Ratio23-4	1.057	1.056	1.059	1.066	1.074	1.080	1.084	1.084	1.082	1.078	1.075	1.073	1.071	1.070	1.069	1.068	1.068	1.068	1.067	1.067	1.067	1.067	1.067	1.066	1.066	1.066	1.064	1.066	1.061
Ratio12-5	1.051	1.053	1.052	1.057	1.063	1.069	1.074	1.076	1.075	1.073	1.071	1.069	1.068	1.067	1.066	1.065	1.064	1.064	1.063	1.063	1.063	1.062	1.062	1.062	1.062	1.061	1.060	1.064	1.056
Ratio23-5	1.053	1.055	1.055	1.061	1.068	1.074	1.078	1.080	1.078	1.076	1.074	1.072	1.070	1.069	1.068	1.068	1.067	1.067	1.066	1.066	1.066	1.066	1.065	1.065	1.065	1.064	1.063	1.067	1.057
Ratio12-6	1.054	1.055	1.053	1.055	1.058	1.061	1.063	1.065	1.066	1.067	1.068	1.068	1.068	1.067	1.066	1.065	1.064	1.063	1.062	1.062	1.061	1.060	1.060	1.060	1.059	1.059	1.058	1.062	1.060
Ratio23-6	1.056	1.057	1.055	1.058	1.061	1.064	1.067	1.068	1.070	1.070	1.071	1.070	1.069	1.068	1.067	1.066	1.066	1.065	1.064	1.064	1.063	1.063	1.063	1.062	1.062	1.061	1.060	1.064	1.060
Ratio12-7	1.054	1.054	1.054	1.055	1.058	1.060	1.061	1.062	1.062	1.062	1.062	1.062	1.061	1.061	1.060	1.059	1.058	1.057	1.057	1.056	1.056	1.056	1.055	1.055	1.055	1.055	1.054	1.058	1.058
Ratio23-7	1.055	1.056	1.056	1.058	1.061	1.063	1.064	1.064	1.064	1.064	1.063	1.062	1.060	1.059	1.059	1.058	1.057	1.057	1.056	1.056	1.056	1.055	1.055	1.055	1.055	1.055	1.054	1.057	1.056
Ratio12-8	1.053	1.053	1.053	1.055	1.058	1.060	1.062	1.063	1.063	1.062	1.061	1.060	1.059	1.058	1.057	1.056	1.055	1.054	1.053	1.053	1.053	1.053	1.053	1.053	1.053	1.054	1.053	1.057	1.057
Ratio23-8	1.054	1.055	1.055	1.058	1.061	1.063	1.064	1.064	1.063	1.062	1.061	1.060	1.059	1.058	1.057	1.056	1.055	1.054	1.054	1.053	1.053	1.053	1.052	1.052	1.052	1.052	1.051	1.054	1.053
Ratio12-9	1.052	1.052	1.052	1.055	1.058	1.061	1.062	1.063	1.063	1.062	1.060	1.059	1.057	1.056	1.055	1.054	1.053	1.052	1.051	1.051	1.051	1.050	1.050	1.051	1.051	1.051	1.051	1.054	1.054
Ratio23-9	1.053	1.054	1.055	1.058	1.061	1.063	1.064	1.064	1.063	1.062	1.061	1.060	1.059	1.057	1.056	1.055	1.055	1.054	1.053	1.053	1.052	1.052	1.052	1.051	1.051	1.051	1.050	1.053	1.052
Ratio12-10	1.052	1.053	1.053	1.055	1.057	1.059	1.060	1.060	1.060	1.059	1.058	1.057	1.056	1.055	1.054	1.053	1.052	1.052	1.052	1.051	1.051	1.051	1.051	1.051	1.051	1.051	1.050	1.053	1.053
Ratio23-10	1.054	1.055	1.055	1.058	1.060	1.062	1.062	1.062	1.062	1.061	1.060	1.059	1.058	1.057	1.056	1.055	1.055	1.054	1.054	1.053	1.053	1.053	1.053	1.052	1.052	1.052	1.051	1.054	1.053
Ratio12-11	1.049	1.051	1.050	1.052	1.054	1.055	1.056	1.057	1.057	1.056	1.056	1.055	1.055	1.054	1.054	1.053	1.053	1.052	1.052	1.052	1.052	1.051	1.051	1.051	1.051	1.051	1.050	1.053	1.051
Ratio23-11	1.052	1.053	1.053	1.055	1.056	1.058	1.059	1.059	1.059	1.059	1.059	1.058	1.057	1.057	1.056	1.056	1.055	1.055	1.055	1.054	1.054	1.054	1.054	1.053	1.053	1.053	1.052	1.055	1.053
Ratio12-12	1.049	1.052	1.050	1.051	1.053	1.054	1.055	1.056	1.056	1.055	1.055	1.054	1.054	1.053	1.052	1.052	1.051	1.051	1.051	1.050	1.050	1.050	1.050	1.050	1.050	1.049	1.048	1.051	1.049
Ratio23-12	1.051	1.054	1.053	1.054	1.055	1.057	1.058	1.058	1.058	1.058	1.057	1.057	1.056	1.055	1.055	1.054	1.054	1.053	1.053	1.053	1.052	1.052	1.052	1.052	1.052	1.051	1.050	1.052	1.051
Ratio12-13	1.045	1.049	1.047	1.047	1.048	1.049	1.050	1.051	1.051	1.051	1.051	1.051	1.050	1.049	1.049	1.048	1.048	1.048	1.047	1.047	1.047	1.046	1.046	1.046	1.046	1.046	1.044	1.045	1.045
Ratio23-13	1.047	1.051	1.049	1.049	1.050	1.051	1.053	1.053	1.054	1.053	1.053	1.053	1.052	1.051	1.051	1.050	1.050	1.049	1.049	1.049	1.048	1.048	1.048	1.048	1.048	1.047	1.046	1.047	1.046
Height weighted average 12	1.05	1.05	1.05	1.05	1.06	1.06	1.06	1.06	1.06	1.06	1.06	1.06	1.06	1.06	1.06	1.06	1.06	1.05	1.05	1.05	1.05	1.05	1.05	1.05	1.05	1.05	1.05	1.06	1.05
Height weighted average 23	1.05	1.05	1.05	1.06	1.06	1.06	1.06	1.06	1.06	1.06	1.06	1.06	1.06	1.06	1.06	1.06	1.06	1.06	1.05	1.05	1.05	1.05	1.05	1.05	1.05	1.05	1.05	1.05	1.05
Volume weighted β_k	β_k= 1.05																												

Table 4.9 Summary of velocity ratio of first, second and third 10 channels when initial incoming velocity equals 0.1m/s

x (mm)	11.25	33.75	67.50	112.50	157.50	202.50	247.50	292.50	337.50	382.50	427.50	472.50	517.50	562.50	607.50	652.50	697.50	742.50	787.50	832.50	877.50	922.50	967.50	1012.50	1057.50	1102.50	1147.50	1192.50	1203.75
Ratio12-2	1.058	1.058	1.061	1.069	1.075	1.079	1.081	1.080	1.078	1.075	1.073	1.070	1.069	1.067	1.066	1.065	1.064	1.064	1.063	1.063	1.063	1.063	1.063	1.063	1.063	1.063	1.060	1.034	1.068
Ratio23-2	1.061	1.061	1.064	1.073	1.079	1.082	1.084	1.083	1.080	1.077	1.074	1.072	1.070	1.069	1.068	1.067	1.067	1.067	1.067	1.066	1.066	1.066	1.066	1.066	1.066	1.066	1.062	1.032	1.073
Ratio12-3	1.050	1.051	1.053	1.057	1.060	1.063	1.065	1.065	1.064	1.063	1.062	1.061	1.060	1.058	1.057	1.057	1.056	1.056	1.055	1.055	1.055	1.055	1.055	1.055	1.055	1.054	1.054	1.056	1.132
Ratio23-3	1.052	1.054	1.056	1.060	1.063	1.066	1.067	1.067	1.066	1.065	1.064	1.062	1.061	1.060	1.059	1.059	1.058	1.058	1.058	1.058	1.058	1.058	1.058	1.057	1.057	1.056	1.056	1.058	1.102
Ratio12-4	1.054	1.054	1.056	1.061	1.065	1.068	1.069	1.069	1.068	1.065	1.063	1.062	1.060	1.059	1.059	1.058	1.058	1.058	1.058	1.058	1.057	1.057	1.057	1.057	1.057	1.057	1.057	1.058	1.070
Ratio23-4	1.058	1.057	1.059	1.064	1.068	1.071	1.073	1.072	1.070	1.067	1.065	1.064	1.063	1.062	1.061	1.061	1.061	1.061	1.061	1.060	1.060	1.060	1.060	1.060	1.060	1.059	1.059	1.059	1.048
Ratio12-5	1.050	1.051	1.052	1.056	1.060	1.062	1.064	1.063	1.062	1.060	1.059	1.057	1.057	1.056	1.056	1.056	1.056	1.056	1.055	1.055	1.055	1.055	1.055	1.055	1.055	1.055	1.055	1.058	1.067
Ratio23-5	1.053	1.054	1.056	1.060	1.064	1.066	1.067	1.066	1.064	1.062	1.061	1.060	1.059	1.059	1.059	1.059	1.059	1.059	1.059	1.058	1.058	1.058	1.058	1.058	1.058	1.057	1.057	1.060	1.068
Ratio12-6	1.049	1.049	1.049	1.050	1.051	1.052	1.053	1.053	1.054	1.054	1.054	1.054	1.054	1.054	1.054	1.054	1.054	1.054	1.054	1.054	1.054	1.053	1.053	1.053	1.053	1.053	1.053	1.053	1.056
Ratio23-6	1.052	1.052	1.052	1.053	1.054	1.055	1.056	1.056	1.057	1.057	1.057	1.057	1.057	1.057	1.057	1.057	1.057	1.057	1.057	1.056	1.056	1.056	1.056	1.056	1.055	1.055	1.055	1.056	1.057
Ratio12-7	1.049	1.049	1.048	1.048	1.048	1.048	1.048	1.048	1.048	1.048	1.048	1.048	1.049	1.049	1.049	1.049	1.049	1.049	1.049	1.049	1.049	1.049	1.049	1.049	1.049	1.049	1.049	1.049	1.049
Ratio23-7	1.052	1.052	1.051	1.051	1.050	1.050	1.051	1.051	1.051	1.051	1.051	1.051	1.052	1.052	1.052	1.052	1.052	1.052	1.052	1.052	1.052	1.053	1.053	1.053	1.053	1.053	1.052	1.052	1.053
Ratio12-8	1.049	1.049	1.048	1.048	1.048	1.048	1.047	1.047	1.047	1.047	1.048	1.048	1.048	1.048	1.048	1.048	1.048	1.048	1.048	1.047	1.047	1.047	1.047	1.047	1.047	1.047	1.047	1.047	1.046
Ratio23-8	1.052	1.052	1.051	1.051	1.050	1.050	1.050	1.050	1.050	1.050	1.050	1.050	1.050	1.050	1.050	1.050	1.050	1.050	1.050	1.050	1.050	1.050	1.050	1.050	1.050	1.050	1.051	1.050	1.050
Ratio12-9	1.049	1.049	1.048	1.048	1.048	1.047	1.047	1.047	1.047	1.047	1.047	1.047	1.047	1.047	1.047	1.047	1.047	1.047	1.047	1.047	1.047	1.047	1.047	1.047	1.047	1.047	1.047	1.047	1.046
Ratio23-9	1.052	1.052	1.051	1.051	1.050	1.050	1.050	1.050	1.050	1.050	1.050	1.050	1.050	1.050	1.050	1.050	1.050	1.050	1.050	1.050	1.050	1.050	1.050	1.050	1.050	1.050	1.050	1.050	1.048
Ratio12-10	1.049	1.049	1.048	1.048	1.047	1.047	1.047	1.047	1.047	1.047	1.047	1.047	1.047	1.047	1.047	1.048	1.048	1.048	1.048	1.048	1.048	1.048	1.048	1.048	1.048	1.048	1.049	1.048	1.048
Ratio23-10	1.052	1.051	1.051	1.051	1.050	1.050	1.050	1.050	1.050	1.050	1.050	1.050	1.050	1.050	1.050	1.050	1.050	1.050	1.050	1.050	1.050	1.050	1.051	1.051	1.051	1.051	1.051	1.051	1.050
Ratio12-11	1.048	1.048	1.048	1.048	1.048	1.048	1.048	1.048	1.048	1.048	1.048	1.049	1.049	1.049	1.049	1.049	1.049	1.049	1.049	1.050	1.050	1.050	1.050	1.050	1.050	1.050	1.050	1.051	1.052
Ratio23-11	1.050	1.050	1.051	1.051	1.051	1.051	1.051	1.051	1.051	1.051	1.051	1.051	1.051	1.052	1.052	1.052	1.052	1.052	1.052	1.052	1.052	1.052	1.052	1.052	1.052	1.052	1.052	1.053	1.054
Ratio12-12	1.049	1.049	1.049	1.049	1.049	1.049	1.049	1.049	1.049	1.049	1.049	1.049	1.050	1.050	1.050	1.050	1.050	1.050	1.050	1.050	1.050	1.051	1.051	1.051	1.051	1.051	1.051	1.052	1.054
Ratio23-12	1.051	1.051	1.051	1.052	1.052	1.051	1.051	1.052	1.052	1.052	1.052	1.052	1.052	1.052	1.053	1.053	1.053	1.053	1.053	1.053	1.053	1.053	1.053	1.053	1.053	1.053	1.053	1.054	1.056
Ratio12-13	1.048	1.048	1.049	1.049	1.049	1.049	1.049	1.049	1.049	1.049	1.049	1.050	1.050	1.050	1.050	1.050	1.050	1.050	1.050	1.051	1.051	1.051	1.051	1.051	1.051	1.051	1.051	1.052	1.055
Ratio23-13	1.051	1.051	1.051	1.052	1.051	1.051	1.051	1.052	1.052	1.052	1.052	1.052	1.053	1.053	1.053	1.053	1.053	1.053	1.053	1.053	1.053	1.053	1.053	1.053	1.053	1.053	1.053	1.054	1.057
Height weighted average 12	1.05	1.05	1.05	1.05	1.05	1.05	1.05	1.05	1.05	1.05	1.05	1.05	1.05	1.05	1.05	1.05	1.05	1.05	1.05	1.05	1.05	1.05	1.05	1.05	1.05	1.05	1.05	1.05	1.05
Height weighted average 23	1.05	1.05	1.05	1.05	1.05	1.05	1.05	1.05	1.05	1.05	1.05	1.05	1.05	1.05	1.05	1.05	1.05	1.05	1.05	1.05	1.05	1.05	1.05	1.05	1.05	1.05	1.05	1.05	1.05
Volume weighted β_v	β_v =1.05																												

Table 4.10 Summary of kinetic energy ratio (β_k) between channels when initial incoming velocity equals 0.05m/s

x(mm)	11.25	33.75	67.50	112.50	157.50	202.50	247.50	292.50	337.50	382.50	427.50	472.50	517.50	562.50	607.50	652.50	697.50	742.50	787.50	832.50	877.50	922.50	967.50	1012.50	1057.50	1102.50	1147.50	1192.50	1203.75
C1/C3	1.02	1.02	1.02	1.02	1.03	1.03	1.04	1.04	1.04	1.04	1.04	1.04	1.04	1.04	1.04	1.04	1.04	1.04	1.04	1.04	1.04	1.04	1.04	1.04	1.04	1.04	1.00	1.12	1.31
C3/C5	0.98	0.95	0.98	1.02	1.04	1.04	1.04	1.04	1.05	1.05	1.05	1.05	1.05	1.05	1.04	1.04	1.04	1.04	1.04	1.04	1.04	1.04	1.04	1.04	1.04	1.04	1.04	0.98	0.98
C5/C7	1.04	1.06	1.05	1.05	1.04	1.04	1.04	1.04	1.04	1.04	1.04	1.04	1.03	1.03	1.03	1.03	1.03	1.03	1.03	1.03	1.03	1.03	1.03	1.03	1.03	1.03	1.03	1.01	1.01
C7/C9	0.98	0.97	1.02	1.05	1.05	1.05	1.05	1.05	1.05	1.05	1.05	1.05	1.05	1.05	1.05	1.05	1.05	1.05	1.05	1.05	1.04	1.04	1.04	1.04	1.05	1.05	1.04	1.03	1.03
AVG_{odd}	1.01	1.00	1.02	1.04	1.04	1.04	1.04	1.04	1.05	1.05	1.05	1.05	1.04	1.04	1.04	1.04	1.04	1.04	1.04	1.04	1.04	1.04	1.04	1.04	1.04	1.04	1.03	1.04	1.08
C2/C4	1.04	1.05	1.04	1.05	1.04	1.04	1.05	1.05	1.05	1.05	1.05	1.05	1.05	1.05	1.05	1.05	1.05	1.05	1.05	1.05	1.05	1.05	1.05	1.05	1.04	1.03	1.02	1.02	1.01
C4/C6	1.01	1.03	1.03	1.04	1.04	1.04	1.04	1.04	1.04	1.04	1.04	1.04	1.04	1.04	1.04	1.04	1.04	1.04	1.04	1.04	1.04	1.04	1.04	1.04	1.03	1.01	0.99	0.98	1.00
C6/C8	0.97	1.05	1.04	1.04	1.04	1.04	1.04	1.04	1.04	1.04	1.04	1.04	1.04	1.04	1.04	1.04	1.05	1.05	1.05	1.05	1.05	1.03	1.04	1.03	1.05	1.03	1.04	1.04	1.09
AVG_{even}	1.01	1.04	1.04	1.04	1.04	1.04	1.04	1.04	1.04	1.04	1.04	1.04	1.04	1.04	1.04	1.04	1.05	1.05	1.05	1.05	1.05	1.04	1.04	1.04	1.04	1.02	1.02	1.01	1.03
Volume weighted β_k	β_k=1.04																												

Note: 1.C1/C3 is height and width weighted kinetic energy ratio at a specific x coordinate between channel 1 and channel 3, and so on so forth. 2. AVG_{odd} and AVG_{even} are the average value of the ratios for odd number and even number of channels.

Table 4.11 Summary of velocity ratio (β_v) between channels when initial incoming velocity equals 0.05m/s

x(mm)	11.25	33.75	67.50	112.50	157.50	202.50	247.50	292.50	337.50	382.50	427.50	472.50	517.50	562.50	607.50	652.50	697.50	742.50	787.50	832.50	877.50	922.50	967.50	1012.50	1057.50	1102.50	1147.50	1192.50	1203.75
C1/C3	1.04	1.04	1.03	1.03	1.03	1.03	1.03	1.03	1.03	1.03	1.03	1.03	1.03	1.03	1.03	1.03	1.03	1.03	1.03	1.03	1.03	1.03	1.03	1.03	1.03	1.03	1.02	1.12	1.27
C3/C5	1.05	1.05	1.05	1.05	1.04	1.04	1.04	1.04	1.04	1.04	1.04	1.04	1.04	1.04	1.04	1.04	1.04	1.04	1.04	1.04	1.04	1.04	1.04	1.04	1.04	1.04	1.04	1.03	1.02
C5/C7	1.03	1.03	1.03	1.03	1.04	1.04	1.04	1.04	1.05	1.05	1.05	1.05	1.05	1.05	1.05	1.05	1.05	1.05	1.05	1.05	1.05	1.05	1.05	1.05	1.05	1.05	1.05	1.05	1.05
C7/C9	1.06	1.06	1.06	1.05	1.05	1.05	1.05	1.05	1.05	1.05	1.05	1.05	1.05	1.05	1.05	1.05	1.05	1.05	1.05	1.04	1.04	1.04	1.04	1.04	1.05	1.05	1.06	1.17	1.21
AVG_{odd}	1.05	1.05	1.04	1.04	1.04	1.04	1.04	1.04	1.04	1.04	1.04	1.04	1.04	1.04	1.04	1.04	1.04	1.04	1.04	1.04	1.04	1.04	1.04	1.04	1.04	1.04	1.04	1.09	1.14
C2/C4	1.09	1.05	1.04	1.04	1.04	1.04	1.04	1.04	1.04	1.04	1.04	1.04	1.03	1.03	1.03	1.03	1.03	1.03	1.03	1.02	1.02	1.02	1.02	1.01	1.01	1.00	1.02	1.02	0.98
C4/C6	1.00	1.00	1.03	1.03	1.03	1.03	1.03	1.03	1.04	1.04	1.04	1.04	1.04	1.04	1.05	1.05	1.05	1.05	1.06	1.06	1.07	1.07	1.08	1.09	1.10	1.11	1.10	1.10	1.16
C6/C8	1.27	1.18	1.20	1.06	1.06	1.06	1.06	1.06	1.06	1.06	1.06	1.06	1.06	1.05	1.05	1.05	1.05	1.05	1.05	1.05	1.04	1.04	1.03	1.03	1.02	1.01	1.02	1.01	0.98
AVG_{even}	1.12	1.08	1.09	1.04	1.04	1.04	1.04	1.04	1.05	1.05	1.05	1.05	1.04	1.04	1.04	1.04	1.04	1.04	1.05	1.04	1.04	1.04	1.04	1.04	1.04	1.04	1.05	1.04	1.04
Volume weighted β_v	β_v=1.04																												

Note: 1.C1/C3 is height and width weighted velocity ratio at a specific x coordinate between channel 1 and channel 3, and so on so forth. 2. AVG_{odd} and AVG_{even} are the average value of the ratios for odd number and even number of channels.

Where u_i is the instantaneous velocity of a point in the ith channel of the flocculator, u_{i+2} is the instantaneous velocity of the corresponding point in the (i+2)th channel. k_i is the kinetic energy of a point in the ith channel of the flocculator, k_{i+2} is the kinetic energy of the corresponding point in the (i+2)th channel. β has a normal particular value for any flocculator, varying slightly with flow characteristics. Here β equals 1.01, 1.03, 1.04, 1.04, 1.04 and 1.07 respectively for the nominal velocities of 0.1, 0.075, 0.065, 0.06, 0.05, 0.035m/s for the 45mm wide channel with a bed slope of 1/30.

4.8 Conclusion

In this chapter, the use of the computational fluid dynamics package FLUENT to simulate the flow in channels was described and the model and experimental results were compared. The following conclusions were drawn from the CFD modelling study of the channel flow:

1. The FLUENT CFD package enabled the convenient set-up and execution of a three-dimensional mathematical model study of fluid flows in channels. It allowed the basic equations of motion and associated turbulence closure to be solved with relative ease, and the use of the software's various facilities allowed the use of variable finite difference grids so as to minimise demand for computer resources whilst still achieving useful simulation results. Convergence can be enhanced by a judicious choice of underrelaxation factors and the appropriate selection of the solution method.

2. The FLUENT CFD model of the channels was, in most of cases tested, capable of producing results giving a good fit to experimentally determined flow velocities and turbulence shear stresses. Where an accurate fit was not attained, the main features of the measured flow were still reproduced qualitatively.

3. The inlet longitudinal velocity profile is the main influence on the magnitude and distribution of turbulence and velocity in the channels. The transversal and vertical velocities and the turbulence at the flocculator inlet zone can be assumed negligible.

4. Point turbulence kinetic energy and velocity are approximately directly proportional to the nominal average forward flow velocities, with the coefficient of proportionality, α, equal to 1.05 for the nominal velocity ranging from 0.035 to 0.1m/s.

5. The relationships coefficient (β) between the velocity and turbulence and the number of channels varies from 1.01 to 1.07 for the nominal velocities of 0.1 to 0.035m/s. With the relationships found in this study, the flow features (velocities and kinetic energy) at any point in any number of channels for any particular flow rate can be easily obtained by calculating the flow features in only one odd and one even numbered channels.

Chapter 5. Laboratory investigation of flocculation and settling

5.1 INTRODUCTION

Following the laboratory investigation (Chapter 3) and the modelling simulation (Chapter 4) of the flow in the channel flocculator, this Chapter presents the details of the laboratory investigation of flocculation in hydraulic flocculators and flocculent settling performance under various flowrates, flocculation times, coagulants, raw water turbidities and arrangements of settling (section 5.2). Flocculation efficiency is assessed not only in terms of turbidity but also floc's size and density measured by means of the video recording technique (section 5.3). Flow characteristics in the flocculators and settling tanks are identified by tracer studies in order to utilise the appropriate equation(s) described in Chapter 6 to calculate the flocculation efficiency in relation to turbulence. Conclusions of this chapter are given in section 5.4.

Flocculation is a process used in water treatment for aggregation or growth of destabilised colloidal particles, which can be removed through subsequent treatment methods such as sedimentation or filtration. Besides the mechanisms of destabilisation as outlined in Chapter 2, the three major collision (transport) mechanisms of flocculation are:

1. Aggregation resulting from random Brownian movement of fluid molecules (perikinetic flocculation). When particles move in water under Brownian motion, they collide with other particles. On contact, they form large particles and continue to do so until they become too large to be affected by Brownian motion. Perikinetic flocculation is predominant for submicron particles. A large initial concentration of particles in the suspension will cause faster floc formation, since the opportunity for collisions is higher.

2. Aggregation induced by fluid motion (orthokinetic flocculation). Orthokinetic flocculation involves particle movement with gentle motion of water with the result that particles will agglomerate if they come close enough to be within a zone of attractive influence of one another. It also considers that particles have negligible settling velocity, hence the need for agitation of the water, or a turbulence intensity to promote the collisions. The rate of flocculation is proportional to the volume of the zone of influence, the

concentration of particles and the turbulence intensity in a specific range. Too vigorous agitation breaks flocs up and consequently demolishes the flocculation.

3. Differential settling, where flocculation is due to the different rates of settling of particles of different sizes. Larger particles settle faster than smaller particles, which also helps in orthokinetic flocculation and causes further agglomeration.

The two main modes of process operations of creating turbulence used in flocculation are the hydraulic flocculator, where hydraulic energy provides the necessary turbulence intensity, and the mechanical flocculator, where the turbulence is created by mechanical power input. Mechanical flocculators use mechanical mixing devices such as paddles, turbines and propellers and require extensive maintenance. Due to difficulties experienced with these mechanical flocculation techniques, flocculators using hydraulic energy have gained prominence in the developing countries. As well as the advantages of less energy cost, no mechanical or moving parts and therefore less maintenance, hydraulic flocculators offer the significant benefits of plug flow. Although it is criticised for its high head loss and inflexibility of mixing intensity, McConnachie's (1995) and Haarhoff's (1998) researches showed that the hydraulic flocculators are able to be much more flexible and versatile than generally recognised.

The most commonly used hydraulic flocculator is the baffled channel flocculator (Schulz and Okun 1984). It is widely employed in many developing countries and performs efficiently over a wide range of flows. It was also used in this study.

5.2 FLOCCULATION AND SETTLING TEST

The main objectives of this part were to perform an experimental investigation on hydraulic flocculation and settling to study the relationship between the flocculation efficiency and the hydrodynamic parameters describing the internal structure of turbulence, such as velocity and kinetic energy, in the hydraulic flocculator and consequently to assess the settling efficiency. Specifically, this study had the following objectives:

1. Experimental study of flocculation performance under various raw water turbidities, flocculation times, types of coagulant, initial mixings and turbulence intensities resulting from different flowrates, widths of channel flocculator and arrangements of baffles.
2. Laboratory research of flocculent settling in a settling tank with and without tubes against time and location.

3. Development of design criteria and operational considerations for flocculation and settling processes.

5.2.1 Introduction

The experimental work conducted included batch laboratory studies (i.e. Jar test), continuous flow experiments of flocculation and settling, tracer studies of flow characteristics of the flocculators and settling tanks.

The independent variables and measuring parameters of this experimental study is firstly given in section 5.2.2. After that the Jar test, which is described in section 5.2.3, was carried out in order to get the optimum dosages of aluminium sulphate and Moringa oleifera (see section 5.2.2.1) for different initial turbidities prior to the continuous flow flocculation and settling tests. Section 5.2.4 presents the details of experimental procedures and relevant facilities. Tracer studies of the flow characteristics are also represented here. The experimental results of flocculation and settling are given in section 5.2.5.

5.2.2 Independent variables and measured parameters

The independent variables and measured parameters throughout the experiments of flocculation and settling are described in this section. The different conditions for conducting the continuous flow experiments are presented in Table 5.1

Table 5.1 Experimental details of flocculation and settling

Test Group	Nominal velocities v(m/s)	Raw water turbidity (NTU)	Coagulant(mg/l)		Flocculation time (min)	Settling time (min)		Channel Width (mm)	Bed Slope	Mesh injection
			Alum	Moringa oleifera		Normal	Tube			
1	0.035, 0.05, 0.06, 0.065, 0.075 and 0.1	100	25	***	17.2	25	***	45	1/30	YES
2	0.035, 0.05, 0.06, 0.065, 0.075 and 0.1	100	25	***	8.6	25	***	45	1/30	YES
3	0.035, 0.05, 0.06, 0.065, 0.075 and 0.1	100	25	***	4.3	25	***	45	1/30	YES
4	0.035, 0.05, 0.06, 0.065, 0.075 and 0.1	265	50	***	17.2	25	***	45	1/30	YES
5	0.035, 0.05, 0.06, 0.065, 0.075 and 0.1	265	50	***	8.6	25	***	45	1/30	YES
6	0.035, 0.05, 0.06, 0.065, 0.075 and 0.1	265	50	***	4.3	25	***	45	1/30	YES
7	0.035, 0.05, 0.06, 0.065, 0.075 and 0.1	950	80	***	17.2	25	***	45	1/30	YES
8	0.035, 0.05, 0.06, 0.065, 0.075 and 0.1	950	80	***	8.6	25	***	45	1/30	YES
9	0.035, 0.05, 0.06, 0.065, 0.075 and 0.1	950	80	***	4.3	25	***	45	1/30	YES
10	0.035, 0.05, 0.06, 0.065, 0.075 and 0.1	265	***	75	17.2	25	***	45	1/30	YES
11	0.035, 0.05, 0.06, 0.065, 0.075 and 0.1	265	***	75	8.6	25	***	45	1/30	YES
12	0.035, 0.05, 0.06, 0.065, 0.075 and 0.1	265	***	75	4.3	25	***	45	1/30	YES
13	0.035, 0.05, 0.06, 0.065, 0.075 and 0.1	950	***	100	17.2	25	***	45	1/30	YES
14	0.035, 0.05, 0.06, 0.065, 0.075 and 0.1	950	***	100	8.6	25	***	45	1/30	YES
15	0.035, 0.05, 0.06, 0.065, 0.075 and 0.1	950	***	100	4.3	25	***	45	1/30	YES
16	0.035, 0.05, 0.06, 0.065, 0.075 and 0.1	265	50	***	17.2	***	25	45	1/30	YES
17	0.035, 0.05, 0.06, 0.065, 0.075 and 0.1	265	50	***	8.6	***	25	45	1/30	YES
18	0.035, 0.05, 0.06, 0.065, 0.075 and 0.1	265	50	***	4.3	***	25	45	1/30	YES
19	0.035, 0.05, 0.06, 0.065, 0.075 and 0.1	265	50	***	17.2	25	***	45 (baffle)	1/30	YES
20	0.035, 0.05, 0.06, 0.065, 0.075 and 0.1	950	50	***	17.2	25	***	45 (baffle)	1/30	YES
21	0.035, 0.05, 0.06, 0.065, 0.075 and 0.1	265	50	***	17.2	25	***	45	1/30	NO
22	0.035, 0.05, 0.06, 0.065, 0.075 and 0.1	265	50	***	17.2	25	***	150	1/80	YES

5.2.2.1 Independent variables

Experimental dependent variables, turbidity and particle characteristics, such as size, settling velocity and density were determined as the functions of type of coagulant, hydrodynamic condition, flocculation and settling time, arrangement of flocculator and settling tank and spatial location of the reactors, such as settling tank. The principal independent variables in this experiment were the type of coagulant, flowrate, flocculation and settling time, arrangement of flocculator, type of settling tank, the concentration of particles, water temperature and pH.

Type of coagulants used

Two coagulants were used in this study, i.e. alum and Moringa oleifera. Alum is one of the most common and effective coagulants used in water treatment operations. Another reason of the choice was the consideration of comparison with previous investigations (McConnachie, 1995; Haarhoff and Joubert, 1997) of which alum was mostly employed.

Moringa oleifera is a natural coagulant made from crushed seeds of an easily grown tree found in parts of Africa and Asia. The use of Moringa oleifera in this study was to compare it with alum for the flocculation and settling performance, interpret their difference and flocculation mechanisms, and assess its capability as a coagulant. The study of a natural coagulant in this investigation was also because synthetic coagulants are expensive commercial products for developing countries while a regular requirement for a natural coagulant, such as Moringa oleifera, from an easily grown crop can be of considerable economic benefit to rural communities (McConnachie, 1995).

Moringa oleifera has been used in Sudan to precipitate solids, including bacteria, from cloudy and muddy water for centuries (Jahn, 1988). Moringa oleifera seeds were found to be a fast-acting plant coagulant which can be used without health risks, according to toxicological tests carried out in the Federal Republic of Germany (Jahn, 1984). They can clarify not only highly turbid muddy water but also waters of medium and low turbidity which may appear milky and opaque or sometimes yellowish or greyish. It performs better and quicker in warm water (Jahn, 1984).

As with all coagulants, the dosage, turbulence, flocculation and settling time have considerable effects on its efficiency, as does the initial raw water quality (Jahn, 1982).

Concentration of raw water

Three raw water turbidities, 100, 265 and 950 NTU, which represent low, medium and high turbidities, were tested in this study. The high turbidity, 950 NTU rarely occurs in treatment plants, but it might be found in tropical countries when drawing river water after a rainstorm. The medium value (265 NTU) was chosen representing the concentration that is commonly found in water treatment plants. The reason why the very low concentration, 100 NTU, was tested was to compare the results from previous studies (Haarhoff and Joubert, 1997).

Kaolin was the particle chosen for creating the three initial turbidities in all the experiments of flocculation and settling. The choice of particles was based on its availability and wide use by many investigators (Argaman, 1968; Bratby, 1980 and McConnachie, 1991).

Flowrates

Six flowrates, 56.4, 42.3, 36.7, 33.8, 28.2, 19.7 l/min corresponding to the nominal velocities of 0.1, 0.075, 0.065, 0.06, 0.05 and 0.035m/s, were used to create various hydrodynamic conditions. The choice of flowrates was also considered to give a suitable retention time for the flocculation and settling.

Arrangement of the channel flocculator

Two channel widths, 45mm and 150mm were tested for the effect on turbulence intensity and hence on the flocculation efficiency. For the 45mm wide channel flocculator, tests with and without baffles for six flow rates with flocculation times of 4.3, 8.6 and 17.2 minutes were investigated for the difference of hydrodynamic conditions and the degree of flocculation (see Table 5.1). 17.2 minutes is the maximum flocculation time for the flow with nominal velocity of 0.1m/s, whilst 8.6, and 4.3 minutes were chosen for the study of the effect of flocculation time on flocculation efficiency. Two plastic grid baffles 10mm thick with the grid wall 1.5mm thick and openings 12.5mm x 12.5mm were located at one third and two thirds of the length in each of the first 28 channels.

Bed slope

Two longitudinal bed slopes, 1/30 for the 45mm wide channel and 1/80 for the 150mm wide channel flocculator, were adopted in this study, which gave approximately 153mm and 44mm overall slope gain to compensate for the water level drop caused by head loss and so

prevent velocity increase along the flocculator length to prevent floc breakup. Variation of bed slope can be an alternative or additional method of variation of turbulence for coping with the change of inflow rates to be accommodated in the same flocculator in addition to the application of baffles.

Water temperature and pH

There are many interdependent factors influencing the processes of coagulation and flocculation (Amirtharajah and O'Melia, 1990), and, as the main objective here was to investigate the effects of turbulence on the degree of flocculation, only the relevant factors such as the flowrate, retention time and channel arrangement were studied, while the basic chemical parameters, such as water temperature and pH were kept constant. Water temperature was set at 20 ± 0.1^{0}C and pH at 7 ± 0.2 in this study. The effect of water temperature and pH on flocculation can be found in Chapter 2.

Type of settling tank

A tank with and without tubes was used to test the effect of the arrangement of the settling tank on the results of flocculation and settling. The horizontal flow settling tank without tubes was adopted in most of the experiments, and was used for the study of the variation of settling performance with time and location. A tube settling tank is likely to improve efficiency by providing better flow conditions for particle aggregation and flocs settling and shortening the distance a particle must fall prior to removal (Montgomery, 1985). It was used in this research for comparison with the settling tank without tubes in terms of flocculation and settling efficiency.

5.2.2.2 Measured parameters

The main measured parameters in the tests were turbidity, water depth in the flocculator, water temperature and pH. The floc characteristics, such as floc size and floc settling velocity will be described in the section 5.3.

Turbidity

Turbidity was measured at the raw water supply tank, the inlet to the flocculator, the outlet of the flocculator, various positions (see 5.2.4.2) in the settling tank and from the outlet of the settling tank. The measurements at the inlet to the flocculator and the outlet of the settling tank were used for the calculation of flocculation performance.

Turbidity was measured by the Hach 2100N turbidimeter with calibration by the manufacturer's standard suspensions. The measurement is based on the interference of light passing through a water sample. The particles contained in the water cause scattering of the light according to their fineness, shape and size. The turbidimeter is used to measure this effect. Inside this instrument is a light source (a tungsten lamp) which is used to illuminate a bottle containing a sample of the water to be tested. These 20ml sample bottles are made of colourless glass and are kept scrupulously clean, both inside and out. Any bottle that is scratched is not used and before placing the bottle in the turbidimeter, the outside is wiped clean with a cloth to guarantee a grease- and dirt-free surface for the light to strike as it is vital to ensure that the light scattering was due to the suspended particles alone.

A photoelectric detector measures the amount of scattered light at 90^0 to the path of the incident light. An LED display connected to the detector gives an instantaneous readout in Nephelometric Turbidity Units (NTU). The instrument has a wide range of 0-2000 NTU, which covered all of the readings in this study, therefore avoiding the process of dilution of the sample and consequent possibility of errors.

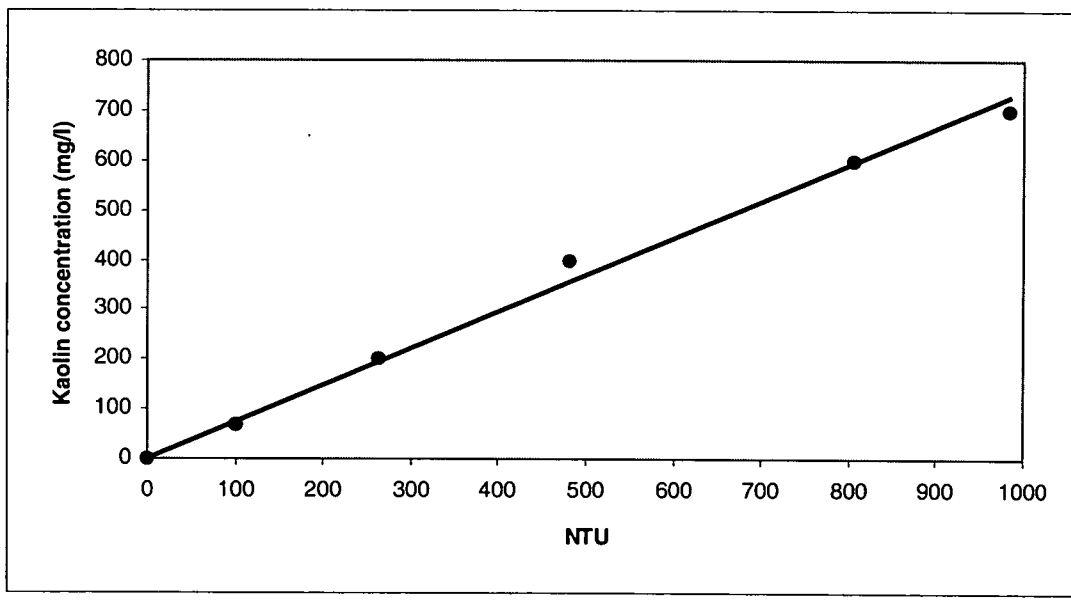

Figure 5.1 Kaolin concentration vs NTU

Before the use of the turbidimeter, it was set to read 10, 20, 50, 75 and 100 NTU for the precalibrated samples. A 20ml sample of the water to be tested was put in one of the sample

bottles and for the final turbidity measurements, if aluminium sulphate was the coagulant used, a drop of concentrated hydrochloric acid was added and the bottle shaken. This was to redissolve any precipitate of aluminium hydroxide which would otherwise give misleadingly high results for the turbidity as the aim was to assess removal of original particles. The sample bottle was wiped clean with a cloth and located in the turbidimeter and the reading noted. The correlation between kaolin concentration and NTU was tested and plotted in Figure 5.1.

pH

pH was measured directly by a pH meter at the supply tank, inlet and outlet of the flocculator to ensure it was 7 ± 0.2 throughout the flocculator for all the tests. Prior to use, the pH meter was calibrated with the manufacturer's samples.

Water depth

Water depth was measured at the head of the first channel and the end of the last channel of the flocculator by a ruler to ±1mm. The water depth was affected by the bed slope, baffling details in the channel and the level of adjustable outlet in the settling tank. The water depth at the head of the first channel was kept as 200 ±1mm giving the nominal forward velocities of 0.1, 0.075, 0.065, 0.06, 0.05, 0.035m/s for the 6 flowrates and 3 retention times of 17.2, 8.6 and 4.3 minutes in the flocculator.

The detailed measurements of water depth are given in section 5.2.6. The head losses in the channel flocculator calculated from the measurements associated the channel bed slope and from the empirical equations are also presented.

5.2.3 Jar test

Jar tests were carried out to determine the optimum dosages of aluminium sulphate ($Al_2(SO_4)_3.14H_2O$) and Moringa oleifera for the removal of suspended matter from synthetic raw waters. These dosages were used in the continuous flow flocculation test for the same synthetic raw waters, although the optimum dosage obtained from the Jar test may not be optimum for the hydraulic flocculators because of the different turbulence generation methods and the limits of the jar test in simulating the hydraulic conditions.

5.2.3.1 Apparatus

The apparatus (Stuart scientific type SW1) consisted of a rack of stirrers, driven by one motor, under which six 1 litre glass beakers were arranged. This allowed six different samples to be tested simultaneously and allowed direct comparison of turbidity removal for different coagulant dosages. The stirrers were flat rectangular blades which could be raised to allow access to the beakers and their speed of rotation was variable using a speed control attached to the motor. An LED display indicated the speed of rotation in revolutions per minutes (rpm). A fluorescent light tube was fixed below the beakers, enabling easy observation of the floc formed. In front of the beakers is a bar to which dosing tubes are attached which allows simultaneous coagulant addition.

5.2.3.2 Experimental procedures

1. To each beaker was added 750ml tap water at 20^0C $\pm 1^0$C plus either 56, 150 or 525 mg kaolin corresponding to 100, 265 and 950 NTU for low, medium and high turbidities respectively The correlation between kaolin concentration and NTU is shown in Figure 5.1. For tests in which aluminium sulphate were to be used as the coagulant, 150 mg sodium bicarbonate and 0.5 ml 5% acetic acid were also added. This increased the alkalinity of the solution as is required to promote formation of aluminium hydroxide floc, and adjusted the pH to around 7.0 ± 0.2, the suitable range of pH for alum coagulant being sweep flocculation (Amirtharajah and Mills, 1982).
2. Beaker contents were stirred at a moderate speed (40rpm) for 10 minutes to ensure a uniform mixture. Using a syringe, 20 ml samples of the solution were taken at a depth of 2 cm below the surface in each beaker to provide measurements of the initial turbidity.
3. To each of the dosing tubes was added various amounts of coagulant, either crushed seeds of Moringa oleifera or aluminium sulphate solution.
4. The coagulant was added to the beakers and this was followed by rapid mixing at 200 rpm for 25 seconds (1 minute, based on suggested procedures (Amirtharajah and O'Melia, 1990), having been found to give poorer results). Turning the bar to which the dosing tubes were attached ensured that the coagulant was added to the central vortex, close to the shaft of the stirrers, thus effecting maximum dispersion in the beakers.
5. The speed of rotation of the stirrers was reduced to 60 rpm for 15 minutes. After this period of slow stirring, the paddles were raised and the beakers were removed to the laboratory bench and the solution was left to settle for 10 minutes.

6. 20ml samples were again taken at a depth of 2 cm in each beaker for the final turbidity measurement.

5.2.3.3 Optimum dosages

The residual turbidity results were plotted against coagulant dosage and the optimum coagulant dosage was that which resulted in the least residual turbidity. The optimum dosages for the two coagulants under three turbidity concentrations are listed in Table 5.2.

Table 5.2 Optimum dosages of alum and Moringa oleifera for three initial turbidities

Turbidity (NTU)	Optimum dosage (mg/l)		pH
	Alum	Moringa Oleifera	
100	25	not tested	7
265	50	75	7
950	80	100	7

5.2.4 Continuous flocculation and settling tests

The continuous flocculation and settling experiments were carried out once the dosage of coagulant was determined by the Jar test. The experimental details are listed in Table 5.1. A flow chart consisting of the hydraulic flocculator, settling tank and supply water tank is shown in Figure 5.2.

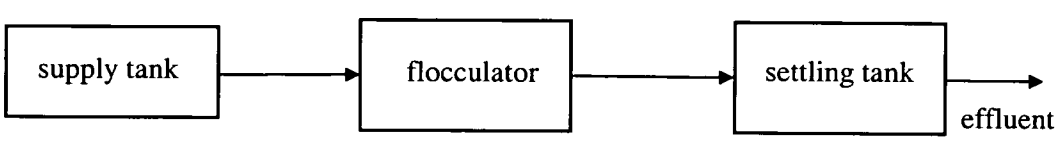

Figure 5.2 Flow chart of flocculation and settling test

5.2.4.1 The hydraulic flocculator and sedimentation tank and Auxiliary devices

Two test units were used for the flocculation test (see Figure 5.3), a horizontal flow flocculator of 85 channels in series each 45mm wide and 1215mm long with 8 mm dividing walls gave effective total flow length of about 103m which was adjustable in longitudinal

slope and into which baffles could be inserted and 22 channels in series each 150mm wide and 1215mm long with 8 mm dividing walls gave effective total flow length of about 26.7m. The water head in the first channel of both units was 200mm. The flocculators used in this study were designed to approximate plug flow conditions, and so were made long, narrow, and rectangular. Two perspex windows were constructed along the channel length (front and rear) to view the growth of flocs.

For the settling tank the effective width is 0.72m without and with tubes, while the effective lengths are 1.96m and 1.72m respectively as shown in Figures 5.4.1 and 5.4.2. The water depth h is dependent on the tested flow rates and settling time. The walls of inlet, outlet and the bottom were made in wood. One side wall was constructed in steel while another was perspex allowing viewing of the particles and their motion in the tank. The inlet zone with a 5mm thick baffle plate was designed to slow down the flocculated water velocity and evenly distribute the flow. The baffle was located 125mm from the bottom of the tank and 100mm from the inlet wall separating the inlet zone from the effective settling area. Four turnable plastic 90^0 bends connected the outlet pipes, which eventually converge into a discharge main. The adjustable elevation of the bends allowed control of the water level in the settling tank and flocculator so that the same initial water head in the flocculator could be achieved for all the tests. A 60mm diameter discharge pipe was constructed at the bottom wall of the tank for the purpose of discharging sediments and emptying the tank.

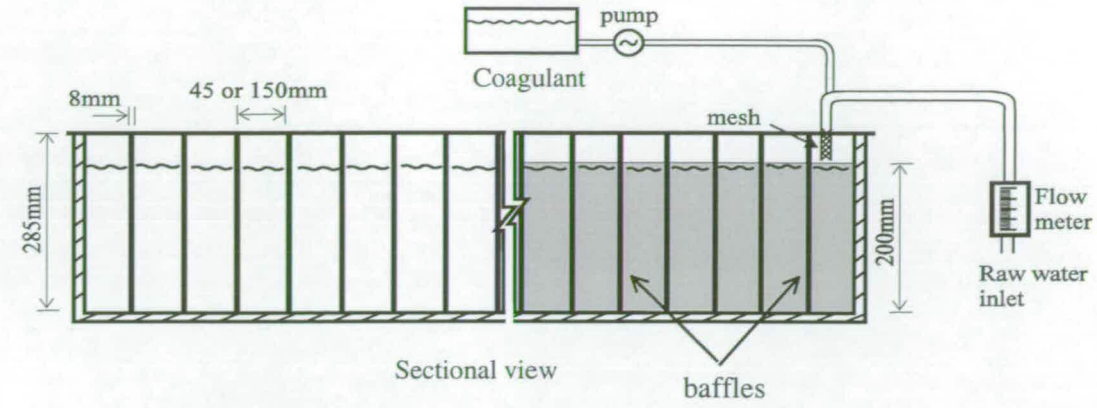

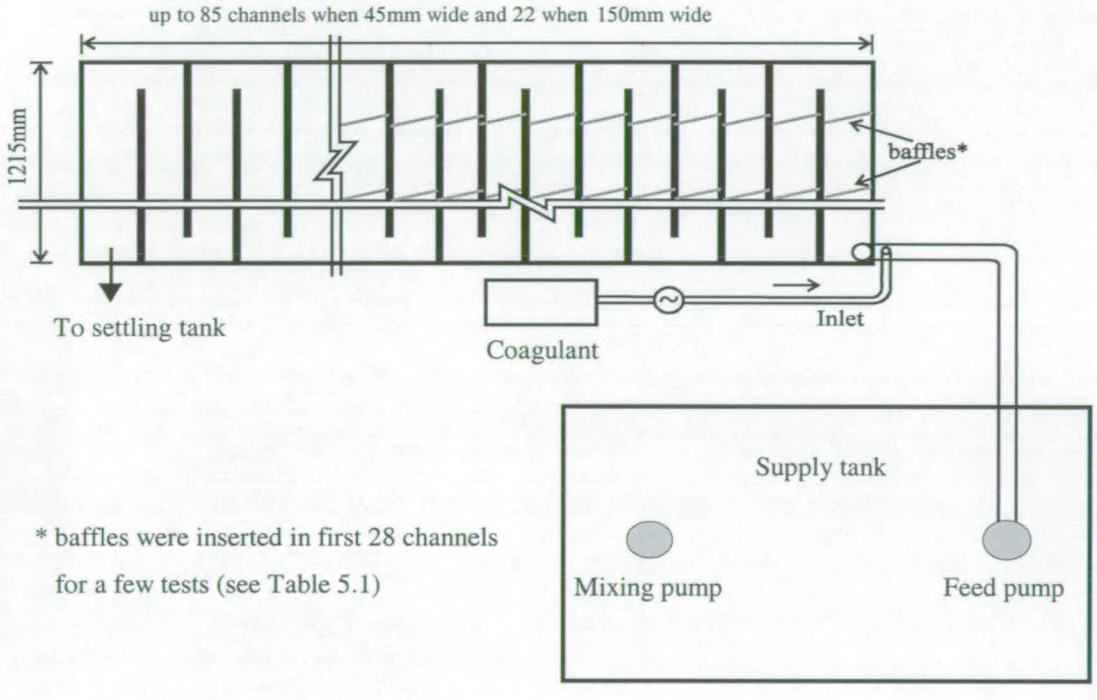

* baffles were inserted in first 28 channels for a few tests (see Table 5.1)

Plan view

Figure 5.3 Hydraulic flocculator and auxiliary devices

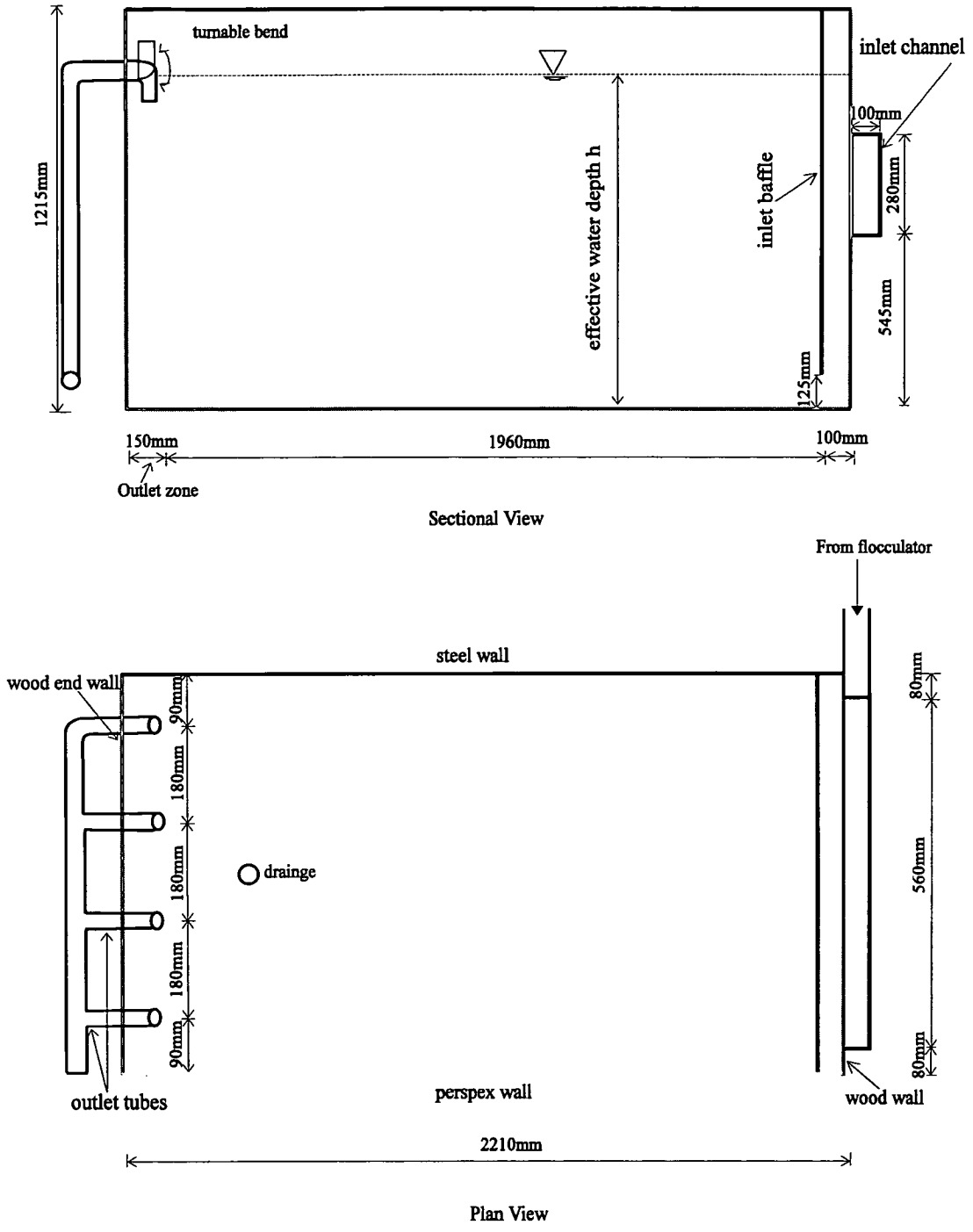

Figure 5.4.1 Settling tank without tubes: Not to scale

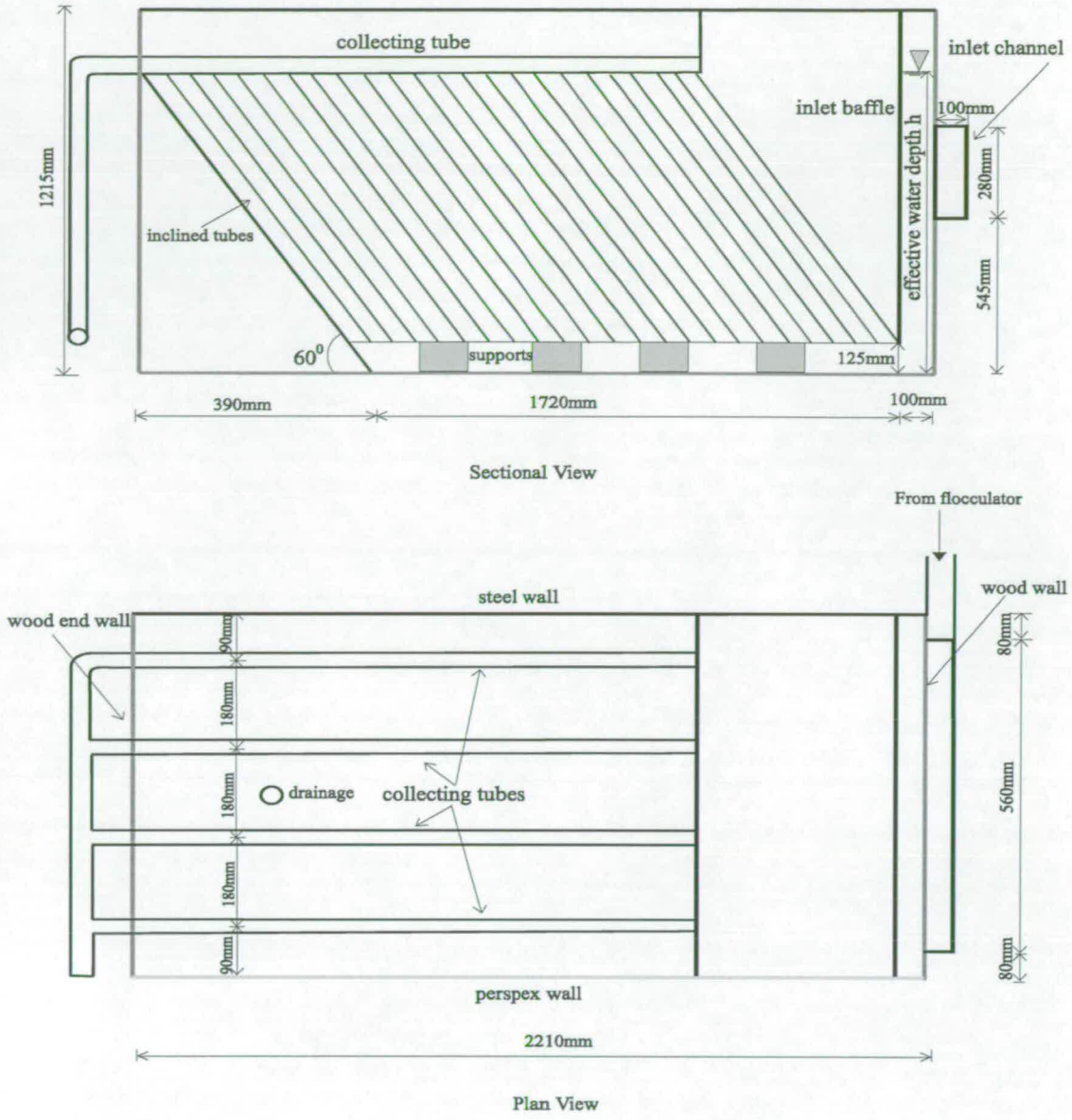

Figure 5.4.2 Settling tank with tubes: Not to scale

For the tank with tubes (see Figure 5.4.2), 4 plastic collecting pipes (1500mm in length, 50mm in diameter) with 16 equally distributed 10mm diameter drilled holes were distributed in the way that water could be evenly collected by each pipe. 286 grey plastic tubes plus 26 clear perspex tubes were located at an angle of 60^0 to the bottom of the tank for the sake of sediment discharge. The clear tubes were arranged immediately adjacent to the perspex side to allow viewing of the flocs inside the tubes. The tubes were 1000mm in length and 50mm in diameter. The effective volume of the tank and the number of the tubes being used were

adjusted by blocking off part of the tank longitudinally according to the flow rates to give a 25 minutes nominal average retention time.

Main auxiliary equipment used in the experiments included a large overhead supply tank with a capacity of approximately 4670 litres; a submerged supplying pump and a mixing pump for equalising the suspension in the supply tank; a 40 litre wood box for dissolving aluminium sulphate and a 55 litre plastic drum for preparation of Moringa oleifera.

5.2.4.2 Experimental procedures

Synthetic water was formed from tap water with added kaolin (75, 200 and 700mg/l corresponding to 100, 265 and 950 NTU for low, medium and high turbidities) + 200 mg/l Na_2HCO_3 (for at least 2meq/l alkalinity (Andreu-Villegas and Letterman, 1978) to promote aluminium hydroxide floc, assuming zero alkalinity in the tap water) + acetic acid to give pH of 7± 0.2 (0.0334 ml concentrated acid per litre water and mixed thoroughly). The alkalinity in water is a buffer system that enables a final coagulation pH in the mixed solution to be achieved by the interaction of the H^+ released by alum hydrolysis with the alkalinity.

In the day before each test run, the 4670 litre steel supply tank was filled with water to about 3/4 full at temperature of about 25^0C with the mixing pump switched on when the tank was about half full. The water temperature was adjusted with hot water supply. Kaolin was weighed out according to the required turbidity (see Figure 5.1), mixed with water in 5 litre beakers and left to soak overnight so that aggregates were broken and a fairly homogeneous suspension of clay particles was produced. The day of the test run, the mixing pump was switched on and hot and cold water completed the filling as necessary to get the final temperature 20 ± 0.1^0C. The kaolin mixture in the beakers was stirred and added to the supply tank. The beakers were rinsed in the supply tank to remove all the kaolin. Bicarbonate was weighed out, added to a 5 litre beaker with warm water and mixed with an electric stirrer until dissolved before being added to the supply tank. Concentrated acetic acid was measured out into a measuring cylinder in a fume cupboard, carefully carried to the supply tank and poured in slowly to avoid fumes. The tank contents were left mixing by the pump for about 30 minutes to even the concentration in the tank before commencing supply to the flocculator and the mixing pump was continuously running throughout the experiment

to assure a constant raw water quality. From the supply tank the turbid water was pumped by a submerged pump into the flocculator via a flow meter. A 30 litre stock solution of 500mg/l (for low turbidity), 1000mg/l (for medium turbidity) or 1700mg/l (for high turbidity) was prepared by dissolving granular aluminium sulphate, $Al_2(SO_4)_3.14H_2O$ of technical grade in tap water. The coagulant was measured and fed by a peristaltic pump into the raw water inlet pipe 300mm before its end with wire mesh inserted into the pipe over this length to increase the agitation. Six runs without the mesh were tested for the effect of initial mixing on flocculation (see Table 5.1). Alum flow rate was adjusted to give a constant dosage of 25, 50 and 85 mg/l for low, medium and high turbidity respectively. For Moringa oleifera as coagulant, 180 g of crushed Moringa oleifera seeds were blended at high speed for 1 minute in warm water and mixed up with cool water in a 55-litre plastic drum to 20 ± 0.1^0C, left to settle for 1.25 hours. Moringa oleifera was drawn from a level in the drum 100 mm above the base and added at rates equivalent to 75 and 100 mg/l for medium and high turbidity as determined by the Jar test.

The number of channels being used in the flocculator and the effective volume of the settling tank were adjusted according to the flow rates to give the predetermined residence times, 17.2, 8.6 and 4.3 minutes for flocculation and 25 minutes for settling.

Effluent from the flocculators passed to the settling tanks with and without tubes where the floc was allowed to settle. Three consecutive samples were taken from a same measuring point, such as the outlet of the settling tank, in a time interval of 5 minutes after the period of flocculation and settling time for each flowrate after the run of the tests. If the turbidity results of these three sample are comparable, it is assumed that the steady-state conditions were reached and samples were taken at the inlet to the flocculator and from the outlet pipes of the settling tanks for assessing flocculation efficiency. To study the flocculent settling against time and location in the settling tank without tubes, samples were also taken for turbidity measurement at 20mm below the water surface, 300 and 600mm from the tank bottom at the quarter, half and full effective length of the settling tank.

5.2.4.3 Flow characteristics of hydraulic flocculators and settling tanks

The flow characteristics of the hydraulic flocculators with 45mm and 150mm wide channels and settling tanks with and without tubes were studied using a tracer technique. The objective of the study for the hydraulic flocculators was aimed at determining whether the

flow states are nearly plug-flow and could be simulated by the modified Argaman's (1968) model, and the study for the settling tanks was intended to explain the effect of the flow characteristics on settling efficiency.

There are two ideal flow states, plug flow and complete mixing flow. Complete mixing flow has the characteristic that the contents of the tank are so completely mixed that the composition is uniform throughout. Therefore the composition of the effluent is the same as that of liquid in the tank; while plug flow, by definition, has no mixing of the fluid in a longitudinal direction and all liquid advances with equal velocity, therefore each fluid particle spends exactly the same amount of time flowing through the reactor, such as flocculator or settling tank (Lo, 1996). For an ideal plug flow, the detention time for each particle can be obtained from the following equation:

$$T = \frac{V}{Q} \qquad (5.1)$$

-where T is the detention time, V is the volume of liquid in the ideal reactor, and Q is the volumetric flowrate of feed.

However, in practice, most real tanks do not behave like the above two flow reactors even though they were intended to be designed as such. Major deviations from the ideal flow conditions are due to density currents caused by temperature and concentration differentials; short circuiting, perhaps because of unevenly manufactured structure of the tank, such as an unbalanced weir outlet of a settling tank; the existence of stagnant regions; and dispersion caused by turbulence and local mixing. The extent of the departure from the ideal can be assessed by residence time distribution analysis with the help of tracer studies.

5.2.4.3.1 The procedures of the tracer study

The tracer study was conducted for the flocculator and settling tank at three flow rates of 56.4, 28.2 and 19.7 l/min, which cover the range of flow rates used in the flocculation and settling tests, correspond to the nominal velocities of 0.1, 0.05 and 0.035m/s according to the following procedures.

1. The effective dimensions of the flocculator and the settling tank were measured. The effective volumes of flocculator for the three flow rates under an average retention time

of 17.2 minutes and the required effective volumes of settling tank under a 25 minutes settling time were calculated.

2. The water was allowed to flow into the tanks for approximately a retention period beyond that required for filling. The tracer, 1600 mg/l methylene blue solution, was injected by pulse as quickly as possible into the liquid entering the flocculator and the settling tank.

3. The progress of the dyed flow was observed and timed along the depth and width of the tank and the visible flow characteristics were recorded with the help of sketches.

4. As the coloured wave approached the outlet, effluent samples of about 5ml were withdrawn and placed in test cells. Samples were collected mainly at a time interval of 1 minute and 0.5 minute around the theoretical retention time during the period from the initial appearance of tracer in the outflow until the effluent concentration approached zero. Sampling was stopped after twice the theoretical retention time.

5. All samples were analysed by a spectrophotometer using 1cm cell at the wavelength of 650nm to obtain percentage light transmission. The calibration chart as shown in Figure 5.5 was used to determine actual dye concentrations.

6. The tank was emptied and refilled with clean water and the procedures repeated for the case of different channel width for the flocculator and arrangements of tubes for the settling tank.

5.2.4.3.2 Results of the tracer study

The ratio, F, of the concentration of the output, c, to the calculated average concentration, C, (i.e. F = c/C) is usually plotted against the ratio of the experimental values of time to the theoretical retention time, t/T, to provide a quantitative measure of tracer study (AWWA, 1990). For the pulse input, the mathematical modelling of the F function for ideal plug flow, complete mixing flow and non-ideal flow can be calculated by a material balance on the tracer and expressed in the following Equations 5.2, 5.3 and 5.4.

$$F = \begin{cases} 0, t \neq T \\ \infty, t = T \end{cases}$$ for plug flow (Lo, 1996); (5.2)

F = exp (-t/T) for complete mixing flow (Lo, 1996); (5.3)

According to Rebhun and Argaman (1965), for non-ideal flow:

$$1 - F(t) = \left[\exp \frac{-1}{(1-p)(1-m)} \right] \left(\frac{t}{T} - p^{1-m} \right) \quad (5.4)$$

where p= fraction of active flow volume acting as plug flow

1-p = fraction of active flow volume acting as mixed flow

m= fraction of total basin volume that is dead space.

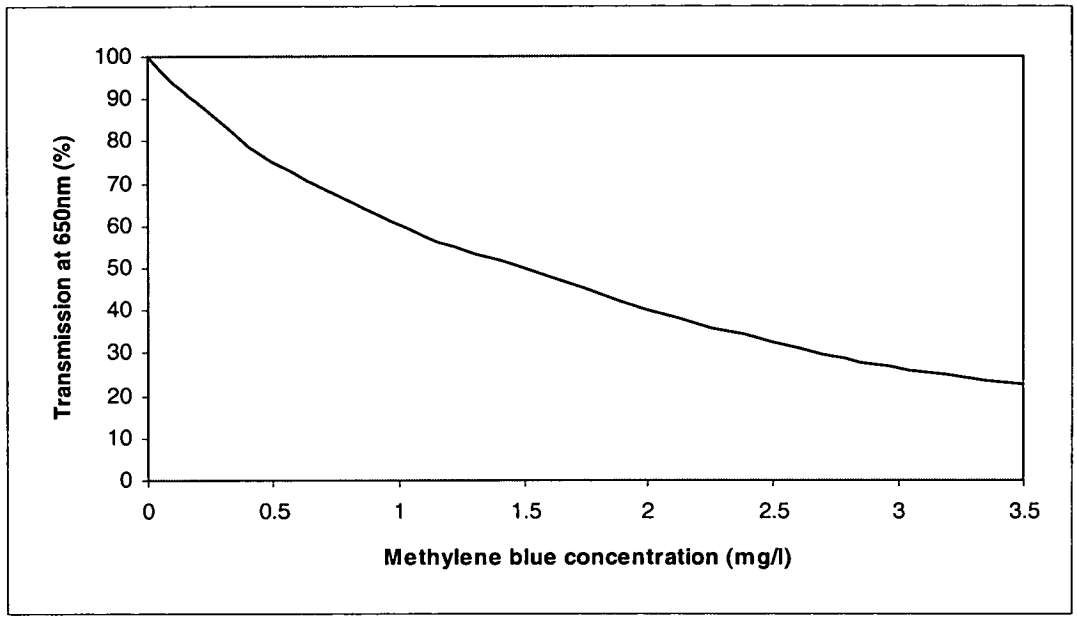

Figure 5.5 Methylene blue concentration vs transmission

The F curves of the above equations for ideal complete mixing, ideal plug flow and real practical flow by pulse input are displayed in Figure 5.6. The theoretical retention time is 17.2 minutes and 4.3 minutes for the 45mm and 150mm wide hydraulic flocculators and 25 minutes for the settling tanks. The F curves of three flowrates corresponding to three nominal velocities, 0.1, 0.05 and 0.035m/s for the flocculators and settling tanks are shown in Figures 5.7.1 to 5.8.6. The mass balance of the tracer was calculated at specific time intervals, the performance indices such as the first tracer efficiency, t_i/T, the modal

efficiency, t_p/T and 50 percent efficiency t_{50}/T are listed in the Tables 5.3.1. T is the theoretical retention time, t_i is the time delay for initial indication of tracer in effluent, t_p the time to reach peak effluent concentration, t_{50}, the time of 50 percent of tracer to have appeared in effluent. The t_{50}/T can also be called the index of mean retention time (AWWA, 1990). Ideally, the above indices approach values of 1.0 under perfect plug-flow conditions.

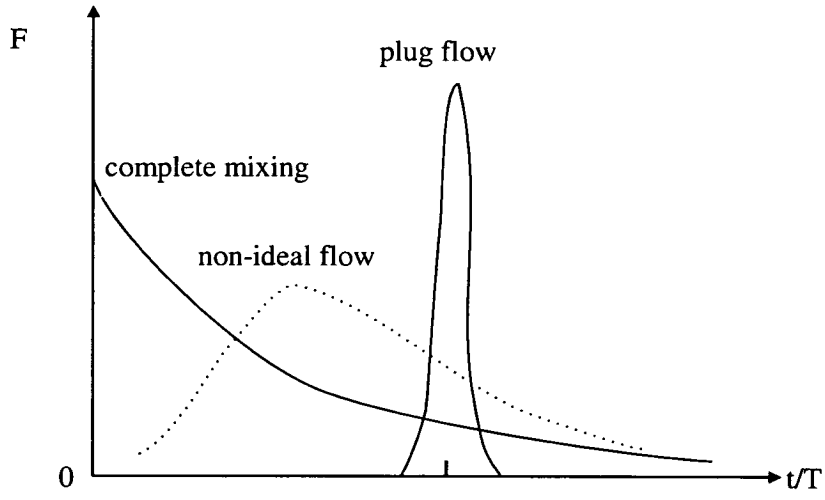

Figure 5.6 Curves of F versus t/T for complete mixing, plug flow, and non-ideal flow

The F curves for the 45mm wide channel flocculator shown in Figures 5.7.1, 5.7.2 and 5.7.3 clearly display that the flows in the flocculator are very close to the ideal plug flow with the index of average retention time of 0.921 to 0.985 as listed in Table 5.3. The flows in the 150mm wide channel flocculator as shown in Figure 5.7.4, 5.7.5 and 5.7.6 are not so close to the ideal plug flow as that in the 45mm wide flocculator but are still close enough with the index of average retention time around 0.9.

The comparison of the flow states in the settling tanks with and without tubes by the tracer study are plotted in the Figures of 5.8.1 to 5.8.6. The Figures show that the flow in the tubes settling tank are closer to ideal plug flow with a 1.02 to 1.07 times ratio of the index of average retention time to the index of the corresponding flow in the tank without tubes. The first tracer efficiency, t_i/T, also called an index of short-circuiting (AWWA, 1990) and the index of modal retention time, t_p/T, show that the time interval for initial indication of tracer in the effluent and the time of the tracer to reach its peak concentration for the tank without

tubes are, respectively, up to 1.3 and 1.1 times earlier than that for the tank with tubes indicating some short circuiting.

Table 5.3.1 Performance indices for hydraulic flocculators and settling tanks

Reactor	Nominal velocity (v) (m/s)	t_i/T	t_p/T	t_{50}/T
45mm wide hydraulic flocculator	0.1	0.27	0.97	0.985
	0.05	0.26	0.93	0.921
	0.035	0.32	0.95	0.952
150mm wide hydraulic flocculator	0.1	0.33	0.89	0.905
	0.05	0.33	0.89	0.906
	0.035	0.33	0.89	0.891
settling tank without tubes	0.1	0.36	0.77	0.833
	0.05	0.29	0.79	0.856
	0.035	0.35	0.83	0.913
settling tank with tubes	0.1	0.42	0.84	0.889
	0.05	0.37	0.87	0.912
	0.035	0.45	0.89	0.935

It can be concluded that both 45mm and 150mm wide channel flocculators are close enough to ideal plug flow reactors to allow their simulation for flocculation performance as plug flow. Flows in the settling tank with tubes are closer to ideal plug flow than those in the tank without tubes.

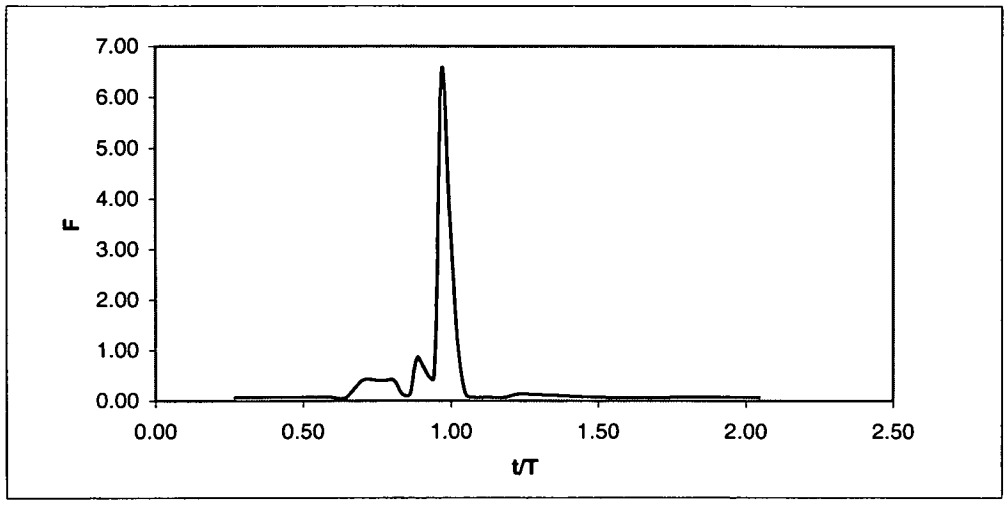

Figure 5.7.1 F curve for 45mm wide hydraulic flocculator (v=0.1m/s)

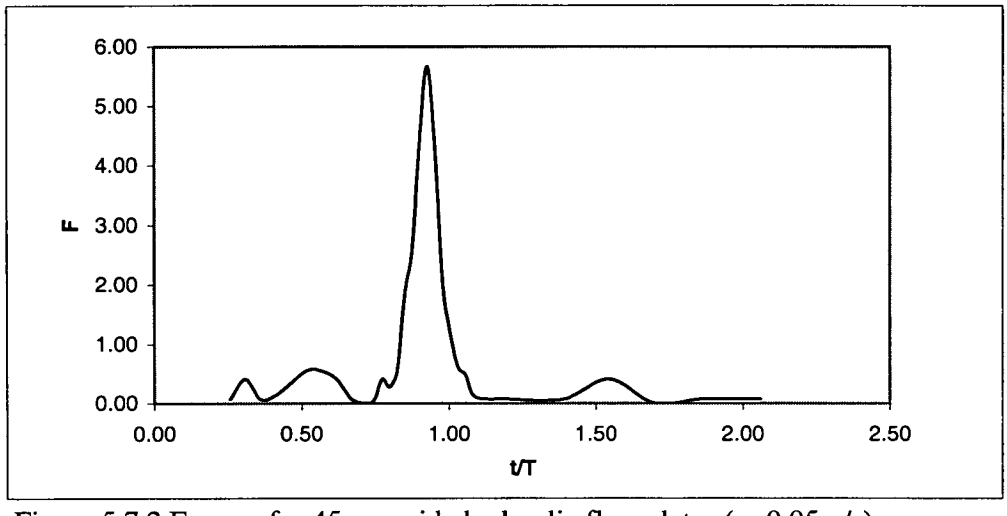

Figure 5.7.2 F curve for 45mm wide hydraulic flocculator (v=0.05m/s)

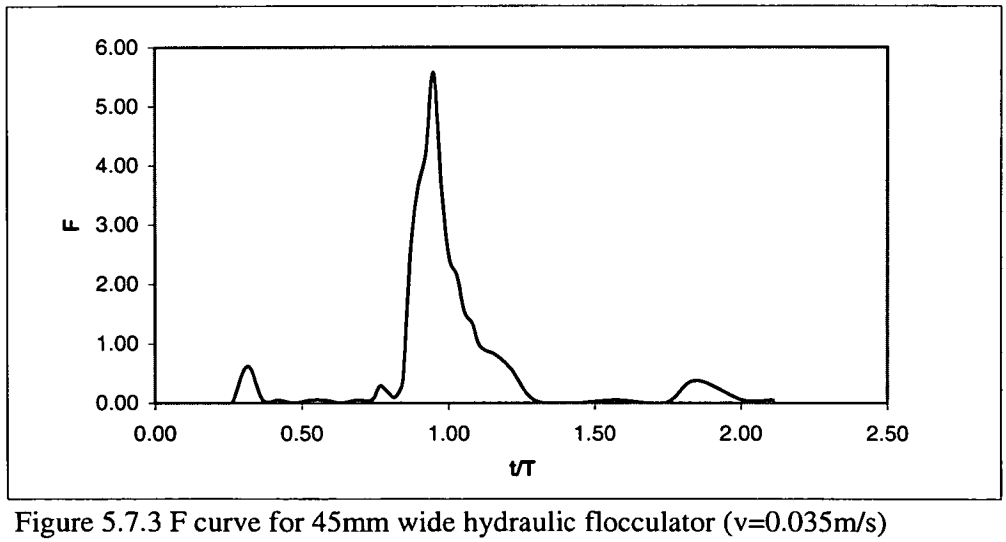

Figure 5.7.3 F curve for 45mm wide hydraulic flocculator (v=0.035m/s)

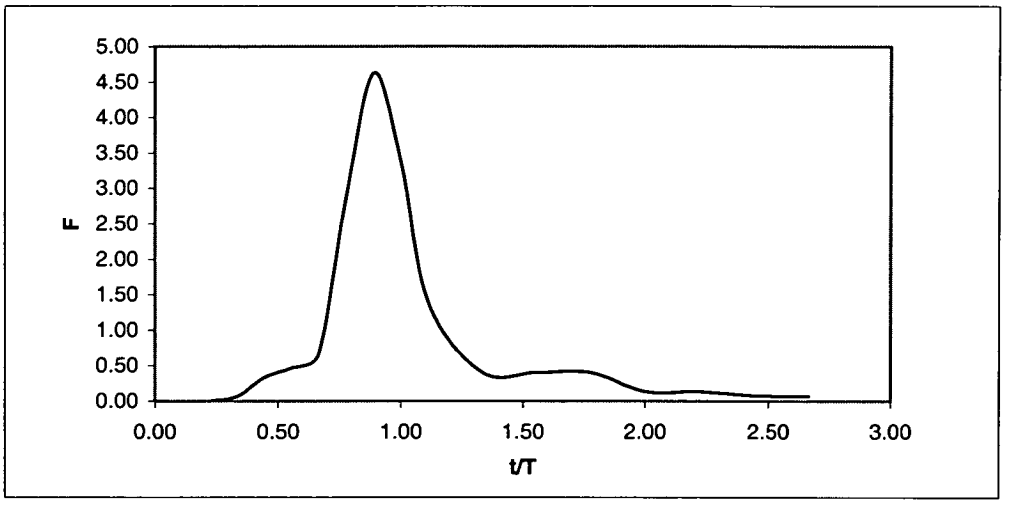

Figure 5.7.4 F curve for 150mm wide hydraulic flocculator (v=0.1m/s)

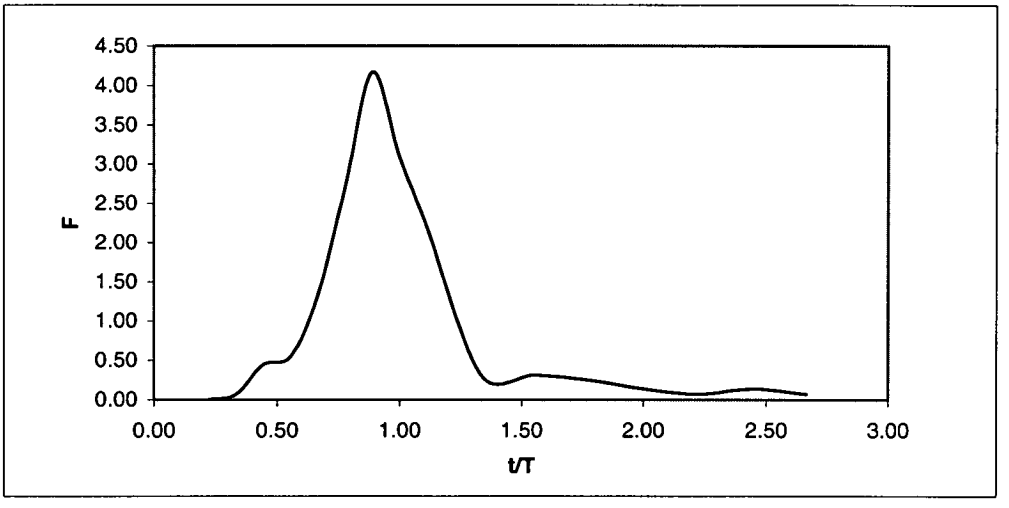

Figure 5.7.5 F curve for 150mm wide hydraulic flocculator (v=0.05m/s)

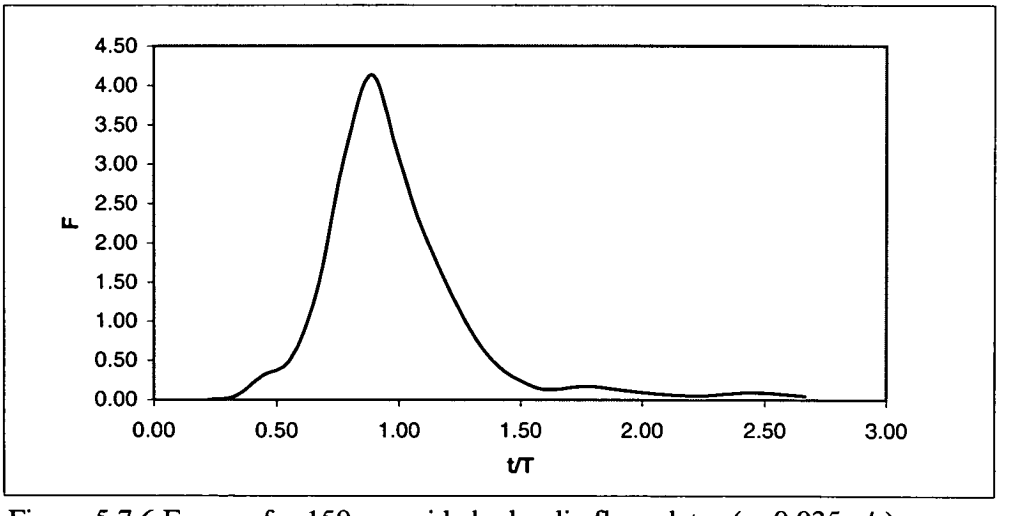

Figure 5.7.6 F curve for 150mm wide hydraulic flocculator (v=0.035m/s)

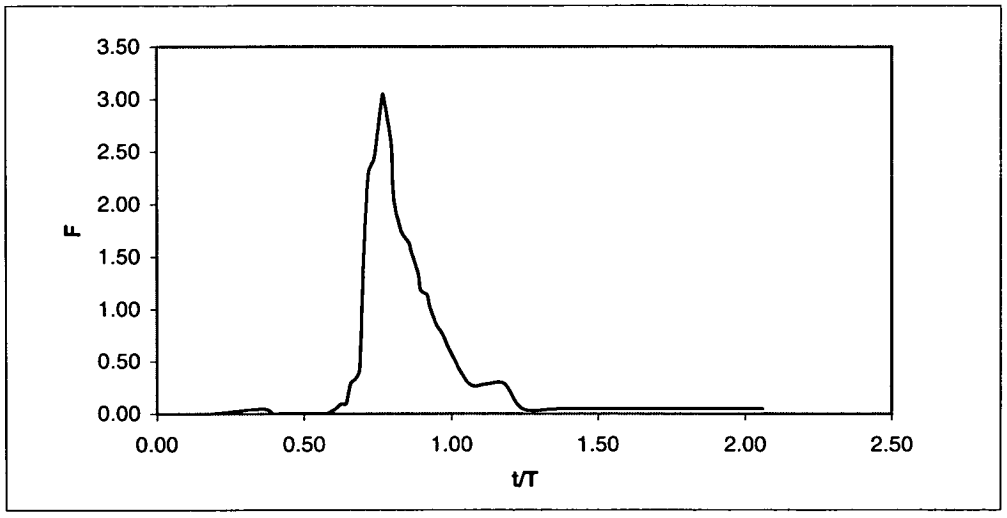

Figure 5.8.1 F curve for settling tank without tubes (v=0.1m/s)

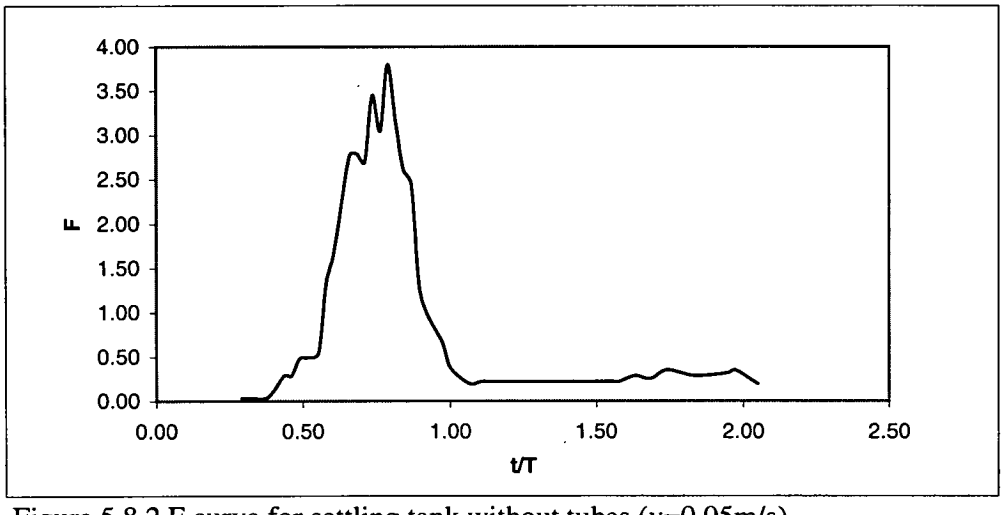

Figure 5.8.2 F curve for settling tank without tubes (v=0.05m/s)

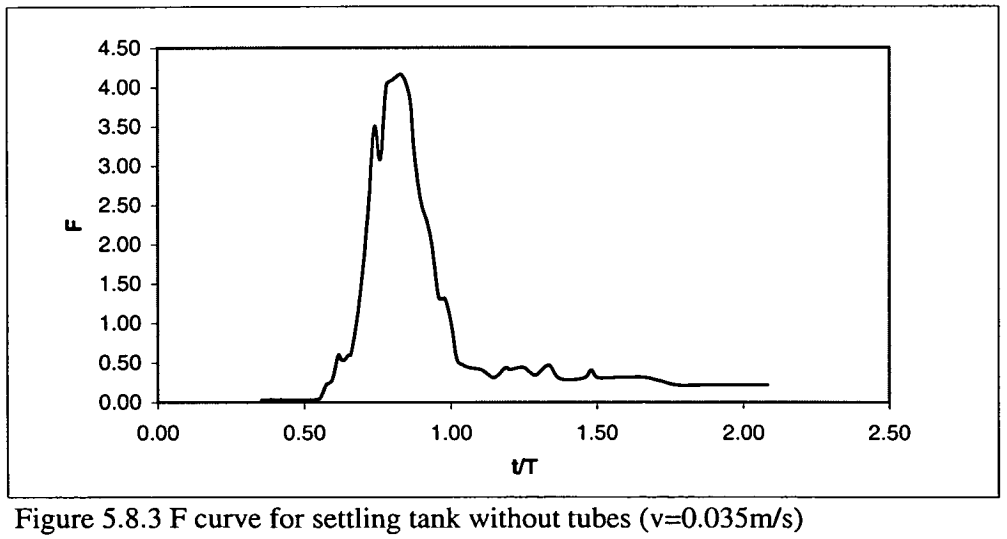

Figure 5.8.3 F curve for settling tank without tubes (v=0.035m/s)

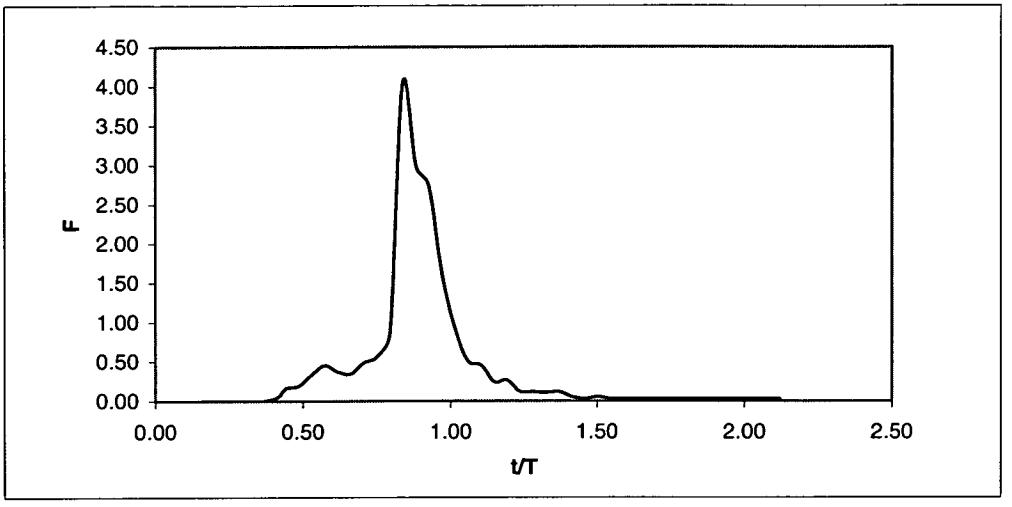

Figure 5.8.4 F curve for settling tank with tubes (v=0.1m/s)

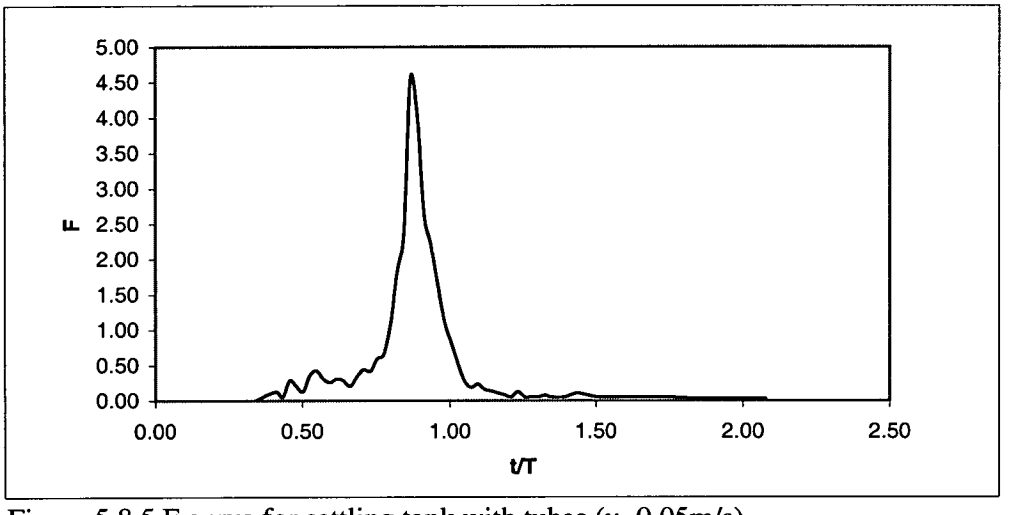

Figure 5.8.5 F curve for settling tank with tubes (v=0.05m/s)

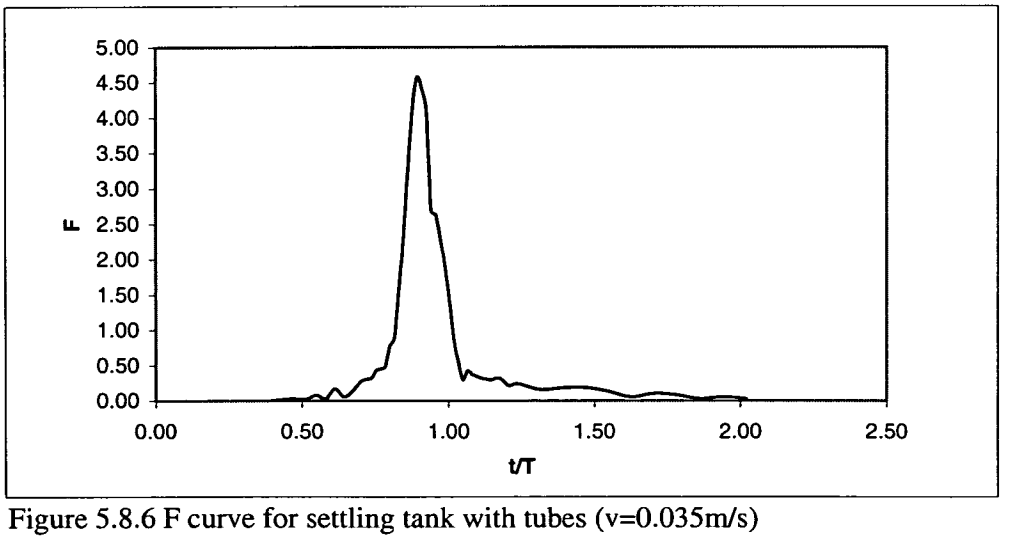

Figure 5.8.6 F curve for settling tank with tubes (v=0.035m/s)

5.2.5 Results of flocculation and settling

Most experiments of flocculation and settling were repeated several times to give reliable data resulting in a maximum ±2 NTU difference in turbidity. The results of 132 tests of flocculation are plotted as volume weighted kinetic energy ($\sum \frac{k_i \forall_i}{\forall}$) vs the turbidity ratio of (n_0/n_1) in Figures 5.9.1. to 5.14.3 and tabulated in Appendix B. The details of the calculation of the volume weighted kinetic energy are given in Chapter 6. n_0 and n_1 represent turbidities of the raw water and flocculated water after 25 minutes settling respectively. Settling spatial and temporal performances are shown in Figures 5.16.1 to 5.17.6 and listed in Tables 5.4.1 and 5.4.2 in section 5.2.5.2.

5.2.5.1 Flocculation

The three different residence times 17.2, 8.6 and 4.3 minutes were employed for various turbulence intensities. Flocculation efficiency was investigated against three raw water turbidities, two coagulants, settling tank with and without tubes and the factors influencing turbulence intensity, such as flowrate, width of channel flocculator, arrangement of baffles and initial mixing. In Figures 5.9.1 to 5.14.3, flocculation results with alum as coagulant are labelled as Alum 100, Alum 265 and Alum 950 for three raw water turbidities of 100, 265 and 950 NTU, Alum 265 (baffle) and Alum 950 (baffle) for the flocculator with baffles, Alum 265 (no mesh) for the inlet pipe without inserted mesh, Alum 265 (150mm) for the flocculator channel of 150mm width, and Tube Alum 265 for the case of the settling tank with tubes, whilst the results with Moringa oleifera as coagulant are labelled as M.Oleifera 265 and 950.

5.2.5.1.1 Effect of turbulence

Increased turbulence accelerates the process of interparticle collisions and formation of flocs. However, if the agitation is too vigorous, then the turbulent shear forces developed will cause floc to break up and consequently demolish the flocculation. Therefore, the analysis for the overall kinetic energy of flocculation needs to combine the processes of aggregation and breakup for a realistic description of the process. In this section, the effect of the turbulence intensity resulting from different flowrates, widths of channel flocculator, arrangements of baffles and initial mixing method on the flocculation are discussed.

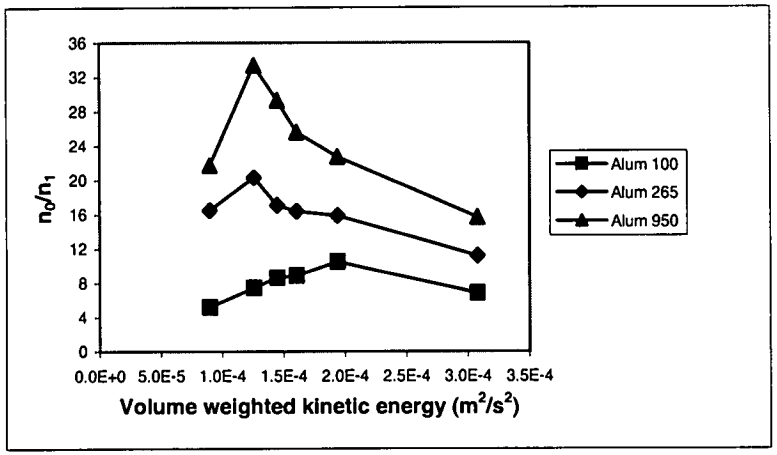

Figure 5.9.1 Flocculation efficiency with three initial concentrations under flocculation time of 17.2 minutes

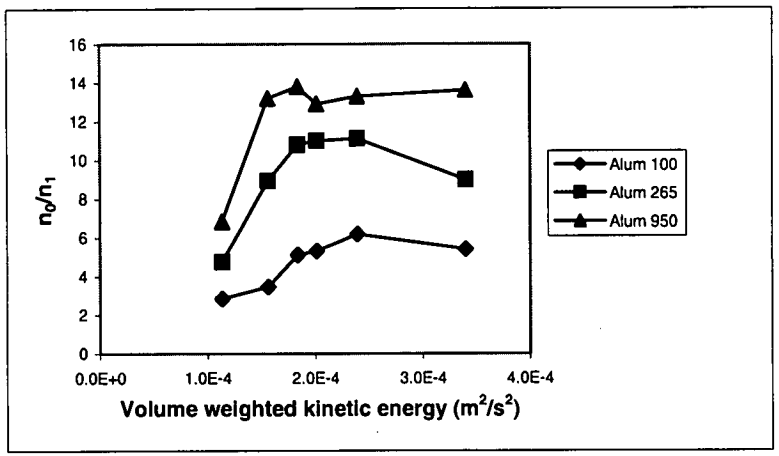

Figure 5.9.2 Flocculation efficiency with three initial concentrations under flocculation time of 8.6 minutes

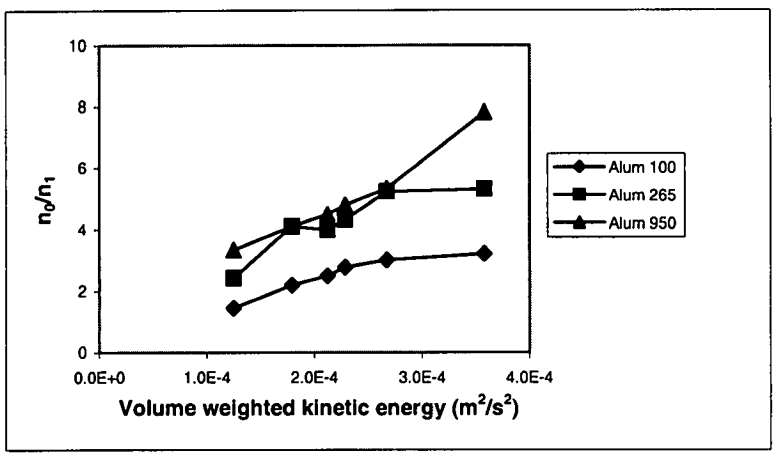

Figure 5.9.3 Flocculation efficiency with three initial concentrations under flocculation time of 4.3 minutes

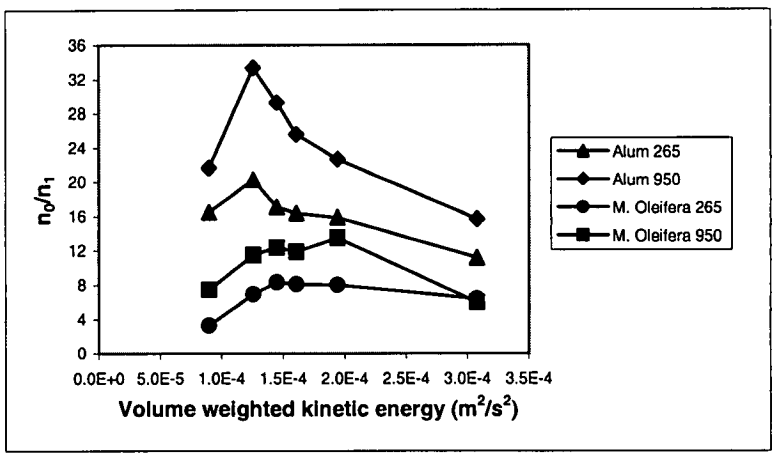

Figure 5.10.1 Flocculation efficiency with Alum and Moringa oleifera under flocculation time of 17.2 minutes

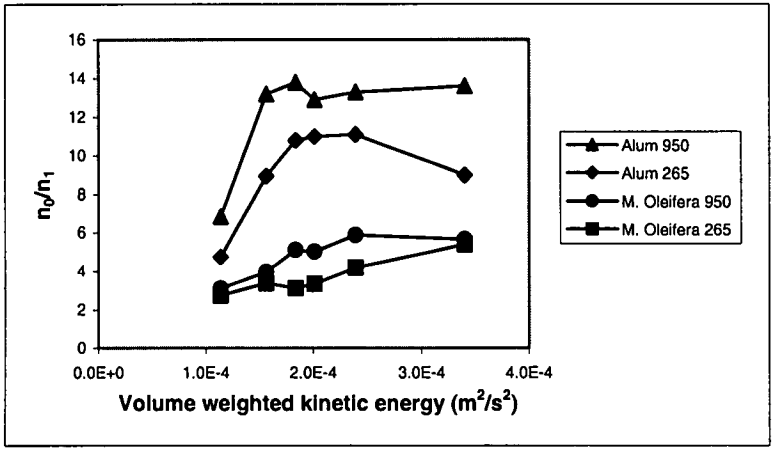

Figure 5.10.2 Flocculation efficiency with Alum and Moringa oleifera under flocculation time of 8.6 minutes

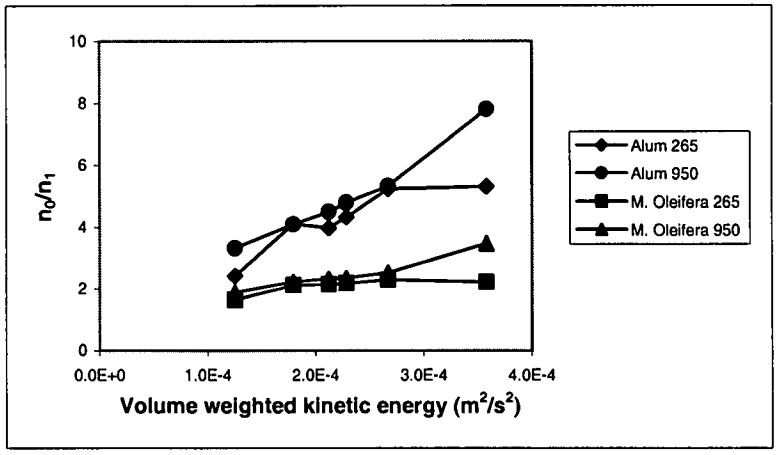

Figure 5.10.3 Flocculation efficiency with Alum and Moringa oleifera under flocculation time of 4.3 minutes

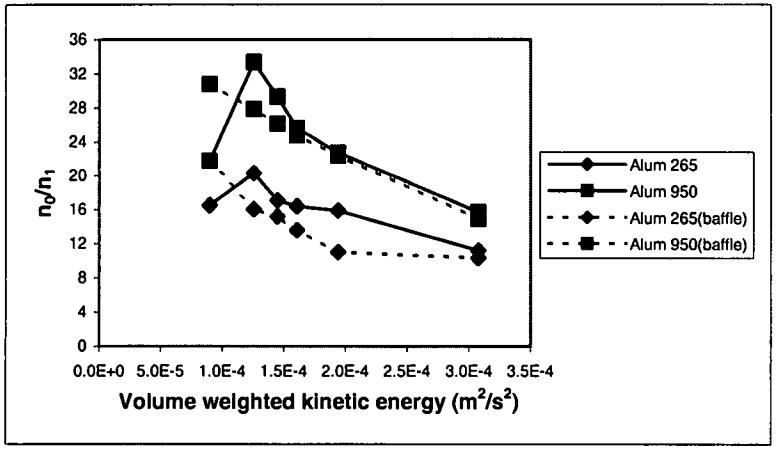

Figure 5.11 Comparison of flocculation efficiency with and without baffles under flocculation time of 17.2 minutes

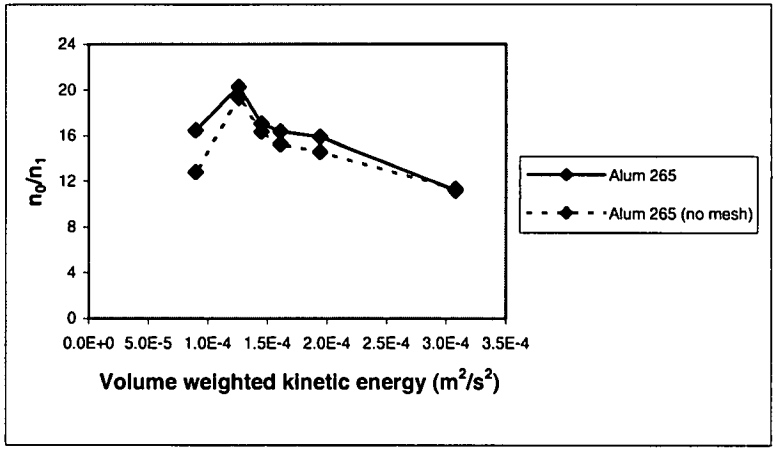

Figure 5.12 Comparison of flocculation efficiency with and without injection of mesh under flocculation time of 17.2 minutes

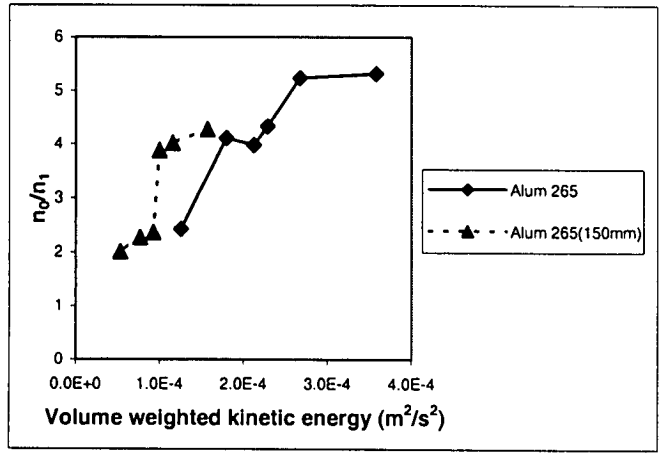

Figure 5.13 Comparison of flocculation efficiency for two channel widths under flocculation time of 4.3 minutes

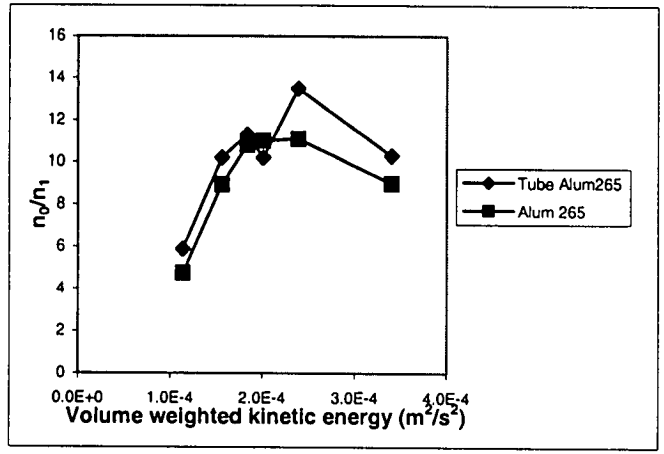

Figure 5.14.2 Flocculation efficiency with and without settling tubes under flocculation time of 8.6 minutes

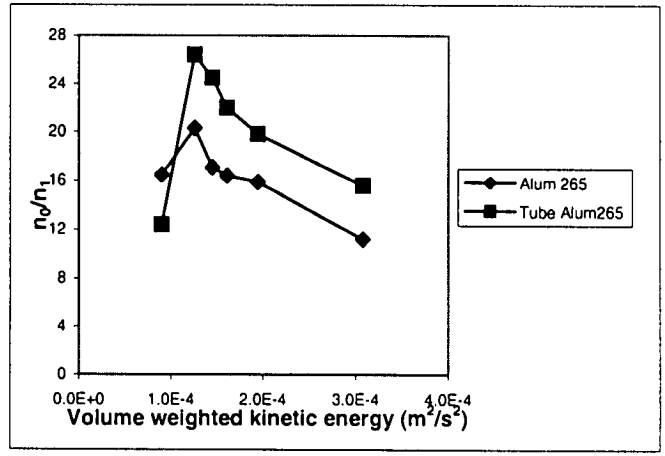

Figure 5.14.1 Flocculation efficiency with and without settling tubes under flocculation time of 17.2 minutes

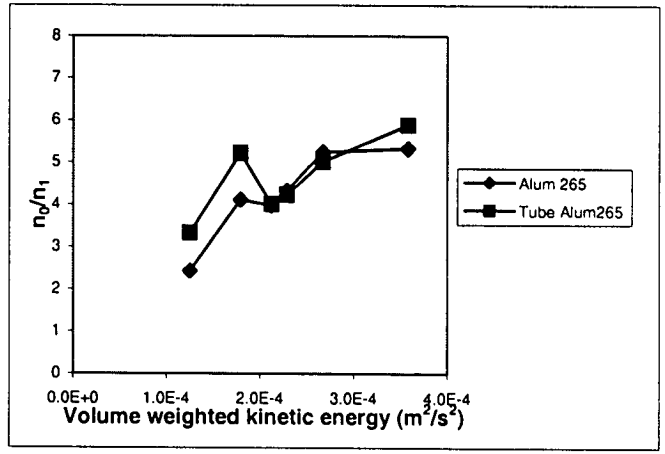

Figure 5.14.3 Flocculation efficiency with and without settling tubes under flocculation time of 4.3 minutes

The effect of flow rate

Six flow rates corresponding to six nominal velocities and various values of kinetic energy as listed in Tables B1, B2 and B3 of Appendix B were tested for the relation between turbulence and flocculation. Figures 5.9.1 to 5.10.3 show the relations for three raw water turbidities, three flocculation times and two coagulants. It is clearly displayed that flocculation efficiency increases as the turbulence intensity quantified by turbulence kinetic energy increases up to a limit beyond which the degree of flocculation decreases for alum treatment for 17.2 and 8.6 minutes and Moringa oleifera for 17.2 minutes. For lower retention times of 4.3 minutes for alum and 4.3 and 8.6 minutes for Moringa oleifera "breakup" of floc is not evident, presumably due to inadequate time for floc formation. The experimental results respond to the theory of flocculation described in Chapter 2 in quality and agree well in quantity with the numerical simulations of turbulence in relation to flocculation in Chapter 6.

Arrangement of baffles

As shown in Figure 5.3, 56 plastic grid baffles of 10mm thick with the grid wall 1.5mm wide and openings 12.5mm x 12.5mm were inserted across the first 28 flocculator channels (i.e. two per channel placed at one-third and two-thirds points along the channel), for the experimental conditions of test groups 19 and 20 as listed in Table 5.1. Results of the flocculation efficiencies with and without baffles are tabulated in Tables B1 and B4 of Appendix B and plotted in Figure 5.11. For the plots in Figure 5.11, the kinetic energies for the unbaffled channel have been calculated (see Chapter 4) but those for the baffled channel are taken to have the same value for each flow velocity as the unbaffled one. However, the plot with baffles shows a forward displacement of kinetic energy indicating that additional turbulence was generated by the baffles and therefore the equality of kinetic energy is not correct. The additional turbulence induced by the grid baffles allows the flocculation efficiency to be improved when there is insufficient agitation and flocculation time. As shown in the Figure 5.11, the flocculation efficiencies are increased by 32% and 42% for the lowest kinetic energy, i.e. the lowest flow rate corresponding to the nominal velocity of 0.035m/s for medium and high raw water turbidities respectively after insertion of the baffles. Baffles of various types, dimensions and arrangements inserted across the flocculator channels can be expected to provide a range of optimum turbulence intensities in terms of flocculation efficiency for different flow rates and can allow the required retention time to be reached over a shorter length by backing the flow up within the flocculator. So,

the application of baffles will allow for variations in inflow rates to be accommodated in the same flocculator while maintaining effective flocculation.

.

Initial mixing.

The purpose of rapid mixing is to disperse coagulants uniformly throughout the raw water as quickly as possible in order to destabilise the colloidal particles present in the raw water (i.e. neutralise the negative charges around the colloid surface). Theoretical and experimental studies have shown (Amirtharajah and Mills, 1982) that the contact between coagulant and colloidal particles should occur before the hydrolysis reaction with alkalinity is completed. This requires very rapid, intensive and sufficient dispersion of coagulant in the mass of water within a few seconds (Vrale and Jordan, 1971). To facilitate the rapid dispersion, the water is agitated vigorously with the aid of mixing devices and the coagulant is added at the most turbulent zone. There are basically two ways of effecting rapid mixing: hydraulically and mechanically. Hydraulic rapid mixing is found to be more economical than mechanical mixing due to the absence of moving parts and power requirements, but it is not as flexible to cope with the variation of raw water quality and quantity as mechanical mixing. Mechanical mixing is used in both developed and developing countries, but hydraulic mixing is currently receiving increased attention according to the research and field experiences of Amirtharajah and Mills (1982).

30 cm-long metal mesh material was inserted into the end section of the raw water inlet pipe just after the point of coagulant injection, for most of the tests, to ensure a high initial mixing force at the coagulant input zone. The flocculation results of six tests without the mesh are listed in Table B4 and a comparison of the flocculation results with and without the mesh with alum as coagulant is shown in Figure 5.12. The result with the mesh is generally up to 10% better than that without the mesh in terms of flocculation efficiency while up to 50% improvement was found according to McConnachie's study (1995) for Moringa oleifera as coagulant. This can be explained by the different flocculation mechanisms of the two coagulants. As described in Chapter 2, the main flocculent protein of Moringa oleifera is comparable to that of a synthetic polymer, such as polyacrylamide, and the flocculation with Moringa oleifera follows the combined mechanisms of patch charge and interparticle bridging (Gassenschmidt et al, 1995) while the dominant flocculation mechanism for alum is sweep flocculation at pH = 7, and alum dosage in the range of 25 to 80mg/l. In the zone where sweep coagulation dominates, there is no significant difference in

flocculation efficiencies between the different intensities of initial mixing according to Amirtharajah and Mills (1982).

Width of channel flocculator

One aim was to study the effect of the channel geometry, such as the channel width and bed slope, on the flow turbulence intensity and consequently flocculation efficiency. Two channel widths, 45mm and 150mm, with bed slopes of 1/30 and 1/80 respectively were adopted. The 45mm wide channel was used for most of the tests. The flocculation results of the six tests with the 150mm wide channel are listed in Table B4 and a comparison of the flocculation results with 45mm wide channel is shown in Figure 5.13. It can be seen that the magnitude of the kinetic energy of the 150mm wide channel is about 43% of that of the 45mm wide channel for every corresponding nominal velocity as listed in Tables B3 and B4 and a poorer flocculation efficiency (up to 45% less) due to the insufficient intensity of turbulence as shown in Figure 5.13.

5.2.5.1.2 Effect of raw water turbidity

Flocculation performances with alum as coagulant for three initial concentrations and three different flocculation times and with Moringa oleifera as coagulant for two initial concentrations and three flocculation times are given in Figures 5.9.1 to 5.10.3.

It is clearly displayed that the higher raw water turbidity has better flocculation performance for all the cases. The maximum flocculation efficiency for the initial turbidity of 950 NTU is up to 3.2 times of that for the initial turbidity of 100 NTU, 1.6 times for 265 NTU with alum as coagulant. For Moringa oleifera as coagulant, the ratio of maximum flocculation efficiency of the initial concentrations of 950 NTU to that of 265 NTU is in range of 1.1 to 1.6 for the three different flocculation times. The variations of the experimental results of flocculation performance with the raw water turbidities are in response to larger initial concentrations of particles in the suspension resulting in faster and more effective floc formation due to the greater opportunity for collisions as mentioned in the mechanisms of flocculation in section 5.1. It is noted that the flocculation efficiencies decrease as the flocculation times decrease from 17.2 to 4.3 minutes for all the three initial concentrations as shown in Figures 5.9.1 to 5.10.3. It is obvious that 4.3 minutes is not a long enough time for particle aggregation. The results from the flocculation time of 8.6 minutes are better by up to 2.3 times higher efficiency for alum as coagulant and 2.1 times for Moringa oleifera as

coagulant than the results from 4.3 minutes but are up to 2.4 times worse for alum as coagulant and 2.3 times worse for Moringa oleifera as coagulant than the results of flocculation time of 17.2 minutes. According to Treweek (1979) and McConnachie (1995), the flocculation time should be more than 7 minutes, usually around 20 minutes, in terms of creating maximum flocculation efficiency.

5.2.5.1.3 Effect of type of coagulant

The flocculation performances with alum as coagulant and with Moringa oleifera as coagulant are given in Figures 5.10.1, 5.10.2 and 5.10.3 for two initial turbidities and three flocculation times. The following points are evident from the Figures:

Under the same conditions, such as initial turbidity, flocculation time and kinetic energy, the flocculation with alum as coagulant always gives better results, 1.5 to 5 times of that of results with Moringa oleifera as coagulant. According to Amirtharajah and Mills (1982), at pH = 7, and alum dosage in the range of 25 to 80mg/l, the same condition as that of this experiment, the dominant flocculation mechanism for alum is sweep flocculation as shown in Figure 2.5 in Chapter 2. In sweep coagulation, the individual characteristics of the particles in suspension are obliterated within fraction of a second of adding the coagulant and the system becomes almost indistinguishable from coagulating metal hydroxide. An important function of the precipitated metal hydroxide is to provide a large number of particles and thereby improve coagulation kinetics very substantially (Packham and Sheiham, 1977). In contrast Moringa oleifera follows the combined mechanisms of patch charge and interparticle bridging and the difference of the flocculation mechanisms would explain the difference of flocculation performances.

5.2.5.1.4 Test with tube settling tank

The flocculation efficiencies with and without tubes for the initial concentration of 265 NTU under three flocculation times are shown in Figures 5.14.1, 5.14.2 and 5.14.3. The tube settling generally gives better results for all the cases in the Figures with a maximum efficiency ratio to the result of settling without tubes of 1.4.

To explain the difference in flocculation and settling performance, the settling area, settling depth and Reynolds number are calculated taking the case of flow rate of 56.4 l/min with a

nominal velocity of 0.1m/s under 17.2 minutes flocculation in the 45mm wide channel flocculator as an example. The effective width (W) and length (L) of the settling tank are 0.72m and 1.96m respectively as shown in Figure 5.4.1, and the water depth in the settling tank without tubes is 1m to give 25 minutes nominal settling time under "ideal" condition. So, the settling area (A), settling depth (H) of the settling tank without tubes are:

$A = 0.72 \times 1.96 = 1.41 m^2$, $H = 1.0m$

For the settling tank with tubes, the tubes were located at an angle of 60^0 to the bottom of the tank and the length (L_{tube}) and the diameter (D) of a tube were 1000mm and 50mm respectively as mentioned in section 5.2.4.1. So, the floc maximum settling depth in the tubes is H_{tube} as shown in Figure 5.15, the total settling area in the tank, A_{tube}, is the sum of settling areas of 312 tubes for the flow rate (Q) of 56.4 l/min. The settling area of each tube is half of the internal surface area of the tube, therefore we have:

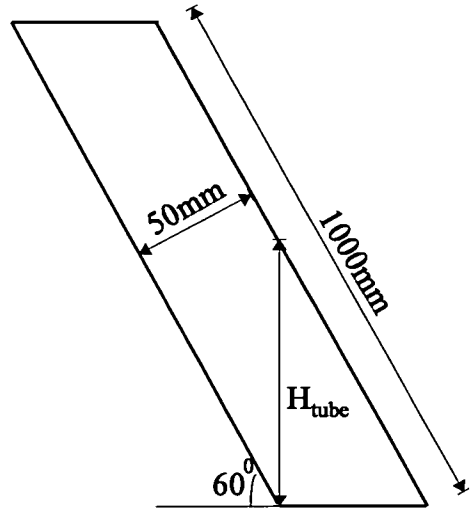

Figure 5.15 Dimensions of settling tube

$H_{tube} = D/\sin 30 = 50mm / 0.5 = 100mm = 0.1m$

$A_{tube} = 312 \times 0.5\pi DL_{tube} = 312 \times 0.5 \times 3.14 \times 0.05 \times 1.0 = 24.49 m^2$

So, $H_{tube}/H = 1/10$ (5.5.1)

$A_{tube}/A = 17.37$ (5.5.2)

The ratio of the Reynolds' number of the settling tanks without tubes (Re) to that of the tank with tubes (Re_{tube}) is given as follows:

$$\frac{Re}{Re_{tube}} = \frac{\frac{vR}{\nu}}{\frac{v_{tube}R_{tube}}{\nu}} \qquad (5.5.3)$$

Here, $v = \frac{Q}{WH}$, the forward flow velocity, $R = \frac{WH}{2H + W}$, the hydraulic radius of the settling tank without tubes, $v_{tube} = \frac{Q}{312\pi\left(\frac{D}{2}\right)^2}$, the velocity in each tube if the flow is uniformly distributed among all 312 tubes, $R_{tube} = \frac{D}{4}$ and ν is the fluid kinetic viscosity. Substituting the values of v, R, v_{tube} and D into Equation 5.5.3 gives:

$$\frac{Re}{Re_{tube}} = 18 \qquad (5.5.4)$$

It can be concluded from Equations 5.5.1, 5.5.2 and 5.5.4 that the settling tank with tubes provides a bigger settling area, a shorter settling depth and improved flow conditions as quantified by the Reynolds number for floc settling. Improvement in flocculation efficiency by the use of tube settling is confirmed in Chapter 6 where calculations show a 1.7% increase in the aggregation constant and about a 16% decrease in the breakup constant compared with the normal settling.

5.2.5.2 Sedimentation against location and time

One of the primary objectives of the experimental work of this research was to study the phenomena of settling and flocculation which occur within the settling tank, and to investigate the conditions that affect such phenomena. The performance of the flocculation and settling was evaluated by the measurement of particle mass concentration quantified by turbidity. The correlation between turbidity and mass concentration of kaolin can be found in section 5.2.2.2. Continuous flow settling experiments were performed with two raw water turbidities and six flow rates as listed in Table 5.3.2. Samples were taken for the measurement of turbidity at various depths during each experiment as a function of time and location.

Table 5.3.2 Settling experimental conditions

Raw water turbidity (NTU)	Flow rate (l/min)	Nominal velocity in the flocculator (m/s)
265	56.4	0.100
265	42.3	0.075
265	36.7	0.065
265	33.8	0.060
265	28.2	0.050
265	19.7	0.035
950	56.4	0.100
950	42.3	0.075
950	36.7	0.065
950	33.8	0.060
950	28.2	0.050
950	19.7	0.035

The weight fraction remaining of the particle concentration (n_1/n_0) vs settling time for six flow rates and three levels, 30, 60 and 90cm from the bottom of the settling tank, are listed in Tables 5.4.1 and 5.4.2 and results plotted in Figures 5.16.1 to 5.17.6. The flow rates correspond to six nominal velocities, 0.1, 0.075, 0.065, 0.06, 0.05 and 0.035m/s, in the flocculator as listed in Table 5.3. The nominal velocities are listed to represent the corresponding flow rates in the Figures. Samples were taken at the three levels for each of the ideal settling times of 6.25, 12.5 and 25 minutes, i.e. at ¼, ½ and full tank length. For simplification these three levels are marked bottom, middle and top in the Figures.

The variation of the turbidity at the top level with settling time for the six nominal velocities and two initial turbidities is shown in Figures 5.16.1 and 5.16.2. It is observed that the flocculent settling performance is a function of flow rate for the same temporal and spatial conditions. The best settling performance occurred at the flow velocity of 0.05m/s for both initial turbidities. As expected settling efficiency improves as the settling time increases, with an increase, up to 76%, when the settling time is extended from 6.25 to 12.5 minutes. Settling with the higher initial turbidity (950 NTU) produced greater solid removal by up to 1.5 times compared with the lower initial turbidity (265 NTU) for corresponding flow.

Table 5.4.1 Weight fraction remaining

Initial concentration NTU	Flow rate (l/min)	Nominal velocity (m/s)	Location	1/4 tank length (6.25 min. retention)	1/2 tank length (12.5 min. retention)	Tank length (25 min. retention)	Effluent
265	56.4	0.100	Top	0.222	0.104	0.085	0.089
			Middle	0.423	0.377	0.231	
			Bottom	0.520	0.500	0.315	
265	42.3	0.075	Top	0.189	0.091	0.061	0.063
			Middle	0.302	0.173	0.151	
			Bottom	0.440	0.200	0.157	
265	36.7	0.065	Top	0.162	0.087	0.061	0.061
			Middle	0.194	0.177	0.142	
			Bottom	0.460	0.173	0.173	
265	33.8	0.060	Top	0.108	0.077	0.059	0.058
			Middle	0.165	0.085	0.069	
			Bottom	0.430	0.123	0.077	
265	28.2	0.050	Top	0.100	0.068	0.049	0.049
			Middle	0.115	0.096	0.075	
			Bottom	0.450	0.105	0.089	
265	19.7	0.035	Top	0.175	0.089	0.061	0.061
			Middle	0.158	0.131	0.123	
			Bottom	0.490	0.146	0.173	

Table 5.4.2 Weight fraction remaining

Initial concentration (NTU)	Flow rate (l/min)	Nominal velocity (m/s)	Location	1/4 tank length (6.25 min.retention)	1/2 tank length (12.5 min retention)	Tank length (25 min retention)	Effluent
950	56.4	0.100	Top	0.084	0.072	0.062	0.064
			Middle	0.140	0.121	0.101	
			Bottom	0.480	0.330	0.220	
950	42.3	0.075	Top	0.065	0.054	0.040	0.044
			Middle	0.111	0.102	0.071	
			Bottom	0.340	0.260	0.180	
950	36.7	0.065	Top	0.054	0.045	0.039	0.039
			Middle	0.090	0.080	0.064	
			Bottom	0.310	0.230	0.140	
950	33.8	0.060	Top	0.055	0.043	0.033	0.034
			Middle	0.088	0.076	0.065	
			Bottom	0.300	0.220	0.130	
950	28.2	0.050	Top	0.042	0.031	0.020	0.030
			Middle	0.068	0.064	0.049	
			Bottom	0.270	0.170	0.110	
950	19.7	0.035	Top	0.056	0.048	0.044	0.046
			Middle	0.074	0.065	0.045	
			Bottom	0.260	0.190	0.110	

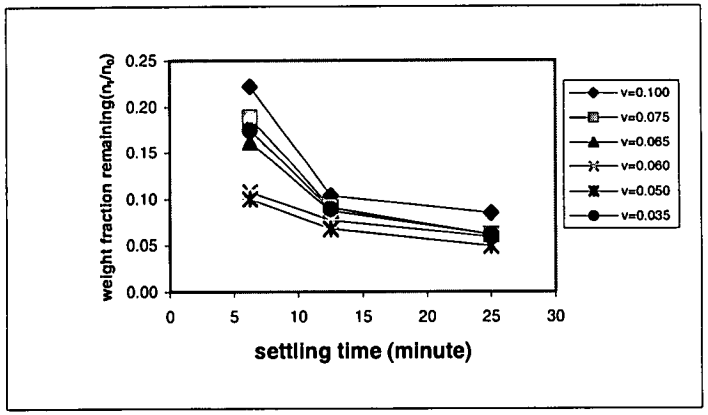

Figure 5.16.1 Settling performance at various flowrates under initial concentration of 265NTU

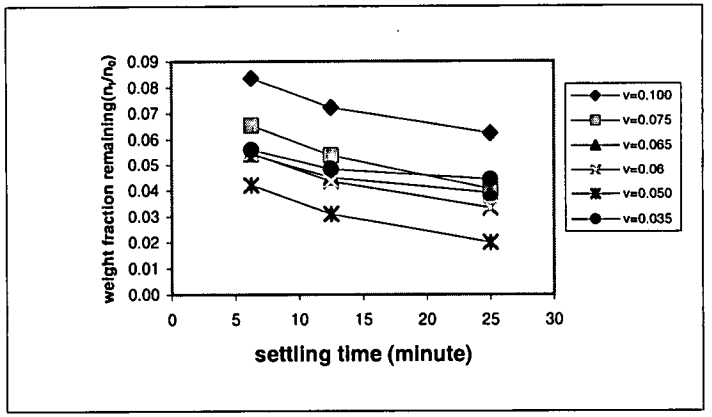

Figure 5.16.2 Settling performance at various flowrates under initial concentration of 950NTU

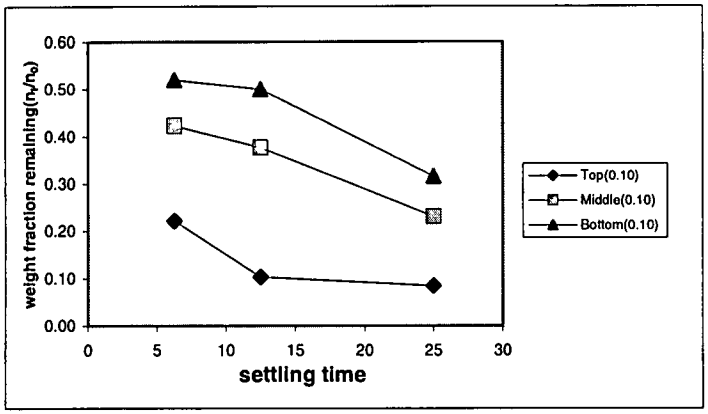

Figure 5.17.1 Settling performance at different levels for nominal velocity of 0.1m/s under initial concentration of 265NTU

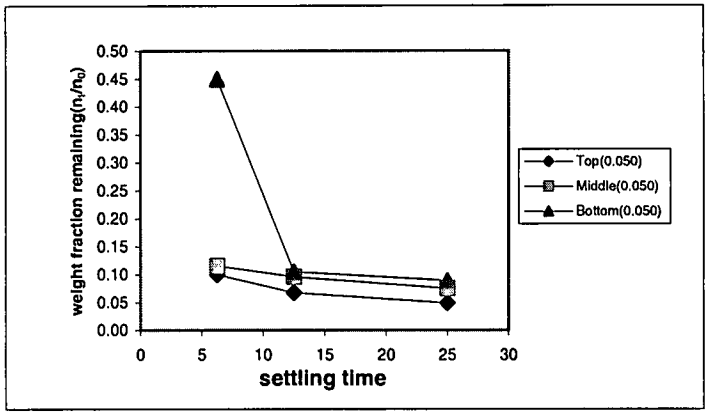

Figure 5.17.2 Settling performance at different levels for nominal velocity of 0.05m/s under initial concentration of 265NTU

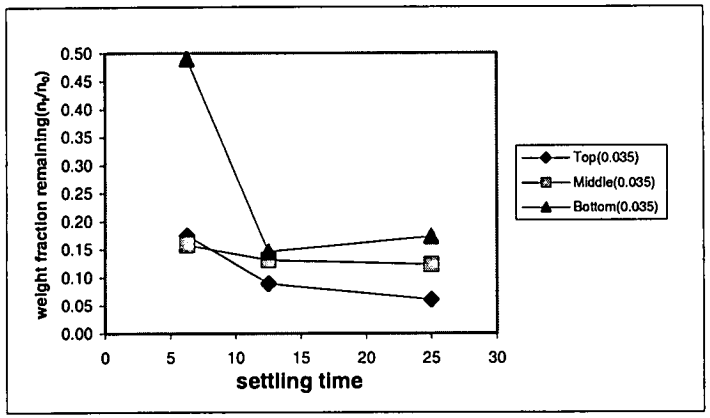

Figure 5.17.3 Settling performance at different levels for nominal velocity of 0.035m/s under initial concentration of 265NTU

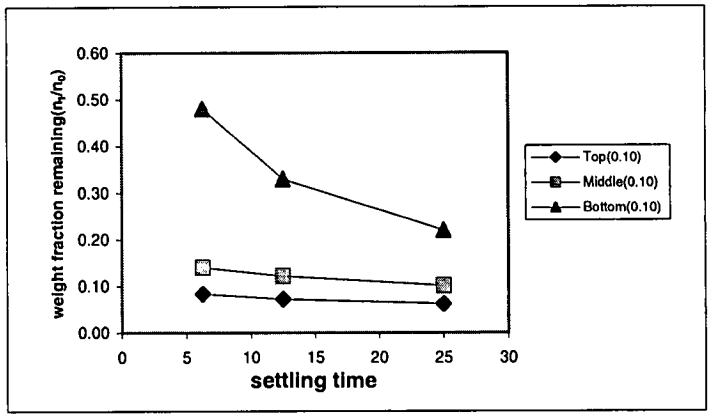

Figure 5.17.4 Settling performance at different levels for nominal velocity of 0.1m/s under initial concentration of 950NTU

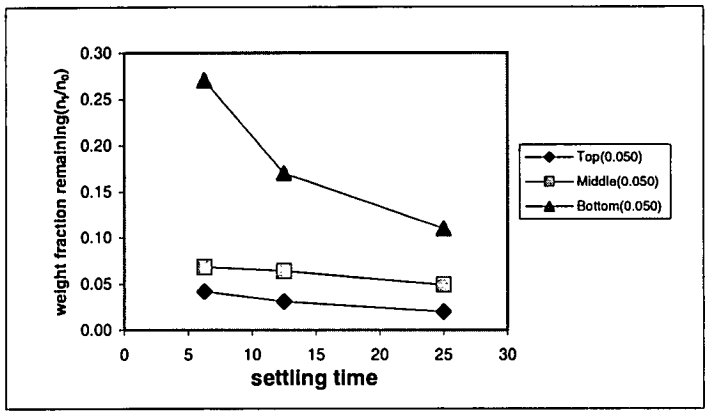

Figure 5.17.5 Settling performance at different levels for nominal velocity of 0.05m/s under initial concentration of 950NTU

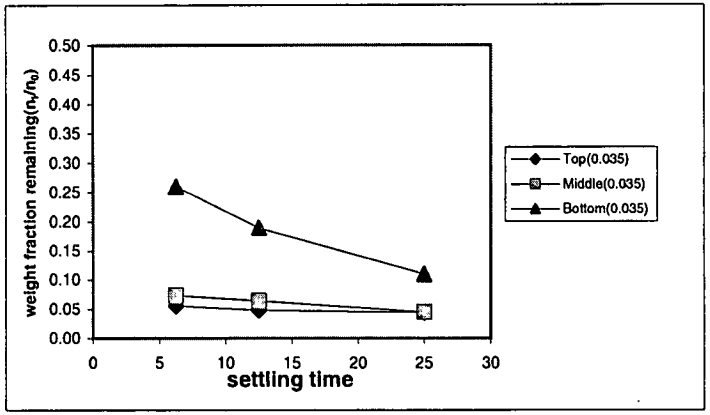

Figure 5.17.6 Settling performance at different levels for nominal velocity of 0.035m/s under initial concentration of 950NTU

The settling performance at the three levels for the two raw water turbidities is illustrated in Figures 5.17.1 to 5.17.6. Up to 63% difference of weight fraction remaining is found between the top level and middle level whilst 23% to 84% between the top and bottom.

It can be concluded that the settling, in agreement with the description of flocculent settling in Chapter 2, depends on the fluid and particle properties as well as the depth of the tank and settling time.

5.2.6 Calculation of head loss

According to Montgomery (1985), the total head loss, H_T, in the flocculator can be calculated as the sum of the head loss from the turbulence and friction on the sides of a channel, h_L and the head losses at bends, h_b, as indicated by Equation 5.6.1.

$$H_T = h_L + h_b = \frac{LV^2}{C^2R} + Nk_{bend}\frac{V^2}{2g} \qquad (5.6.1)$$

-where L is the flow travel length, V is the mean flow velocity, C is the Chezy coefficient, R is the hydraulic radius, N is the number of bends, and k_{bend} is an empirical friction coefficient. Manning's friction factor, n, is the most widely used friction factor for open channel flow and is related to C by $C = \frac{R^{\frac{1}{6}}}{n}$. A value of n = 0.012 is appropriate for the wooden sides and base of the flocculator used here (Chow, 1959) and has been used to calculate the total head loss within the straight sections using the average velocity and an effective length of 1.215m for each channel.

For two random flows with mean velocities of V_i and V_j, their corresponding total head losses, H_i, H_j, the head losses due to turbulence and friction on the sides of a channel, h_{iL}, h_{jL} and the head losses at bends, h_{ib}, h_{jb}, under the same retention time, t, can be expressed by Equations 5.6.2 to 5.8.2.

The total head loss for a specific average velocity and a certain length of channel is calculated as follows:

$$H_i = h_{iL} + h_{ib} \qquad (5.6.2)$$

$$H_j = h_{jL} + h_{jb} \tag{5.6.3}$$

-where $$h_{iL} = \frac{L_i V_i^2}{C_i^2 R_i} = \frac{n^2 V_i t V_i^2}{R_i^{4/3}} = V_i^3 \frac{n^2 t}{R_i^{4/3}} \tag{5.7.1}$$

$$h_{jL} = \frac{L_j V_j^2}{C_j^2 R_j} = \frac{n^2 V_j t V_j^2}{R_j^{4/3}} = V_j^3 \frac{n^2 t}{R_j^{4/3}} \tag{5.7.2}$$

$$h_{ib} = k_{bend} \frac{V_i^2}{2g} N_i \tag{5.8.1}$$

$$h_{jb} = k_{bend} \frac{V_j^2}{2g} N_j \tag{5.8.2}$$

If the change of the hydraulic radius for flows in the flocculator can be ignored, the ratio of the head loss due to turbulence and friction on the sides of the channel for two arbitrary mean velocities can be calculated as follows,

$$\frac{h_{iL}}{h_{jL}} = \frac{V_i^3 \frac{n^2 t}{R_i^{4/3}}}{V_j^3 \frac{n^2 t}{R_j^{4/3}}} = \frac{V_i^3}{V_j^3} \tag{5.9}$$

The water head in the first channel of the flocculators and the water depth at the outlet of the flocculators were measured for all the tests as listed in Table 5.5. These measurements were used for the calculation of the head loss of the flocculators and for setting boundary conditions for the modelling simulation as mentioned in Chapter 4. The water depth in the 45mm wide channel flocculator for the six flow rates is in the range of 200mm to 265mm and consequently R varies from 20.2 to 20.7mm. Therefore, calculation of the head loss by Equation 5.9 is acceptable with a maximum relative error of 0.3%.

For a particular retention time, the ratio of the number of bends passed through by different flows is given by Equations 5.10.1 and 5.10.2.

$$N_j = N_i \frac{V_j}{V_i}, \quad \text{if both } N_i \text{ and } N_j \text{ are integers; and} \tag{5.10.1}$$

$$N_j = N_i \frac{V_j}{V_i} \pm 1, \text{ if either } N_i \text{ or } N_j \text{ from Eq.5.10.1 is a non-integer.} \tag{5.10.2}$$

Table 5.5 Water depth measurements

Average velocity (m/s)	Flocculation time (minutes)	Water head (D_1) (mm)	Water depth at outlet (D_n) (mm)	Channel width (mm)
0.100	17.2	200	240	45
0.075	17.2	200	261	45
0.065	17.2	200	262	45
0.060	17.2	200	265	45
0.050	17.2	200	259	45
0.035	17.2	200	246	45
0.100	8.6	200	213	45
0.075	8.6	200	229	45
0.065	8.6	200	230	45
0.060	8.6	200	230	45
0.050	8.6	200	227	45
0.035	8.6	200	224	45
0.100	4.3	200	207	45
0.075	4.3	200	209	45
0.065	4.3	200	214	45
0.060	4.3	200	215	45
0.050	4.3	200	205	45
0.035	4.3	200	210	45
0.100	4.3	200	209	150
0.075	4.3	200	215	150
0.065	4.3	200	217	150
0.060	4.3	200	217	150
0.050	4.3	200	216	150
0.035	4.3	200	213	150

If N_i and N_j are greater than 1, as is always the case for a channel flocculator, the ratio of the head loss at a bend for two random flows is expressed by Equation 5.11 with a maximum relative error of 4.7% for this study.

$$\frac{h_{ib}}{h_{jb}} = \frac{k_{bend}\frac{V_i^2}{2g}N_i}{k_{bend}\frac{V_j^2}{2g}\frac{V_j}{V_i}N_i} = \frac{V_i^3}{V_j^3} \qquad (5.11)$$

So, the correlation of total head loss for two flows can be derived as,

$$\frac{H_i}{H_j} = \frac{h_{iL} + h_{ib}}{h_{jL} + h_{jb}} = \frac{V_i^3}{V_j^3} \qquad (5.12)$$

Table 5.6 Flocculator head loss

Test set	Flow (l/min)	Nominal velocity (m/s)	Average velocity (m/s)	Bed slope	Calculated mean head loss (mm)			k_{bend}	Channel width (mm)	Chezy C ($m^{0.5}/s$)
					Total (H_T)	Sides (H_L)	Bend (H_b)			
1	56.4	0.100	0.091	1/30	113.0	22.0	91.0	2.6	45	43.56
2	42.3	0.075	0.065	1/30	51.8	11.1	40.6	3.1	45	43.60
3	36.7	0.065	0.056	1/30	35.5	8.3	27.1	3.3	45	43.60
4	33.8	0.060	0.052	1/30	26.8	7.1	19.7	2.9	45	43.60
5	28.2	0.050	0.043	1/30	16.5	5.0	11.5	3.1	45	43.59
6	19.7	0.035	0.031	1/30	6.6	2.6	3.9	3.4	45	43.57

However, previous studies (Haarhoff, 1998) and the experimental results as shown in Table 5.6 do not agree well with the calculated ratio as expressed in Equation 5.12. For example the ratios of total head losses, head losses due to turbulence and friction on the sides of channels, and the head losses at bends of test sets 1 to 2 are not equal to the power of 3 of their average velocity ratio as follows:

ratio of average velocity cubed:	$(0.091/0.065)^3$	= 2.7
ratio of H_T :	113.0/51.8	= 2.2
ratio of H_L:	22.0/11.0	= 2.0
ratio of H_b :	91.0/40.6	= 2.2

One important reason is that the empirical friction coefficient, k_{bend}, is not a constant for all the cases, which is explained by the following calculations.

Table 5.6 gives calculated head losses due to turbulence and friction on the sides of a channel, the head losses at bends and the total head loss measured over the number of channels, N, required for 17.2 minutes retention. The derived values of Chezy C, and k_{bend} are also listed in the table. The measured total head loss $\Delta H = (D_1 - D_n$ + drop in elevation of

the bed over N channels), where D_1 is the depth at the initial channel and D_n the depth in the Nth channel as listed in Table 5.5. For example, for test set 1:

17.2 minutes retention was over 85 channels at a bed slope of 1/30 giving H_T = 200 - 240 + 85 x 54/30 = 113 mm. Hydraulic radius, R = 0.0204m giving $C = \frac{R^{1/6}}{n} = \frac{0.0206^{1/6}}{0.012} =$ 43.56. Average velocity for 85 channel for 56.4 l/min and average depth 220mm is 0.091 m/s as calculated and from Equation 5.7.1or 5.7.2 the head loss from the bed and sides of the 85 channels totals 22.0 mm. The resulting head loss from the bend is taken to be 113 – 22 = 91 mm, which gives k_{bend} = 2.6 from Equation 5.8.1 or 5.8.2. The flow measurement was accurate to around ±2.5 l/min and the measured depths to ±1 mm resulting in possible error of calculated k_{bend} mainly within ±0.2.

Suggested design values for k_{bend} for an open channel with 180^0 bend and the channel width w_c, equal to the bend width w_b, as for the flocculator used here, are 3.2 to 3.5 (Kawamura, 1991) and 3.2 (Montgomery, 1985). For w_b/w_c = 1.5, k_{bend} = 2.4 to 4.0 (Okun and Schulz, 1984) and $w_b/w_c < 1$, k_{bend} = 1.5 (Kawamura, 1991). As shown in Table 5.6, the value of k_{bend} ranges from 2.6 to 3.4, which is close to the range of 3.2 to 3.5 recommended by Kawamura (1991) and Montgomery (1985) as noted above.

5.3 FLOC CHARACTERISTICS

Turbidity measurements indicate in a macro view the flocculation and settling efficiency whilst floc characteristics, such as floc size, floc density and floc settling velocity are important parameters in assessing flocculation and settling performance from a micro aspect. So, both measurements of turbidity and particle characteristics provide a complete picture for analysing and evaluating the processes of flocculation and settling (Kavanaugh, et al, 1980).

A review of determination of floc size, settling velocity and density is given in Chapter 2. In this study, the floc size and floc settling velocity were measured by a video recording technique as this can record floc size and settling velocity simultaneously, and is relatively easy to operate. The apparatus used for the measurements is described in section 5.3.1. The

measurement procedures of floc size and floc settling are presented in section 5.3.2. The calculation of floc density is found in section 5.3.3.

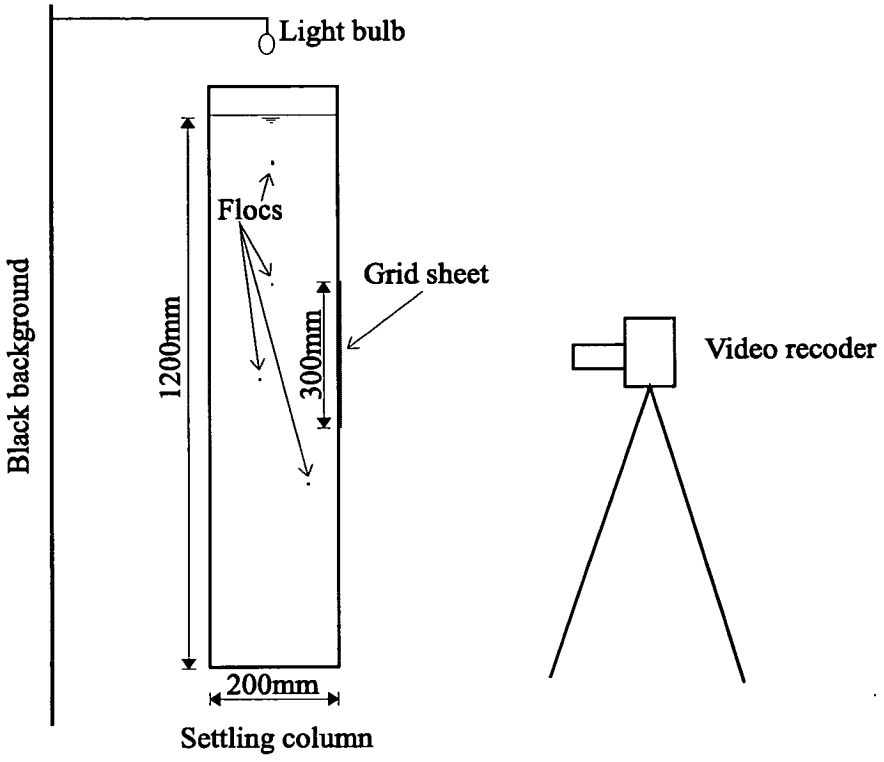

Figure 5.18 Video recorder and settling column in position for recording floc size and settling velocity

5.3.1 Introduction

The set up of the equipment for experimental measurement is shown in Figure 5.18. One item of the equipment used for the measurement of floc size and settling velocity was a quiescent settling column, which was constructed of perspex and had dimensions of 1200mm in depth, 200mm x 200mm in cross section. The column was designed to be deep and wide enough to minimise wall effects, while at the same time to allow for the constraints posed by the photographic techniques used. The height of the tank allowed a sufficient settling time for a natural distribution of floc size to occur before they reached the bottom. After each of these settling tests the tank was emptied, cleaned, and refilled before a new test was conducted to ensure liquid temperature 20 ± 0.1^{0}C and inhibit any other physical changes which may have occurred as a result of the previous sample, since small

temperature differences between the floc and the liquid surround it in the settling column could result in serious experimental errors (Kimpel, 1984).

The settling flocs were recorded against a black background using a 12 zoom Panasonic VHS video recorder. A 500 watt light bulb was used to illuminate the area surrounding the settling column, and was placed in such way to ensure an appropriate depth of field and to minimise unnecessary reflections. A 1mm x 1mm mesh grid transparent sheet (300mm x 200mm) was placed directly against the outside of the settling column to serve as a focusing basis, and to enable the floc size to be determined directly from the screen by playing back the recording tape.

5.3.2 Measurement of particle size and settling velocity

The measurements of floc size, settling velocity and thereafter the calculation of floc density were carried out from flocs established under three different initial raw water turbidities, six flow rates, two flocculation times and two coagulants as listed in Table 5.7.

For the measurements of floc size and settling velocity, approximately 1.5ml of the flocculated suspension was gently taken up from the outlet of the flocculator and introduced into the settling column by using a L-shaped glass tube of inside diameter 7mm. It was found that a sample size of 1.5ml allowed for individual settling of the flocs, thus avoiding turbulence, and/or streaming in the settling tank (Kimpel, 1984). The glass tube diameter was significantly greater than the diameter of the flocs contained in the suspension to prevent breakage or alterations in agglomerate structure. The number of flocs in the settling column was few, therefore most flocs settled down independently. Extreme care was taken when choosing the flocs to be measured in order to meet the requirements of discrete particle settling formula given by Equation 5.13. First, in order to obtain data free from wall effects and hydrodynamic interaction, only the flocs settling individually through the central part of the column were selected for recording; Second, since the flocs were assumed to be spherical, those few flocs which did not closely resemble spheres were not measured. This approach applied to all the tests of this study to allow the comparison of the size, settling velocity and density of the same kind of flocs for the tests conditions as listed in Table 5.7. A running timer was also recorded in order to determine floc settling velocity. The motion of a discrete particle was timed over a distance up to 50mm in this study as used by Tambo and Watanabe (1979). This procedure was repeated for a number of discrete flocs (20 in

most cases) in order to obtain a representative value for each case. Floc size and settling velocity were simultaneously measured on the monitor by playing back the videotape after calculation of the magnification ratio. The enlarged picture allowed floc size to be measured directly to ± 0.01mm and velocities to ±0.01mm/s.

Results of the measurement of floc size and settling velocity are listed in Table 5.7.

5.3.3 Calculation of floc Density

The measurements of floc size and settling velocity allow the floc density to be calculated. The basic equation used to calculate the effective floc buoyant density, ρ_f - ρ_l, and hence the floc density, is the discrete particle settling formula given by Newton's Law:

$$V_s = \sqrt{\frac{4g(\rho_f - \rho_l)d_f}{3C_d\rho_l}} \tag{5.13}$$

-where V_s is the floc free settling velocity, g is the gravitational acceleration, ρ_f, ρ_l are densities of floc and water respectively, d_f is the floc diameter, Newton's drag coefficient, C_d, is a function of the Reynolds number, Re, and the shape of the particle. Here,

$$Re = \frac{V_s d_f \rho_l}{\mu} \tag{5.14}$$

-where, Re is the Reynolds number for the settling of spheres, and μ is the liquid viscosity.

Much more sensitivity is given by using floc effective density (ρ_f - ρ_l) as a parameter indicating the variation of floc density than by directly using floc density (Tambo and Watanabe, 1979), therefore floc effective density is used here. Rearranging Equation 5.13 gives,

Table 5.7 Experimental details of measurements of floc size and settling velocity and calculated floc effective density

Raw water turbidity (NTU)	Coagulant (mg/l)		Flocculation time	Nominal velocity	Kinetic energy	Floc size (±0.01mm)	Settling velocity (±0.01mm/s)	Effective floc density
	Alum	Moringa oleifera	(min.)	v(m/s)	(m^2/s^2)	(mm)	(mm/s)	(g/cm^3)
100	25	***	17.2	0.035	8.966E-5	0.40	1.79	0.024
100	25	***	17.2	0.050	1.256E-4	0.35	3.13	0.056
100	25	***	17.2	0.060	1.448E-4	0.32	2.75	0.058
100	25	***	17.2	0.065	1.606E-4	0.32	2.73	0.057
100	25	***	17.2	0.075	1.941E-4	0.30	2.54	0.060
100	25	***	17.2	0.100	3.077E-4	0.25	2.12	0.070
100	25	***	8.6	0.035	1.137E-4	0.38	1.66	0.024
100	25	***	8.6	0.050	1.563E-4	0.33	2.86	0.057
100	25	***	8.6	0.060	1.836E-4	0.30	2.66	0.063
100	25	***	8.6	0.065	2.011E-4	0.28	2.69	0.073
100	25	***	8.6	0.075	2.391E-4	0.25	2.34	0.078
100	25	***	8.6	0.100	3.401E-4	0.20	1.98	0.100
265	50	***	17.2	0.035	8.966E-5	0.42	1.92	0.023
265	50	***	17.2	0.050	1.256E-4	0.40	3.48	0.049
265	50	***	17.2	0.060	1.448E-4	0.38	3.33	0.051
265	50	***	17.2	0.065	1.606E-4	0.36	2.99	0.050
265	50	***	17.2	0.075	1.941E-4	0.33	2.65	0.052
265	50	***	17.2	0.100	3.077E-4	0.27	2.22	0.063
265	50	***	8.6	0.035	1.137E-4	0.40	1.79	0.024
265	50	***	8.6	0.050	1.563E-4	0.37	3.57	0.058
265	50	***	8.6	0.060	1.836E-4	0.35	3.43	0.062
265	50	***	8.6	0.065	2.011E-4	0.35	3.3	0.059
265	50	***	8.6	0.075	2.391E-4	0.30	2.77	0.066
265	50	***	8.6	0.100	3.401E-4	0.23	2.32	0.090
950	80	***	17.2	0.035	8.966E-5	0.53	2.86	0.023
950	80	***	17.2	0.050	1.256E-4	0.72	7.64	0.041
950	80	***	17.2	0.060	1.448E-4	0.65	6.43	0.040
950	80	***	17.2	0.065	1.606E-4	0.62	6.33	0.043
950	80	***	17.2	0.075	1.941E-4	0.57	5.77	0.045
950	80	***	17.2	0.100	3.077E-4	0.42	4.32	0.057
950	80	***	8.6	0.035	1.137E-4	0.45	2.36	0.025
950	80	***	8.6	0.050	1.563E-4	0.62	6.7	0.046
950	80	***	8.6	0.060	1.836E-4	0.60	5.56	0.039
950	80	***	8.6	0.065	2.011E-4	0.60	5.76	0.041
950	80	***	8.6	0.075	2.391E-4	0.52	5.48	0.050
950	80	***	8.6	0.100	3.401E-4	0.35	3.89	0.071
265	***	75	17.2	0.035	8.966E-5	0.15	1.01	0.086
265	***	75	17.2	0.050	1.256E-4	0.09	1.34	0.352
265	***	75	17.2	0.060	1.448E-4	0.08	1.51	0.449
265	***	75	17.2	0.065	1.606E-4	0.07	1.54	0.563
265	***	75	17.2	0.075	1.941E-4	0.07	1.7	0.659
265	***	75	17.2	0.100	3.077E-4	0.07	1.21	0.537
950	***	100	17.2	0.035	8.966E-5	0.12	0.91	0.120
950	***	100	17.2	0.050	1.256E-4	0.08	1.29	0.364
950	***	100	17.2	0.060	1.448E-4	0.08	1.37	0.462
950	***	100	17.2	0.065	1.606E-4	0.07	1.47	0.569
950	***	100	17.2	0.075	1.941E-4	0.07	1.67	0.685
950	***	100	17.2	0.100	3.077E-4	0.06	1.01	0.622

$$\rho_f - \rho_l = \frac{3C_d\rho_l V_s^2}{4d_f g} \tag{5.15}$$

Fair, Geyer and Okun (1968) have used multiple regression analysis to determine that the relation between C_d and Re is,

$$C_d = \frac{24}{Re} + \frac{3}{Re^{0.5}} + 0.34 \tag{5.16.1}$$

In a flow regime for which Re < 1, where laminar flow prevails, the relationship between C_d and Re takes the limiting form,

$$C_d = \frac{24}{Re} = \frac{24\mu}{d_p\rho_l V_s} \tag{5.16.2}$$

For Reynolds number ranging from 0.01 to 50, Concha and Almenda (1979) developed an equation describing the drag coefficient, C_d, of a solid settling sphere given by Equation 5.17. It was derived through combination of boundary layer theory, and experimental data for the pressure distribution and boundary layer thickness over the surface of the sphere.

$$C_d = 0.28\ (1 + \frac{9.06}{Re^{1/2}})^2 \tag{5.17}$$

This specific expression was used here due to its applicability over the entire Reynolds number range of interest. Although the flocs are porous spheres, Kimpel's (1984) study found that the effect of permeability is minimal for flocs ranging in size from 20 to 1000 micrometres. The effect of permeability is not considered in this study as all the floc sizes measured lie in the above range. The floc sizes and calculated floc densities are given in Tables 5.7.

5.3.4 Variation of floc size and density

The floc size and density vs turbulence kinetic energy for various raw water turbidities, types of coagulant, and flocculation times are shown in Figures 5.19 to 5.22. In the Figures,

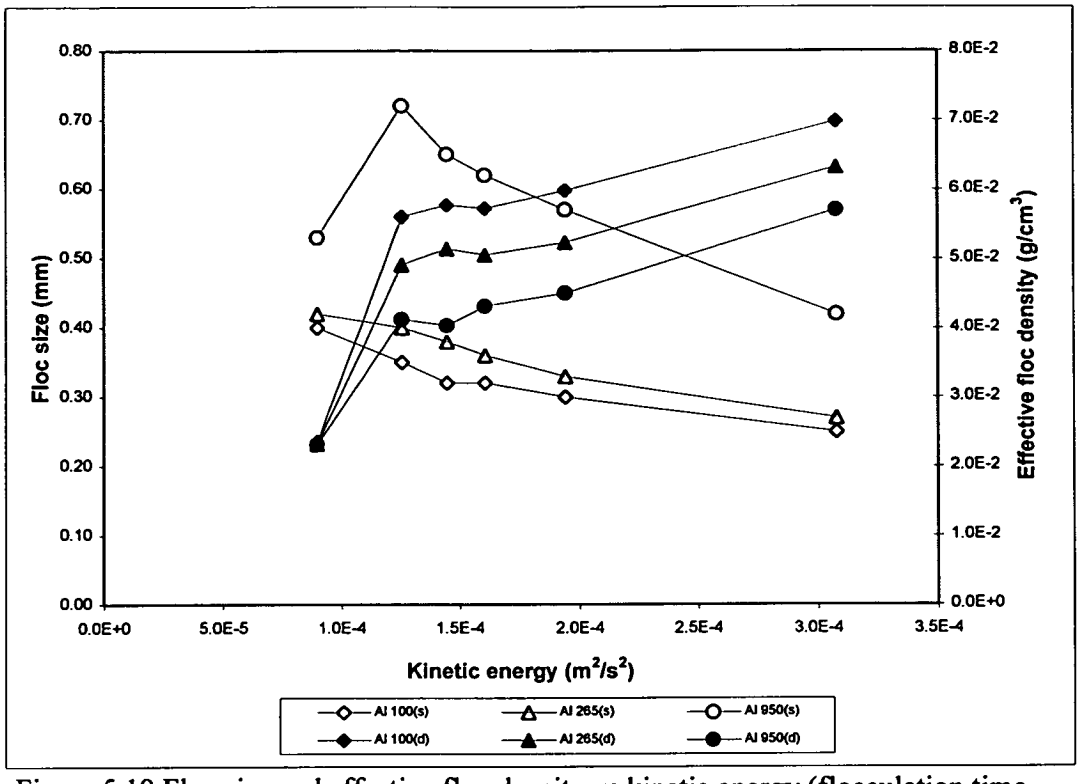

Figure 5.19 Floc size and effective floc density vs kinetic energy (flocculation time of 17.2 minutes)

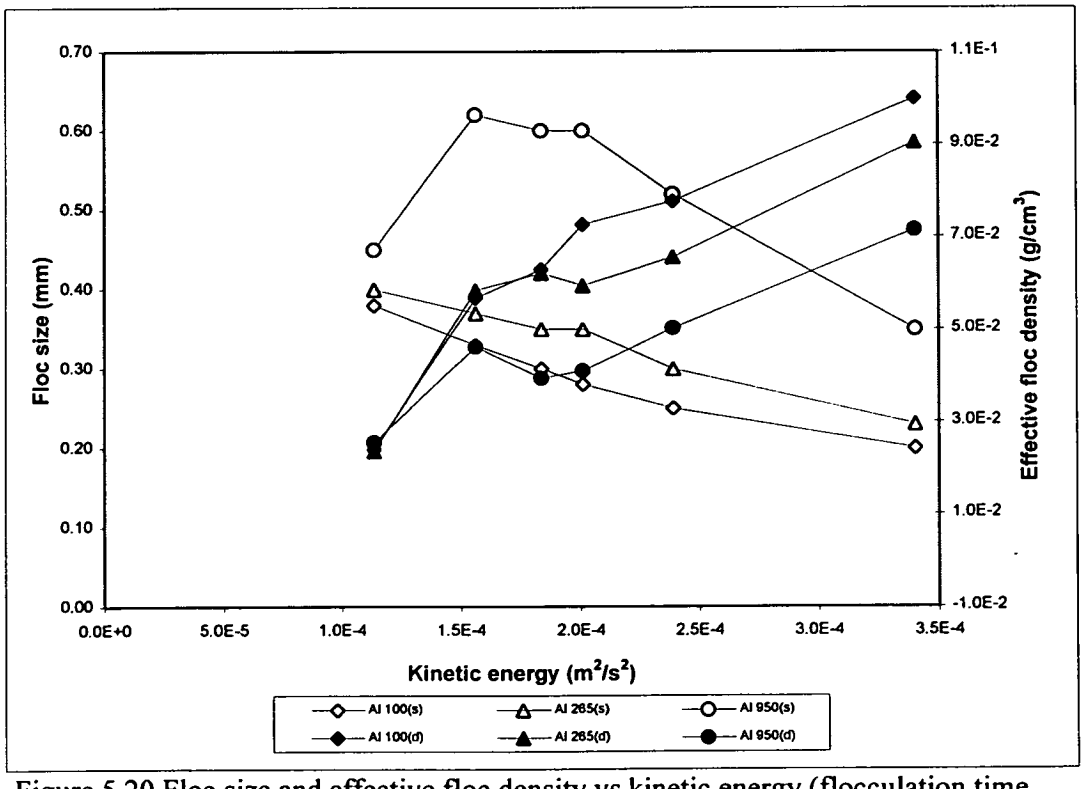

Figure 5.20 Floc size and effective floc density vs kinetic energy (flocculation time of 8.6 minutes)

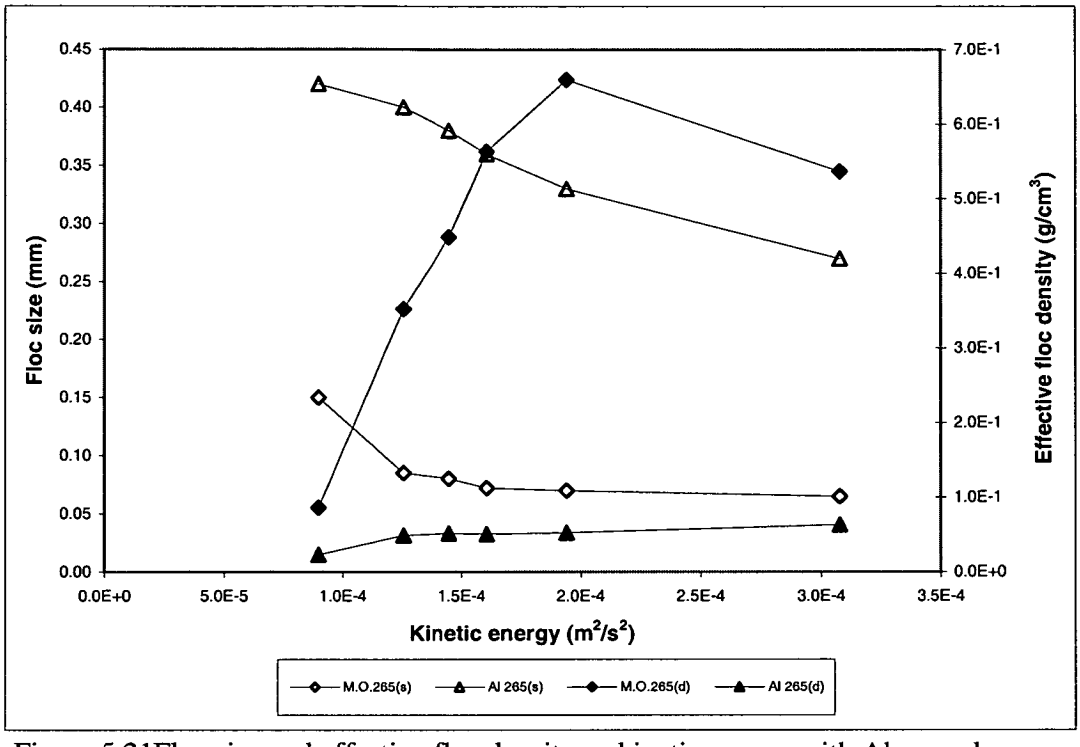

Figure 5.21Floc size and effective floc density vs kinetic energy with Alum and Moringa Oleifera as coagulant (flocculation time of 17.2 minutes)

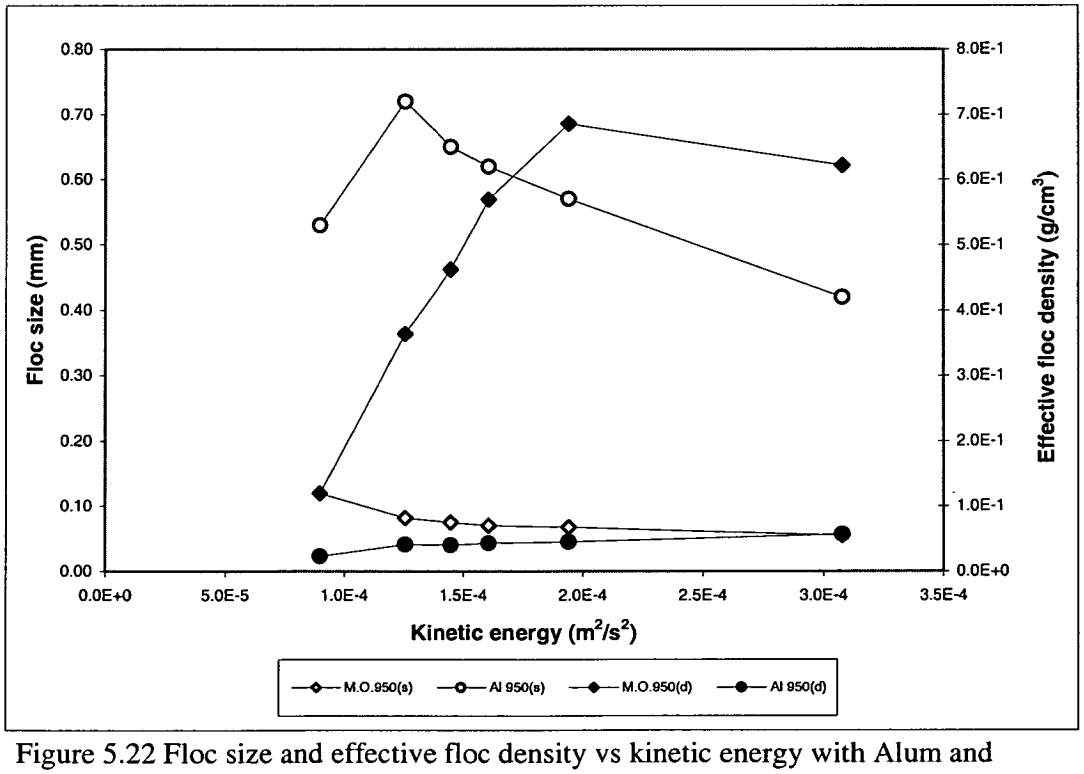

Figure 5.22 Floc size and effective floc density vs kinetic energy with Alum and Moringa Oleifera as coagulant (flocculation time of 8.6 minutes)

floc sizes with alum as coagulant for turbidities of 100, 265 and 950 NTU are marked as Al 100(s), Al 265(s) and Al 950(s) respectively, and the corresponding floc densities are Al 100(d), Al 265(d) and Al 950(d). Floc size and density with Moringa oleifera as coagulant are labelled as M.O 265(s), M.O. 950 (s) and M.O. 265(d), M.O. 950 (d), respectively. For the raw water turbidities of 265 and 100 NTU, the floc size consistently decreases as the turbulence kinetic energy increases, whereas the floc density increases. It is as expected and agrees with previous studies (Argaman, 1968; Parker et al, 1972) that floc size depends on the strength of turbulence and is inversely proportional to the value of turbulence intensity. The density of flocs generally increases with increase of turbulence, while this is accompanied by a significant decrease in the size (Kimpel 1984). However, for highest raw water turbidity of 950 NTU, it is noted that there is an initial increase in floc size prior to eventual decrease as the increase of turbulence intensity as shown in Figures 5.19 and 5.20. Turbulence has two opposite effects on floc size, it can enhance floc aggregation and consequently bring more particles into one floc resulting in a bigger floc size, or demolish floc size by causing floc breakup. It may be explained that the initial build up of the floc size from the highest turbidity was due to the former effect dominating in the solution which has a large number of particles but not very vigorous turbulence.

Figure 5.19 gives the floc size and density from three initial turbidities. There is a general trend that the higher the initial turbidity the larger the floc size and the lower the floc density. The diameter of floc from the turbidity of 950 NTU is 1.3 to 2.1 times that from the lowest turbidity of 100 NTU, while its effective density is mainly around 70 to 80% of that from the turbidity of 100 NTU. This probably results from the higher possibilities of collision in the higher concentration solution and so each floc containing more particles. The more particles the bigger the floc size will be and the less the solid volume fraction becomes resulting in relatively low density.

Comparison of the floc size and density under two flocculation times of 17.2 and 8.6 minutes with alum as coagulant can be made from Figures 5.19 and 5.20. It is shown that slightly bigger and looser flocs are generated under the longer flocculation time, with up to 30% larger floc size and 30% lower effective floc density compared with the shorter flocculation time. This confirms Healy's (1961) observation that floc growth proceeds as flocculation time increases, whilst the floc porosity increases since collisions are most likely to occur at the outermost particles of the floc, increasing the tendency for long chains to

form leaving significant voidage in the developed structure. According to Argaman (1968), flocs reach their ultimate size after approximately 6 minutes, but Glasgow and Hsw (1982) showed that this initial formation of smaller and denser agglomerates collide later to form larger, less dense agglomerates.

The results of floc size and density with alum and Moringa oleifera as coagulant are compared in Figures 5.21 and 5.22 for two flocculation times. It is clearly shown that flocs with Moringa oleifera as coagulant have higher density and smaller size for all the cases, with up to 14.2 times greater effective floc density and 89% lower floc size. Kimple (1984) also found that there are coagulant effects on the floc density and size. He found that the flocs formed using a combination of the low molecular weight polyacrylamide and inorganic salt of Calcium Chloride ($CaCl_2$) as the flocculant appear to be less dense and larger than those formed from the high molecular weight cationic polyacrylamide only. Gassenschmidt et al (1995) found the main flocculent protein of Moringa oleifera was comparable to that of a synthetic polymer, such as polyacrylamide, and as both alum and Calcium Chloride are inorganic salts, the results shown here support Kimple's studies.

The effect of particle size on the effective diffusivity of the floc is composed of two opposing factors: an increase in particle size results in a decrease of the entrainment factor and an increase of the collision radius due to reduction in available particles for aggregation. As the diffusivity is directly proportional to the entrainment factor and the collision radius, the combined effect depends on the relative significance of these two factors.

5.4 CONCLUSIONS

In this chapter, experimental studies of flocculation and settling were carried out under various flow rates, types of coagulant, raw water turbidities, times of flocculation and settling, and arrangements of flocculator and settling tank. Flocculation efficiency is presented not only in terms of turbidity but also floc size, settling velocity and density. The following conclusions are drawn from these experimental investigations:

1. Turbulence intensity in a hydraulic flocculator can be adjusted by inserting grid baffles, varying bed slope and channel width to cope with the variation of raw water quality and rate of flow. The adjusted turbulence allows the flocculation efficiency to be improved

when there is insufficient or excessive agitation and flocculation time. The flocculation efficiencies could increase by up to 42% according to this research.

2. The maximum flocculation efficiency for the highest initial turbidity of 950 NTU is up to 3.2 times of that for the initial turbidity of 100 NTU, 1.6 times for 265 NTU with alum as coagulant. For Moringa oleifera as coagulant, the ratio of maximum flocculation efficiency of the initial concentrations of 950 NTU to that of 265 NTU is in the range of 1.1 to 1.6.

3. Flocculation time should be more than 7 minutes, and around 20 minutes in general, for effective treatment.

4. Alum, as a whole, provides better flocculation than Moringa oleifera. Stronger initial mixing gives an increase in flocculation efficiency for both the testes with alum and Moringa oleifera as coagulant. However, it has more significant effect on the tests with Moringa oleifera. Flocs with Moringa oleifera as coagulant have higher density and smaller size, with up to 14.2 times greater effective floc density and 89% lower floc size compared with the flocs with alum as coagulant.

5. Settling with the higher initial turbidity (950 NTU) produced greater solids removal by up to 1.5 times compared with the lower initial turbidity (265 NTU) for a corresponding flow. The tube settling tank provides an about 16.4 times larger settling area, is 9 times shorter in settling distance and 17 times less in Reynolds number than those of the tank without tubes for a specific flow, and this allows the tube settling tank to give greater removal of solids. Up to 76% increase in settling efficiency was obtained by extending the settling time from 6.25 minutes to 12.5 minutes.

6. Tracer studies showed that both the 45mm and 150mm wide channel flocculators are close enough to ideal plug flow reactors to allow their simulation for flocculation performance as plug flow. Flow in the settling tank with tubes is closer to ideal plug flow than that in the tank without tubes.

7. Measurements of head loss in the channel flocculators indicate that the empirical friction coefficient at the bend is not a fixed value but is dependent on many factors,

such as flow velocity and the geometry of the flocculator. Here it fell in the range of 2.6 to 3.4.

Chapter 6 Computation of turbulence and flocculation

6.1 Introduction

It is well known that turbulence can be used as a measure of the effectiveness of promoting flocculation, an extensively used and most important method of water treatment. Although the overall turbulence should be the integration of that of the individual points in the flocculator rather than an averaged velocity gradient (G) and the use of the averaged velocity gradient has been criticised by many investigators (see Chapter 2), the averaged velocity gradient still has generally been employed as the turbulence parameter in assessing flocculation efficiency and designing the flocculation process as it can be evaluated relatively simply. With the use of the verified Computational Fluid Dynamics (CFD) package FLUENT (see Chapter 4), the current study is able to provide the accurate values of the turbulence and velocity at any point in the flocculator. The relationships between the velocity and turbulence and the number of the channels and the nominal velocity established in Chapter 4 enable an easy and accurate approach to calculating the flocculation in relation to turbulence by inserting the individual turbulence intensities and the velocities into Argaman's equation (Amirtharajah and O'Melia, 1990) for a plug flow, which was the flow states of the flocculators of this study tested by the tracer study described in Chapter 5. The aggregation and breakup constants during the flocculation were determined under various flow rates, raw water turbidities, retention times, types of coagulants, flocculator geometry and arrangements of settling.

6.2 Computation of turbulence in relation to flocculation

The theoretical background of turbulence in relation to flocculation was discussed in Chapter 2. Argaman's flocculation equation (1968) for a plug flow can be expressed as follows:

$$\frac{n_1}{n_0} = \frac{K_b}{K_a}\frac{\overline{u'^2}}{K_p} + \left(1 - \frac{K_b}{K_a}\frac{\overline{u'^2}}{K_p}\right)e^{-K_a\frac{\overline{u'^2}}{K_p}t} \qquad (6.1)$$

n_1 and n_0 are the particle concentrations at times t and 0. The coefficients of formation and breakup of flocs are given by K_a and K_b respectively, K_p is a coefficient and has a particular

value for a specific flocculator, and $\overline{u'^2}$ is the square of the averaged flow velocity fluctuation in a flocculator. According to Argaman (1968) $\overline{u'^2}$ can be expressed in terms of velocity gradient G in a mechanical flocculator:

$$G = \overline{u'^2}/K_p \tag{6.2}$$

Therefore, Equation 6.1 can be rewritten as the commonly used (Amirtharajah and O'Melia, 1990) design equation:

$$\frac{n_1}{n_0} = \frac{K_b}{K_a}G + (1 - \frac{K_b}{K_a}G)e^{-K_aG\ t} \tag{6.3}$$

Here, it should be noted that G is the averaged velocity gradient rather than the integration of the square of the individual velocity fluctuation (u'^2) and t is the averaged hydraulic retention time rather than the real flocculation time for each individual unit in the flocculator. Therefore Argaman's equation is still a formula based on the average of turbulence and hydraulic retention time which has been being criticised (Ives 1968, Lai 1975, Andreu-Villegas and Letterman 1976, Cleasby 1984, Clark 1985, McConnachie 1991). Although the previous investigators tried to compensate for the use of averaged velocity gradient (G) by adopting some new terms still associated with the G such as Gt, G^nt and GtC, where n is a constant, C is the concentration of coagulant and t is the retention time, they still kept using the average concept whilst the fundamental discrete methodology was not addressed. To do so, the calculation domain of the flocculators in this study was discreted into a number of control volumes. The averaged velocity gradient, G, in Argaman's equation was replaced by the integration of the square of the velocity function $u_i'^2$ of each control volume $\forall_i$, and the averaged hydraulic retention time t was replaced by the real flocculation time for each control volume, t_i, which is expressed as

$$t_i = L_i/u_i \tag{6.4}$$

-where L_i is the length of the control volume in the i direction, u_i is the instantaneous velocity of the corresponding control volume in the i direction. In the current study, the

length and velocity in the x direction were used because of the reliable experimental readings and good fit with the modelling results in the direction of the x coordinate.
By definition, kinetic energy,

$$k_i = \frac{1}{2}(u_i'^2 + v_i'^2 + w_i'^2) \tag{6.5}$$

-where u_i', v_i' and w_i' are the velocity fluctuations in three dimensions for the control volume of $\forall_i$.

So a new integration equation for calculating flocculation in relation to turbulence can be produced by replacing G in Equation 6.3 with the sum of the square of individual velocity fluctuation quantified by turbulence kinetic energy as expressed in Equations 6.5 and substituting t_i for t, giving,

$$\frac{n_1}{n_0} = \frac{K_b}{K_a}\sum_i^N \frac{\frac{2}{K_p}k_i\forall_i}{\forall} + (1 - \frac{K_b}{K_a}\sum_i^N \frac{\frac{2}{K_p}k_i\forall_i}{\forall})e^{-K_a\sum_i^N \frac{\frac{2}{K_p}k_i\forall_i}{\forall}\frac{L_i}{u_i}} \tag{6.6}$$

-where $\forall$ is the effective total volume of the flocculator and N is the total number of control volumes. Substituting η for $\frac{2}{K_p}$ gives,

$$\frac{n_1}{n_0} = \eta\frac{K_b}{K_a}\sum_i^N \frac{k_i\forall_i}{\forall} + (1 - \eta\frac{K_b}{K_a}\sum_i^N \frac{k_i\forall_i}{\forall})e^{-\eta K_a\sum_i^N \frac{k_i\forall_i}{\forall}\frac{L_i}{u_i}} \tag{6.7}$$

For channel number N', the Equation can be rewritten as follows:

$$\frac{n_1}{n_0} = \eta\frac{K_b}{K_a}\sum_{i=1}^X\sum_{i=1}^Y\sum_{i=1}^Z\sum_{i=1}^{N'} \frac{k_i\forall_i}{\forall} + (1 - \eta\frac{K_b}{K_a}\sum_{i=1}^X\sum_{i=1}^Y\sum_{i=1}^Z\sum_{i=1}^{N'} \frac{k_i\forall_i}{\forall})e^{-\eta K_a\sum_{i=1}^X\sum_{i=1}^Y\sum_{i=1}^Z\sum_{i=1}^{N'}\frac{k_i\forall_i}{\forall}\frac{L_i}{u_i}} \tag{6.8}$$

-where X, Y and Z are the number of control volumes in x, y and z directions in one channel. From a theoretical view, Equations 6.7 and 6.8 are much more accurate than Equation 6.3, but it is obviously a time consuming process to obtain the kinetic energy and

the velocity of each control volume in all the channels by directly using these two equations and it is not appropriate for engineering design. However, accurate and simplified equations can be generated on the basis of the relationships between velocity and kinetic energy and the nominal velocity and the number of channels expressed by Equations 4.21 and 4.24, and repeated here,

$$u_i/u_j \approx k_i/k_j \approx \alpha\, V_i/V_j \tag{6.9}$$

$$u_i/u_{i+2} = k_i/k_{i+2} = \beta \tag{6.10}$$

These 'simplified' equations for calculating flocculation efficiency under any nominal average velocity, for example V_k, and any number, for example N', of the channels of the hydraulic flocculator can be produced by inserting Equations 6.9 and 6.10 into Equation 6.8 on the basis of knowing the velocity and kinetic energy in the first two channels in the flocculator under nominal average velocity V_i.

To simplify the final equations substitutions A, A1, B and B1 have been made where,

$$A = \eta \frac{K_b}{K_a} \sum_{i1}^{N} \frac{k_{i1} \forall_{i1}}{\forall} \tag{6.11.1}$$

$$A1 = \eta K_a \sum_{i1}^{N} \frac{k_{i1} \forall_{i1}}{\forall} \frac{L_{i1}}{u_{i1}} \tag{6.11.2}$$

$$B = \eta \frac{K_b}{K_a} \sum_{i2}^{N} \frac{k_{i2} \forall_{i2}}{\forall} \tag{6.11.3}$$

$$B1 = \eta K_a \sum_{i2}^{N} \frac{k_{i2} \forall_{i2}}{\forall} \frac{L_{i2}}{u_{i2}} \tag{6.11.4}$$

-where k_{i1}, $\forall_{i1}$, L_{i1} and u_{i1} are the kinetic energy, volume, length and instantaneous velocity of the control volume i1 in the first channel and k_{i2}, $\forall_{i2}$, L_{i2} and u_{i2} are the corresponding parameters in the second channel.

Thus, if N' is an odd number,

$$\frac{n_1}{n_0} = \alpha \frac{V_i}{V_k} A \sum_{j=1,3,5...}^{N'} \beta^{\frac{j-1}{2}} + (1-\alpha \frac{V_i}{V_k} A \sum_{j=1,3,5...}^{N'} \beta^{\frac{j-1}{2}}) e^{-\alpha A 1 \sum_{j=1,3,5...}^{N'} \beta^{\frac{j-1}{2}}}$$

$$+\alpha \frac{V_i}{V_k} B \sum_{j=2,4,6...}^{N'-1} \beta^{\frac{j-2}{2}} + (1-\alpha \frac{V_i}{V_k} B \sum_{j=2,4,6...}^{N'-1} \beta^{\frac{j-2}{2}}) e^{-\alpha B 1 \sum_{j=2,4,6...}^{N'-1} \beta^{\frac{j-2}{2}}} \quad (6.12)$$

-where j is the number of channels.

If N' is an even number,

$$\frac{n_1}{n_0} = \alpha \frac{V_i}{V_k} A \sum_{j=1,3,5...}^{N'-1} \beta^{\frac{j-1}{2}} + (1-\alpha \frac{V_i}{V_k} A \sum_{j=1,3,5...}^{N'-1} \beta^{\frac{j-1}{2}}) e^{-\alpha A 1 \sum_{j=1,3,5...}^{N'-1} \beta^{\frac{j-1}{2}}}$$

$$+\alpha \frac{V_i}{V_k} B \sum_{j=2,4,6...}^{N'} \beta^{\frac{j-2}{2}} + (1-\alpha \frac{V_i}{V_k} B \sum_{j=2,4,6...}^{N'} \beta^{\frac{j-2}{2}}) e^{-\alpha B 1 \sum_{j=2,4,6...}^{N'} \beta^{\frac{j-2}{2}}} \quad (6.13)$$

Here, Equation 6.8 is called the "point to point method", Equations 6.12 and 6.13 are called the "simplified method" and Equation 6.3 is called the "average G method". To test the validity of the Equations 6.12 and 6.13, comparison between the calculation of flocculation efficiency vs turbulence kinetic energy by the "simplified method" and by the "point to point method" is made for the cases listed in Table 6.1 and is shown in Figures 6.1.1 to 6.1.6. The results of the "point to point method" and the "simplified method" were also compared with experimental data. In the Figures, the Relative error (S) and the Relative error (P) represent the relative errors in respect of the experimental results for the results of the "simplified method" and the "point to point method" respectively. The experiments were carried out in the 45mm wide channel flocculator with a 1/30 longitudinal bed slope; aluminium sulphate was used as coagulant. The particle concentrations n_0 and n_1 should be replaced by an appropriate parameter for different types of water under test (Bratby, 1980). For example, UV spectrophototmetric measurements for a coloured water, turbidity for a turbid water. Therefore the measurements of turbidity before flocculation and after flocculation and 25 minutes settling were substituted for the particle concentrations n_0 and n_1 to calculate the extent of flocculation in this study. This principle was also used by Haarhoff (1997).

Table 6.1 Test conditions

Case No.	Nominal Velocities (m/s)	Flocculation Time (minutes)	Raw water turbidity n_0 (NTU)
1	0.035, 0.05, 0.06, 0.065, 0.075 and 0.1	17.2	100
2	0.035, 0.05, 0.06, 0.065, 0.075 and 0.1	8.6	100
3	0.035, 0.05, 0.06, 0.065, 0.075 and 0.1	17.2	265
4	0.035, 0.05, 0.06, 0.065, 0.075 and 0.1	8.6	265
5	0.035, 0.05, 0.06, 0.065, 0.075 and 0.1	17.2	950
6	0.035, 0.05, 0.06, 0.065, 0.075 and 0.1	8.6	950

According to Montgomery (1985), the average velocity gradient G in a baffled channel flocculator is expressed as follows:

$$G = \sqrt{\frac{g\rho h}{\mu t}} \tag{6.14}$$

-where g is the gravity constant, ρ is the fluid density, μ is the fluid absolute viscosity, t is the average hydraulic retention time and h is the total head loss. Head loss can be calculated or directly measured from experiment (see Chapter 5).

Comparison between the results of the "average G method" and the experimental data is given in Figures 6.2.1 to 6.2.6 under the same conditions listed in Table 6.1.

It is shown from the Figures 6.1.1 to 6.1.6 that there is an excellent fit between the results of the "simplified method" and the results of the "point to point method". Both calculation values quantitatively agree very well with the experimentally determined rate of flocculation under three different raw water turbidities and two nominal flocculation times and the basic shape of the variations of flocculation efficiency with turbulence kinetic energy are well reproduced by the two methods. The relative errors of these two methods to the experimental results are mainly below 20%.

Figures 6.2.1 to 6.2.6 show the results calculated by the "average G method" against the efficiency of flocculation directly from the experiments under the same conditions as that of the "simplified method" and the "point to point method". The fit between the results of the "average G method" and the experimental data is not quite so good, however, as that for the

"simplified method" and the "point to point method". The relative error is up to 115% and about half of the relative errors exceed 20%.

It is concluded that comparison of the experimental data with the results of the proposed "simplified method" and the "point to point method" of calculating rate of flocculation show that the "simplified method" is sufficiently accurate to predict the flocculation efficiency of a hydraulic channel flocculator. Also it is not accurate to directly apply the Argaman's equation to assess the hydraulic flocculator although it has been shown to give a relatively good fit in quantifying the flocculation efficiency in a mechanical flocculator (Argaman, 1968).

6.3 Determination of aggregation and breakup constants

The most practical contribution of the Argaman's equation to the real engineering design might be the flocculation constants, which are able to generalise the flocculation behaviour and can be obtained from a few, simple tests in the laboratory. Tables 6.2 lists the aggregation constant and the breakup constant empirically determined in the laboratory for a mechanical flocculator by previous investigators. Amirtharajah and O'Melia (1990) suggested that the aggregation constant K_a is in the range of 1.8 to 4.5×10^{-5} and K_b is in range of 0.8 to 1.0 x 10^{-7} sec. for kaolin clay-alum system and alum coagulation of natural particles. However the application of the flocculation constants to the real engineering design has not been widely adopted due to the lack of comparability, general validity and scalability although the standardisation of experimental apparatus and method recommended by Bratby et al (1977) makes it possible to compare the flocculation constants determined by different researchers for a specific particle-coagulant system and a specific mechanical flocculator.

Little relevant information is found on the study of flocculation constants for a hydraulic flocculator. However, this is needed and the current study of flocculation constants is attempting to guide hydraulic flocculator design and give the designers a better understanding of the potential use of the flocculation constants in designing flocculators and their influencing factors.

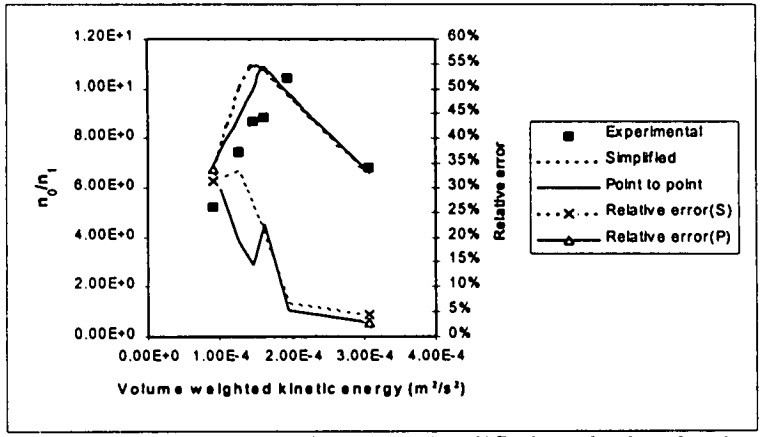

Figure 6.1.1 Comparison between simplified method and point to point method with experimental results (case 1)

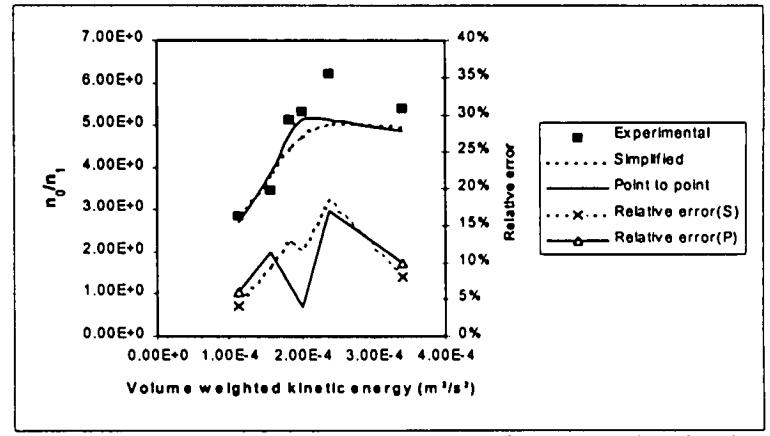

Figure 6.1.2 Comparison between simplified method and point to point method experimental results (case 2)

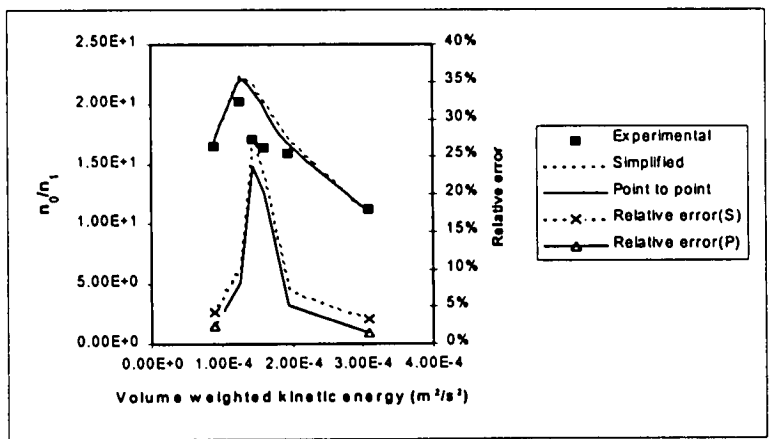

Figure 6.1.3 Comparison between simplified method and point to point method experimental results (case 3)

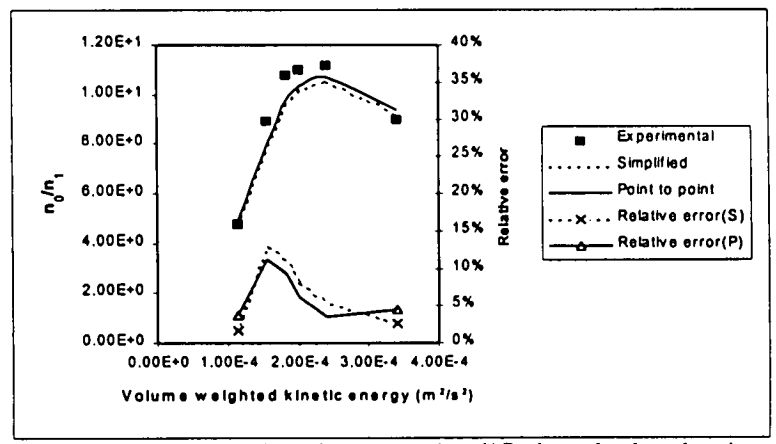

Figure 6.1.4 Comparison between simplified method and point to point method experimental results (case 4)

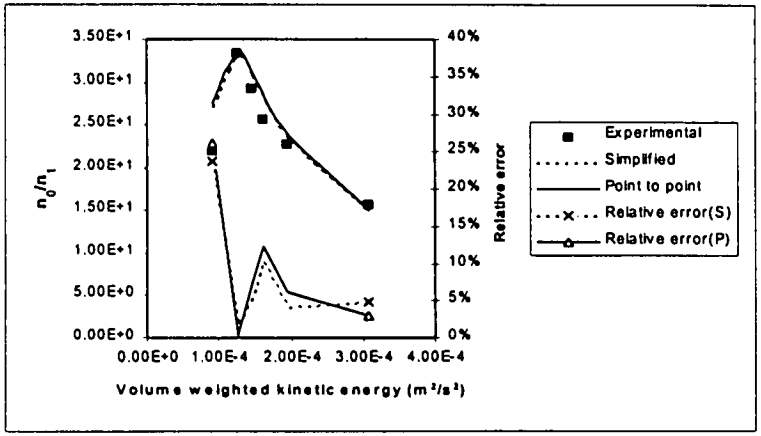

Figure 6.1.5 Comparison between simplified method and point to point method experimental results (case 5)

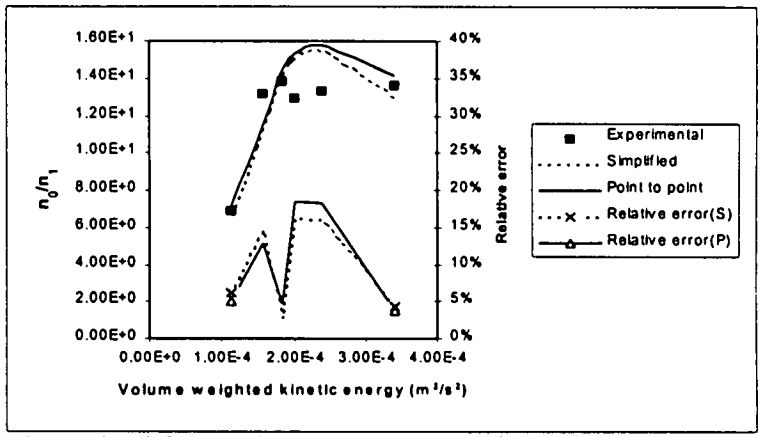

Figure 6.1.6 Comparison between simplified method and point to point method experimental results (case 6)

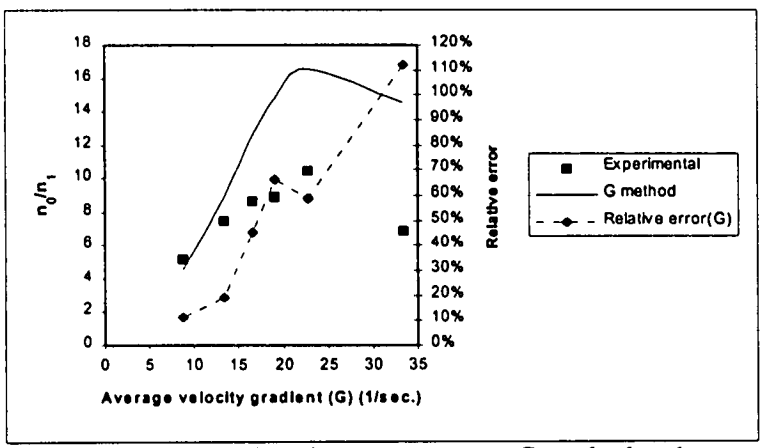

Figure 6.2.1 Comparison between average G method and experimental results (case 1)

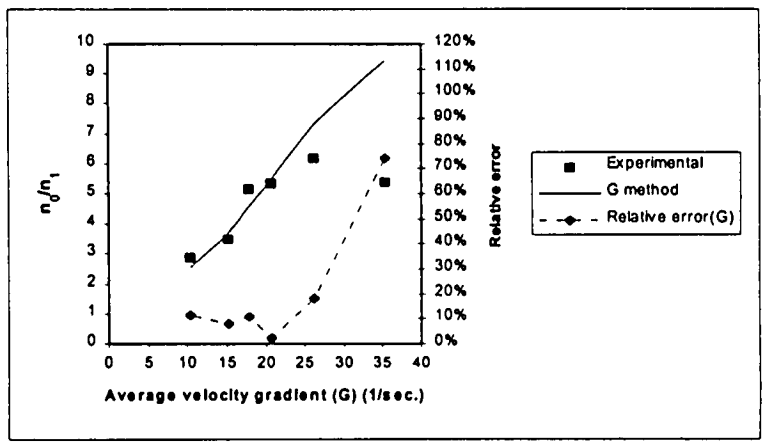

Figure 6.2.2 Comparison between average G method and experimental results (case 2)

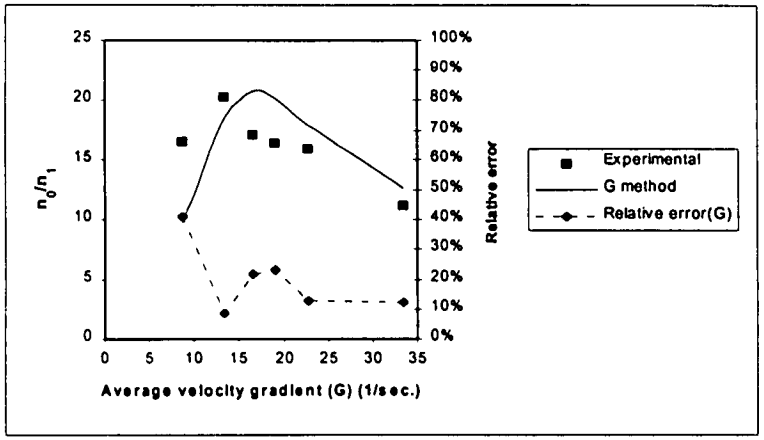

Figure 6.2.3 Comparison between average G method and experimental results (case 3)

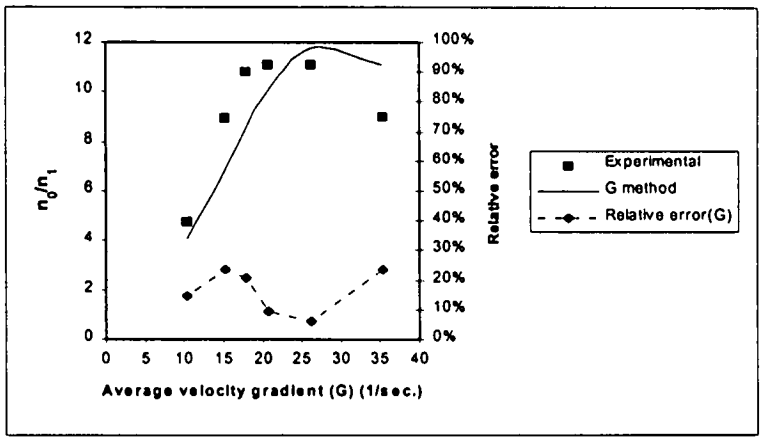

Figure 6.2.4 Comparison between average G method and experimental results (case 4)

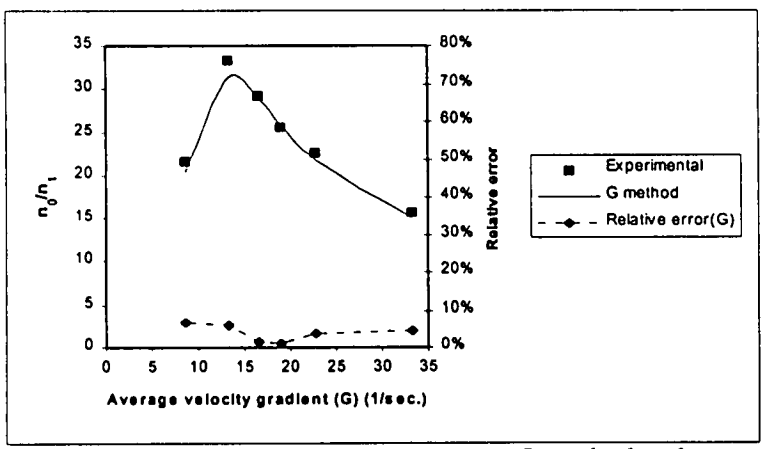

Figure 6.2.5 Comparison between average G method and experimental results and (case 5)

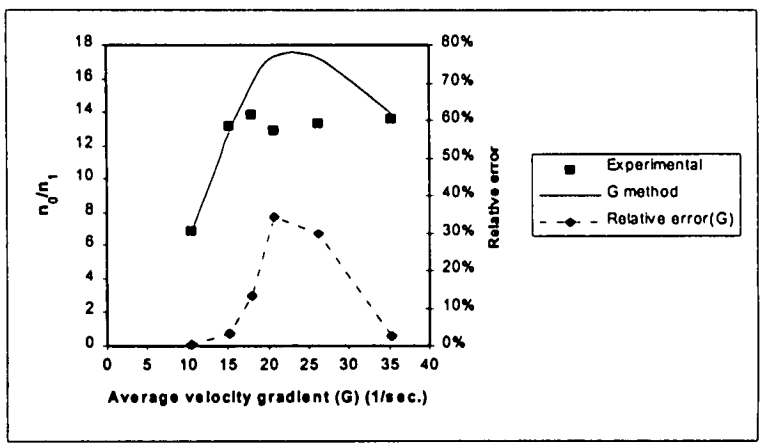

Figure 6.2.6 Comparison between average G method and experimental results (case 6)

Table 6.2 Aggregation constant K_a and Breakup constant K_b (Abstracted from Montgomery, 1985)

System	K_a	K_b (sec.)	Reference
Kaolin-alum	4.5×10^{-5}	1×10^{-7}	Argaman (1970)
Kaolin-alum	2.5×10^{-4}	4.5×10^{-7}	Bratby (1977)
Natural particulate-alum	1.8×10^{-5}	0.8×10^{-7}	Argaman (1971)
Alum-phosphate precipitate	2.8×10^{-4}	3.4×10^{-7}	Argaman (1971)
Alum-phosphate plus polymer	2.7×10^{-4}	1×10^{-7}	Odegaard (1979)
Lime-phosphate, pH 11	5.6×10^{-4}	2.4×10^{-7}	Odegaard (1979)

Increased turbulence accelerates the process of interparticle collisions and formation of flocs. However, if the agitation is too vigorous, then the turbulent shear forces developed will cause floc to break up and consequently demolish the flocculation. Therefore, the analysis for the overall kinetic energy of flocculation needs to combine the processes of aggregation and breakup for a realistic description of the process. In this section, the effects of raw water turbidity, type of coagulant and arrangement of settling on the determination of aggregation and breakup constants during the flocculation in the 45mm wide channel flocculator are discussed. The details of the experiments are described in Chapter 5 and the conditions of the tests are listed in Table 6.3.

Table 6.3 Details of test conditions

Test Designation	Nominal velocity v(m/s)	n_0 (NTU)	Coagulant (mg/l)		Settling time (min)	
			Alum	M.Oleifera	Tank with no tube	Tank with tube
A	0.035, 0.05, 0.06, 0.065, 0.075 and 0.1	100	25	***	25	***
B	0.035, 0.05, 0.06, 0.065, 0.075 and 0.1	265	50	***	25	***
C	0.035, 0.05, 0.06, 0.065, 0.075 and 0.1	950	80	***	25	***
D	0.035, 0.05, 0.06, 0.065, 0.075 and 0.1	265	***	75	25	***
E	0.035, 0.05, 0.06, 0.065, 0.075 and 0.1	950	***	100	25	***
F	0.035, 0.05, 0.06, 0.065, 0.075 and 0.1	265	50	***	***	25

The flocculation constants, K_a and K_b, can be calculated either by Equations 6.12 or 6.13 by knowing local kinetic energy, velocity, geometry of each control volume and η. In this study the value of η is set as 400,000 on the basis of K_p ranging from $\frac{1}{200000}$ to $\frac{1}{400000}$ according to Argaman (1968). Different magnitudes of the flocculation constants are

calculated resulting from different values of K_p. However, the value of K_p was kept the same for all the relative cases of the flocculation study therefore the degree of errors (if any) is the same. And because the main interest of this part is to compare the variation of the flocculation constants rather than their absolute values under various conditions, the error due to the setting of η is acceptable.

Theoretically, from two sets of experimental data, the flocculation constants, K_a and K_b, can be calculated either by Equation 6.12 or 6.13. However, Haarhoff et al (1996) studied the minimum number of tests to be performed to derive the two flocculation constants (K_a and K_b) from the experimental data. He concluded that for a reliable estimation of the flocculation constants, nine is the minimum number of tests which should include a sufficiently short flocculation time of 6 minutes or less to demonstrate the effect of the aggregation constant, K_a, and a sufficiently high turbulence intensity and long flocculation time of 12 to 18 minutes to demonstrate the effect of the breakup constant, K_b. This is because the effect of the aggregation constant K_a is especially evident early in the flocculation process, while the effect of the breakup constant K_b is only evident later in the flocculation process, and especially at high velocity gradients. In this study as described in Chapter 5, considering the accuracy of determination of the flocculation constants and research interest in the range of their variation with turbulence and flocculation time, eighteen tests, namely six turbulence intensities quantified by kinetic energy corresponding to six nominal velocities (v = 0.035, 0.05, 0.06, 0.065, 0.075 and 0.1m/s) and three nominal flocculation times (t = 4.3, 8.6 and 17.2 minutes), were carried out which consequently generated (n-1)! estimations of flocculation constants. Here, n equals 18, the number of tests. To determine the flocculation constants from (n-1)! estimations, the ratio of n_1/n_0 rather than n_0/n_1 was plotted with the volume weighted averaged kinetic energy and used as the basis for fitting lines of best fit of the flocculation constants. This was suggested by Bratby et al (1977) to minimise the error whilst determining the flocculation constants. From the curves of volume weighted kinetic energy ($\sum \frac{k_i \forall_i}{\forall}$) vs flocculation performance (n_1/n_0) (values of kinetic energy and flocculation efficiency listed in Appendix B), the aggregation and breakup constants, K_a and K_b can be determined by fitting either Equation 6.12 or 6.13 to the curves and are shown in Figures 6.3.1 and 6.3.2. The choice of the settling time of 25 minutes in this study is based on the principle that it should be slightly greater than the time beyond which no significant improvement of the water quality is

evident according to Bratby (1980) and previous investigators' experience (Argaman, 1968; McConnachie, 1991).

6.3.1 Effect of raw water turbidity

In Figures 6.3.1, 6.3.2 and 6.3.3, three different raw water turbidities with Alum as coagulant labelled as Alum 100 (i.e. turbidity = 100 NTU), Alum 265 and Alum 950, and two different raw water turbidities with Moringa oleifera as coagulant labelled as M.Oleifera 265 and M. Oleifera 950, are used to study the effect of raw water turbidity on the flocculation constants. The influence of the tube settling is included for Alum 265.

The Figures show that the aggregation constant consistently increases whilst the raw water turbidity is increased form 100 to 950 NTU for both the cases with Alum and Moringa oleifera, the magnitude of the aggregation constant for the turbidity of 950 NTU is 1.8 times of that for the turbidity of 100 NTU with the alum as coagulant. The effect of raw water turbidity makes the breakup constant consistently decrease, about 21% decrease from 950 NTU to 100 NTU, for the cases with Alum, but 10% increase for the cases with Moringa oleifera from 265 NTU to 950 NTU. The ratio of the breakup constant to aggregation constant constantly decreases in the range of about 18% to 56% for all the five cases.

It is concluded that the flocculation constants are, contrary to the Argaman flocculation model, dependent on the initial particle concentration. This was also found by the work done by Haarhoff (1997).

The variation of the flocculation constants due to the change of raw water turbidity resulted in different flocculation performances vs kinetic energy as exhibited in the Figures 6.4.1 to 6.5.2. It is clearly displayed that the higher raw water turbidity the better the flocculation performance for all the cases, which is corresponding to the increase of aggregation constants with the increase of raw water turbidity. The maximum flocculation efficiency for

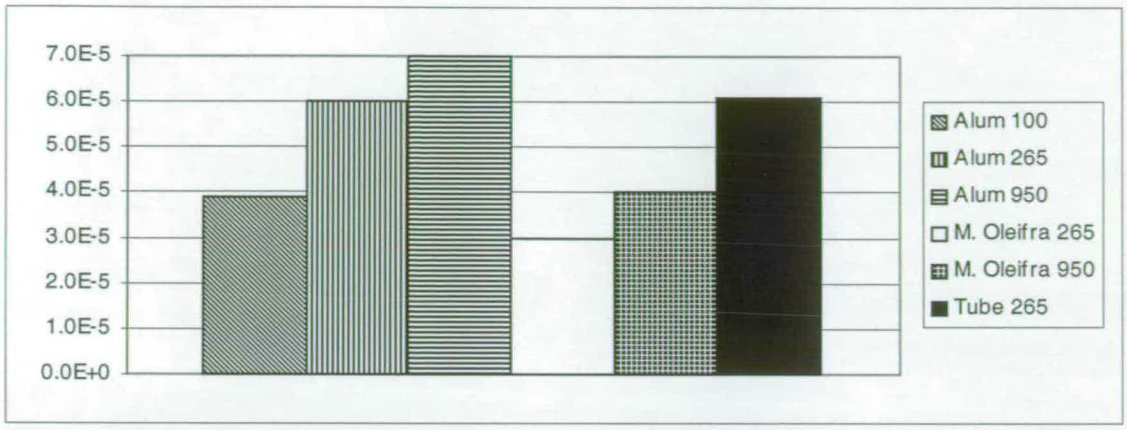

Figure 6.3.1 Variation of aggregation constants K_a with initial turbidity, type of coagulant and arrangement of settling

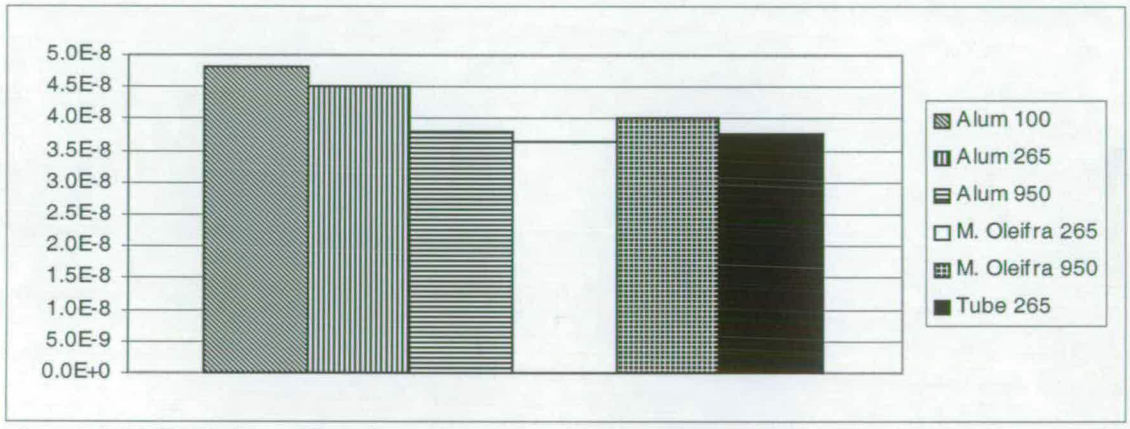

Figure 6.3.2 Variation of breakup constants K_b with initial turbidity, type of coagulant and arrangement of settling

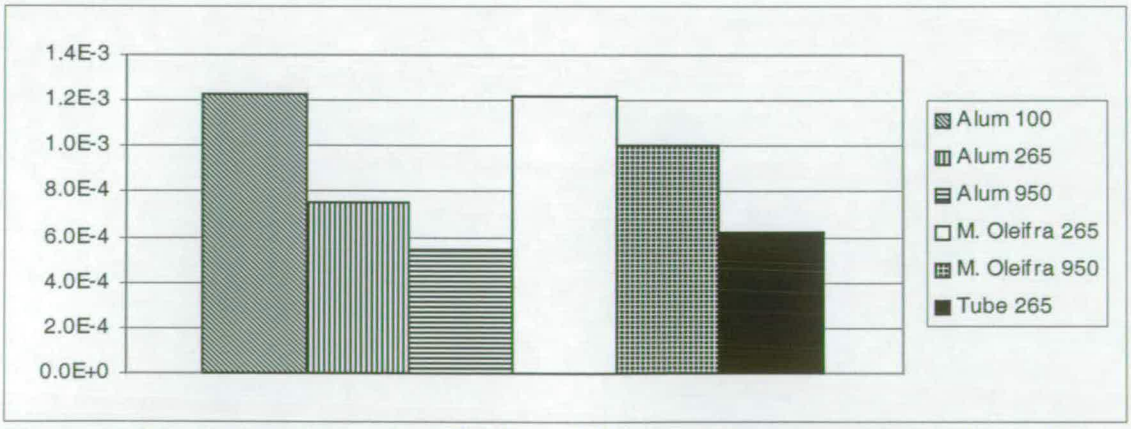

Figure 6.3.3 Variation of the ratio of K_b/K_a with initial turbidity, type of coagulant and arrangement of settling

the raw water turbidity of 950 NTU is about 3 times of that for the raw water turbidity of 100 NTU, 1.5 times for 265 NTU with alum as coagulant, and about 2.5 times and 3.9 times respectively for the two initial concentrations of 950 and 265 NTU with Moringa oleifera as coagulant. Comparison of Figures 6.4.1 and 6.4.2, Figures 6.5.1 and 6.5.2 show that 4.3 minutes is not a long enough flocculation time for the particle aggregation and consequently producing the maximum rate of flocculation. Treweek (1979) and McConnachie (1995) suggested that the flocculation time should be more than 7 minutes, and usually around 20 minutes, in terms of creating maximum flocculation efficiency.

6.3.2 Effect of types of coagulant

In Figures 6.3.1, 6.3.2 and 6.3.3 the columns labelled Alum 265, Alum 950 and M.Oleifera 265 and M. Oleifera 950 are used to assess the effect of types of coagulant on the determination of flocculation constants. The corresponding aggregation and breakup constants are expressed as $K_{a(Alum)}$ and $K_{b(Alum)}$ for the tests with Alum and expressed as $K_{a(M.\ O)}$ and $K_{b(M.O)}$ for the tests with coagulant of Moringa oleifera.

The following points are evident from the Figures:

The aggregation constants $K_{a(Alum)}$, are around 2.0 and 1.8 times of $K_{a(M.\ O)}$ for the two corresponding medium and high raw water turbidities. This might be explained by the following: as mentioned in Chapter 5, at pH = 7, and alum dosage in the range of 25 to 80mg/l, the dominant flocculation mechanism for alum is sweep flocculation (Amirtharajah and Mills, 1982), while Gassenschmidt et al (1995) found the main flocculent protein of the Moringa oleifera was comparable to that of synthetic polymer, such as polyacrylamide, and the flocculation with Moringa oleifera follows the combined mechanisms of patch charge and interparticle bridging. In sweep coagulation, the individual characteristics of the particles in suspension are obliterated within fraction of a second of adding the coagulant and the system becomes almost indistinguishable from coagulating metal hydroxide. An important function of the precipitated metal hydroxide is to provide a large number of particles and thereby improve coagulation kinetics very substantially (Packham and Sheiham, 1977).

The effect of the types of coagulant on the breakup constant is not consistent for the two different raw water turbidities. At the raw water turbidity of 265 NTU, the breakup constant $K_{b(Alum)}$ is about 24% greater than $K_{b(M.O)}$. At the raw water turbidity of 950 NTU, the

breakup constant $K_{b(Alum)}$ is 5% less than $K_{b(M.O)}$. There is very little fundamental understanding of the factors affecting the strength of aggregates or their mode of breakage under stress, and most work has been of an empirical nature (Thomas et al, 1999). According to Muhle (1993), the floc strength is proportional to a floc's size. However, Yeung and Pelton (1996) found that the strength of floc is related to floc compactness rather than floc size. Either the floc size or floc compactness is dependent on the type of coagulant and water turbidity. For the case mentioned above both coagulant and turbidity varied, therefore there is no consistent effect on the breakup constant.

The effect of the types of coagulant on the ratio of breakup constant to aggregation constant is consistent for the two different raw water turbidities. The ratio of constants $K_{b(Alum)}/K_{a(Alum)}$ are 38% and 46% less than $K_{b(M.O)}/K_{a(M.O)}$ for the two corresponding medium and high raw water turbidities.

The variation of the flocculation constants due to the use of the two types of coagulants affected the flocculation performances vs kinetic energy as exhibited in Figures 6.4.1 to 6.5.2. It is clearly shown that the flocculation performances are poorer with Moringa oleifera than with alum.

6.3.3 Effect of arrangement of settling

The following observations are made from the two columns labelled Alum 265 and Tube Alum 265 in Figures 6.3.1, 6.3.2 and 6.3.3 for the comparison of test B with normal settling and test F with tube settling under the raw water turbidity of 265 NTU.

Tube settling gave a slight increase, 1.7%, to the aggregation constant and about 16% decrease to the breakup constant compared with the normal settling. The ratio of breakup constant to aggregation constant with the tube settling is 17.6% less than that without tube settling.

Figures 6.6.1 and 6.6.2 present the difference of the flocculation efficiency due to the variation of the flocculation constants from the settling tank without and with tubes. It is due to the increased settling area, shorter settling depth and improved flow conditions, which can be expressed by Reynolds number, for the floc settling and consequently enhances the

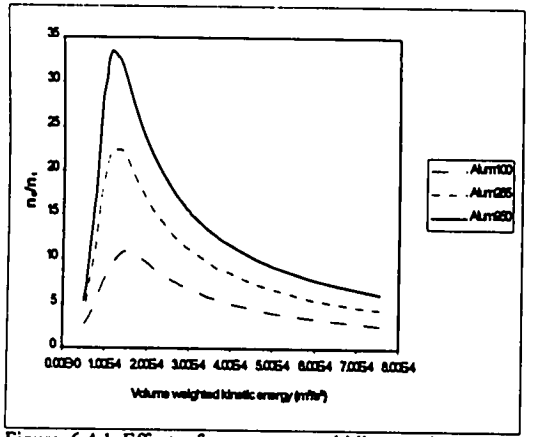

Figure 6.4.1 Effect of raw water turbidity on flocculation efficiency (Nominal flocculation time=17.2 minutes)

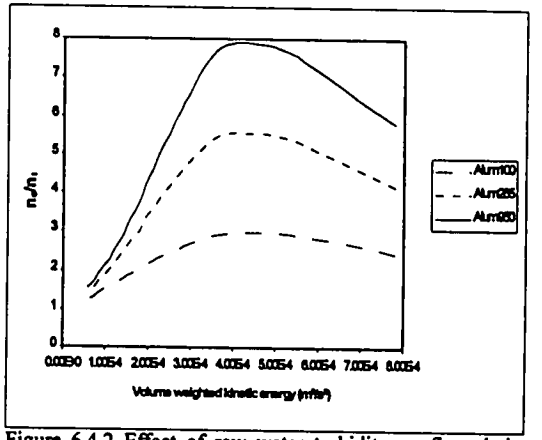

Figure 6.4.2 Effect of raw water turbidity on flocculation efficiency (Nominal flocculation time=4.3 minutes)

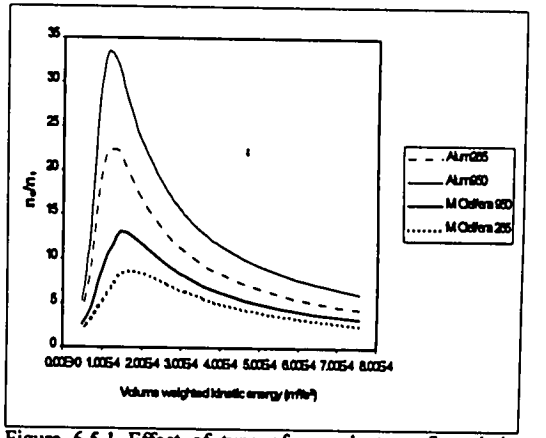

Figure 6.5.1 Effect of type of coagulant on flocculation efficiency (Nominal flocculation time=17.2 minutes)

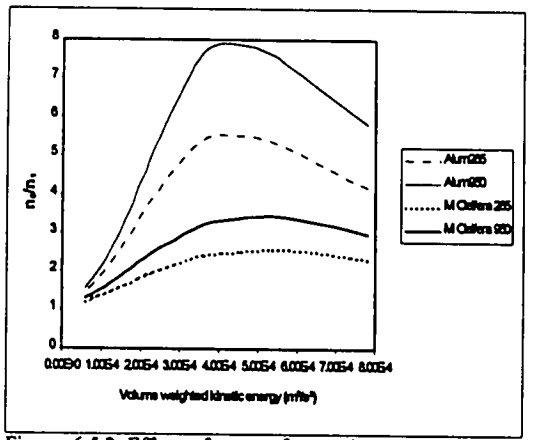

Figure 6.5.2 Effect of type of coagulant on flocculation efficiency (Nominal flocculation time=4.3 minutes)

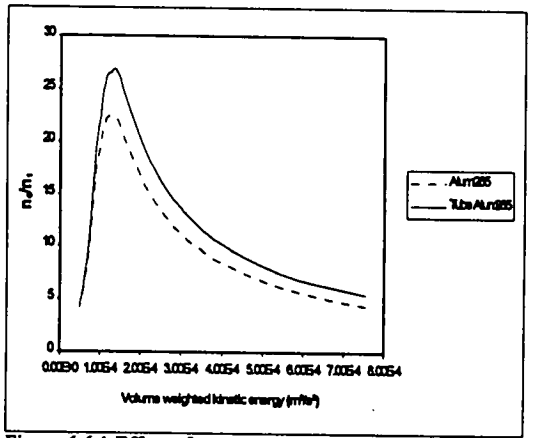

Figure 6.6.1 Effect of arrangement of settling on flocculation efficiency (Nominal flocculation time=17.2 minutes)

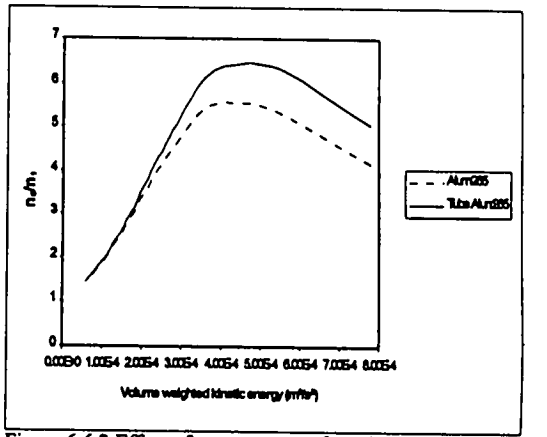

Figure 6.6.2 Effect of arrangement of settling on flocculation efficiency (Nominal flocculation time=4.3 minutes)

aggregation and settling of flocs and minimises the breaking of aggregated flocs. According to the calculation in Chapter 5, for a flow rate under a specific hydraulic retention time, such as 25 minutes, the settling area of the tube settling tank was increased almost 16 times while the settling depth was decreased 9 times of that of the tank without tubes. The Reynolds number with the tank having tubes is only about 6% of that of the tank without tubes indicating smoother flow achieved in the tube settling tank.

6.4 Conclusions

In this chapter, a modified Argaman's equation for calculating the extent of flocculation in relation to turbulence is derived and the determination of flocculation constants under various raw water turbidities, types of coagulant and arrangements of settling is given. The following conclusions are drawn from the computation of the degree of flocculation in the channel flocculator:

1. The modified equation allows calculation of the degree of flocculation in relation to turbulence in an accurate and easy way based on the relationships between turbulence and velocity and the nominal mean velocities and the number of channels.

2. Comparison of the experimental data with the results of the proposed "simplified method" and "point to point method" of calculating the extent of flocculation show that the "simplified method" is sufficiently accurate to predict the flocculation efficiency.

3. It is not accurate to directly apply the Argaman's equation to assess the efficiency of the hydraulic flocculator.

4. The flocculation constants are, contrary to Argaman's flocculation model, dependent on the initial particle concentration. The aggregation constant increases with the increase of initial particle concentration. The flocculation constants are also dependent on the type of coagulant. Improved settling conditions, such as tube settling, can enhance aggregation and minimise breaking of flocs and therefore increase aggregation constants and decrease breakup constants.

Chapter 7. Conclusions and recommendations for future research

7.1 Introduction

The main objectives of this research have been to investigate the correlation between turbulence and flocculation. The research consists of experimental study and numerical simulation. The experimental studies were conducted for the investigation of turbulence and velocity in channel flocculators and flocculation and settling performance under various conditions. Simultaneously, numerical simulations were carried out for the flow characteristics in the flocculator and degree of flocculation and settling. This chapter aims to draw the main conclusions of the works described in previous chapters, and gives recommendations for further work in the field of experimental and numerical studies of flocculation in relation to turbulence in general.

7.2 Summary conclusions

General conclusions of the experimental and theoretical studies of turbulence in relation to flocculation are summarised as follows:

1. Laboratory investigation of flow characteristics in the channel flocculator shows that the longitudinal flow velocity at the inlet end of the effective channel length exhibits a logarithmic profile from the channel bottom to the water surface. The absolute value of the longitudinal velocity gradually decreases approaching a channel bend and continuously increases from the end wall and reaches a steady value after about 50mm downstream from the bend, whilst the value of the transversal and vertical velocities go through an opposite process. The magnitudes of the longitudinal velocities near the channel bottom are generally 1.1 to 1.6 times of those at the middle level and 1.0 to 2.7 times of those at the level near the surface where the lowest values occur. Beyond the bend, the lowest magnitude of u velocity was at the level near the channel bottom. This is partly due to the redistribution of flow as it passes along the straight channel section, and

partly to backing up effects from the bend. The variation trends of the velocities of v and w remained essentially the same for the different levels.

2. Velocities vary across the width of the channel. Due to the influence of the channel bend, in the upstream channel the maximum longitudinal velocity, u, is generally at the outside wall of the channel but in the downstream channel it is closer to the inside wall. Transversal velocity, v, has a similar variation trend as that of u-velocity. The vertical velocity, w, has a slight variation with the width of the channel and goes to zero 50mm downstream from the bend.

3. There is a general trend that the kinetic energy decreases from about x=0.45m towards the end wall in an upstream channel due to the backup effect of the bend and decreases downstream from the end wall. The minimum magnitude of kinetic energy lies at the level near the water surface. There is no obvious variation trend of the kinetic energy with the channel width.

4. Assessment of measurement errors shows that the measurements of velocity and turbulence are quite steady and reliable, especially for the longitudinal velocity and kinetic energy under different nominal velocities.

5. The FLUENT CFD package enabled the convenient set-up and execution of a three-dimensional mathematical model study of fluid flows in the channels. It allowed the basic equations of motion and associated turbulence closure to be solved with relative ease, and the use of the software's various facilities allowed the use of variable finite difference grids so as to minimise demand for computer resources whilst still achieving useful simulation results. Convergence can be enhanced by a judicious choice of underrelaxation factors and the appropriate selection of the solution method.

6. The FLUENT CFD model of the channels was, in most of cases tested, capable of producing results giving a good fit to experimentally determined flow velocities and turbulence shear stresses. Where an accurate fit was not attained, the main features of the measured flow were still reproduced qualitatively. It was found that the inlet longitudinal velocity profile has a determinative effect on the magnitude and distribution of

turbulence and velocity in the channels. The initial transversal and vertical velocities and initial turbulence can be assumed negligible.

7. Experimental measurement by using LDA and numerical simulation by employing the FLUENT CFD package show that turbulence kinetic energy and velocity are approximately directly proportional to the nominal velocities, the kinetic energy and velocity related coefficient α was calculated as 1.05. The relationships coefficient (β) between the velocity and turbulence and the number of channels varies from 1.01 to 1.07 for the nominal velocities of 0.1 to 0.035m/s. With the relationships found in this study, the flow features (velocities and kinetic energy) at any point in any number of channels for any particular flow rate can be easily obtained by calculating the flow features in only one odd and one even numbered of channels.

8. Turbulence intensity in a hydraulic flocculator can be adjusted by inserting grid baffles, varying bed slope and channel width to cope with the variation of raw water quality and rate of flow. The adjusted turbulence allows the flocculation efficiency to be improved when there is insufficient or excessive agitation and flocculation time.

9. The maximum flocculation efficiency for the highest initial turbidity of 950 NTU is up to 3.2 times of that for the initial turbidity of 100 NTU, 1.6 times for 265 NTU with alum as coagulant. For Moringa oleifera as coagulant, the ratio of maximum flocculation efficiency of the initial concentrations of 950 NTU to that of 265 NTU is in the range of 1.1 to 1.6. Flocculation time should be more than 7 minutes, and around 20 minutes in general for effective treatment.

10. Alum, as a whole, provides better flocculation than Moringa oleifera. Stronger initial mixing gives an increase in flocculation efficiency for both the tests with alum and Moringa oleifera as coagulant. However, it has more significant effect on the tests with Moringa oleifera. Flocs with Moringa oleifera as coagulant have higher density and smaller size, with up to 14.2 times greater effective floc density and 89% lower floc size compared with the flocs with alum as coagulant.

11. Settling with the higher initial turbidity (950 NTU) produced greater solids removal by up to 1.5 times compared with the lower initial turbidity (265 NTU) for a corresponding flow. The tube settling tank provides an about 16.4 times larger in settling area, is 9 times shorter in settling distance and 17 times less in Reynolds number than those of the tank without tubes for a specific flow, and this allows the tube settling tank to give greater removal of solids. Up to 76% increase in settling efficiency was obtained by extending the settling time from 6.25 minutes to 12.5 minutes.

12. Measurements of head loss in the channel flocculators indicate that the empirical friction coefficient at the bend is not a fixed value but is dependent on many factors, such as flow velocity and the geometry of the flocculator. Here it fell in the range of 2.6 to 3.4.

13. Tracer studies showed that both the 45mm and 150mm wide channel flocculators are close enough to ideal plug flow reactor to allow their simulation for flocculation performance as plug flow.

14. A modified Argaman's equation is derived, which allows calculation of the degree of flocculation in relation to turbulence in an accurate and simplified way based on the relationships between turbulence and velocity and the nominal mean velocities and the number of channels. Comparison of the flocculation experimental data with the results of the proposed simplified method of calculating the extent of flocculation show that the simplified method is sufficiently accurate to predict the flocculation efficiency, however, it is not accurate to directly apply the Argaman's equation to assess the efficiencies of the hydraulic flocculator.

15. The flocculation constants are, contrary to Argaman's flocculation model, dependent on the initial particle concentration. The aggregation constant increases with the increase of initial particle concentration. The flocculation constants are also dependent on the type of coagulant. Improved settling conditions, such as tube settling, can enhance aggregation and minimise breaking of flocs and therefore increase aggregation constants and decrease breakup constants.

7.3 Recommendations for future research

This section is included as a summary of the areas of further research which have been highlighted through the work carried for this thesis. These are summarised below:

1. Floc density was calculated by using modified Stokes' settling formula under some assumptions (see Chapter 5) according to the published data (Tambo and Watanabe, 1979; Adachi and Tanaka, 1997; Gregory, 1997; Bache et al, 1991; Kusuda et al, 1981; Klimpel and Hogg, 1986). A power function correlation between floc density and floc size was therefore established. However, considerable difference in the magnitude of the coefficients in the function was found by different investigators for similar flocculation characteristics (Adachi and Tanaka, 1997). There is a need to judge the accuracy of the calculated floc density and valid various mathematical simulations of the correlation between floc density and size by directly measuring floc density. However, the existing experimental methods are time consuming, uncertain in accuracy and difficult to operate under realistic condition. It is suggested that a quick, accurate and easily operated measuring method should be developed.

2. The relationships between turbulence and velocity and the nominal mean velocities and the number of channels were found in this study and therefore a modified Argaman's equation is proposed allowing calculation of the degree of flocculation in relation to turbulence in an accurate and simplified way. It would be of benefit to extend the study of the relationships for a wider range of flow rates and geometry of the channel flocculator, such as various bed slopes, channel widths, and the ratios of channel slot to width.

3. Flocculent settling against time and location was experimentally investigated under many factors in this study, such as raw water turbidities, flow rates, types of coagulant, and flocculation times. It is recommended to carry out a numerical simulation of the settling phenomena to give an extended picture of the settling activities.

References

Adachi, Y. and Tanaka, Y. (1997), Settling velocity of an aluminimum-kaolinite floc, *Water Research*, Vol.31, No.3, pp.449-454.

Amirtharajah, A. and Mills, K.M. (1982), Rapid-mix design for mechanisms of alum coagulation, *Journal of American Water Works Association*, Vol.74, No.4 p211-216.

Amirtharajah, A. and Trusler, S.L. (1986), Destabilization of particles by turbulent repid mixing, Journal of Engineering Engineering, Vol.112, No.6, pp1085-1108.

Amirtharajah, A. and O'Melia, C.R. (1990), Water quality and treatment, *American Water Works Association, 4th edition.*

Amirtharajah, A. and Tambo, N. (1991), Mixing in water treatment, In: Amirtharajah A, Clark M.M., Trussell RR, eds. Mixing in coagulation and flocculation, Denver, CO: *American Water Works Association*, pp256-281.

Andreu-Villegas, R. and Letterman, R.D. (1976), Optimising flocculator power input, *Journal of Environmental Engineering Division, ASCE,* Vol.102, No.2, pp.251-263.

Argaman, Y. (1968), Turbulence in orthokinetic flocculation, Ph.D.thesis, the University of California, America.

Argaman, Y. and Kaufman, W.J. (1968), Turbulence in Orthokinetic Flocculation, *Journal of the Sanitary Engineering Division, ASCE*, SAZ Vol.96.

Argaman, Y. and Kaufman, W.J. (1970), Turbulence and flocculation, *Journal Sanitary Engineering Division, ASCE,* Vol. 96, pp.223-241.

Argaman, Y. (1971), Pilot-plant studies of flocculation, *Journal of American Water Works Association*, Vol.63, pp.775-777.

atTRACKtion Technical reference manual (1989), Dantec Elektronik, Developed by Dantec Electronics, Inc. Allendale, NJ, USA.

AWWA (1990), Water quality and treatment, *McGraw-Hill, Inc., New York.*

Bache, D.H.; Hossain, M.D.; Al-Ani S.H.; and Jackson P.J. (1991), Optimum coagulation conditions for a coloured water in terms of floc size, density and strength, *Water supply*, Vol.9, pp.93-102.

Bache, D.H.; Ali, A.; Rasool, E.; McGilligan, J.F. and Johnson C. (1996), Temperature and coagulation control in the sweep floc domain, *Journal of Water SRT-Aqua*, Vol.45, No.4, pp.195-202.

Bernard, P.S. (1986), Limitations of the near-wall k-epsilon turbulence model, *AIAA Journal*, Vol.24, No.4, pp.619-622.

Bratby, J.; Miller, M. W.; and Marais, G.V.R. (1977), Design of flocculation system from batch test data, *Water SA,* Vol.3, pp.173-182.

Bratby, J. (1980), Coagulation and flocculation, *Uplands Press Ltd, Croydon, England*

Camp, T.R.; Root, D.A.; and Bhoota, B.V. (1940), Effects of temperature on rate of floc formation, *Journal of American Water Works Association,* Vol.32, pp.1913.

Camp, T.R. and Stein, P.C. (1943), Velocity gradients and internal work in fluid motion, *Journal of Boston Society of Civil Engineering,* Vol.30, No.4, pp.219-237.

Camp, T.R. (1946), Sedimentation and the Design of Settling Tanks. *Transactions of the American Society of Civil Engineers*, Vol.111, pp.895.

Camp, T.R. (1955), Flocculation and flocculation basin, *Trans, ASCE*, Vol.120, pp.1-16.

Casson L.W. and Lawler D.F. (1990), Flocculation in turbulent flow: measurement and modelling of particle size distributions, *Journal of American Water Works Association,* Vol.68, No. 8, pp.54-68.

Casulli, V. (1998), Numerical methods for free surface hydrodynamics, Handout of training course, *Manchester Metropolitan University.*

Chellam, S. and Wiesner, M.R. (1993), Fluid mechanics and fractal aggregates, *Water Research*, Vol.27, pp.1493-1496.

Chen, C.P, and Guo, K. I. (1991), Non-isotropic multiple-scale turbulence model, *Applied Mathematics and Mechanics*, Vol.12, No.10, pp.981-991.

Chojnacki, A. (1968), Influence of temperature on rate of floc formation, *Gas Woda Technol Sanit, Vol.42, No.5*, pp.153.

Chow, V.T. (1959), Open-channel hydraulics, *McGraw-Hill, New York.*

Clark, M.M. (1985), Critique of Camp and Stein's RMS velocity gradient, *Journal of Environmental Engineering*, ASCE, Vol.111, No.6, pp.741-754.

Cleasby, J.L. (1984), Is velocity gradient a valid turbulence flocculation parameter?, *Journal of Environmental Engineering*, ASCE, Vol.110, No.5, pp.875-897.

Concha, F. and Almendra, E.R. (1979), Settling velocities of particulate system, 1. settling velocities of individual spherical particles. *International Journal of Mineral processing*, Vol.5. pp.349.

Crapper, M. (1995), Fluid mud modelling, Ph.D. Thesis, the University of Liverpool, England.

DeBoer, GBJ.; DeWeerd. C. and Thoenes, D. (1989), Coagulation in turbulent flow: Part II, *Chemical Engineering Research and Design*, Vol.67, No.3, pp.308-315

De Vriend, H.J. (1977), A mathematical model of steady flow in curved shallow channel, *Journal of Hydraulic Research*, Vol. 15, No 1, pp. 37-53.

Dian Desa (1985), Water purification with Moringa seeds, *Waterlines*, Vol.3, No.4.

Dirican, C. (1981), The structure and growth of aggregates in flocculation, M.S. Thesis, The Pennsylvania state University.

DISA Laser Doppler Anemometry (1983), DISA Information Department, Bristol, UK.

Dolejs, P. (1984), Interaction of temperature, alkalinity and alum dose by coagulation of humid water. In: Pawlowski L, Verdier AJ, Lacy WJ, eds. *Chemistry for protection of the Environment*, Amsterdam: Elsevier, pp. 169-178.

Fadel A.A (1985), Model for horizontal tube settlers, Ph.D. thesis, Iowa State University, at Ames, Iowa.

Fadel A.A and Baumann E.R. (1990), Tube Settler Modelling, *Journal of Environmental Engineering*, Vol.16, No.1, pp.107-124.

Fair, G.M.; Geyer, J.C.; and Okun, D.A. (1968), Water and wastewater Engineering, Vol.2, Water Purification and Wastewater Treatment and Disposal. *John Wiley and Sons, Inc. New York.*

FLUENT Incorporated (1993), *Fluent version 4.2.2 user's guide, Fluent Incorporated, Lebanon, New Hampshire, USA.*

Gassenschmidt, U.; Jany, K. D.; Tauscher, B.; and Niebergall, H. (1995), Isolation and characterisation of a flocculating protein from Moringa oleifera Lam, *Biochimica et Biophydica Acta,* Vol.1234, pp.477-481.

Glasgow, L.A. and Hsw, J.D. (1982), An experimental study of floc strength, *AIChE Journal*, Vol.28, pp.779-785.

Graham, D.I.; James, P.W.; Jones, T.E.R.; Davies, J.M. and Delo, E.A. (1992), Measurement and prediction of surface shear stress in annular flume, *Journal of Hydraulic Engineering, ASCE,* Vol.118, No.9.

Gregory, J. (1997), The density of particle aggregates, *Water Science and Technology*, Vol.36, No.4, pp.1-13.

Haarhoff, J.; Van Beek C.J.; and Van Wyk H.J. (1996), Practical Application of the Argaman-Kaufman Flocculation model, Proceedings of the 1996 Biennial conference of the water institute of southern Africa held in port Elizabeth, South Africa.

Haarhoff, J. and Joubert, H. (1997), Determination of aggregation and breakup constants during flocculation, *Water Science and Technology*, Vol.36, No.4, pp.33-40.

Haarhoff, J. (1998), Design of around-the-end hydraulic flocculators, *Journal of Water SRT-Aqua,* Vol.47, No.3, pp.142-152.

Hafez, Y.I. (1995), A-epsilon turbulence model for predicting the three-dimensional velocity field and boundary shear in closed and open channels, Ph.D. Thesis, Colorado state University, America.

Han M and Lawler D.F. (1992), The relative (insignificance) of G in flocculation, *Journal of American Water Works Association*, Vol.84, No.10, pp.79-91.

Healy, T.W. (1961), Flocculation-dispersion behaviour of quartz in the presence of a polyacrylamide flocculant, *Journal of Colloid and Interface Science,* Vol.16, pp.609-617.

Henderson, F.M. (1966), Open Channel Flow, *MacMillan.*

Hodson H.E., Wanger E.G. (1981), Conduct and uses of jar tests, *Journal of American Water Works Association*, Vol.73, No.4, pp.218-223.

Ives, K.J. (1968), Theory and operation of sludge blanket clarifiers, *Proceedings of Institution of Civil Engineers,* Vol.39, pp.243-260.

Jahn, S.A.A. (1982), Traditional water purification in tropical developing counties, German Agency for Technical Cooperation (GTZ), Eschborn, Germany, pp.20-22.

Jahn, S.A.A. (1984), Traditional water clarification methods-using scientific observation to maximise efficiency, *Waterlines,* Vol.2, No.3, pp.27-28.

Jahn, S.A.A. (1988), Using Moringa seeds as coagulants in developing countries, *Journal of the America Water Association*, Vol.80, No.6, pp.43-50.

Kavanaugh, M.C.; Tate, C.H.; Trussel, A.R.; Trussel R.R.; Treweek G. (1980), Use of particle size distribution measurements for selection and control of solid/liquid separation

processes, *Particulates in Water: Characterisation, Fate, Effects, and Removal*, M.C. Kavanaugh and Leckie, J.O. ed., Advances in Chemistry Series 189, *American Chemical Society, Washington, D. C.*

Kawanura, S. (1991), Integrated design of water treatment facilities, *John Wiley, New York.*

Kimpel, R.C (1984), The structure of agglomerates in flocculated suspensions, M.S.Thesis, The Pennsylvania State University.

Kimpel, R.C.; Dirican, C.; and Hogg, R. (1986), Measurement of agglomerate density in flocculated fine particle suspension, *Particle science and technology*, Vol.4, pp.45-59.

Kimpel, R.C. and Hogg, R. (1986), Effects of flocculation conditions on agglomerate structure, *Journal of Colloid and Interface Science*, Vol.113, No.1, pp.121-131.

Knocke, W.R.; Dishman, M.C.; and Miller, G.F. (1993), Measurement of chemical sludge floc density and implications related to sludge dewatering, *Water Environment Research*, No.6, pp.735-743.

Kolmogorov, A.N.(1941), Local structure of turbulence in an incompressible fluid at a very high Reynolds number, *Dokl Akad Nauk SSSR*, Vol.30 pp.299-302

Kurotani, K.; Kubota, M.; Zaitsu, Y.; Ohto, T; Inoue, K.; and Nakayama, T. (1995), Advanced control of coagulation process by applying a floc sensor, *Water Supply*, Vol.13, No.3-4, pp.239-244.

Kusuda, T.; Koga, K.; Yorozu, H.; and Awaya, Y. (1981), Density and settling velocity of flocs, *Memorios of the faculty of engineering, Kyushu University*, Vol.41, No.3.

Lagvankar, A.L. and Gemmell, R.S. (1968), A size-density relationship for flocs, *Journal of American Water Works Association*, Vol.60, pp.1040-1046.

Lai, R.J. (1975), Physical aspects of mixing in coagulation control, Ph.D thesis, the University of Florida, America.

Lane, S.N. and Richards, K.S (1998), High resolution, two-dimensional spatial modelling of flow processes in a multi-thread channel, *Hydrological Processes*, Vol.12, No.8, pp.1279-1298.

Launder, B.E.; Reece, G.J.; and Rodi, W. (1975), Progress in the development of a Reynolds-stress turbulence closure, *Journal of Fluid. Mechanics*, Vol. 68, pp.537-566.

Lawler, D.F. (1979), A particle Approach to the Thickening Process, Ph.D Thesis, the University of North Carolina at Chapel Hill, America.

Leipold C. (1934), Mechanical agitation and floc formation, *Journal of the America Water Association*, Vol.82, pp.1070.

Leschziner, M.A. and Rodi, W (1979), Calculation of strong curved open channel flow, *Journal of the Hydraulic Division, ASCE,* Vol. 105, pp.1279-1314.

Levich, V.G. (1962), Physicochemical hydrodynamics, *Prentice-Hall, Englewood Cliffs, N.J.*

Li, Y.C. (1988), Experimental techniques of water treatment, *China Architecture Industry Press, Beijing, China.*

Liggett, J.A. and Vasudev, S.U. (1965), Slope and friction effects in two dimensional high speed flow, *Proceedings of 11th international congress IAHR*, Leningrad, U.S.S.R., Vol.1. pp.1-12.

Lo, I.M.C. (1996), Hand out of physical and chemical wastewater treatment, Department of Civil and Structural Engineering, University of Hongkong of Science and Technology.

Matsumoto, K. and Mori, Y. (1975), Settling velocity of floc-new measurement method of floc density, *Journal of Chemical engineering of Japan*, Vol.8, pp.143-147.

McConnachie, G.L. (1991), Turbulence intensity of mixing in relation to flocculation, *Journal of Environmental Engineering, ASCE,* Vol.117, No.6, pp.731-750.

McConnachie, G.L. (1995), Establishment of design principles for hydraulic flocculators, Final report to Overseas Development Administration (ODA).

Mendis, M.M. (1987), Improvement of flow distribution at deep open channel bends, M.Eng. Thesis, University of Liverpool.

Montgomery J.M. (1985), Water treatment principal and design, *John Wiley, New York.*

Morris J.K. and Knocke W.R. (1984), Temperature effects on the use of metal-ion coagulants for water treatment, *Journal of the America Water Association*, Vol.76, pp.74-79.

Muhle, K. (1993), In coagulation and flocculation, *ed. B. Dobias. Marcel Dekker, New York*, pp.355-390.

Odegaard, H. (1979), Orthokinetic flocculation of phosphate precipitates in a multicomponent reactor with non-ideal flow, *Progress of Water Technology*, Vol.11, pp.61-88.

Okun D.A. and Schulz C.R. (1984), Surface water treatment for communities in developing countries, Water and Sanitation for Health (WASH) Project, Tech. report no. 29, Arlington VA, USA.

Packham, R.F. and Sheiham I. (1977), Developments in the theory of coagulation and flocculation, *Journal of Institution of Water Engineering Science,* Vol.31, No.2, pp.96-108.

Parker, D.S.; Kaufman, W.J.; and Jenkins, D. (1972), Floc breakup in turbulence flocculation process, *Journal Sanitary Engineering Division, ASCE,* Vol. 98, pp.79.

Patankar, S.V. (1980), Numerical heat transfer and fluid flow, *Washington, DC: Hemisphere publish Corp.*

Petersen, O. and Krishnappan, B.G. (1994), Measurement and analysis of flow characteristics in a rotating circular flume, *Journal of Hydraulic Research*, Vol. 32, No.4.

Rebhun, M. and Argaman, Y. (1965), Evaluation of hydraulic efficiency of sedimentation basin, *Proceedings of ASCE*, Vol.91(SA5), pp.37.

Rosovskii, I.L. (1965), Flow of water in bends of open channels, *Programme for Scientific Translation*, Jerusalem, Israel.

Schulz, C.R. and Okun, D.A. (1984), Surface water treatment for Communities in developing countries, *John Wiley &Sons, New York.*

Sharma, S.K.; Stanley, D.A.; and Harris, J. (1994), Determining the Effect of Physico-Chemical Parameters on Floc Size Using a Population Balance Model, *Minerals & Metallurgical Processing*, Vol.11, No.3, pp.168-173.

Smoluchowski, M. (1917), Versuch Einer Mathematischen Theorie der Koaglations-Kinetik Killoider Losungen, *Zeitschrigt fur Physikalische Chemie*, Wiesbaden, West Germany, Vol.92, pp.129-168.

Spielman, L.A. (1978), Hydrodynamic aspects of flocculation, in K.J. Ives (ed.), *the scientific basis of flocculation*, Sijthoff and Noorhoff, The Netherlands.

Steven, R.G. (1990), Air flow through and above a forest of widely spaced trees, Ph.D. Thesis, the University of Edinburgh, Scotland.

Streamflo velocity meter 400, *Nixon instrumentation, Gloucestershire, England.*

Strickland, T.K. (1982), Transportation of the particle size distribution during thickening, Master Thesis, the University of Texas at Austin.

Tambo, N. and Watanabe, Y. (1979), Physical characteristics of flocs-1. The floc density function and aluminium floc, *Water Research*, Vol.13, pp409-419.

Tambo N. and Hozumi H. (1979a), Physical characteristics of flocs-II. Strength of floc, Water Research, Vol.13, pp.421-427.

Thomas, D.N.; Judd, S.J.; and Fawcett, N. (1999), Flocculation modelling: a review, *Water Research*, Vol.33, No.7, pp.1579-1592.

Treweek, G.P. (1979), Optimisation of flocculation time prior to direct filtration, *Journal of American Water Work Association*, Vol.71, No.2, pp.96.

Treweek, G. P. and. Morgan, J.J. (1980), Prediction of suspension turbidities from aggregate size distributions, *Particulates in water: Characterisation, Fate, Effects, and Removal*, M. C. Kavanaugh and J. O. Leckie, ed., Advances in Chemistry Series 189, *American Chemical Society, Washington, D. C.*

Velz, C.J. (1934), Influence of temperature on coagulation, *Civil Engineering,* Vol.7, pp.345-349.

Vrale, L. and Jordan, R.M. (1971), Rapid mixing in water treatment, *Journal of American Water Work Association*, Vol.63, pp.52.

Webber, N.B. (1968), Fluid mechanics for civil engineers, *Chapman and Hall.*

Willis, R.M. (1978), Tubular settlers-A technical Review, *Journal of American Water Works Association.*

Wirojanagud, W. (1983), Particle size distributions in flocculent sedimentation, Ph.D. Thesis, the University of Texas at Austin, America.

Yang, H.D. (1995), Advanced turbulence models for recalculating flows, Ph.D. Thesis, Texas technical University, America.

Yeung, A.K.C. and Pelton, R. (1996), Micromechanics: a new approach to studying the strength and break-up of flocs, *Journal of colloid interface Science,* Vol.184, pp.579-585.

Younus, M. and Chaudhry, M.H. (1994), Depth-averaged k-epsilon turbulence model for the computation of free-surface flow, *Journal of Hydraulic Research*, Vol.32, No.3, pp.415-444.

Zhang, H.Z. (1993), Study of a numerical turbulence model for flow pass smooth and rough surfaces (pipe flow, smooth surfaces), Ph.D Thesis, the University of Rhode island.

APPENDICES

APPENDIX A

Table A 1.1 LDA readings for the flowrate of 180l/min (nominal velocity of 0.1m/s) level 1 (z=20mm)

Section 1ow (y=25mm)

X	u-velocity	v-velocity	w-velocity	u'u'	v'v'	w'w'	u'	v'	w'	k
(m)	(m/s)	(m/s)	(m/s)	(m^2/s^2)	(m^2/s^2)	(m^2/s^2)	(m/s)	(m/s)	(m/s)	(m^2/s^2)
5.00E-2	4.32E-2	-2.01E-2	-9.28E-3	8.83E-5	1.01E-4	8.54E-5	9.40E-3	1.01E-2	9.24E-3	1.38E-4
1.00E-1	8.27E-2	-1.82E-2	-7.43E-3	1.10E-4	1.08E-4	8.66E-5	1.05E-2	1.04E-2	9.31E-3	1.53E-4
1.50E-1	1.18E-1	-1.62E-2	8.92E-4	1.43E-4	1.15E-4	9.31E-5	1.20E-2	1.07E-2	9.65E-3	1.76E-4
2.00E-1	1.35E-1	-6.44E-3	2.38E-3	1.78E-4	1.22E-4	1.03E-4	1.33E-2	1.11E-2	1.02E-2	2.02E-4
3.00E-1	1.39E-1	2.54E-3	1.83E-3	2.44E-4	1.40E-4	1.26E-4	1.56E-2	1.18E-2	1.12E-2	2.55E-4
4.50E-1	1.28E-1	3.54E-3	5.11E-4	3.00E-4	1.58E-4	1.51E-4	1.73E-2	1.26E-2	1.23E-2	3.05E-4

Section 1c (y=60mm)

X	u-velocity	v-velocity	w-velocity	u'u'	v'v'	w'w'	u'	v'	w'	k
(m)	(m/s)	(m/s)	(m/s)	(m^2/s^2)	(m^2/s^2)	(m^2/s^2)	(m/s)	(m/s)	(m/s)	(m^2/s^2)
5.00E-2	4.38E-2	-2.30E-2	-5.77E-3	1.11E-4	1.09E-4	9.16E-5	1.05E-2	1.04E-2	9.57E-3	1.56E-4
1.00E-1	7.95E-2	-3.02E-2	2.53E-3	1.21E-4	1.03E-4	8.48E-5	1.10E-2	1.01E-2	9.21E-3	1.54E-4
1.50E-1	1.12E-1	-2.94E-2	6.88E-3	1.46E-4	1.16E-4	9.07E-5	1.21E-2	1.08E-2	9.52E-3	1.76E-4
2.00E-1	1.19E-1	-1.23E-2	6.20E-3	1.69E-4	1.20E-4	9.69E-5	1.30E-2	1.09E-2	9.84E-3	1.93E-4
3.00E-1	1.12E-1	6.87E-4	3.88E-3	2.04E-4	1.23E-4	1.08E-4	1.43E-2	1.11E-2	1.04E-2	2.18E-4
4.50E-1	1.05E-1	5.92E-3	1.16E-3	2.44E-4	1.33E-4	1.26E-4	1.56E-2	1.15E-2	1.12E-2	2.51E-4

Section 1iw (y=100mm)

X	u-velocity	v-velocity	w-velocity	u'u'	v'v'	w'w'	u'	v'	w'	k
(m)	(m/s)	(m/s)	(m/s)	(m^2/s^2)	(m^2/s^2)	(m^2/s^2)	(m/s)	(m/s)	(m/s)	(m^2/s^2)
5.00E-2	3.50E-2	-4.06E-2	-3.02E-3	1.27E-4	9.41E-5	8.69E-5	1.13E-2	9.70E-3	9.32E-3	1.54E-4
1.00E-1	5.53E-2	-6.75E-2	8.29E-3	1.15E-4	1.13E-4	7.80E-5	1.07E-2	1.06E-2	8.83E-3	1.53E-4
1.50E-1	6.36E-2	-4.85E-2	8.76E-3	1.35E-4	1.15E-4	8.40E-5	1.16E-2	1.07E-2	9.17E-3	1.67E-4
2.00E-1	2.87E-2	-1.31E-2	5.48E-3	1.11E-4	7.65E-5	6.26E-5	1.05E-2	8.75E-3	7.91E-3	1.25E-4
3.00E-1	-1.41E-2	-1.35E-3	2.14E-3	1.21E-4	5.86E-5	5.76E-5	1.10E-2	7.65E-3	7.59E-3	1.19E-4
4.50E-1	8.11E-3	2.32E-3	-1.37E-3	2.12E-4	7.62E-5	7.44E-5	1.45E-2	8.73E-3	8.62E-3	1.81E-4

Section 2iw (y=208mm)

X	u-velocity	v-velocity	w-velocity	u'u'	v'v'	w'w'	u'	v'	w'	k
(m)	(m/s)	(m/s)	(m/s)	(m^2/s^2)	(m^2/s^2)	(m^2/s^2)	(m/s)	(m/s)	(m/s)	(m^2/s^2)
5.00E-2	3.06E-3	-3.26E-2	-2.07E-3	9.32E-5	4.98E-5	5.55E-5	9.65E-3	7.06E-3	7.45E-3	9.93E-5
1.00E-1	-3.32E-2	-4.37E-2	3.95E-3	1.01E-4	7.07E-5	5.94E-5	1.01E-2	8.41E-3	7.71E-3	1.16E-4
1.50E-1	-6.84E-2	-3.13E-2	2.11E-3	1.39E-4	7.67E-5	7.79E-5	1.18E-2	8.76E-3	8.83E-3	1.47E-4
2.00E-1	-7.21E-2	-1.29E-2	8.38E-4	1.47E-4	7.78E-5	7.48E-5	1.21E-2	8.82E-3	8.65E-3	1.50E-4
3.00E-1	-7.03E-2	-2.03E-3	5.35E-6	1.47E-4	7.70E-5	7.08E-5	1.21E-2	8.78E-3	8.41E-3	1.47E-4
4.50E-1	-7.02E-2	1.20E-4	-6.83E-5	1.45E-4	7.36E-5	6.94E-5	1.21E-2	8.58E-3	8.33E-3	1.44E-4

Section 2c (y=248mm)

X	u-velocity	v-velocity	w-velocity	u'u'	v'v'	w'w'	u'	v'	w'	k
(m)	(m/s)	(m/s)	(m/s)	(m^2/s^2)	(m^2/s^2)	(m^2/s^2)	(m/s)	(m/s)	(m/s)	(m^2/s^2)
5.00E-2	5.45E-3	-1.80E-2	-4.72E-3	9.15E-5	4.56E-5	5.45E-5	9.56E-3	6.75E-3	7.38E-3	9.58E-5
1.00E-1	-1.99E-2	-2.06E-2	2.83E-3	7.58E-5	4.98E-5	4.66E-5	8.71E-3	7.06E-3	6.83E-3	8.61E-5
1.50E-1	-5.01E-2	-2.06E-2	2.10E-3	1.20E-4	6.72E-5	6.58E-5	1.09E-2	8.20E-3	8.11E-3	1.26E-4
2.00E-1	-6.39E-2	-1.08E-2	9.46E-4	1.37E-4	7.32E-5	7.30E-5	1.17E-2	8.56E-3	8.54E-3	1.42E-4
3.00E-1	-7.11E-2	-2.06E-3	7.83E-5	1.45E-4	7.59E-5	7.60E-5	1.20E-2	8.71E-3	8.72E-3	1.48E-4
4.50E-1	-7.17E-2	9.30E-5	-2.99E-5	1.45E-4	7.60E-5	7.60E-5	1.20E-2	8.71E-3	8.72E-3	1.48E-4

Section 2ow (y=283mm)

X	u-velocity	v-velocity	w-velocity	u'u'	v'v'	w'w'	u'	v'	w'	k
(m)	(m/s)	(m/s)	(m/s)	(m^2/s^2)	(m^2/s^2)	(m^2/s^2)	(m/s)	(m/s)	(m/s)	(m^2/s^2)
5.00E-2	1.10E-2	-2.41E-3	-7.85E-3	7.51E-5	3.75E-5	4.45E-5	8.67E-3	6.13E-3	6.67E-3	7.86E-5
1.00E-1	1.02E-2	8.78E-4	2.17E-3	4.50E-5	3.16E-5	3.32E-5	6.71E-3	5.62E-3	5.76E-3	5.49E-5
1.50E-1	-4.61E-3	-2.37E-3	2.79E-3	6.46E-5	3.14E-5	3.12E-5	8.04E-3	5.60E-3	5.58E-3	6.36E-5
2.00E-1	-3.22E-2	-4.23E-3	1.40E-3	8.76E-5	4.57E-5	4.56E-5	9.36E-3	6.76E-3	6.76E-3	8.95E-5
3.00E-1	-4.35E-2	-3.51E-4	2.07E-4	1.09E-4	5.27E-5	5.27E-5	1.04E-2	7.26E-3	7.26E-3	1.07E-4
4.50E-1	-4.37E-2	-5.76E-5	-8.62E-5	1.09E-4	5.40E-5	5.40E-5	1.05E-2	7.35E-3	7.35E-3	1.09E-4

Table A1.2 LDA readings for the flowrate of 180l/min (nominal velocity of 0.1m/s) level 2 (z=60mm)

Section 1ow (y=25mm)

X	u-velocity	v-velocity	w-velocity	u'u'	v'v'	w'w'	u'	v'	w'	k
(m)	(m/s)	(m/s)	(m/s)	(m^2/s^2)	(m^2/s^2)	(m^2/s^2)	(m/s)	(m/s)	(m/s)	(m^2/s^2)
5.00E-2	3.46E-2	-2.09E-2	-2.19E-2	8.48E-5	1.48E-4	1.02E-4	9.21E-3	1.22E-2	1.01E-2	1.67E-4
1.00E-1	7.75E-2	-2.31E-2	-4.77E-3	8.99E-5	1.68E-4	1.02E-4	9.48E-3	1.30E-2	1.01E-2	1.80E-4
1.50E-1	1.15E-1	-2.13E-2	2.89E-3	1.09E-4	1.78E-4	9.73E-5	1.04E-2	1.34E-2	9.86E-3	1.92E-4
2.00E-1	1.32E-1	-5.74E-3	1.20E-2	1.41E-4	1.62E-4	4.42E-5	1.19E-2	1.27E-2	6.65E-3	1.74E-4
3.00E-1	1.36E-1	2.15E-3	4.44E-3	2.13E-4	1.39E-4	9.65E-5	1.46E-2	1.18E-2	9.82E-3	2.24E-4
4.50E-1	1.26E-1	2.36E-3	4.00E-3	2.17E-4	1.19E-4	3.36E-5	1.47E-2	1.09E-2	5.80E-3	1.85E-4

Section 1c (y=60mm)

X	u-velocity	v-velocity	w-velocity	u'u'	v'v'	w'w'	u'	v'	w'	k
(m)	(m/s)	(m/s)	(m/s)	(m^2/s^2)	(m^2/s^2)	(m^2/s^2)	(m/s)	(m/s)	(m/s)	(m^2/s^2)
5.00E-2	5.00E-2	-4.55E-2	-1.20E-2	1.27E-4	1.39E-4	7.90E-5	1.13E-2	1.18E-2	8.89E-3	1.73E-4
1.00E-1	8.10E-2	-5.13E-2	8.95E-3	9.96E-5	1.38E-4	6.80E-5	9.98E-3	1.18E-2	8.25E-3	1.53E-4
1.50E-1	1.00E-1	-3.46E-2	9.26E-3	8.80E-5	1.21E-4	6.20E-5	9.38E-3	1.10E-2	7.87E-3	1.36E-4
2.00E-1	7.00E-2	-1.24E-2	7.50E-3	1.21E-4	1.07E-4	4.70E-5	1.10E-2	1.03E-2	6.86E-3	1.37E-4
3.00E-1	1.10E-1	1.33E-3	6.43E-3	1.78E-4	1.08E-4	5.70E-5	1.33E-2	1.04E-2	7.55E-3	1.72E-4
4.50E-1	6.00E-2	4.61E-3	3.42E-3	2.85E-4	1.51E-4	4.20E-5	1.69E-2	1.23E-2	6.48E-3	2.39E-4

Section 1iw (y=100mm)

X	u-velocity	v-velocity	w-velocity	u'u'	v'v'	w'w'	u'	v'	w'	k
(m)	(m/s)	(m/s)	(m/s)	(m^2/s^2)	(m^2/s^2)	(m^2/s^2)	(m/s)	(m/s)	(m/s)	(m^2/s^2)
5.00E-2	2.00E-2	-6.91E-2	-5.42E-3	7.50E-5	1.10E-4	1.07E-4	8.66E-3	1.05E-2	1.03E-2	1.46E-4
1.00E-1	2.70E-2	-8.88E-2	1.69E-2	1.71E-4	1.02E-4	8.08E-5	1.31E-2	1.01E-2	8.99E-3	1.77E-4
1.50E-1	3.12E-2	-3.94E-2	1.83E-2	9.60E-5	1.41E-4	7.87E-5	9.80E-3	1.19E-2	8.87E-3	1.58E-4
2.00E-1	2.25E-2	-6.50E-3	9.15E-3	1.93E-4	1.31E-4	1.72E-5	1.39E-2	1.14E-2	4.15E-3	1.71E-4
3.00E-1	2.04E-2	9.16E-4	5.25E-3	2.13E-4	1.63E-4	1.72E-4	1.46E-2	1.28E-2	1.31E-2	2.74E-4
4.50E-1	2.82E-2	2.45E-3	-4.70E-3	2.20E-4	2.17E-4	3.36E-5	1.48E-2	1.47E-2	5.80E-3	2.35E-4

Section 2iw (y=208mm)

X	u-velocity	v-velocity	w-velocity	u'u'	v'v'	w'w'	u'	v'	w'	k
(m)	(m/s)	(m/s)	(m/s)	(m^2/s^2)	(m^2/s^2)	(m^2/s^2)	(m/s)	(m/s)	(m/s)	(m^2/s^2)
5.00E-2	-3.20E-2	-4.28E-2	-3.54E-3	2.56E-4	6.06E-5	9.52E-5	1.60E-2	7.79E-3	9.76E-3	2.06E-4
1.00E-1	-6.20E-2	-4.57E-2	6.55E-3	2.19E-4	5.60E-5	6.79E-5	1.48E-2	7.48E-3	8.24E-3	1.71E-4
1.50E-1	-1.10E-1	-3.12E-2	3.84E-3	1.97E-4	4.83E-5	4.91E-5	1.40E-2	6.95E-3	7.01E-3	1.47E-4
2.00E-1	-8.12E-2	-9.92E-3	1.54E-3	2.43E-4	4.32E-5	5.03E-5	1.56E-2	6.58E-3	7.09E-3	1.68E-4
3.00E-1	-3.43E-2	-1.44E-3	-1.59E-5	1.93E-4	4.25E-5	5.56E-5	1.39E-2	6.52E-3	7.46E-3	1.46E-4
4.50E-1	-8.34E-2	6.84E-5	-2.12E-4	1.74E-4	4.28E-5	5.65E-5	1.32E-2	6.54E-3	7.52E-3	1.37E-4

Section 2c (y=248mm)

X	u-velocity	v-velocity	w-velocity	u'u'	v'v'	w'w'	u'	v'	w'	k
(m)	(m/s)	(m/s)	(m/s)	(m^2/s^2)	(m^2/s^2)	(m^2/s^2)	(m/s)	(m/s)	(m/s)	(m^2/s^2)
5.00E-2	-2.60E-2	-2.20E-2	-4.50E-3	2.20E-4	6.01E-5	7.80E-5	1.48E-2	7.75E-3	8.83E-3	1.79E-4
1.00E-1	-5.12E-2	-2.43E-2	5.70E-3	1.59E-4	6.02E-5	4.70E-5	1.26E-2	7.76E-3	6.86E-3	1.33E-4
1.50E-1	-7.10E-2	-1.87E-2	6.50E-3	1.07E-4	5.61E-5	4.20E-5	1.03E-2	7.49E-3	6.48E-3	1.03E-4
2.00E-1	-8.54E-2	-9.28E-3	1.90E-3	1.12E-4	4.95E-5	3.40E-5	1.06E-2	7.03E-3	5.83E-3	9.77E-5
3.00E-1	-7.76E-2	-1.66E-3	2.00E-4	6.56E-5	4.50E-5	3.80E-5	8.10E-3	6.71E-3	6.16E-3	7.43E-5
4.50E-1	-7.31E-2	3.88E-5	-3.10E-4	1.08E-4	4.45E-5	3.84E-5	1.04E-2	6.67E-3	6.20E-3	9.55E-5

Section 2ow (y=283mm)

X	u-velocity	v-velocity	w-velocity	u'u'	v'v'	w'w'	u'	v'	w'	k
(m)	(m/s)	(m/s)	(m/s)	(m^2/s^2)	(m^2/s^2)	(m^2/s^2)	(m/s)	(m/s)	(m/s)	(m^2/s^2)
5.00E-2	-3.10E-2	-2.36E-3	-1.37E-2	1.11E-4	5.21E-5	8.14E-5	1.05E-2	7.22E-3	9.02E-3	1.22E-4
1.00E-1	-4.10E-2	-2.36E-3	-6.49E-4	1.32E-4	6.72E-5	8.28E-5	1.15E-2	8.20E-3	9.10E-3	1.41E-4
1.50E-1	-5.20E-2	-2.03E-3	3.66E-3	1.52E-4	8.43E-5	7.75E-5	1.23E-2	9.18E-3	8.80E-3	1.57E-4
2.00E-1	-6.64E-2	-3.19E-3	2.07E-3	1.08E-4	7.95E-5	6.92E-5	1.04E-2	8.92E-3	8.32E-3	1.28E-4
3.00E-1	-8.20E-2	-2.36E-4	3.68E-4	1.59E-4	8.10E-5	6.21E-5	1.26E-2	9.00E-3	7.88E-3	1.51E-4
4.50E-1	-8.00E-2	4.31E-5	-7.94E-5	1.59E-4	8.10E-5	6.05E-5	1.26E-2	9.00E-3	7.78E-3	1.50E-4

Table A1.3 LDA readings for the flowrate of 180l/min (nominal velocity of 0.1m/s) level 3 (z=100mm)

Section 1ow (y=25mm)

X	u-velocity	v-velocity	w-velocity	u'u'	v'v'	w'w'	u'	v'	w'	k
(m)	(m/s)	(m/s)	(m/s)	(m^2/s^2)	(m^2/s^2)	(m^2/s^2)	(m/s)	(m/s)	(m/s)	(m^2/s^2)
5.00E-2	3.01E-2	-2.40E-2	-1.65E-2	8.75E-5	1.36E-4	7.81E-5	9.35E-3	1.17E-2	8.83E-3	1.51E-4
1.00E-1	7.48E-2	-2.40E-2	-6.55E-3	8.73E-5	1.28E-4	7.33E-5	9.34E-3	1.13E-2	8.56E-3	1.44E-4
1.50E-1	1.12E-1	-5.24E-2	3.58E-3	1.31E-4	1.32E-4	7.34E-5	1.14E-2	1.15E-2	8.57E-3	1.68E-4
2.00E-1	1.30E-1	-5.79E-3	6.45E-3	1.81E-4	1.09E-4	7.39E-5	1.34E-2	1.05E-2	8.60E-3	1.82E-4
3.00E-1	1.34E-1	3.16E-3	4.95E-3	2.41E-4	1.02E-4	8.13E-5	1.55E-2	1.01E-2	9.02E-3	2.12E-4
4.50E-1	1.23E-1	6.27E-3	1.80E-3	2.83E-4	9.41E-5	9.04E-5	1.68E-2	9.70E-3	9.51E-3	2.34E-4

Section 1c (y=60mm)

X	u-velocity	v-velocity	w-velocity	u'u'	v'v'	w'w'	u'	v'	w'	k
(m)	(m/s)	(m/s)	(m/s)	(m^2/s^2)	(m^2/s^2)	(m^2/s^2)	(m/s)	(m/s)	(m/s)	(m^2/s^2)
5.00E-2	2.74E-2	-5.86E-2	-1.14E-2	1.05E-4	1.01E-4	7.22E-5	1.02E-2	1.01E-2	8.50E-3	1.39E-4
1.00E-1	6.61E-2	-6.06E-2	5.06E-3	8.58E-5	8.16E-5	6.87E-5	9.26E-3	9.03E-3	8.29E-3	1.18E-4
1.50E-1	9.87E-2	-3.30E-2	1.43E-2	7.81E-5	8.02E-5	6.81E-5	8.84E-3	8.96E-3	8.25E-3	1.13E-4
2.00E-1	1.06E-1	-9.87E-3	1.54E-2	8.08E-5	7.48E-5	6.60E-5	8.99E-3	8.65E-3	8.12E-3	1.11E-4
3.00E-1	1.06E-1	2.63E-3	1.10E-2	1.15E-4	7.87E-5	7.30E-5	1.07E-2	8.87E-3	8.54E-3	1.33E-4
4.50E-1	9.79E-2	4.34E-3	4.28E-3	2.17E-4	1.11E-4	1.09E-4	1.47E-2	1.06E-2	1.05E-2	2.19E-4

Section 1iw (y=100mm)

X	u-velocity	v-velocity	w-velocity	u'u'	v'v'	w'w'	u'	v'	w'	k
(m)	(m/s)	(m/s)	(m/s)	(m^2/s^2)	(m^2/s^2)	(m^2/s^2)	(m/s)	(m/s)	(m/s)	(m^2/s^2)
5.00E-2	5.52E-3	-7.83E-2	-5.42E-3	1.38E-4	6.58E-5	7.19E-5	1.17E-2	8.11E-3	8.48E-3	1.38E-4
1.00E-1	3.06E-2	-8.91E-2	1.24E-2	1.22E-4	6.37E-5	7.47E-5	1.11E-2	7.98E-3	8.65E-3	1.30E-4
1.50E-1	4.09E-2	-3.28E-2	1.76E-2	1.07E-4	7.59E-5	7.48E-5	1.03E-2	8.71E-3	8.65E-3	1.29E-4
2.00E-1	2.29E-2	-4.11E-3	1.43E-2	1.58E-4	6.37E-5	8.01E-5	1.26E-2	7.98E-3	8.95E-3	1.51E-4
3.00E-1	2.08E-2	4.21E-3	1.48E-3	2.80E-4	1.42E-4	1.57E-4	1.67E-2	1.19E-2	1.25E-2	2.89E-4
4.50E-1	3.18E-2	4.03E-3	-4.55E-3	3.33E-4	1.82E-4	1.75E-4	1.83E-2	1.35E-2	1.32E-2	3.45E-4

Section 2iw (y=208mm)

X	u-velocity	v-velocity	w-velocity	u'u'	v'v'	w'w'	u'	v'	w'	k
(m)	(m/s)	(m/s)	(m/s)	(m^2/s^2)	(m^2/s^2)	(m^2/s^2)	(m/s)	(m/s)	(m/s)	(m^2/s^2)
5.00E-2	-4.69E-2	-4.36E-2	-4.51E-3	1.54E-4	4.25E-5	7.15E-5	1.24E-2	6.52E-3	8.46E-3	1.34E-4
1.00E-1	-7.49E-2	-4.38E-2	5.85E-4	9.56E-5	3.69E-5	5.11E-5	9.78E-3	6.07E-3	7.15E-3	9.18E-5
1.50E-1	-9.34E-2	-2.45E-2	1.51E-3	5.62E-5	3.42E-5	3.48E-5	7.49E-3	5.85E-3	5.90E-3	6.26E-5
2.00E-1	-9.52E-2	-1.01E-2	3.53E-4	4.63E-5	2.87E-5	3.02E-5	6.80E-3	5.36E-3	5.49E-3	5.26E-5
3.00E-1	-9.24E-2	-1.46E-3	-1.53E-4	5.46E-5	2.86E-5	3.01E-5	7.39E-3	5.35E-3	5.48E-3	5.66E-5
4.50E-1	-9.13E-2	-5.36E-5	-4.26E-4	5.47E-5	2.83E-5	3.05E-5	7.40E-3	5.32E-3	5.53E-3	5.68E-5

Section 2c (y=248mm)

X	u-velocity	v-velocity	w-velocity	u'u'	v'v'	w'w'	u'	v'	w'	k
(m)	(m/s)	(m/s)	(m/s)	(m^2/s^2)	(m^2/s^2)	(m^2/s^2)	(m/s)	(m/s)	(m/s)	(m^2/s^2)
5.00E-2	-4.34E-2	-2.29E-2	-6.58E-3	1.67E-4	5.20E-5	7.81E-5	1.29E-2	7.21E-3	8.84E-3	1.48E-4
1.00E-1	-6.68E-2	-2.52E-2	-1.16E-3	1.22E-4	4.89E-5	6.49E-5	1.10E-2	6.99E-3	8.05E-3	1.18E-4
1.50E-1	-8.28E-2	-1.78E-2	2.11E-4	8.35E-5	4.23E-5	4.76E-5	9.14E-3	6.51E-3	6.90E-3	8.67E-5
2.00E-1	-8.89E-2	-8.58E-3	1.77E-4	6.39E-5	3.61E-5	3.83E-5	7.99E-3	6.01E-3	6.19E-3	6.91E-5
3.00E-1	-9.15E-2	-1.50E-3	-2.02E-4	5.42E-5	3.20E-5	3.37E-5	7.36E-3	5.66E-3	5.80E-3	5.99E-5
4.50E-1	-9.16E-2	3.83E-5	-4.16E-4	5.28E-5	3.09E-5	3.33E-5	7.27E-3	5.56E-3	5.77E-3	5.85E-5

Section 2ow (y=283mm)

X	u-velocity	v-velocity	w-velocity	u'u'	v'v'	w'w'	u'	v'	w'	k
(m)	(m/s)	(m/s)	(m/s)	(m^2/s^2)	(m^2/s^2)	(m^2/s^2)	(m/s)	(m/s)	(m/s)	(m^2/s^2)
5.00E-2	-3.02E-2	-2.35E-3	-8.26E-3	1.18E-4	6.71E-5	8.21E-5	1.09E-2	8.19E-3	9.06E-3	1.34E-4
1.00E-1	-5.14E-2	-2.43E-3	-4.28E-3	1.72E-4	8.30E-5	8.36E-5	1.31E-2	9.11E-3	9.14E-3	1.69E-4
1.50E-1	-6.05E-2	-2.03E-3	-2.10E-3	1.62E-4	8.11E-5	7.30E-5	1.27E-2	9.01E-3	8.55E-3	1.58E-4
2.00E-1	-6.59E-2	-3.17E-3	1.85E-4	1.62E-4	7.11E-5	6.36E-5	1.27E-2	8.43E-3	7.98E-3	1.48E-4
3.00E-1	-7.64E-2	-5.25E-4	2.38E-4	1.52E-4	7.12E-5	5.64E-5	1.23E-2	8.44E-3	7.51E-3	1.40E-4
4.50E-1	-7.66E-2	4.14E-4	2.87E-4	1.52E-4	7.12E-5	5.46E-5	1.23E-2	8.44E-3	7.39E-3	1.39E-4

Table A1.4 LDA readings for the flowrate of 180l/min (nominal velocity of 0.1m/s) level 4 (z=140mm)

Section 1ow (y=25mm)

X	u-velocity	v-velocity	w-velocity	u'u'	v'v'	w'w'	u'	v'	w'	k
(m)	(m/s)	(m/s)	(m/s)	(m^2/s^2)	(m^2/s^2)	(m^2/s^2)	(m/s)	(m/s)	(m/s)	(m^2/s^2)
5.00E-2	2.73E-2	-2.41E-2	-6.84E-3	7.14E-5	1.32E-4	6.06E-5	8.45E-3	1.15E-2	7.78E-3	1.32E-4
1.00E-1	7.58E-2	-2.42E-2	-5.36E-3	7.58E-5	9.87E-5	5.50E-5	8.70E-3	9.94E-3	7.42E-3	1.15E-4
1.50E-1	1.11E-1	-2.31E-2	1.05E-3	1.21E-4	1.09E-4	5.58E-5	1.10E-2	1.04E-2	7.47E-3	1.42E-4
2.00E-1	1.28E-1	-5.72E-3	4.37E-3	1.71E-4	1.08E-4	5.60E-5	1.31E-2	1.04E-2	7.49E-3	1.67E-4
3.00E-1	1.32E-1	1.24E-3	3.70E-3	2.21E-4	1.07E-4	6.21E-5	1.49E-2	1.04E-2	7.88E-3	1.95E-4
4.50E-1	1.24E-1	3.22E-3	1.34E-3	2.51E-4	1.07E-4	7.10E-5	1.58E-2	1.03E-2	8.43E-3	2.15E-4

Section 1c (y=60mm)

X	u-velocity	v-velocity	w-velocity	u'u'	v'v'	w'w'	u'	v'	w'	k
(m)	(m/s)	(m/s)	(m/s)	(m^2/s^2)	(m^2/s^2)	(m^2/s^2)	(m/s)	(m/s)	(m/s)	(m^2/s^2)
5.00E-2	1.54E-2	-6.04E-2	-1.65E-3	1.06E-4	9.20E-5	7.70E-5	1.03E-2	9.59E-3	8.77E-3	1.38E-4
1.00E-1	7.70E-2	-5.73E-2	4.20E-3	9.30E-5	7.00E-5	5.80E-5	9.64E-3	8.37E-3	7.62E-3	1.11E-4
1.50E-1	1.10E-1	-6.48E-2	6.13E-3	8.20E-5	8.00E-5	7.10E-5	9.06E-3	8.94E-3	8.43E-3	1.17E-4
2.00E-1	1.02E-1	-1.16E-2	7.72E-3	2.40E-5	6.10E-5	7.30E-5	4.90E-3	7.81E-3	8.54E-3	7.90E-5
3.00E-1	1.19E-1	1.24E-2	8.20E-3	2.70E-5	6.10E-5	7.20E-5	5.20E-3	7.81E-3	8.49E-3	8.00E-5
4.50E-1	1.02E-1	7.86E-3	5.34E-3	1.68E-4	7.11E-5	3.20E-5	1.30E-2	8.43E-3	5.66E-3	1.36E-4

Section 1iw (y=100mm)

X	u-velocity	v-velocity	w-velocity	u'u'	v'v'	w'w'	u'	v'	w'	k
(m)	(m/s)	(m/s)	(m/s)	(m^2/s^2)	(m^2/s^2)	(m^2/s^2)	(m/s)	(m/s)	(m/s)	(m^2/s^2)
5.00E-2	4.90E-3	-6.55E-2	-4.40E-3	9.00E-6	4.82E-5	5.66E-5	3.00E-3	6.94E-3	7.52E-3	5.69E-5
1.00E-1	2.00E-2	-7.12E-2	4.53E-3	8.90E-5	5.46E-5	6.58E-5	9.43E-3	7.39E-3	8.11E-3	1.05E-4
1.50E-1	2.00E-2	-3.52E-2	8.40E-3	1.00E-4	6.46E-5	6.84E-5	1.00E-2	8.04E-3	8.27E-3	1.17E-4
2.00E-1	3.10E-2	1.31E-2	1.07E-2	2.81E-5	5.14E-5	7.17E-5	5.30E-3	7.17E-3	8.47E-3	7.56E-5
3.00E-1	4.42E-2	1.24E-2	1.46E-3	7.90E-5	9.80E-5	1.10E-4	8.89E-3	9.90E-3	1.05E-2	1.44E-4
4.50E-1	5.74E-2	1.04E-2	-3.42E-3	2.03E-4	1.27E-4	1.20E-4	1.42E-2	1.13E-2	1.10E-2	2.25E-4

Section 2iw (y=208mm)

X	u-velocity	v-velocity	w-velocity	u'u'	v'v'	w'w'	u'	v'	w'	k
(m)	(m/s)	(m/s)	(m/s)	(m^2/s^2)	(m^2/s^2)	(m^2/s^2)	(m/s)	(m/s)	(m/s)	(m^2/s^2)
5.00E-2	-5.20E-2	-6.97E-2	-4.05E-3	1.30E-4	4.09E-5	6.18E-5	1.14E-2	6.40E-3	7.86E-3	1.16E-4
1.00E-1	-8.01E-2	-8.34E-2	-2.31E-3	1.40E-4	3.28E-5	4.05E-5	1.18E-2	5.72E-3	6.37E-3	1.07E-4
1.50E-1	-9.80E-2	-1.57E-2	-1.59E-3	2.20E-4	2.64E-5	2.55E-5	1.48E-2	5.14E-3	5.05E-3	1.36E-4
2.00E-1	-1.02E-1	-3.82E-3	-4.41E-4	2.25E-4	2.61E-5	2.14E-5	1.50E-2	5.11E-3	4.62E-3	1.36E-4
3.00E-1	-1.09E-1	-2.00E-4	-2.63E-4	2.13E-4	3.21E-5	2.14E-5	1.46E-2	5.67E-3	4.62E-3	1.33E-4
4.50E-1	-7.00E-2	3.09E-4	-5.20E-4	3.03E-4	3.21E-5	2.14E-5	1.74E-2	5.66E-3	4.62E-3	1.78E-4

Section 2c (y=248mm)

X	u-velocity	v-velocity	w-velocity	u'u'	v'v'	w'w'	u'	v'	w'	k
(m)	(m/s)	(m/s)	(m/s)	(m^2/s^2)	(m^2/s^2)	(m^2/s^2)	(m/s)	(m/s)	(m/s)	(m^2/s^2)
5.00E-2	-4.90E-3	-6.20E-3	-1.10E-3	1.40E-4	5.10E-5	6.80E-5	1.18E-2	7.14E-3	8.25E-3	1.30E-4
1.00E-1	-7.80E-2	-8.70E-2	-3.70E-3	9.70E-5	6.00E-5	4.90E-5	9.85E-3	7.75E-3	7.00E-3	1.03E-4
1.50E-1	-9.00E-2	-7.70E-2	-3.14E-3	2.10E-5	4.60E-5	4.10E-5	4.58E-3	6.78E-3	6.40E-3	5.40E-5
2.00E-1	-1.09E-1	-7.84E-3	-2.20E-3	5.76E-5	4.20E-5	2.80E-5	7.59E-3	6.48E-3	5.29E-3	6.38E-5
3.00E-1	-1.29E-1	-4.50E-3	-7.60E-4	2.70E-5	3.20E-5	2.80E-5	5.20E-3	5.66E-3	5.29E-3	4.35E-5
4.50E-1	-1.02E-1	5.00E-3	-1.10E-3	2.70E-5	2.40E-5	1.30E-5	5.20E-3	4.90E-3	3.61E-3	3.20E-5

Section 2ow (y=283mm)

X	u-velocity	v-velocity	w-velocity	u'u'	v'v'	w'w'	u'	v'	w'	k
(m)	(m/s)	(m/s)	(m/s)	(m^2/s^2)	(m^2/s^2)	(m^2/s^2)	(m/s)	(m/s)	(m/s)	(m^2/s^2)
5.00E-2	-1.54E-2	-2.35E-3	1.49E-3	3.51E-5	3.50E-5	7.14E-5	5.93E-3	5.91E-3	8.45E-3	7.08E-5
1.00E-1	-5.63E-2	-2.46E-3	-7.72E-3	1.27E-4	7.30E-5	7.52E-5	1.13E-2	8.55E-3	8.67E-3	1.38E-4
1.50E-1	-5.94E-2	-2.38E-3	-6.12E-3	1.79E-4	9.77E-5	6.92E-5	1.34E-2	9.88E-3	8.32E-3	1.73E-4
2.00E-1	-8.30E-2	-3.19E-3	-1.61E-3	1.52E-4	7.11E-5	6.12E-5	1.23E-2	8.43E-3	7.82E-3	1.42E-4
3.00E-1	-1.19E-1	-2.35E-4	3.75E-4	1.52E-4	7.11E-5	5.42E-5	1.23E-2	8.43E-3	7.36E-3	1.39E-4
4.50E-1	-7.46E-2	-1.58E-5	7.27E-4	1.52E-4	7.12E-5	5.21E-5	1.23E-2	8.44E-3	7.22E-3	1.38E-4

Table A1.5 LDA readings for the flowrate of 180l/min (nominal velocity of 0.1m/s) level 5 (z=180mm)

Section 1ow (y=25mm)

X	u-velocity	v-velocity	w-velocity	u'u'	v'v'	w'w'	u'	v'	w'	k
(m)	(m/s)	(m/s)	(m/s)	(m^2/s^2)	(m^2/s^2)	(m^2/s^2)	(m/s)	(m/s)	(m/s)	(m^2/s^2)
5.00E-2	2.63E-2	-2.34E-2	-2.40E-3	2.12E-5	1.58E-5	1.47E-5	4.60E-3	3.97E-3	3.83E-3	2.58E-5
1.00E-1	7.78E-2	-3.98E-2	-1.47E-3	1.80E-5	1.30E-5	1.32E-5	4.24E-3	3.61E-3	3.63E-3	2.21E-5
1.50E-1	1.11E-1	-2.79E-2	3.60E-4	2.02E-5	1.47E-5	1.49E-5	4.50E-3	3.83E-3	3.86E-3	2.49E-5
2.00E-1	1.31E-1	-6.50E-3	1.43E-3	2.14E-5	1.60E-5	1.63E-5	4.62E-3	4.00E-3	4.04E-3	2.68E-5
3.00E-1	1.37E-1	1.10E-3	1.35E-3	2.22E-5	1.60E-5	1.44E-5	4.71E-3	4.00E-3	3.79E-3	2.63E-5
4.50E-1	1.32E-1	2.37E-3	4.79E-4	2.32E-5	1.95E-5	1.61E-5	4.82E-3	4.41E-3	4.01E-3	2.94E-5

Section 1iw (y=100mm)

X	u-velocity	v-velocity	w-velocity	u'u'	v'v'	w'w'	u'	v'	w'	k
(m)	(m/s)	(m/s)	(m/s)	(m^2/s^2)	(m^2/s^2)	(m^2/s^2)	(m/s)	(m/s)	(m/s)	(m^2/s^2)
5.00E-2	3.00E-2	-8.33E-2	-2.35E-3	6.70E-5	1.21E-5	1.23E-5	8.19E-3	3.47E-3	3.51E-3	4.57E-5
1.00E-1	4.20E-2	-9.45E-2	1.40E-4	3.10E-5	1.68E-5	1.72E-5	5.57E-3	4.09E-3	4.14E-3	3.25E-5
1.50E-1	5.70E-2	-3.43E-2	3.06E-3	5.70E-5	2.28E-5	2.41E-5	7.55E-3	4.77E-3	4.91E-3	5.19E-5
2.00E-1	4.89E-2	5.30E-3	4.36E-3	6.20E-5	2.67E-5	3.10E-5	7.87E-3	5.17E-3	5.57E-3	5.98E-5
3.00E-1	5.29E-2	8.49E-3	6.39E-4	2.70E-5	2.79E-5	3.33E-5	5.20E-3	5.29E-3	5.77E-3	4.41E-5
4.50E-1	5.74E-2	4.62E-3	-1.24E-3	2.40E-5	2.59E-5	2.76E-5	4.90E-3	5.08E-3	5.26E-3	3.88E-5

Section 2c (y=248mm)

X	u-velocity	v-velocity	w-velocity	u'u'	v'v'	w'w'	u'	v'	w'	k
(m)	(m/s)	(m/s)	(m/s)	(m^2/s^2)	(m^2/s^2)	(m^2/s^2)	(m/s)	(m/s)	(m/s)	(m^2/s^2)
5.00E-2	-3.00E-2	6.20E-3	-1.13E-3	4.90E-5	1.75E-5	1.81E-5	7.00E-3	4.18E-3	4.26E-3	4.23E-5
1.00E-1	-5.00E-2	-8.25E-3	-2.87E-3	1.33E-5	1.60E-5	1.39E-5	3.65E-3	4.00E-3	3.72E-3	2.16E-5
1.50E-1	-8.90E-2	-7.84E-3	-1.78E-3	2.81E-5	1.69E-5	1.24E-5	5.30E-3	4.11E-3	3.52E-3	2.87E-5
2.00E-1	-9.60E-2	-4.90E-3	-7.98E-4	3.36E-5	1.69E-5	1.10E-5	5.80E-3	4.11E-3	3.32E-3	3.08E-5
3.00E-1	-9.39E-2	-4.50E-3	-2.47E-4	1.10E-5	1.01E-5	1.01E-5	3.32E-3	3.17E-3	3.19E-3	1.56E-5
4.50E-1	-1.02E-1	-5.20E-3	-2.74E-4	1.30E-5	9.91E-6	1.00E-5	3.60E-3	3.15E-3	3.17E-3	1.64E-5

Section 1c (y=60mm)

X	u-velocity	v-velocity	w-velocity	u'u'	v'v'	w'w'	u'	v'	w'	k
(m)	(m/s)	(m/s)	(m/s)	(m^2/s^2)	(m^2/s^2)	(m^2/s^2)	(m/s)	(m/s)	(m/s)	(m^2/s^2)
5.00E-2	1.64E-2	-5.52E-2	-3.25E-3	3.70E-5	1.33E-5	1.32E-5	6.08E-3	3.65E-3	3.63E-3	3.17E-5
1.00E-1	7.00E-2	-6.33E-2	-5.29E-4	2.30E-5	1.39E-5	1.41E-5	4.80E-3	3.73E-3	3.76E-3	2.55E-5
1.50E-1	9.20E-2	-3.88E-2	2.33E-3	3.20E-5	1.72E-5	1.81E-5	5.66E-3	4.15E-3	4.26E-3	3.37E-5
2.00E-1	9.60E-2	-7.12E-3	3.80E-3	3.40E-5	2.08E-5	2.11E-5	5.83E-3	4.56E-3	4.60E-3	3.80E-5
3.00E-1	1.04E-1	4.05E-3	3.25E-3	2.70E-5	2.33E-5	2.43E-5	5.20E-3	4.83E-3	4.93E-3	3.73E-5
4.50E-1	1.02E-1	4.13E-3	1.51E-3	2.81E-5	2.43E-5	2.55E-5	5.30E-3	4.93E-3	5.05E-3	3.90E-5

Section 2iw (y=208mm)

X	u-velocity	v-velocity	w-velocity	u'u'	v'v'	w'w'	u'	v'	w'	k
(m)	(m/s)	(m/s)	(m/s)	(m^2/s^2)	(m^2/s^2)	(m^2/s^2)	(m/s)	(m/s)	(m/s)	(m^2/s^2)
5.00E-2	-3.10E-2	-4.33E-2	-1.64E-3	2.00E-5	1.24E-5	1.42E-5	4.47E-3	3.52E-3	3.76E-3	2.33E-5
1.00E-1	-8.06E-2	-5.43E-2	-1.52E-3	2.20E-5	1.21E-5	1.17E-5	4.69E-3	3.48E-3	3.41E-3	2.29E-5
1.50E-1	-8.10E-2	-3.29E-2	-1.02E-3	2.00E-5	1.53E-5	1.03E-5	4.47E-3	3.91E-3	3.20E-3	2.28E-5
2.00E-1	-1.02E-1	-1.21E-2	-3.78E-4	2.20E-5	1.51E-5	9.83E-6	4.69E-3	3.89E-3	3.14E-3	2.35E-5
3.00E-1	-5.89E-2	-1.36E-3	-1.29E-4	3.90E-5	2.86E-5	1.01E-5	6.24E-3	5.34E-3	3.17E-3	3.88E-5
4.50E-1	-5.74E-2	6.40E-4	-2.38E-4	3.84E-5	2.99E-5	1.03E-5	6.20E-3	5.47E-3	3.20E-3	3.93E-5

Section 2ow (y=283mm)

X	u-velocity	v-velocity	w-velocity	u'u'	v'v'	w'w'	u'	v'	w'	k
(m)	(m/s)	(m/s)	(m/s)	(m^2/s^2)	(m^2/s^2)	(m^2/s^2)	(m/s)	(m/s)	(m/s)	(m^2/s^2)
5.00E-2	3.22E-2	1.60E-3	5.39E-3	4.26E-5	2.93E-5	3.29E-5	6.53E-3	5.41E-3	5.73E-3	5.24E-5
1.00E-1	-3.62E-2	-4.20E-3	-3.79E-3	2.97E-5	1.82E-5	1.68E-5	5.45E-3	4.27E-3	4.10E-3	3.24E-5
1.50E-1	-6.20E-2	-4.84E-3	-3.21E-3	2.88E-5	1.94E-5	1.73E-5	5.36E-3	4.40E-3	4.16E-3	3.27E-5
2.00E-1	-4.20E-2	-2.42E-3	-1.13E-3	2.94E-5	2.14E-5	1.72E-5	5.42E-3	4.63E-3	4.15E-3	3.40E-5
3.00E-1	-7.30E-2	-6.94E-4	1.53E-4	3.20E-5	2.17E-5	1.69E-5	5.65E-3	4.65E-3	4.11E-3	3.53E-5
4.50E-1	-5.88E-2	-3.36E-4	4.23E-4	3.34E-5	2.28E-5	1.71E-5	5.78E-3	4.78E-3	4.14E-3	3.67E-5

Table A2.1 LDA readings for the flowrate of 90l/min (nominal velocity of 0.05m/s) level 1 (z=20mm)

Section 1ow (y=25mm)

X	u-velocity	v-velocity	w-velocity	u'u'	v'v'	w'w'	u'	v'	w'	k
(m)	(m/s)	(m/s)	(m/s)	(m^2/s^2)	(m^2/s^2)	(m^2/s^2)	(m/s)	(m/s)	(m/s)	(m^2/s^2)
5.00E-2	2.87E-2	-3.16E-3	-7.67E-3	4.38E-5	5.18E-5	4.57E-5	6.62E-3	7.20E-3	6.76E-3	7.06E-5
1.00E-1	5.57E-2	-4.15E-3	-5.33E-3	6.78E-5	6.25E-5	5.15E-5	8.23E-3	7.91E-3	7.18E-3	9.09E-5
1.50E-1	7.92E-2	-4.11E-3	8.31E-4	9.76E-5	7.13E-5	6.01E-5	9.88E-3	8.44E-3	7.75E-3	1.14E-4
2.00E-1	9.11E-2	3.16E-4	1.24E-3	1.25E-4	7.91E-5	7.07E-5	1.12E-2	8.89E-3	8.41E-3	1.38E-4
3.00E-1	9.29E-2	2.22E-3	1.01E-3	1.63E-4	9.09E-5	8.32E-5	1.28E-2	9.53E-3	9.12E-3	1.69E-4
4.50E-1	8.38E-2	2.71E-3	2.10E-4	1.75E-4	9.45E-5	9.11E-5	1.32E-2	9.72E-3	9.54E-3	1.80E-4

Section 1c (y=60mm)

X	u-velocity	v-velocity	w-velocity	u'u'	v'v'	w'w'	u'	v'	w'	k
(m)	(m/s)	(m/s)	(m/s)	(m^2/s^2)	(m^2/s^2)	(m^2/s^2)	(m/s)	(m/s)	(m/s)	(m^2/s^2)
5.00E-2	2.89E-2	-1.65E-2	-3.28E-3	6.49E-5	6.26E-5	5.23E-5	8.05E-3	7.91E-3	7.23E-3	8.99E-5
1.00E-1	5.14E-2	-2.52E-2	2.45E-3	7.50E-5	7.14E-5	5.18E-5	8.66E-3	8.45E-3	7.20E-3	9.91E-5
1.50E-1	7.06E-2	-2.22E-2	5.61E-3	9.65E-5	8.45E-5	5.98E-5	9.83E-3	9.19E-3	7.73E-3	1.20E-4
2.00E-1	6.81E-2	-8.76E-3	4.36E-3	1.10E-4	7.60E-5	6.58E-5	1.05E-2	8.72E-3	8.11E-3	1.26E-4
3.00E-1	6.77E-2	1.25E-3	2.50E-3	1.11E-4	6.10E-5	6.54E-5	1.05E-2	7.81E-3	8.09E-3	1.19E-4
4.50E-1	6.71E-2	4.27E-3	5.33E-4	1.31E-4	6.21E-5	7.59E-5	1.14E-2	7.88E-3	8.71E-3	1.34E-4

Section 1iw (y=100mm)

X	u-velocity	v-velocity	w-velocity	u'u'	v'v'	w'w'	u'	v'	w'	k
(m)	(m/s)	(m/s)	(m/s)	(m^2/s^2)	(m^2/s^2)	(m^2/s^2)	(m/s)	(m/s)	(m/s)	(m^2/s^2)
5.00E-2	2.54E-2	-3.04E-2	-1.83E-3	7.16E-5	5.96E-5	5.12E-5	8.46E-3	7.72E-3	7.16E-3	9.12E-5
1.00E-1	3.98E-2	-4.92E-2	6.03E-3	7.35E-5	7.84E-5	5.14E-5	8.57E-3	8.85E-3	7.17E-3	1.02E-4
1.50E-1	4.55E-2	-3.24E-2	5.61E-3	9.08E-5	8.17E-5	5.77E-5	9.53E-3	9.04E-3	7.59E-3	1.15E-4
2.00E-1	2.53E-2	-7.86E-3	3.28E-3	6.56E-5	5.30E-5	4.21E-5	8.10E-3	7.28E-3	6.49E-3	8.04E-5
3.00E-1	-2.56E-3	-5.52E-4	1.54E-3	4.35E-5	3.02E-5	2.89E-5	6.59E-3	5.49E-3	5.38E-3	5.13E-5
4.50E-1	1.42E-2	2.09E-3	-6.78E-4	6.69E-5	4.34E-5	4.20E-5	8.18E-3	6.58E-3	6.48E-3	7.61E-5

Section 2iw (y=208mm)

X	u-velocity	v-velocity	w-velocity	u'u'	v'v'	w'w'	u'	v'	w'	k
(m)	(m/s)	(m/s)	(m/s)	(m^2/s^2)	(m^2/s^2)	(m^2/s^2)	(m/s)	(m/s)	(m/s)	(m^2/s^2)
5.00E-2	2.26E-3	-2.18E-2	-2.03E-3	5.32E-5	3.30E-5	3.32E-5	7.30E-3	5.75E-3	5.76E-3	5.98E-5
1.00E-1	-2.20E-2	-2.65E-2	2.42E-3	7.26E-5	4.83E-5	4.04E-5	8.52E-3	6.95E-3	6.35E-3	8.07E-5
1.50E-1	-4.52E-2	-2.20E-2	1.44E-3	9.42E-5	5.21E-5	5.15E-5	9.70E-3	7.22E-3	7.18E-3	9.89E-5
2.00E-1	-4.82E-2	-8.69E-3	5.52E-4	9.58E-5	5.08E-5	5.01E-5	9.79E-3	7.13E-3	7.08E-3	9.84E-5
3.00E-1	-4.59E-2	-1.46E-3	-7.06E-7	9.38E-5	5.01E-5	4.85E-5	9.68E-3	7.08E-3	6.96E-3	9.62E-5
4.50E-1	-4.48E-2	8.67E-5	-5.22E-5	9.26E-5	4.85E-5	4.75E-5	9.62E-3	6.96E-3	6.89E-3	9.43E-5

Section 2c (y=248mm)

X	u-velocity	v-velocity	w-velocity	u'u'	v'v'	w'w'	u'	v'	w'	k
(m)	(m/s)	(m/s)	(m/s)	(m^2/s^2)	(m^2/s^2)	(m^2/s^2)	(m/s)	(m/s)	(m/s)	(m^2/s^2)
5.00E-2	3.48E-3	-1.24E-2	-3.54E-3	5.00E-5	2.65E-5	3.09E-5	7.07E-3	5.15E-3	5.56E-3	5.38E-5
1.00E-1	-1.22E-2	-1.36E-2	1.65E-3	4.66E-5	3.14E-5	2.90E-5	6.82E-3	5.60E-3	5.38E-3	5.35E-5
1.50E-1	-3.27E-2	-1.37E-2	1.30E-3	7.76E-5	4.38E-5	4.27E-5	8.81E-3	6.62E-3	6.54E-3	8.20E-5
2.00E-1	-4.23E-2	-7.34E-3	5.92E-4	9.02E-5	4.82E-5	4.80E-5	9.49E-3	6.94E-3	6.92E-3	9.31E-5
3.00E-1	-4.73E-2	-1.45E-3	4.55E-5	9.58E-5	5.02E-5	5.02E-5	9.79E-3	7.09E-3	7.09E-3	9.81E-5
4.50E-1	-4.77E-2	6.18E-5	-2.43E-5	9.59E-5	5.02E-5	5.02E-5	9.79E-3	7.09E-3	7.09E-3	9.82E-5

Section 2ow (y=283mm)

X	u-velocity	v-velocity	w-velocity	u'u'	v'v'	w'w'	u'	v'	w'	k
(m)	(m/s)	(m/s)	(m/s)	(m^2/s^2)	(m^2/s^2)	(m^2/s^2)	(m/s)	(m/s)	(m/s)	(m^2/s^2)
5.00E-2	6.20E-3	-4.27E-3	-5.07E-3	3.28E-5	2.21E-5	2.79E-5	5.73E-3	4.70E-3	5.28E-3	4.14E-5
1.00E-1	5.87E-3	-3.22E-3	1.04E-3	2.76E-5	1.93E-5	1.98E-5	5.26E-3	4.39E-3	4.45E-3	3.33E-5
1.50E-1	-2.33E-3	-4.22E-3	1.50E-3	3.27E-5	2.12E-5	2.32E-5	5.72E-3	4.60E-3	4.82E-3	3.86E-5
2.00E-1	-2.14E-2	-2.14E-3	8.13E-4	6.47E-5	3.29E-5	3.40E-5	8.04E-3	5.73E-3	5.83E-3	6.58E-5
3.00E-1	-2.82E-2	-6.36E-4	1.42E-4	6.59E-5	3.64E-5	3.84E-5	8.12E-3	6.03E-3	6.20E-3	7.03E-5
4.50E-1	-3.23E-2	-4.65E-5	1.22E-4	7.61E-5	3.95E-5	3.94E-5	8.72E-3	6.28E-3	6.28E-3	7.75E-5

Table A2.2 LDA readings for the flowrate of 90l/min (nominal velocity of 0.05m/s) level 2 (z=60mm)

Section 1ow (y=25mm)

X	u-velocity	v-velocity	w-velocity	u'u'	v'v'	w'w'	u'	v'	w'	k
(m)	(m/s)	(m/s)	(m/s)	(m^2/s^2)	(m^2/s^2)	(m^2/s^2)	(m/s)	(m/s)	(m/s)	(m^2/s^2)
5.00E-2	2.27E-2	-8.19E-3	-1.64E-2	5.04E-5	8.55E-5	5.76E-5	7.10E-3	9.25E-3	7.59E-3	9.68E-5
1.00E-1	5.18E-2	-1.20E-2	-8.36E-3	6.49E-5	9.02E-5	6.57E-5	8.06E-3	9.50E-3	8.11E-3	1.10E-4
1.50E-1	7.71E-2	-1.04E-2	1.47E-3	1.05E-4	1.06E-4	7.56E-5	1.02E-2	1.03E-2	8.69E-3	1.43E-4
2.00E-1	8.89E-2	-2.46E-3	3.73E-3	1.11E-4	1.09E-4	8.54E-5	1.05E-2	1.05E-2	9.24E-3	1.53E-4
3.00E-1	7.76E-2	1.62E-3	2.80E-3	1.21E-4	8.80E-5	1.06E-4	1.10E-2	9.38E-3	1.03E-2	1.57E-4
4.50E-1	9.05E-2	2.08E-3	8.26E-4	1.11E-4	1.11E-4	1.11E-4	1.05E-2	1.05E-2	1.05E-2	1.66E-4

Section 1c (y=60mm)

X	u-velocity	v-velocity	w-velocity	u'u'	v'v'	w'w'	u'	v'	w'	k
(m)	(m/s)	(m/s)	(m/s)	(m^2/s^2)	(m^2/s^2)	(m^2/s^2)	(m/s)	(m/s)	(m/s)	(m^2/s^2)
5.00E-2	1.87E-2	-3.49E-2	-7.61E-3	7.82E-5	7.67E-5	6.00E-5	8.84E-3	8.76E-3	7.75E-3	1.07E-4
1.00E-1	5.32E-2	-4.08E-2	6.98E-3	7.81E-5	7.77E-5	5.11E-5	8.84E-3	8.81E-3	7.15E-3	1.03E-4
1.50E-1	8.10E-2	-2.59E-2	1.14E-2	7.01E-5	7.06E-5	4.62E-5	8.38E-3	8.40E-3	6.80E-3	9.35E-5
2.00E-1	8.54E-2	-8.69E-3	1.10E-2	7.37E-5	6.25E-5	4.33E-5	8.59E-3	7.91E-3	6.58E-3	8.98E-5
3.00E-1	7.76E-2	1.32E-3	6.11E-3	1.25E-4	6.70E-5	5.66E-5	1.12E-2	8.19E-3	7.52E-3	1.24E-4
4.50E-1	7.30E-2	3.44E-3	1.76E-3	1.82E-4	8.81E-5	8.10E-5	1.35E-2	9.39E-3	9.00E-3	1.76E-4

Section 1iw (y=100mm)

X	u-velocity	v-velocity	w-velocity	u'u'	v'v'	w'w'	u'	v'	w'	k
(m)	(m/s)	(m/s)	(m/s)	(m^2/s^2)	(m^2/s^2)	(m^2/s^2)	(m/s)	(m/s)	(m/s)	(m^2/s^2)
5.00E-2	1.29E-2	-4.64E-2	-3.82E-3	1.06E-4	5.76E-5	6.14E-5	1.03E-2	7.59E-3	7.84E-3	1.12E-4
1.00E-1	2.90E-2	-5.96E-2	1.26E-2	9.36E-5	5.72E-5	4.98E-5	9.68E-3	7.56E-3	7.06E-3	1.00E-4
1.50E-1	3.30E-2	-2.71E-2	1.22E-2	7.95E-5	6.23E-5	5.03E-5	8.92E-3	7.89E-3	7.09E-3	9.61E-5
2.00E-1	3.43E-2	-5.06E-3	7.59E-3	9.67E-5	4.37E-5	4.67E-5	9.83E-3	6.61E-3	6.83E-3	9.35E-5
3.00E-1	1.20E-2	7.93E-4	2.48E-3	1.58E-4	7.92E-5	8.15E-5	1.26E-2	8.90E-3	9.03E-3	1.59E-4
4.50E-1	3.43E-2	2.08E-3	-2.00E-3	1.79E-4	1.02E-4	9.76E-5	1.34E-2	1.01E-2	9.88E-3	1.90E-4

Section 2iw (y=208mm)

X	u-velocity	v-velocity	w-velocity	u'u'	v'v'	w'w'	u'	v'	w'	k
(m)	(m/s)	(m/s)	(m/s)	(m^2/s^2)	(m^2/s^2)	(m^2/s^2)	(m/s)	(m/s)	(m/s)	(m^2/s^2)
5.00E-2	-1.81E-2	-2.83E-2	-3.46E-3	1.30E-4	3.55E-5	5.43E-5	1.14E-2	5.96E-3	7.37E-3	1.10E-4
1.00E-1	-5.22E-2	-3.03E-2	4.35E-3	9.03E-5	3.24E-5	4.38E-5	9.50E-3	5.69E-3	6.62E-3	8.33E-5
1.50E-1	-6.47E-2	-1.98E-2	2.63E-3	5.26E-5	3.13E-5	3.15E-5	7.25E-3	5.59E-3	5.61E-3	5.77E-5
2.00E-1	-2.47E-2	-7.36E-3	1.10E-3	5.05E-5	3.03E-5	2.87E-5	7.10E-3	5.50E-3	5.36E-3	5.47E-5
3.00E-1	-2.24E-2	-1.13E-3	1.23E-4	5.44E-5	3.13E-5	2.87E-5	7.38E-3	5.59E-3	5.36E-3	5.72E-5
4.50E-1	-2.68E-2	3.20E-5	2.85E-5	5.65E-5	3.03E-5	2.87E-5	7.51E-3	5.50E-3	5.36E-3	5.77E-5

Section 2c (y=248mm)

X	u-velocity	v-velocity	w-velocity	u'u'	v'v'	w'w'	u'	v'	w'	k
(m)	(m/s)	(m/s)	(m/s)	(m^2/s^2)	(m^2/s^2)	(m^2/s^2)	(m/s)	(m/s)	(m/s)	(m^2/s^2)
5.00E-2	-7.81E-3	-1.50E-2	-6.65E-3	1.15E-4	3.44E-5	5.20E-5	1.07E-2	5.87E-3	7.21E-3	1.01E-4
1.00E-1	-4.23E-2	-1.65E-2	2.17E-3	1.00E-4	3.60E-5	4.75E-5	1.00E-2	6.00E-3	6.89E-3	9.19E-5
1.50E-1	-5.64E-2	-1.27E-2	2.05E-3	7.20E-5	3.40E-5	3.79E-5	8.48E-3	5.83E-3	6.15E-3	7.19E-5
2.00E-1	-5.08E-2	-6.38E-3	9.71E-4	5.59E-5	3.04E-5	3.17E-5	7.48E-3	5.51E-3	5.63E-3	5.90E-5
3.00E-1	-4.40E-2	-1.19E-3	5.11E-5	4.77E-5	2.79E-5	2.83E-5	6.91E-3	5.28E-3	5.32E-3	5.20E-5
4.50E-1	-5.32E-2	1.20E-5	-1.08E-4	4.67E-5	2.76E-5	2.80E-5	6.83E-3	5.25E-3	5.29E-3	5.12E-5

Section 2ow (y=283mm)

X	u-velocity	v-velocity	w-velocity	u'u'	v'v'	w'w'	u'	v'	w'	k
(m)	(m/s)	(m/s)	(m/s)	(m^2/s^2)	(m^2/s^2)	(m^2/s^2)	(m/s)	(m/s)	(m/s)	(m^2/s^2)
5.00E-2	-2.96E-3	-5.25E-3	-9.10E-3	6.42E-5	3.13E-5	4.14E-5	8.01E-3	5.59E-3	6.43E-3	6.84E-5
1.00E-1	-2.02E-2	-5.24E-3	-9.13E-4	8.70E-5	3.94E-5	4.51E-5	9.33E-3	6.28E-3	6.72E-3	8.58E-5
1.50E-1	-3.24E-2	-4.22E-3	1.96E-3	9.25E-5	4.53E-5	4.95E-5	9.62E-3	6.73E-3	7.04E-3	9.37E-5
2.00E-1	-4.03E-2	-2.13E-3	1.21E-3	8.71E-5	5.06E-5	4.56E-5	9.33E-3	7.11E-3	6.75E-3	9.17E-5
3.00E-1	-4.24E-2	-4.24E-4	3.21E-4	9.12E-5	4.65E-5	5.16E-5	9.55E-3	6.82E-3	7.19E-3	9.47E-5
4.50E-1	-4.36E-2	2.18E-5	-1.21E-4	8.91E-5	4.66E-5	5.17E-5	9.44E-3	6.82E-3	7.19E-3	9.37E-5

Table A2.3 LDA readings for the flowrate of 90l/min (nominal velocity of 0.05m/s) level 3 (z=100mm)

Section 1ow (y=25mm)

X	u-velocity	v-velocity	w-velocity	u'u'	v'v'	w'w'	u'	v'	w'	k
(m)	(m/s)	(m/s)	(m/s)	(m^2/s^2)	(m^2/s^2)	(m^2/s^2)	(m/s)	(m/s)	(m/s)	(m^2/s^2)
5.00E-2	2.06E-2	-1.63E-2	-1.22E-2	4.88E-5	7.89E-5	4.46E-5	6.98E-3	8.88E-3	6.68E-3	8.61E-5
1.00E-1	5.31E-2	-1.66E-2	-6.43E-3	6.43E-5	7.66E-5	5.24E-5	8.02E-3	8.75E-3	7.24E-3	9.66E-5
1.50E-1	7.71E-2	-8.65E-3	1.23E-3	8.97E-5	8.70E-5	6.43E-5	9.47E-3	9.33E-3	8.02E-3	1.21E-4
2.00E-1	8.76E-2	-3.50E-3	2.44E-3	1.04E-4	9.65E-5	7.44E-5	1.02E-2	9.82E-3	8.62E-3	1.37E-4
3.00E-1	8.91E-2	8.14E-4	2.32E-3	1.11E-4	1.08E-4	9.49E-5	1.05E-2	1.03E-2	9.74E-3	1.56E-4
4.50E-1	8.07E-2	1.20E-3	9.91E-4	1.21E-4	1.11E-4	1.05E-4	1.10E-2	1.05E-2	1.03E-2	1.68E-4

Section 1c (y=60mm)

X	u-velocity	v-velocity	w-velocity	u'u'	v'v'	w'w'	u'	v'	w'	k
(m)	(m/s)	(m/s)	(m/s)	(m^2/s^2)	(m^2/s^2)	(m^2/s^2)	(m/s)	(m/s)	(m/s)	(m^2/s^2)
5.00E-2	1.69E-2	-4.49E-2	-6.57E-3	7.03E-5	7.87E-5	4.28E-5	8.38E-3	8.87E-3	6.54E-3	9.59E-5
1.00E-1	4.35E-2	-5.03E-2	5.85E-3	5.63E-5	5.13E-5	4.12E-5	7.50E-3	7.17E-3	6.42E-3	7.44E-5
1.50E-1	6.37E-2	-2.34E-2	1.13E-2	5.06E-5	4.38E-5	4.12E-5	7.11E-3	6.62E-3	6.42E-3	6.78E-5
2.00E-1	6.72E-2	-6.05E-3	1.12E-2	5.18E-5	4.53E-5	3.89E-5	7.20E-3	6.73E-3	6.24E-3	6.81E-5
3.00E-1	6.72E-2	2.63E-3	7.07E-3	6.11E-5	4.53E-5	4.86E-5	9.01E-3	6.73E-3	6.97E-3	8.75E-5
4.50E-1	5.66E-2	3.35E-3	1.30E-3	1.37E-4	4.76E-5	7.19E-5	1.17E-2	6.90E-3	8.48E-3	1.28E-4

Section 1iw (y=100mm)

X	u-velocity	v-velocity	w-velocity	u'u'	v'v'	w'w'	u'	v'	w'	k
(m)	(m/s)	(m/s)	(m/s)	(m^2/s^2)	(m^2/s^2)	(m^2/s^2)	(m/s)	(m/s)	(m/s)	(m^2/s^2)
5.00E-2	4.87E-3	-5.60E-2	-3.36E-3	8.26E-5	3.68E-5	4.30E-5	9.09E-3	6.06E-3	6.56E-3	8.12E-5
1.00E-1	2.09E-2	-6.19E-2	1.02E-2	7.50E-5	4.03E-5	4.58E-5	8.66E-3	6.35E-3	6.77E-3	8.06E-5
1.50E-1	2.77E-2	-1.89E-2	1.14E-2	6.34E-5	4.64E-5	4.52E-5	7.97E-3	6.81E-3	6.72E-3	7.75E-5
2.00E-1	1.57E-2	-1.11E-3	8.36E-3	8.22E-5	3.56E-5	4.38E-5	9.06E-3	5.96E-3	6.62E-3	8.08E-5
3.00E-1	1.47E-2	2.77E-3	1.35E-3	1.33E-4	6.93E-5	7.58E-5	1.15E-2	8.32E-3	8.70E-3	1.39E-4
4.50E-1	2.36E-2	2.48E-3	-2.62E-3	1.54E-4	8.68E-5	8.26E-5	1.24E-2	9.31E-3	9.09E-3	1.62E-4

Section 2iw (y=208mm)

X	u-velocity	v-velocity	w-velocity	u'u'	v'v'	w'w'	u'	v'	w'	k
(m)	(m/s)	(m/s)	(m/s)	(m^2/s^2)	(m^2/s^2)	(m^2/s^2)	(m/s)	(m/s)	(m/s)	(m^2/s^2)
5.00E-2	-3.08E-2	-2.75E-2	-3.09E-3	9.14E-5	2.57E-5	4.13E-5	9.56E-3	5.07E-3	6.42E-3	7.92E-5
1.00E-1	-5.31E-2	-2.86E-2	1.08E-3	5.38E-5	2.13E-5	3.07E-5	7.33E-3	4.62E-3	5.54E-3	5.29E-5
1.50E-1	-6.54E-2	-1.87E-2	1.10E-3	3.44E-5	2.19E-5	2.21E-5	5.86E-3	4.68E-3	4.70E-3	3.92E-5
2.00E-1	-6.57E-2	-6.71E-3	9.47E-4	3.28E-5	2.18E-5	2.22E-5	5.73E-3	4.67E-3	4.71E-3	3.84E-5
3.00E-1	-6.52E-2	-1.02E-3	-8.73E-5	3.29E-5	2.18E-5	2.42E-5	5.73E-3	4.67E-3	4.92E-3	3.94E-5
4.50E-1	-6.25E-2	-7.51E-5	-3.01E-4	3.29E-5	2.18E-5	2.52E-5	5.74E-3	4.67E-3	5.02E-3	3.99E-5

Section 2c (y=248mm)

X	u-velocity	v-velocity	w-velocity	u'u'	v'v'	w'w'	u'	v'	w'	k
(m)	(m/s)	(m/s)	(m/s)	(m^2/s^2)	(m^2/s^2)	(m^2/s^2)	(m/s)	(m/s)	(m/s)	(m^2/s^2)
5.00E-2	-2.80E-2	-1.55E-2	-4.97E-3	1.01E-4	3.18E-5	4.67E-5	1.01E-2	5.64E-3	6.83E-3	9.00E-5
1.00E-1	-4.51E-2	-1.72E-2	-7.17E-4	7.43E-5	2.99E-5	3.92E-5	8.62E-3	5.47E-3	6.26E-3	7.17E-5
1.50E-1	-5.68E-2	-1.22E-2	2.45E-4	5.08E-5	2.58E-5	2.89E-5	7.13E-3	5.08E-3	5.38E-3	5.28E-5
2.00E-1	-6.14E-2	-5.91E-3	1.76E-4	3.88E-5	2.20E-5	2.33E-5	6.23E-3	4.69E-3	4.83E-3	4.21E-5
3.00E-1	-6.35E-2	-1.07E-3	-1.38E-4	3.27E-5	1.96E-5	2.05E-5	5.72E-3	4.42E-3	4.52E-3	3.64E-5
4.50E-1	-6.36E-2	1.97E-5	-3.11E-4	3.18E-5	1.89E-5	2.02E-5	5.64E-3	4.35E-3	4.49E-3	3.54E-5

Section 2ow (y=283mm)

X	u-velocity	v-velocity	w-velocity	u'u'	v'v'	w'w'	u'	v'	w'	k
(m)	(m/s)	(m/s)	(m/s)	(m^2/s^2)	(m^2/s^2)	(m^2/s^2)	(m/s)	(m/s)	(m/s)	(m^2/s^2)
5.00E-2	-1.62E-2	-5.24E-3	-6.08E-3	8.64E-5	3.79E-5	4.41E-5	9.29E-3	6.16E-3	6.64E-3	8.42E-5
1.00E-1	-3.03E-2	-5.28E-3	-3.02E-3	1.05E-4	5.49E-5	5.59E-5	1.02E-2	7.41E-3	7.48E-3	1.08E-4
1.50E-1	-4.03E-2	-4.21E-3	-4.69E-4	9.13E-5	6.09E-5	5.47E-5	9.55E-3	7.80E-3	7.40E-3	1.03E-4
2.00E-1	-4.38E-2	-2.11E-3	1.54E-4	8.14E-5	5.73E-5	5.57E-5	9.02E-3	7.57E-3	7.47E-3	9.72E-5
3.00E-1	-4.62E-2	-3.15E-4	2.08E-4	8.15E-5	5.76E-5	5.58E-5	9.03E-3	7.59E-3	7.47E-3	9.74E-5
4.50E-1	-5.04E-2	1.32E-4	1.20E-4	7.15E-5	5.77E-5	5.48E-5	8.45E-3	7.60E-3	7.40E-3	9.20E-5

Table A2.4 LDA readings for the flowrate of 90l/min (nominal velocity of 0.05m/s) level 4 (z=140mm)

Section 1ow (y=25mm)

X	u-velocity	v-velocity	w-velocity	u'u'	v'v'	w'w'	u'	v'	w'	k
(m)	(m/s)	(m/s)	(m/s)	(m^2/s^2)	(m^2/s^2)	(m^2/s^2)	(m/s)	(m/s)	(m/s)	(m^2/s^2)
5.00E-2	1.82E-2	-1.93E-2	-7.11E-3	3.97E-5	6.06E-5	3.31E-5	6.30E-3	7.78E-3	5.76E-3	6.67E-5
1.00E-1	5.22E-2	-1.91E-2	-4.25E-3	6.33E-5	6.16E-5	4.13E-5	7.96E-3	7.85E-3	6.43E-3	8.31E-5
1.50E-1	7.77E-2	-3.52E-2	1.47E-3	8.31E-5	7.50E-5	5.43E-5	9.12E-3	8.66E-3	7.37E-3	1.06E-4
2.00E-1	8.86E-2	-2.45E-3	3.02E-3	1.03E-4	7.46E-5	6.33E-5	1.02E-2	8.64E-3	7.96E-3	1.21E-4
3.00E-1	8.82E-2	6.12E-4	2.04E-3	1.05E-4	8.43E-5	6.38E-5	1.02E-2	9.18E-3	7.99E-3	1.26E-4
4.50E-1	8.02E-2	1.08E-3	6.37E-4	1.06E-4	8.42E-5	9.43E-5	1.03E-2	9.17E-3	9.71E-3	1.42E-4

Section 1c (y=60mm)

X	u-velocity	v-velocity	w-velocity	u'u'	v'v'	w'w'	u'	v'	w'	k
(m)	(m/s)	(m/s)	(m/s)	(m^2/s^2)	(m^2/s^2)	(m^2/s^2)	(m/s)	(m/s)	(m/s)	(m^2/s^2)
5.00E-2	2.60E-2	-5.02E-2	-4.39E-3	5.59E-5	4.36E-5	3.26E-5	7.48E-3	6.60E-3	5.71E-3	6.61E-5
1.00E-1	3.90E-2	-5.03E-2	2.42E-3	4.52E-5	3.48E-5	3.47E-5	6.73E-3	5.90E-3	5.89E-3	5.74E-5
1.50E-1	7.70E-2	-2.01E-2	7.84E-3	4.08E-5	3.71E-5	3.79E-5	6.37E-3	6.09E-3	6.15E-3	5.77E-5
2.00E-1	8.10E-2	-3.06E-3	8.92E-3	4.04E-5	3.13E-5	3.58E-5	6.36E-3	5.59E-3	5.98E-3	5.37E-5
3.00E-1	9.90E-2	4.09E-3	5.65E-3	5.70E-5	3.36E-5	4.13E-5	7.55E-3	5.80E-3	6.43E-3	6.59E-5
4.50E-1	8.80E-2	3.58E-3	1.10E-3	8.11E-5	4.55E-5	5.58E-5	9.00E-3	6.75E-3	7.47E-3	9.12E-5

Section 1iw (y=100mm)

X	u-velocity	v-velocity	w-velocity	u'u'	v'v'	w'w'	u'	v'	w'	k
(m)	(m/s)	(m/s)	(m/s)	(m^2/s^2)	(m^2/s^2)	(m^2/s^2)	(m/s)	(m/s)	(m/s)	(m^2/s^2)
5.00E-2	4.10E-2	-5.91E-2	-2.41E-3	6.75E-5	2.95E-5	3.40E-5	8.22E-3	5.43E-3	5.83E-3	6.55E-5
1.00E-1	1.70E-2	-6.20E-2	4.55E-3	6.57E-5	3.49E-5	4.14E-5	8.10E-3	5.91E-3	6.43E-3	7.10E-5
1.50E-1	2.30E-2	-1.37E-2	7.28E-3	5.21E-5	3.78E-5	4.03E-5	7.22E-3	6.15E-3	6.35E-3	6.51E-5
2.00E-1	1.65E-2	2.26E-3	6.82E-3	6.08E-5	2.84E-5	3.88E-5	7.80E-3	5.33E-3	6.23E-3	6.40E-5
3.00E-1	1.28E-2	4.76E-3	6.62E-4	8.79E-5	4.85E-5	5.38E-5	9.38E-3	6.96E-3	7.33E-3	9.51E-5
4.50E-1	1.98E-2	3.05E-3	-2.08E-3	1.09E-4	6.12E-5	5.77E-5	1.04E-2	7.83E-3	7.60E-3	1.14E-4

Section 2iw (y=208mm)

X	u-velocity	v-velocity	w-velocity	u'u'	v'v'	w'w'	u'	v'	w'	k
(m)	(m/s)	(m/s)	(m/s)	(m^2/s^2)	(m^2/s^2)	(m^2/s^2)	(m/s)	(m/s)	(m/s)	(m^2/s^2)
5.00E-2	-2.88E-2	-3.02E-2	-2.36E-3	8.26E-5	2.24E-5	3.47E-5	9.09E-3	4.74E-3	5.89E-3	6.99E-5
1.00E-1	-3.76E-2	-3.27E-2	-8.16E-4	4.48E-5	1.90E-5	2.24E-5	6.69E-3	4.35E-3	4.74E-3	4.31E-5
1.50E-1	-5.98E-2	-1.87E-2	-5.27E-4	2.76E-5	1.75E-5	1.76E-5	5.25E-3	4.18E-3	4.19E-3	3.13E-5
2.00E-1	-3.43E-2	-7.03E-3	-3.16E-4	3.20E-5	1.83E-5	1.83E-5	5.66E-3	4.28E-3	4.28E-3	3.43E-5
3.00E-1	-2.53E-2	-9.17E-4	-1.75E-4	3.21E-5	2.01E-5	2.14E-5	5.66E-3	4.49E-3	4.62E-3	3.68E-5
4.50E-1	-3.73E-2	8.74E-5	-5.40E-4	3.21E-5	2.01E-5	2.14E-5	5.66E-3	4.49E-3	4.62E-3	3.68E-5

Section 2c (y=248mm)

X	u-velocity	v-velocity	w-velocity	u'u'	v'v'	w'w'	u'	v'	w'	k
(m)	(m/s)	(m/s)	(m/s)	(m^2/s^2)	(m^2/s^2)	(m^2/s^2)	(m/s)	(m/s)	(m/s)	(m^2/s^2)
5.00E-2	-2.54E-2	-1.47E-2	-2.51E-3	9.84E-5	2.93E-5	4.15E-5	9.92E-3	5.41E-3	6.44E-3	8.46E-5
1.00E-1	-6.86E-2	-1.81E-2	-2.88E-3	7.02E-5	2.76E-5	3.43E-5	8.38E-3	5.25E-3	5.86E-3	6.60E-5
1.50E-1	-6.70E-2	-1.29E-2	-1.54E-3	4.49E-5	2.27E-5	2.45E-5	6.70E-3	4.76E-3	4.95E-3	4.60E-5
2.00E-1	-8.70E-2	-6.24E-3	-6.84E-4	3.22E-5	1.83E-5	1.68E-5	5.67E-3	4.28E-3	4.34E-3	3.47E-5
3.00E-1	-8.30E-2	-1.14E-3	-3.20E-4	2.55E-5	1.55E-5	1.57E-5	5.05E-3	3.93E-3	3.96E-3	2.83E-5
4.50E-1	-8.80E-2	-3.37E-6	-4.44E-4	2.41E-5	1.46E-5	1.50E-5	4.90E-3	3.83E-3	3.88E-3	2.69E-5

Section 2ow (y=283mm)

X	u-velocity	v-velocity	w-velocity	u'u'	v'v'	w'w'	u'	v'	w'	k
(m)	(m/s)	(m/s)	(m/s)	(m^2/s^2)	(m^2/s^2)	(m^2/s^2)	(m/s)	(m/s)	(m/s)	(m^2/s^2)
5.00E-2	-1.52E-3	-4.22E-3	4.52E-4	5.27E-5	2.18E-5	2.19E-5	7.26E-3	4.67E-3	4.68E-3	4.82E-5
1.00E-1	-2.18E-2	-5.29E-3	-4.13E-3	8.79E-5	4.26E-5	4.64E-5	9.37E-3	6.52E-3	6.81E-3	8.84E-5
1.50E-1	-3.29E-2	-4.24E-3	-2.70E-3	9.11E-5	4.62E-5	5.62E-5	9.55E-3	6.80E-3	7.50E-3	9.68E-5
2.00E-1	-4.36E-2	-2.13E-3	-9.29E-4	1.13E-4	4.70E-5	5.70E-5	1.06E-2	6.86E-3	7.55E-3	1.09E-4
3.00E-1	-4.41E-2	-4.23E-4	2.37E-4	1.14E-4	5.17E-5	5.74E-5	1.07E-2	7.19E-3	7.58E-3	1.12E-4
4.50E-1	-4.42E-2	8.15E-6	3.60E-4	1.04E-4	5.17E-5	5.75E-5	1.02E-2	7.19E-3	7.58E-3	1.07E-4

Table A2.5 LDA readings for the flowrate of 90l/min (nominal velocity of 0.05m/s) level 5 (z=180mm)

Section 1ow (y=25mm)

X	u-velocity	v-velocity	w-velocity	u'u'	v'v'	w'w'	u'	v'	w'	k
(m)	(m/s)	(m/s)	(m/s)	(m^2/s^2)	(m^2/s^2)	(m^2/s^2)	(m/s)	(m/s)	(m/s)	(m^2/s^2)
5.00E-2	1.82E-2	-1.28E-2	-2.03E-3	9.27E-6	7.07E-6	7.02E-6	3.04E-3	2.66E-3	2.65E-3	1.17E-5
1.00E-1	5.27E-2	-2.09E-2	-1.10E-3	9.91E-5	8.04E-6	7.85E-6	9.96E-3	2.84E-3	2.80E-3	5.75E-5
1.50E-1	7.92E-2	-3.53E-2	3.51E-4	1.24E-5	8.31E-6	8.10E-6	3.52E-3	2.88E-3	2.85E-3	1.44E-5
2.00E-1	8.93E-2	-2.43E-3	8.11E-4	1.35E-5	9.91E-6	9.11E-6	3.67E-3	3.15E-3	3.02E-3	1.62E-5
3.00E-1	8.29E-2	8.45E-4	6.90E-4	1.41E-5	1.12E-5	1.02E-5	3.75E-3	3.35E-3	3.19E-3	1.77E-5
4.50E-1	8.29E-2	1.22E-3	1.21E-4	1.65E-5	1.20E-5	1.17E-5	4.06E-3	3.47E-3	3.42E-3	2.01E-5

Section 1c (y=60mm)

X	u-velocity	v-velocity	w-velocity	u'u'	v'v'	w'w'	u'	v'	w'	k
(m)	(m/s)	(m/s)	(m/s)	(m^2/s^2)	(m^2/s^2)	(m^2/s^2)	(m/s)	(m/s)	(m/s)	(m^2/s^2)
5.00E-2	3.00E-3	-5.02E-2	-1.75E-3	1.06E-5	7.47E-6	7.69E-6	3.26E-3	2.73E-3	2.77E-3	1.29E-5
1.00E-1	5.32E-2	-5.05E-2	6.96E-4	1.57E-5	1.01E-5	1.12E-5	3.96E-3	3.18E-3	3.35E-3	1.85E-5
1.50E-1	7.23E-2	-1.95E-2	2.48E-3	1.92E-5	1.35E-5	1.35E-5	4.38E-3	3.67E-3	3.67E-3	2.31E-5
2.00E-1	9.39E-2	-2.17E-4	3.25E-3	2.02E-5	1.51E-5	1.57E-5	4.49E-3	3.88E-3	3.96E-3	2.55E-5
3.00E-1	6.89E-2	4.58E-3	2.22E-3	2.24E-5	1.60E-5	1.68E-5	4.73E-3	4.01E-3	4.10E-3	2.76E-5
4.50E-1	7.29E-2	3.60E-3	6.44E-4	2.24E-5	1.56E-5	1.68E-5	4.73E-3	3.95E-3	4.09E-3	2.74E-5

Section 1iw (y=100mm)

X	u-velocity	v-velocity	w-velocity	u'u'	v'v'	w'w'	u'	v'	w'	k
(m)	(m/s)	(m/s)	(m/s)	(m^2/s^2)	(m^2/s^2)	(m^2/s^2)	(m/s)	(m/s)	(m/s)	(m^2/s^2)
5.00E-2	1.00E-2	-5.93E-2	-1.04E-3	1.15E-5	7.98E-6	8.22E-6	3.40E-3	2.82E-3	2.87E-3	1.39E-5
1.00E-1	1.77E-2	-6.32E-2	9.19E-4	1.83E-5	1.19E-5	1.23E-5	4.28E-3	3.45E-3	3.51E-3	2.13E-5
1.50E-1	1.88E-2	-1.21E-2	2.46E-3	2.12E-5	1.54E-5	1.55E-5	4.60E-3	3.93E-3	3.94E-3	2.61E-5
2.00E-1	1.12E-2	4.20E-3	2.77E-3	2.41E-5	1.59E-5	1.79E-5	4.91E-3	3.99E-3	4.23E-3	2.89E-5
3.00E-1	3.31E-2	5.89E-3	2.45E-4	2.41E-5	1.62E-5	1.79E-5	4.91E-3	4.02E-3	4.23E-3	2.91E-5
4.50E-1	4.25E-2	3.21E-3	-7.80E-4	2.06E-5	1.45E-5	1.53E-5	4.54E-3	3.81E-3	3.91E-3	2.52E-5

Section 2iw (y=208mm)

X	u-velocity	v-velocity	w-velocity	u'u'	v'v'	w'w'	u'	v'	w'	k
(m)	(m/s)	(m/s)	(m/s)	(m^2/s^2)	(m^2/s^2)	(m^2/s^2)	(m/s)	(m/s)	(m/s)	(m^2/s^2)
5.00E-2	-3.60E-2	-2.73E-2	-4.19E-3	1.10E-5	7.81E-6	8.13E-6	3.32E-3	2.80E-3	2.85E-3	1.35E-5
1.00E-1	-6.01E-2	-3.29E-2	-2.09E-4	1.02E-5	7.55E-6	7.66E-6	3.19E-3	2.75E-3	2.77E-3	1.27E-5
1.50E-1	-6.99E-2	-2.19E-2	-3.19E-4	1.09E-5	7.67E-6	7.68E-6	3.30E-3	2.77E-3	2.77E-3	1.31E-5
2.00E-1	-4.75E-2	-8.04E-3	-2.53E-4	1.11E-5	7.65E-6	7.87E-6	3.33E-3	2.77E-3	2.80E-3	1.33E-5
3.00E-1	-6.05E-2	-8.13E-4	-6.11E-4	1.21E-5	8.67E-6	8.68E-6	3.48E-3	2.95E-3	2.95E-3	1.47E-5
4.50E-1	-6.15E-2	5.31E-4	-5.91E-4	1.31E-5	8.69E-6	9.69E-6	3.62E-3	2.95E-3	3.11E-3	1.57E-5

Section 2c (y=248mm)

X	u-velocity	v-velocity	w-velocity	u'u'	v'v'	w'w'	u'	v'	w'	k
(m)	(m/s)	(m/s)	(m/s)	(m^2/s^2)	(m^2/s^2)	(m^2/s^2)	(m/s)	(m/s)	(m/s)	(m^2/s^2)
5.00E-2	-1.64E-2	-1.13E-2	-2.17E-4	1.38E-5	9.30E-6	9.55E-6	3.72E-3	3.05E-3	3.09E-3	1.63E-5
1.00E-1	-4.01E-2	-1.95E-2	-1.76E-4	1.19E-5	8.74E-6	8.81E-6	3.45E-3	2.96E-3	2.97E-3	1.47E-5
1.50E-1	-4.99E-2	-1.44E-2	-4.81E-4	1.10E-5	8.03E-6	8.09E-6	3.31E-3	2.83E-3	2.84E-3	1.35E-5
2.00E-1	-8.70E-2	-7.24E-3	-1.04E-3	9.74E-6	7.24E-6	7.29E-6	3.12E-3	2.69E-3	2.70E-3	1.21E-5
3.00E-1	-5.53E-2	-1.42E-3	-1.65E-3	8.91E-6	6.72E-6	6.77E-6	2.98E-3	2.59E-3	2.60E-3	1.12E-5
4.50E-1	-5.37E-2	-2.56E-5	-6.46E-4	8.78E-6	6.65E-6	6.72E-6	2.96E-3	2.58E-3	2.59E-3	1.11E-5

Section 2ow (y=283mm)

X	u-velocity	v-velocity	w-velocity	u'u'	v'v'	w'w'	u'	v'	w'	k
(m)	(m/s)	(m/s)	(m/s)	(m^2/s^2)	(m^2/s^2)	(m^2/s^2)	(m/s)	(m/s)	(m/s)	(m^2/s^2)
5.00E-2	2.12E-2	-1.41E-3	2.51E-3	1.98E-5	1.35E-5	1.34E-5	4.45E-3	3.67E-3	3.66E-3	2.33E-5
1.00E-1	4.69E-3	-2.07E-3	-2.07E-3	1.42E-5	1.02E-5	1.04E-5	3.77E-3	3.20E-3	3.23E-3	1.75E-5
1.50E-1	-2.12E-2	-5.28E-3	-1.68E-3	1.89E-5	1.23E-5	1.23E-5	4.34E-3	3.51E-3	3.51E-3	2.18E-5
2.00E-1	-3.23E-2	-2.16E-3	-6.63E-4	2.34E-5	1.36E-5	1.36E-5	4.83E-3	3.69E-3	3.69E-3	2.53E-5
3.00E-1	-3.51E-2	-7.51E-4	8.18E-5	2.61E-5	1.37E-5	1.47E-5	5.11E-3	3.71E-3	3.84E-3	2.73E-5
4.50E-1	-3.53E-2	-3.27E-4	1.36E-4	2.78E-5	1.48E-5	1.48E-5	5.27E-3	3.85E-3	3.85E-3	2.87E-5

Table A3.1 Standard deviations and relative errors for the flowrate of 90l/min (nominal velocity of 0.05m/s) level 1 (z=20mm)

Section 1ow (y=25mm)

X	SDu	SDv	SDw	REu	REv	REw	SDu'	SDv'	SDw'	SDk	REk
(m)	(m/s)	(m/s)	(m/s)	(%)	(%)	(%)	(m/s)	(m/s)	(m/s)	(m2/s2)	(%)
5.00E-02	7.54E-03	9.83E-04	2.55E-03	26.30%	31.12%	33.30%	1.76E-03	1.05E-03	1.23E-03	1.62E-05	22.90%
1.00E-01	1.50E-02	1.21E-03	2.05E-03	26.98%	29.18%	38.37%	1.48E-03	1.21E-03	1.21E-03	1.78E-05	19.54%
1.50E-01	1.42E-02	1.05E-03	2.51E-04	17.92%	25.60%	30.22%	1.52E-03	1.21E-03	1.33E-03	2.09E-05	18.26%
2.00E-01	1.42E-02	1.20E-04	4.12E-04	15.60%	37.97%	33.10%	1.63E-03	1.10E-03	1.10E-03	2.26E-05	16.44%
3.00E-01	1.31E-02	6.31E-04	3.11E-04	14.13%	28.46%	30.70%	1.52E-03	9.52E-04	9.82E-04	2.33E-05	13.79%
4.50E-01	9.75E-03	7.85E-04	6.25E-05	11.63%	28.93%	29.78%	1.21E-03	7.77E-04	5.89E-04	1.86E-05	10.30%

Section 1c (y=60mm)

X	SDu	SDv	SDw	REu	REv	REw	SDu'	SDv'	SDw'	SDk	REk
(m)	(m/s)	(m/s)	(m/s)	(%)	(%)	(%)	(m/s)	(m/s)	(m/s)	(m2/s2)	(%)
5.00E-02	5.61E-03	5.75E-03	7.21E-04	19.40%	34.89%	21.96%	1.79E-03	1.21E-03	1.04E-03	1.89E-05	20.99%
1.00E-01	8.64E-03	6.13E-03	7.12E-04	16.82%	24.34%	29.11%	1.43E-03	1.11E-03	1.21E-03	1.78E-05	17.97%
1.50E-01	1.51E-02	5.44E-03	1.82E-03	21.44%	24.50%	32.45%	1.22E-03	1.21E-03	1.09E-03	1.84E-05	15.27%
2.00E-01	1.13E-02	1.86E-03	1.53E-03	16.61%	21.29%	35.13%	1.11E-03	1.08E-03	9.72E-04	1.69E-05	13.44%
3.00E-01	8.24E-03	3.76E-04	9.20E-04	12.17%	30.08%	36.74%	9.62E-04	4.54E-04	4.52E-04	1.13E-05	9.56%
4.50E-01	5.68E-03	1.11E-03	2.14E-04	8.46%	25.93%	40.19%	1.07E-03	3.43E-04	3.54E-04	1.29E-05	9.59%

Section 1iw (y=100mm)

X	SDu	SDv	SDw	REu	REv	REw	SDu'	SDv'	SDw'	SDk	REk
(m)	(m/s)	(m/s)	(m/s)	(%)	(%)	(%)	(m/s)	(m/s)	(m/s)	(m2/s2)	(%)
5.00E-02	5.34E-03	7.98E-03	5.11E-04	21.01%	26.28%	27.91%	1.88E-03	1.08E-03	1.13E-03	1.96E-05	21.54%
1.00E-01	8.60E-03	1.36E-02	2.40E-03	21.59%	27.53%	39.86%	1.79E-03	1.08E-03	1.08E-03	1.97E-05	19.36%
1.50E-01	7.58E-03	6.92E-03	1.45E-03	16.64%	21.39%	25.88%	1.38E-03	1.11E-03	1.20E-03	1.89E-05	16.39%
2.00E-01	4.06E-03	1.54E-03	1.02E-03	16.06%	19.62%	31.21%	1.45E-03	1.02E-03	1.11E-03	1.56E-05	19.44%
3.00E-01	5.72E-04	1.63E-04	3.10E-04	22.33%	29.59%	20.08%	1.13E-03	7.54E-04	3.89E-04	8.77E-06	17.10%
4.50E-01	1.13E-03	7.35E-04	2.26E-04	7.99%	35.09%	33.28%	1.11E-03	5.80E-04	4.81E-04	1.03E-05	13.55%

Section 2iw (y=208mm)

X	SDu	SDv	SDw	REu	REv	REw	SDu'	SDv'	SDw'	SDk	REk
(m)	(m/s)	(m/s)	(m/s)	(%)	(%)	(%)	(m/s)	(m/s)	(m/s)	(m2/s2)	(%)
5.00E-02	5.06E-04	6.93E-03	5.10E-04	22.46%	31.76%	25.14%	1.72E-03	9.75E-04	7.12E-04	1.43E-05	24.02%
1.00E-01	4.73E-03	8.11E-03	6.52E-04	21.49%	30.64%	26.91%	1.21E-03	1.07E-03	1.09E-03	1.45E-05	17.94%
1.50E-01	8.29E-03	6.03E-03	4.51E-04	18.33%	27.47%	31.44%	1.13E-03	1.05E-03	1.09E-03	1.55E-05	15.66%
2.00E-01	8.42E-03	2.02E-03	1.63E-04	17.47%	23.22%	29.54%	1.21E-03	1.11E-03	1.10E-03	1.62E-05	16.49%
3.00E-01	7.93E-03	3.86E-04	3.45E-07	17.29%	26.38%	48.86%	1.31E-03	6.42E-04	9.52E-04	1.50E-05	15.62%
4.50E-01	5.32E-03	2.00E-05	1.91E-05	11.88%	23.04%	36.65%	9.69E-04	7.34E-04	3.41E-04	1.09E-05	11.54%

Section 2c (y=248mm)

X	SDu	SDv	SDw	REu	REv	REw	SDu'	SDv'	SDw'	SDk	REk
(m)	(m/s)	(m/s)	(m/s)	(%)	(%)	(%)	(m/s)	(m/s)	(m/s)	(m2/s2)	(%)
5.00E-02	6.81E-04	2.75E-03	1.21E-03	19.55%	22.23%	34.18%	1.46E-03	7.05E-04	9.61E-04	1.22E-05	22.69%
1.00E-01	2.07E-03	3.03E-03	3.74E-04	16.95%	22.23%	22.63%	1.21E-03	9.80E-04	8.82E-04	1.10E-05	20.56%
1.50E-01	5.71E-03	3.76E-03	4.65E-04	17.46%	27.38%	35.66%	1.09E-03	7.46E-04	8.91E-04	1.22E-05	14.92%
2.00E-01	6.22E-03	1.96E-03	1.73E-04	14.73%	26.75%	29.27%	1.11E-03	7.61E-04	9.36E-04	1.34E-05	14.43%
3.00E-01	7.42E-03	4.36E-04	1.52E-05	15.69%	30.13%	33.42%	9.70E-04	5.42E-04	4.23E-04	1.07E-05	10.88%
4.50E-01	4.51E-03	1.64E-05	7.54E-06	9.45%	26.57%	31.00%	9.72E-04	2.36E-04	3.25E-04	9.93E-06	10.12%

Section 2ow (y=283mm)

X	SDu	SDv	SDw	REu	REv	REw	SDu'	SDv'	SDw'	SDk	REk
(m)	(m/s)	(m/s)	(m/s)	(%)	(%)	(%)	(m/s)	(m/s)	(m/s)	(m2/s2)	(%)
5.00E-02	1.31E-03	1.22E-03	1.62E-03	21.10%	28.59%	31.97%	1.43E-03	8.10E-04	7.10E-04	9.78E-06	23.62%
1.00E-01	1.25E-03	1.01E-03	3.20E-04	21.37%	31.34%	30.70%	1.22E-03	1.09E-03	5.78E-04	8.42E-06	25.24%
1.50E-01	4.56E-04	8.86E-04	4.05E-04	19.54%	20.99%	26.95%	9.11E-04	8.79E-04	6.69E-04	7.35E-06	19.04%
2.00E-01	4.36E-03	5.43E-04	2.73E-04	20.41%	25.29%	33.58%	1.05E-03	9.31E-04	7.31E-04	1.09E-05	16.53%
3.00E-01	6.27E-03	2.23E-04	5.48E-05	22.27%	35.13%	38.71%	8.71E-04	6.72E-04	7.82E-04	9.49E-06	13.48%
4.50E-01	4.68E-03	1.21E-05	4.30E-05	14.48%	26.00%	35.23%	8.08E-04	4.48E-04	4.38E-04	8.07E-06	10.42%

Table A3.2 Standard deviations and relative errors for the flowrate of 90l/min (nominal velocity of 0.05m/s) level 2 (z=60mm)

Section 1ow (y=25mm)

X	SDu	SDv	SDw	REu	REv	REw	SDu'	SDv'	SDw'	SDk	REk
(m)	(m/s)	(m/s)	(m/s)	(%)	(%)	(%)	(m/s)	(m/s)	(m/s)	(m2/s2)	(%)
5.00E-02	5.38E-03	2.54E-03	5.54E-03	23.70%	30.98%	33.81%	2.80E-03	5.23E-04	1.23E-03	2.25E-05	23.24%
1.00E-01	1.02E-02	5.10E-03	2.46E-03	19.70%	42.40%	29.44%	2.03E-03	7.23E-04	1.12E-03	1.99E-05	18.04%
1.50E-01	1.20E-02	2.31E-03	5.12E-04	15.58%	22.26%	34.73%	2.33E-03	6.23E-04	1.32E-03	2.73E-05	19.04%
2.00E-01	1.20E-02	1.20E-03	1.20E-03	13.51%	48.91%	32.17%	2.60E-03	9.60E-04	9.50E-04	3.04E-05	19.89%
3.00E-01	1.12E-02	6.11E-04	1.12E-03	14.43%	37.69%	39.95%	2.28E-03	5.23E-04	8.23E-04	2.69E-05	17.10%
4.50E-01	5.19E-03	7.52E-04	2.52E-04	5.73%	36.16%	30.50%	1.10E-03	7.71E-04	8.91E-04	1.70E-05	10.21%

Section 1c (y=60mm)

X	SDu	SDv	SDw	REu	REv	REw	SDu'	SDv'	SDw'	SDk	REk
(m)	(m/s)	(m/s)	(m/s)	(%)	(%)	(%)	(m/s)	(m/s)	(m/s)	(m2/s2)	(%)
5.00E-02	2.52E-03	7.50E-03	2.11E-03	13.48%	21.46%	27.65%	1.87E-03	1.11E-03	1.42E-03	2.21E-05	20.59%
1.00E-01	6.43E-03	6.33E-03	1.21E-03	12.09%	15.53%	17.31%	1.32E-03	1.07E-03	1.09E-03	1.69E-05	16.35%
1.50E-01	1.05E-02	3.62E-03	2.01E-03	12.98%	14.01%	17.73%	1.11E-03	1.05E-03	9.10E-04	1.43E-05	15.25%
2.00E-01	7.42E-03	1.64E-03	3.02E-03	8.69%	18.89%	27.50%	8.43E-04	8.25E-04	7.16E-04	1.08E-05	12.05%
3.00E-01	8.42E-03	3.61E-04	2.01E-03	10.85%	27.28%	32.90%	6.21E-04	5.42E-04	5.23E-04	9.12E-06	7.35%
4.50E-01	6.81E-03	1.06E-03	4.04E-04	9.33%	30.99%	22.87%	6.87E-04	4.34E-04	5.41E-04	1.12E-05	6.40%

Section 1iw (y=100mm)

X	SDu	SDv	SDw	REu	REv	REw	SDu'	SDv'	SDw'	SDk	REk
(m)	(m/s)	(m/s)	(m/s)	(%)	(%)	(%)	(m/s)	(m/s)	(m/s)	(m2/s2)	(%)
5.00E-02	3.38E-03	9.83E-03	1.06E-03	26.19%	21.17%	27.64%	2.37E-03	7.52E-04	1.28E-03	2.70E-05	23.99%
1.00E-01	6.01E-03	1.51E-02	4.02E-03	20.73%	25.24%	32.07%	1.48E-03	7.80E-04	8.11E-04	1.65E-05	16.45%
1.50E-01	5.76E-03	6.23E-03	4.51E-03	17.46%	23.03%	36.92%	1.38E-03	5.62E-04	1.03E-03	1.50E-05	15.60%
2.00E-01	4.61E-03	1.42E-03	2.31E-03	13.45%	28.06%	30.47%	1.48E-03	5.10E-04	5.50E-04	1.54E-05	16.46%
3.00E-01	1.61E-03	3.26E-04	1.01E-03	13.43%	41.13%	40.84%	1.28E-03	5.42E-04	8.92E-04	1.86E-05	11.68%
4.50E-01	3.46E-03	7.45E-04	5.63E-04	10.09%	35.90%	28.14%	1.08E-03	7.97E-04	8.09E-04	1.84E-05	9.69%

Section 2iw (y=208mm)

X	SDu	SDv	SDw	REu	REv	REw	SDu'	SDv'	SDw'	SDk	REk
(m)	(m/s)	(m/s)	(m/s)	(%)	(%)	(%)	(m/s)	(m/s)	(m/s)	(m2/s2)	(%)
5.00E-02	4.11E-03	9.25E-03	1.04E-03	22.78%	32.65%	29.97%	2.09E-03	9.75E-04	1.21E-03	2.61E-05	23.70%
1.00E-01	7.32E-03	1.05E-02	2.04E-03	14.03%	34.71%	46.88%	1.08E-03	7.28E-04	8.81E-04	1.25E-05	15.05%
1.50E-01	9.32E-03	6.31E-03	4.51E-04	14.41%	31.90%	17.12%	9.83E-04	5.46E-04	9.10E-04	9.29E-06	16.09%
2.00E-01	1.98E-03	1.74E-03	3.23E-04	8.02%	23.67%	29.45%	8.26E-04	8.51E-04	7.55E-04	8.53E-06	15.58%
3.00E-01	3.02E-03	3.29E-04	4.51E-05	13.50%	29.12%	36.76%	6.09E-04	4.23E-04	5.23E-04	5.80E-06	10.13%
4.50E-01	3.24E-03	9.75E-06	1.26E-05	12.11%	30.50%	44.06%	6.87E-04	3.38E-04	4.08E-04	5.91E-06	10.23%

Section 2c (y=248mm)

X	SDu	SDv	SDw	REu	REv	REw	SDu'	SDv'	SDw'	SDk	REk
(m)	(m/s)	(m/s)	(m/s)	(%)	(%)	(%)	(m/s)	(m/s)	(m/s)	(m2/s2)	(%)
5.00E-02	1.31E-03	4.98E-03	2.11E-03	16.75%	33.13%	31.65%	2.07E-03	7.05E-04	1.03E-03	2.37E-05	23.59%
1.00E-01	4.31E-03	3.29E-03	7.40E-04	10.19%	19.99%	34.06%	9.83E-04	9.78E-04	8.19E-04	1.28E-05	13.90%
1.50E-01	5.13E-03	3.62E-03	6.45E-04	9.10%	28.42%	31.52%	8.70E-04	4.56E-04	9.10E-04	9.64E-06	13.40%
2.00E-01	4.92E-03	1.64E-03	3.23E-04	9.70%	25.75%	33.27%	8.27E-04	6.05E-04	3.55E-04	7.30E-06	12.39%
3.00E-01	4.22E-03	3.61E-04	2.10E-05	9.60%	30.43%	41.12%	7.01E-04	4.23E-04	2.28E-04	5.47E-06	10.52%
4.50E-01	4.13E-03	4.75E-06	3.56E-05	7.76%	39.71%	32.88%	7.18E-04	3.58E-04	2.48E-04	5.42E-06	10.59%

Section 2ow (y=283mm)

X	SDu	SDv	SDw	REu	REv	REw	SDu'	SDv'	SDw'	SDk	REk
(m)	(m/s)	(m/s)	(m/s)	(%)	(%)	(%)	(m/s)	(m/s)	(m/s)	(m2/s2)	(%)
5.00E-02	7.90E-04	1.21E-03	2.10E-03	26.65%	23.04%	23.11%	1.30E-03	1.03E-03	1.03E-03	1.36E-05	19.90%
1.00E-01	4.08E-03	1.11E-03	2.04E-04	20.24%	21.09%	22.35%	1.33E-03	8.91E-04	7.82E-04	1.46E-05	17.01%
1.50E-01	3.79E-03	6.31E-04	4.51E-04	11.70%	14.96%	23.05%	1.11E-03	7.91E-04	9.00E-04	1.35E-05	14.45%
2.00E-01	9.64E-03	4.25E-04	3.02E-04	23.92%	20.00%	24.96%	1.52E-03	3.06E-04	3.12E-04	1.45E-05	15.83%
3.00E-01	7.21E-03	2.33E-04	8.45E-05	17.02%	54.91%	26.35%	7.13E-04	7.23E-04	8.23E-04	1.03E-05	10.86%
4.50E-01	4.09E-03	9.75E-06	3.01E-05	9.37%	44.80%	24.90%	8.80E-04	4.81E-04	4.81E-04	9.58E-06	10.22%

Table A3.3 Standard deviations and relative errors for the flowrate of 90l/min (nominal velocity of 0.05m/s) level 3 (z=100mm)

Section 1ow (y=25mm)

X	SDu	SDv	SDw	REu	REv	REw	SDu'	SDv'	SDw'	SDk	REk
(m)	(m/s)	(m/s)	(m/s)	(%)	(%)	(%)	(m/s)	(m/s)	(m/s)	(m2/s2)	(%)
5.00E-02	4.51E-03	4.54E-03	3.15E-03	21.90%	27.89%	25.87%	1.75E-03	1.21E-03	1.11E-03	1.79E-05	20.77%
1.00E-01	1.09E-02	4.10E-03	1.61E-03	20.58%	24.65%	25.02%	1.42E-03	1.31E-03	1.11E-03	1.80E-05	18.67%
1.50E-01	1.43E-02	4.08E-03	3.01E-04	18.58%	47.17%	24.41%	1.21E-03	1.10E-03	1.09E-03	1.77E-05	14.65%
2.00E-01	1.65E-02	1.05E-03	6.13E-04	18.87%	30.09%	25.14%	1.29E-03	9.94E-04	9.74E-04	1.84E-05	13.40%
3.00E-01	1.11E-02	2.14E-04	6.13E-04	12.45%	26.32%	26.42%	1.31E-03	8.99E-04	9.97E-04	1.92E-05	12.35%
4.50E-01	1.07E-02	3.94E-04	3.43E-04	13.23%	32.76%	34.59%	1.11E-03	9.53E-04	8.92E-04	1.82E-05	10.82%

Section 1c (y=60mm)

X	SDu	SDv	SDw	REu	REv	REw	SDu'	SDv'	SDw'	SDk	REk
(m)	(m/s)	(m/s)	(m/s)	(%)	(%)	(%)	(m/s)	(m/s)	(m/s)	(m2/s2)	(%)
5.00E-02	3.67E-03	1.43E-02	1.81E-03	21.66%	31.89%	27.53%	1.74E-03	1.21E-03	1.11E-03	1.95E-05	20.36%
1.00E-01	7.51E-03	1.24E-02	1.60E-03	17.26%	24.74%	27.40%	1.51E-03	1.31E-03	9.94E-04	1.60E-05	21.51%
1.50E-01	1.53E-02	4.76E-03	3.52E-03	24.08%	20.35%	31.15%	1.21E-03	1.09E-03	1.09E-03	1.33E-05	19.56%
2.00E-01	1.21E-02	9.90E-04	3.20E-03	18.01%	16.37%	28.53%	1.11E-03	8.09E-04	7.91E-04	1.09E-05	15.96%
3.00E-01	1.01E-02	7.13E-04	1.71E-03	15.04%	27.09%	24.22%	1.23E-04	8.38E-04	7.64E-04	7.83E-06	8.96%
4.50E-01	6.01E-03	7.14E-04	4.40E-04	10.62%	21.33%	33.96%	1.12E-03	7.63E-04	7.52E-04	1.55E-05	12.09%

Section 1iw (y=100mm)

X	SDu	SDv	SDw	REu	REv	REw	SDu'	SDv'	SDw'	SDk	REk
(m)	(m/s)	(m/s)	(m/s)	(%)	(%)	(%)	(m/s)	(m/s)	(m/s)	(m2/s2)	(%)
5.00E-02	1.08E-03	1.51E-02	1.06E-03	22.21%	26.98%	31.61%	1.43E-03	1.11E-03	1.09E-03	1.63E-05	20.09%
1.00E-01	3.95E-03	1.78E-02	2.22E-03	18.86%	28.77%	21.85%	1.43E-03	1.10E-03	1.01E-03	1.58E-05	19.59%
1.50E-01	6.03E-03	4.32E-03	3.16E-03	21.75%	22.83%	27.62%	1.14E-03	1.08E-03	7.75E-04	1.28E-05	16.53%
2.00E-01	3.40E-03	3.61E-04	2.22E-03	21.61%	32.48%	26.48%	1.11E-03	9.94E-04	8.75E-04	1.30E-05	16.10%
3.00E-01	2.42E-03	8.15E-04	2.85E-04	16.41%	29.46%	21.14%	1.21E-03	9.84E-04	6.83E-04	1.72E-05	12.40%
4.50E-01	2.21E-03	6.10E-04	9.98E-04	9.36%	24.61%	38.03%	1.08E-03	6.83E-04	5.82E-04	1.57E-05	9.72%

Section 2iw (y=208mm)

X	SDu	SDv	SDw	REu	REv	REw	SDu'	SDv'	SDw'	SDk	REk
(m)	(m/s)	(m/s)	(m/s)	(%)	(%)	(%)	(m/s)	(m/s)	(m/s)	(m2/s2)	(%)
5.00E-02	6.62E-03	8.02E-03	8.61E-04	21.51%	29.17%	27.86%	1.48E-03	1.21E-03	1.05E-03	1.69E-05	21.29%
1.00E-01	8.63E-03	8.18E-03	2.22E-04	16.25%	28.57%	20.58%	1.30E-03	1.20E-03	1.08E-04	1.11E-05	20.91%
1.50E-01	1.09E-02	3.59E-03	2.15E-04	16.71%	19.22%	19.60%	9.91E-04	1.11E-03	8.78E-04	8.82E-06	22.49%
2.00E-01	1.11E-02	1.77E-03	2.21E-04	16.84%	26.40%	23.37%	1.04E-03	1.09E-03	4.67E-04	8.13E-06	21.17%
3.00E-01	7.53E-03	2.52E-04	3.78E-05	11.55%	24.75%	43.31%	9.45E-04	4.68E-04	4.80E-04	6.30E-06	15.98%
4.50E-01	6.42E-03	2.71E-05	1.27E-04	10.28%	36.11%	42.21%	7.76E-04	6.88E-04	4.38E-04	5.91E-06	14.81%

Section 2c (y=248mm)

X	SDu	SDv	SDw	REu	REv	REw	SDu'	SDv'	SDw'	SDk	REk
(m)	(m/s)	(m/s)	(m/s)	(%)	(%)	(%)	(m/s)	(m/s)	(m/s)	(m2/s2)	(%)
5.00E-02	5.63E-03	4.42E-03	1.71E-03	20.10%	28.53%	34.38%	1.65E-03	1.10E-03	9.11E-04	1.88E-05	20.84%
1.00E-01	8.14E-03	4.30E-03	1.61E-04	18.07%	25.06%	22.44%	1.21E-03	1.10E-03	1.12E-03	1.39E-05	19.44%
1.50E-01	8.13E-03	3.84E-03	8.43E-05	14.33%	31.55%	34.37%	1.21E-03	9.89E-04	6.88E-04	1.06E-05	20.18%
2.00E-01	1.10E-02	1.33E-03	4.22E-05	17.90%	22.51%	23.94%	8.91E-04	6.69E-04	6.59E-04	7.12E-06	16.94%
3.00E-01	8.98E-03	2.97E-04	4.21E-05	14.14%	27.84%	30.58%	7.78E-04	4.67E-04	4.56E-04	5.32E-06	14.63%
4.50E-01	7.06E-03	4.41E-06	1.20E-04	11.10%	22.36%	38.68%	4.58E-04	2.24E-04	2.25E-04	2.94E-06	8.29%

Section 2ow (y=283mm)

X	SDu	SDv	SDw	REu	REv	REw	SDu'	SDv'	SDw'	SDk	REk
(m)	(m/s)	(m/s)	(m/s)	(%)	(%)	(%)	(m/s)	(m/s)	(m/s)	(m2/s2)	(%)
5.00E-02	3.41E-03	1.21E-03	1.54E-03	21.06%	23.11%	25.39%	1.57E-03	1.21E-03	8.75E-04	1.73E-05	20.60%
1.00E-01	4.89E-03	1.57E-03	8.98E-04	16.17%	29.82%	29.70%	1.30E-03	1.24E-03	1.11E-03	1.82E-05	16.87%
1.50E-01	7.81E-03	1.35E-03	1.21E-04	19.37%	32.07%	25.69%	1.21E-03	1.10E-03	1.07E-03	1.64E-05	15.89%
2.00E-01	6.72E-03	5.08E-04	3.63E-05	15.34%	24.10%	23.52%	1.13E-03	1.01E-03	7.90E-04	1.40E-05	14.42%
3.00E-01	5.90E-03	8.11E-05	7.06E-05	12.78%	25.76%	33.89%	1.02E-03	8.11E-04	7.10E-04	1.23E-05	12.62%
4.50E-01	5.66E-03	4.43E-05	3.21E-05	11.22%	33.49%	26.72%	8.10E-04	7.89E-04	5.79E-04	1.01E-05	10.94%

Table A3.4 Standard deviations and relative errors for the flowrate of 90l/min (nominal velocity of 0.05m/s) level 4 (z=140mm)

Section 1ow (y=25mm)

X	SDu	SDv	SDw	REu	REv	REw	SDu'	SDv'	SDw'	SDk	REk
(m)	(m/s)	(m/s)	(m/s)	(%)	(%)	(%)	(m/s)	(m/s)	(m/s)	(m2/s2)	(%)
5.00E-02	5.14E-03	4.25E-03	1.54E-03	28.24%	22.06%	21.70%	1.53E-03	9.85E-04	8.75E-04	1.33E-05	19.96%
1.00E-01	9.28E-03	4.03E-03	8.28E-04	17.79%	21.06%	19.45%	1.21E-03	1.10E-03	9.61E-04	1.43E-05	17.22%
1.50E-01	1.32E-02	8.10E-03	3.13E-04	16.93%	23.03%	21.29%	1.09E-03	9.72E-04	8.73E-04	1.45E-05	13.65%
2.00E-01	1.53E-02	5.42E-04	6.26E-04	17.30%	22.12%	20.70%	1.21E-03	9.35E-04	9.45E-04	1.65E-05	13.67%
3.00E-01	9.10E-03	2.43E-04	6.31E-04	10.32%	39.73%	30.88%	1.11E-03	9.94E-04	9.73E-04	1.65E-05	13.04%
4.50E-01	6.78E-03	3.44E-04	2.34E-04	8.46%	31.78%	36.78%	1.06E-03	9.34E-04	9.22E-04	1.65E-05	11.59%

Section 1c (y=60mm)

X	SDu	SDv	SDw	REu	REv	REw	SDu'	SDv'	SDw'	SDk	REk
(m)	(m/s)	(m/s)	(m/s)	(%)	(%)	(%)	(m/s)	(m/s)	(m/s)	(m2/s2)	(%)
5.00E-02	6.71E-03	1.33E-02	9.85E-04	25.80%	26.40%	22.41%	1.41E-03	9.75E-04	9.85E-04	1.36E-05	20.56%
1.00E-01	7.09E-03	1.23E-02	4.17E-04	18.19%	24.47%	17.21%	1.05E-03	9.55E-04	9.44E-04	1.06E-05	18.51%
1.50E-01	1.33E-02	4.63E-03	2.04E-03	17.29%	23.00%	26.04%	1.11E-03	9.41E-04	9.40E-04	1.08E-05	18.64%
2.00E-01	9.87E-03	9.01E-04	1.97E-03	12.18%	29.43%	22.10%	1.01E-03	8.94E-04	9.08E-04	9.77E-06	18.17%
3.00E-01	1.10E-02	1.27E-03	1.21E-03	11.11%	31.07%	21.36%	9.94E-04	8.84E-04	7.39E-04	1.03E-05	15.55%
4.50E-01	8.76E-03	1.41E-03	4.02E-04	9.95%	39.29%	36.70%	7.42E-04	6.30E-04	5.21E-04	8.83E-06	9.68%

Section 1iw (y=100mm)

X	SDu	SDv	SDw	REu	REv	REw	SDu'	SDv'	SDw'	SDk	REk
(m)	(m/s)	(m/s)	(m/s)	(%)	(%)	(%)	(m/s)	(m/s)	(m/s)	(m2/s2)	(%)
5.00E-02	8.24E-03	1.52E-02	6.05E-04	20.10%	25.74%	25.15%	1.32E-03	1.08E-03	9.33E-04	1.35E-05	20.60%
1.00E-01	3.01E-03	1.82E-02	9.28E-04	17.68%	29.38%	20.41%	1.31E-03	9.89E-04	8.79E-05	1.21E-05	17.08%
1.50E-01	3.33E-03	3.24E-03	1.60E-03	14.46%	23.64%	22.03%	1.07E-03	8.42E-04	7.53E-04	1.04E-05	16.02%
2.00E-01	2.22E-03	6.11E-04	1.51E-03	13.43%	27.02%	22.10%	1.11E-03	9.44E-04	7.47E-04	1.10E-05	17.20%
3.00E-01	1.72E-03	1.52E-03	1.61E-04	13.44%	31.95%	24.31%	9.45E-04	8.44E-04	8.34E-04	1.23E-05	12.90%
4.50E-01	2.05E-03	1.03E-03	5.00E-04	10.37%	33.67%	24.00%	7.58E-04	8.33E-04	8.20E-04	1.20E-05	10.52%

Section 2iw (y=208mm)

X	SDu	SDv	SDw	REu	REv	REw	SDu'	SDv'	SDw'	SDk	REk
(m)	(m/s)	(m/s)	(m/s)	(%)	(%)	(%)	(m/s)	(m/s)	(m/s)	(m2/s2)	(%)
5.00E-02	6.24E-03	8.15E-03	6.11E-04	21.67%	26.95%	25.91%	1.43E-03	1.11E-03	1.09E-03	1.54E-05	22.10%
1.00E-01	6.30E-03	8.82E-03	1.81E-04	16.76%	26.93%	22.17%	1.33E-03	1.10E-03	7.88E-05	1.01E-05	23.48%
1.50E-01	9.33E-03	3.92E-03	1.46E-04	15.61%	20.94%	27.70%	1.02E-03	9.84E-04	7.75E-04	7.48E-06	23.90%
2.00E-01	6.22E-03	1.71E-03	1.35E-04	18.14%	24.26%	42.72%	1.05E-03	9.35E-04	6.75E-04	7.74E-06	22.54%
3.00E-01	3.32E-03	2.15E-04	7.82E-05	13.11%	23.47%	44.70%	7.94E-04	6.84E-04	8.03E-04	6.59E-06	17.92%
4.50E-01	4.21E-03	2.10E-05	2.10E-04	11.27%	24.06%	38.87%	5.78E-04	6.83E-04	3.82E-04	4.82E-06	13.10%

Section 2c (y=248mm)

X	SDu	SDv	SDw	REu	REv	REw	SDu'	SDv'	SDw'	SDk	REk
(m)	(m/s)	(m/s)	(m/s)	(%)	(%)	(%)	(m/s)	(m/s)	(m/s)	(m2/s2)	(%)
5.00E-02	6.27E-03	4.21E-03	9.08E-04	24.69%	28.67%	36.25%	1.54E-03	1.11E-03	1.10E-03	1.79E-05	21.14%
1.00E-01	1.41E-02	4.31E-03	8.42E-04	20.51%	23.78%	29.19%	1.11E-03	1.00E-03	1.21E-03	1.28E-05	19.36%
1.50E-01	1.34E-02	4.06E-03	4.32E-04	20.05%	31.60%	28.14%	1.21E-03	9.94E-04	7.94E-04	1.02E-05	22.12%
2.00E-01	9.99E-03	1.31E-03	1.97E-04	11.48%	20.97%	28.80%	9.10E-04	6.89E-04	5.91E-04	6.48E-06	18.68%
3.00E-01	8.81E-03	2.71E-04	1.21E-04	10.62%	23.86%	37.73%	7.99E-04	4.88E-04	4.74E-04	4.85E-06	17.11%
4.50E-01	7.60E-03	1.41E-06	2.04E-04	8.64%	41.72%	45.95%	6.74E-04	3.63E-04	2.52E-04	3.72E-06	13.84%

Section 2ow (y=283mm)

X	SDu	SDv	SDw	REu	REv	REw	SDu'	SDv'	SDw'	SDk	REk
(m)	(m/s)	(m/s)	(m/s)	(%)	(%)	(%)	(m/s)	(m/s)	(m/s)	(m2/s2)	(%)
5.00E-02	3.41E-04	9.98E-04	1.54E-04	22.33%	23.67%	34.11%	1.65E-03	1.10E-03	7.53E-04	1.35E-05	28.04%
1.00E-01	4.93E-03	1.74E-03	9.83E-04	22.62%	32.88%	23.78%	1.32E-03	1.21E-03	1.10E-03	1.65E-05	18.63%
1.50E-01	8.13E-03	1.51E-03	5.31E-04	24.68%	35.56%	19.70%	1.11E-03	1.11E-03	1.09E-03	1.53E-05	15.85%
2.00E-01	7.15E-03	5.84E-04	3.63E-04	16.40%	27.48%	39.04%	1.27E-03	8.94E-04	9.04E-04	1.63E-05	15.04%
3.00E-01	9.01E-03	1.72E-04	7.63E-05	20.44%	40.80%	32.19%	1.22E-03	1.13E-03	1.01E-03	1.72E-05	15.38%
4.50E-01	5.78E-03	3.44E-06	1.23E-04	13.08%	42.25%	34.31%	1.02E-03	8.93E-04	7.92E-04	1.36E-05	12.74%

Table A3.5 Standard deviations and relative errors for the flowrate of 90l/min (nominal velocity of 0.05m/s) level 5 (z=180mm)

Section 1ow (y=25mm)

X	SDu	SDv	SDw	REu	REv	REw	SDu'	SDv'	SDw'	SDk	REk
(m)	(m/s)	(m/s)	(m/s)	(%)	(%)	(%)	(m/s)	(m/s)	(m/s)	(m2/s2)	(%)
5.00E-02	4.22E-03	2.54E-03	5.43E-04	23.15%	19.91%	26.69%	7.71E-04	3.77E-04	2.77E-04	2.66E-06	22.74%
1.00E-01	7.52E-03	4.28E-03	2.76E-04	14.26%	20.48%	25.18%	1.06E-03	1.01E-03	9.11E-04	1.12E-05	19.48%
1.50E-01	1.15E-02	1.00E-02	1.26E-04	14.57%	28.36%	35.91%	5.78E-04	2.28E-04	3.28E-04	2.33E-06	16.19%
2.00E-01	1.34E-02	4.23E-04	2.59E-04	14.96%	17.37%	31.92%	5.08E-04	3.51E-04	4.45E-04	2.55E-06	15.69%
3.00E-01	1.02E-02	3.21E-04	3.13E-04	12.24%	38.04%	45.28%	5.77E-04	3.56E-04	2.66E-04	2.61E-06	14.73%
4.50E-01	8.15E-03	4.43E-04	2.72E-05	9.84%	36.18%	22.57%	5.76E-04	3.38E-04	2.23E-04	2.72E-06	13.55%

Section 1c (y=60mm)

X	SDu	SDv	SDw	REu	REv	REw	SDu'	SDv'	SDw'	SDk	REk
(m)	(m/s)	(m/s)	(m/s)	(%)	(%)	(%)	(m/s)	(m/s)	(m/s)	(m2/s2)	(%)
5.00E-02	7.07E-04	1.26E-02	4.98E-04	23.56%	25.09%	28.42%	7.66E-04	5.43E-04	5.05E-04	3.22E-06	25.01%
1.00E-01	7.93E-03	1.21E-02	1.68E-04	14.90%	23.94%	24.15%	5.25E-04	5.48E-04	4.39E-04	3.09E-06	16.68%
1.50E-01	1.31E-02	4.68E-03	7.82E-04	18.13%	23.98%	31.55%	5.45E-04	4.06E-04	4.01E-04	3.17E-06	13.76%
2.00E-01	8.67E-03	9.10E-05	9.81E-04	9.23%	41.93%	30.21%	5.04E-04	4.13E-04	4.09E-04	3.21E-06	12.62%
3.00E-01	9.97E-03	1.72E-03	6.17E-04	14.47%	37.60%	27.86%	4.33E-04	3.99E-04	3.90E-04	3.05E-06	11.06%
4.50E-01	7.60E-03	1.08E-03	2.22E-04	10.43%	29.97%	34.43%	4.22E-04	3.02E-04	2.10E-04	2.48E-06	9.07%

Section 1iw (y=100mm)

X	SDu	SDv	SDw	REu	REv	REw	SDu'	SDv'	SDw'	SDk	REk
(m)	(m/s)	(m/s)	(m/s)	(%)	(%)	(%)	(m/s)	(m/s)	(m/s)	(m2/s2)	(%)
5.00E-02	2.25E-03	2.01E-02	2.12E-04	22.54%	33.92%	20.34%	7.27E-04	4.38E-04	3.28E-04	2.92E-06	21.05%
1.00E-01	3.05E-03	2.13E-02	2.33E-04	17.26%	33.73%	25.37%	9.11E-04	8.91E-04	7.91E-05	4.97E-06	23.37%
1.50E-01	3.25E-03	4.22E-03	4.42E-04	17.31%	34.81%	18.01%	6.58E-04	4.23E-04	5.33E-04	4.04E-06	15.50%
2.00E-01	2.15E-03	1.08E-03	8.29E-04	19.23%	25.81%	29.92%	5.33E-04	4.35E-04	4.67E-04	3.71E-06	12.82%
3.00E-01	5.04E-03	2.15E-03	8.00E-05	15.23%	36.46%	32.61%	4.46E-04	4.36E-04	3.43E-04	3.16E-06	10.85%
4.50E-01	5.42E-03	1.28E-03	2.78E-04	12.75%	39.87%	35.71%	5.78E-04	3.34E-04	2.02E-04	3.02E-06	11.99%

Section 2iw (y=208mm)

X	SDu	SDv	SDw	REu	REv	REw	SDu'	SDv'	SDw'	SDk	REk
(m)	(m/s)	(m/s)	(m/s)	(%)	(%)	(%)	(m/s)	(m/s)	(m/s)	(m2/s2)	(%)
5.00E-02	7.69E-03	4.98E-03	9.81E-04	21.35%	18.25%	23.43%	6.55E-04	4.29E-04	4.78E-04	2.84E-06	21.01%
1.00E-01	7.27E-03	8.01E-03	8.01E-05	12.09%	24.33%	38.39%	5.54E-04	4.78E-04	3.95E-04	2.46E-06	19.37%
1.50E-01	1.11E-02	6.82E-03	8.22E-05	15.83%	31.14%	25.79%	4.77E-04	4.56E-04	4.09E-04	2.32E-06	17.65%
2.00E-01	6.67E-03	2.12E-03	8.12E-05	14.04%	26.39%	32.11%	4.22E-04	3.47E-04	4.89E-04	2.19E-06	16.43%
3.00E-01	6.86E-03	2.10E-04	1.10E-04	11.34%	25.81%	17.97%	4.11E-04	4.03E-04	3.95E-04	2.19E-06	14.89%
4.50E-01	6.01E-03	1.78E-04	1.61E-04	9.78%	33.47%	27.22%	4.44E-04	2.25E-04	2.05E-04	1.85E-06	11.76%

Section 2c (y=248mm)

X	SDu	SDv	SDw	REu	REv	REw	SDu'	SDv'	SDw'	SDk	REk
(m)	(m/s)	(m/s)	(m/s)	(%)	(%)	(%)	(m/s)	(m/s)	(m/s)	(m2/s2)	(%)
5.00E-02	4.64E-03	3.94E-03	8.94E-05	28.27%	34.90%	41.27%	7.12E-04	5.61E-04	6.13E-04	3.68E-06	22.51%
1.00E-01	6.69E-03	4.05E-03	4.49E-05	16.67%	20.77%	25.46%	6.07E-04	4.46E-04	4.61E-04	2.83E-06	19.20%
1.50E-01	6.01E-03	3.38E-03	7.89E-05	12.05%	23.39%	16.40%	5.71E-04	4.56E-04	3.61E-04	2.51E-06	18.54%
2.00E-01	6.13E-03	1.41E-03	4.14E-04	7.04%	19.49%	39.98%	3.71E-04	2.26E-04	5.71E-04	2.02E-06	16.66%
3.00E-01	5.66E-03	4.22E-04	4.41E-04	10.24%	29.85%	26.82%	6.37E-04	1.23E-04	1.03E-04	1.95E-06	17.38%
4.50E-01	5.56E-03	1.12E-05	2.04E-04	10.37%	43.78%	31.63%	3.46E-04	1.02E-04	1.11E-04	1.10E-06	9.91%

Section 2ow (y=283mm)

X	SDu	SDv	SDw	REu	REv	REw	SDu'	SDv'	SDw'	SDk	REk
(m)	(m/s)	(m/s)	(m/s)	(%)	(%)	(%)	(m/s)	(m/s)	(m/s)	(m2/s2)	(%)
5.00E-02	4.66E-03	5.00E-04	5.23E-04	22.04%	35.51%	20.85%	1.11E-03	3.47E-04	5.71E-04	5.50E-06	23.58%
1.00E-01	1.46E-03	4.97E-04	4.23E-04	31.19%	24.05%	20.45%	7.98E-04	5.71E-04	4.71E-04	3.84E-06	21.98%
1.50E-01	4.06E-03	1.51E-03	5.32E-04	19.18%	28.49%	31.59%	5.80E-04	6.55E-04	5.71E-04	3.96E-06	18.18%
2.00E-01	7.91E-03	4.52E-04	2.35E-04	24.48%	20.91%	35.42%	8.10E-04	4.71E-04	7.10E-04	5.02E-06	19.87%
3.00E-01	5.46E-03	3.02E-04	3.23E-05	15.57%	40.27%	39.56%	7.81E-04	4.17E-04	6.71E-04	4.99E-06	18.31%
4.50E-01	4.62E-03	9.42E-05	4.23E-05	13.11%	28.83%	31.19%	5.81E-04	4.04E-04	3.71E-04	3.72E-06	12.95%

Table A4.1 Standard deviations and relative errors for the flowrate of 180l/min (nominal velocity of 0.1m/s) level 1 (z=20mm)

Section 1ow (y=25mm)

X	SDu	SDv	SDw	REu	REv	REw	SDu'	SDv'	SDw'	SDk	REk
(m)	(m/s)	(m/s)	(m/s)	(%)	(%)	(%)	(m/s)	(m/s)	(m/s)	(m2/s2)	(%)
5.00E-02	8.41E-03	5.11E-03	3.12E-03	19.46%	25.41%	33.56%	1.05E-03	1.48E-03	1.72E-03	2.39E-05	17.40%
1.00E-01	7.41E-03	6.22E-03	1.61E-03	8.96%	34.09%	21.62%	1.20E-03	1.02E-03	1.05E-03	1.92E-05	12.56%
1.50E-01	9.81E-03	5.05E-03	3.51E-04	8.33%	31.11%	39.38%	8.43E-04	6.42E-04	9.12E-04	1.51E-05	8.57%
2.00E-01	1.31E-02	1.52E-03	5.82E-04	9.70%	23.63%	24.45%	7.24E-04	7.02E-04	8.16E-04	1.49E-05	7.39%
3.00E-01	1.02E-02	6.49E-04	5.12E-04	7.31%	25.57%	27.97%	6.24E-04	6.31E-04	7.04E-04	1.46E-05	5.73%
4.50E-01	6.40E-03	7.71E-04	1.64E-04	4.98%	21.78%	32.13%	4.24E-04	5.14E-04	8.25E-04	1.41E-05	4.62%

Section 1c (y=60mm)

X	SDu	SDv	SDw	REu	REv	REw	SDu'	SDv'	SDw'	SDk	REk
(m)	(m/s)	(m/s)	(m/s)	(%)	(%)	(%)	(m/s)	(m/s)	(m/s)	(m2/s2)	(%)
5.00E-02	9.78E-03	5.71E-03	2.03E-03	22.32%	24.86%	35.20%	1.63E-03	6.17E-04	1.65E-03	2.42E-05	15.55%
1.00E-01	1.01E-02	6.51E-03	8.61E-04	12.69%	21.59%	34.04%	1.74E-03	6.18E-04	1.59E-03	2.49E-05	16.15%
1.50E-01	7.68E-03	6.24E-03	2.34E-03	6.88%	21.25%	34.04%	1.13E-03	1.92E-04	1.02E-03	1.69E-05	9.58%
2.00E-01	7.92E-03	2.77E-03	1.53E-03	6.67%	22.49%	24.71%	9.01E-04	4.33E-04	8.91E-04	1.54E-05	7.98%
3.00E-01	8.80E-03	2.31E-04	1.52E-03	7.83%	33.64%	39.13%	1.11E-03	1.74E-04	9.46E-04	1.88E-05	8.63%
4.50E-01	5.49E-03	1.21E-03	3.79E-04	5.25%	20.43%	32.63%	1.01E-03	1.15E-04	1.00E-03	1.95E-05	7.75%

Section 1iw (y=100mm)

X	SDu	SDv	SDw	REu	REv	REw	SDu'	SDv'	SDw'	SDk	REk
(m)	(m/s)	(m/s)	(m/s)	(%)	(%)	(%)	(m/s)	(m/s)	(m/s)	(m2/s2)	(%)
5.00E-02	6.44E-03	8.17E-03	1.02E-03	18.41%	20.13%	33.79%	2.22E-03	4.24E-04	4.38E-04	2.57E-05	16.67%
1.00E-01	5.47E-03	1.92E-02	2.04E-03	9.90%	28.44%	24.62%	1.71E-03	9.11E-04	1.01E-03	2.25E-05	14.72%
1.50E-01	5.34E-03	1.33E-02	2.93E-03	8.40%	27.35%	33.48%	1.32E-03	6.59E-04	8.68E-04	1.87E-05	11.18%
2.00E-01	2.28E-03	2.98E-03	1.92E-03	7.95%	22.85%	35.11%	6.98E-04	4.49E-04	3.45E-04	8.77E-06	7.01%
3.00E-01	1.24E-03	2.96E-04	6.94E-04	8.78%	21.90%	32.38%	5.10E-04	6.85E-04	4.97E-04	8.55E-06	7.22%
4.50E-01	1.04E-03	7.21E-04	4.98E-04	12.85%	31.13%	36.36%	6.81E-04	6.49E-04	7.11E-04	1.30E-05	7.15%

Section 2iw (y=208mm)

X	SDu	SDv	SDw	REu	REv	REw	SDu'	SDv'	SDw'	SDk	REk
(m)	(m/s)	(m/s)	(m/s)	(%)	(%)	(%)	(m/s)	(m/s)	(m/s)	(m2/s2)	(%)
5.00E-02	8.19E-04	6.71E-03	6.71E-04	26.77%	20.57%	32.35%	3.78E-03	7.45E-04	7.45E-04	3.73E-05	37.58%
1.00E-01	7.24E-03	8.09E-03	7.49E-04	21.83%	18.53%	18.94%	3.91E-03	2.24E-04	2.24E-04	3.94E-05	34.07%
1.50E-01	1.47E-02	6.71E-03	6.39E-04	21.49%	21.45%	30.34%	2.62E-03	2.42E-04	7.54E-04	3.17E-05	21.58%
2.00E-01	1.94E-02	6.71E-03	3.09E-04	26.87%	51.82%	36.83%	1.78E-03	5.10E-04	5.10E-04	2.25E-05	15.03%
3.00E-01	1.35E-02	9.67E-04	2.64E-06	19.16%	47.64%	49.34%	2.78E-03	5.10E-04	5.10E-04	3.43E-05	23.28%
4.50E-01	1.29E-02	6.71E-05	3.64E-05	18.43%	55.80%	53.27%	1.62E-03	5.10E-04	5.10E-04	2.05E-05	14.20%

Section 2c (y=248mm)

X	SDu	SDv	SDw	REu	REv	REw	SDu'	SDv'	SDw'	SDk	REk
(m)	(m/s)	(m/s)	(m/s)	(%)	(%)	(%)	(m/s)	(m/s)	(m/s)	(m2/s2)	(%)
5.00E-02	9.14E-04	2.24E-03	1.02E-03	16.78%	12.47%	21.66%	1.08E-03	3.66E-04	3.66E-04	1.10E-05	11.44%
1.00E-01	1.42E-03	6.14E-03	7.59E-04	7.13%	29.77%	26.82%	8.80E-04	5.10E-04	5.10E-04	9.15E-06	10.63%
1.50E-01	6.13E-03	5.10E-03	5.59E-04	12.23%	24.77%	26.58%	9.54E-04	6.88E-04	5.21E-04	1.26E-05	9.96%
2.00E-01	5.19E-03	2.24E-03	2.24E-04	8.13%	20.66%	23.69%	9.76E-04	4.89E-04	4.89E-04	1.29E-05	9.08%
3.00E-01	6.01E-03	4.24E-04	2.24E-05	8.46%	20.63%	28.61%	8.98E-04	5.49E-04	7.49E-04	1.35E-05	9.10%
4.50E-01	5.42E-03	2.24E-05	1.22E-05	7.56%	24.09%	40.89%	8.98E-04	6.49E-04	9.49E-04	1.47E-05	9.93%

Section 2ow (y=283mm)

X	SDu	SDv	SDw	REu	REv	REw	SDu'	SDv'	SDw'	SDk	REk
(m)	(m/s)	(m/s)	(m/s)	(%)	(%)	(%)	(m/s)	(m/s)	(m/s)	(m2/s2)	(%)
5.00E-02	2.08E-03	6.71E-04	1.41E-03	18.88%	27.87%	17.91%	1.62E-03	5.77E-04	6.87E-04	1.52E-05	19.37%
1.00E-01	1.07E-03	3.81E-04	6.75E-04	10.53%	43.36%	31.10%	1.44E-03	4.32E-04	4.22E-04	1.03E-05	18.71%
1.50E-01	5.15E-04	6.71E-04	6.39E-04	11.18%	28.32%	22.93%	1.03E-03	2.42E-04	4.75E-04	8.82E-06	13.87%
2.00E-01	2.19E-03	6.71E-04	3.09E-04	6.80%	15.88%	22.09%	1.12E-03	1.05E-04	9.11E-05	1.05E-05	11.77%
3.00E-01	3.13E-03	9.67E-05	3.64E-05	7.21%	27.55%	17.58%	8.11E-04	5.35E-04	4.25E-04	9.82E-06	9.15%
4.50E-01	3.46E-03	1.11E-05	3.46E-05	7.92%	19.21%	40.19%	6.10E-04	2.45E-04	4.54E-04	7.43E-06	6.83%

Table A4.2 Standard deviations and relative errors for the flowrate of 180l/min (nominal velocity of 0.1m/s) level 2 (z=60mm)

Section 1ow (y=25mm)

X	SDu	SDv	SDw	REu	REv	REw	SDu'	SDv'	SDw'	SDk	REk
(m)	(m/s)	(m/s)	(m/s)	(%)	(%)	(%)	(m/s)	(m/s)	(m/s)	(m2/s2)	(%)
5.00E-02	4.11E-03	5.03E-03	3.41E-03	11.86%	24.03%	15.60%	5.43E-04	1.25E-03	1.20E-03	2.01E-05	12.00%
1.00E-01	4.10E-03	6.07E-03	1.21E-03	5.29%	26.28%	25.32%	3.96E-04	1.20E-03	1.46E-03	2.18E-05	12.10%
1.50E-01	8.11E-03	5.51E-03	5.12E-04	7.07%	25.86%	17.71%	8.43E-04	4.25E-04	1.24E-03	1.61E-05	8.38%
2.00E-01	1.14E-02	1.15E-03	2.82E-03	8.66%	20.06%	23.47%	2.36E-04	1.70E-04	1.63E-03	1.14E-05	6.59%
3.00E-01	1.08E-02	6.86E-04	1.16E-03	7.96%	31.95%	26.03%	2.43E-04	3.13E-04	1.70E-03	1.75E-05	7.81%
4.50E-01	4.00E-03	6.13E-04	6.43E-04	3.17%	26.00%	16.07%	2.36E-04	1.41E-04	9.82E-04	6.85E-06	3.70%

Section 1c (y=60mm)

X	SDu	SDv	SDw	REu	REv	REw	SDu'	SDv'	SDw'	SDk	REk
(m)	(m/s)	(m/s)	(m/s)	(%)	(%)	(%)	(m/s)	(m/s)	(m/s)	(m2/s2)	(%)
5.00E-02	7.80E-03	7.10E-03	3.21E-03	15.60%	15.62%	26.77%	1.30E-03	1.73E-04	1.65E-03	2.09E-05	12.09%
1.00E-01	1.09E-02	5.12E-03	1.42E-03	13.48%	9.98%	15.88%	1.41E-03	1.84E-04	1.53E-03	1.90E-05	12.45%
1.50E-01	6.80E-03	6.24E-03	3.41E-03	6.80%	18.05%	36.86%	1.30E-03	2.10E-04	1.10E-03	1.52E-05	11.18%
2.00E-01	5.79E-03	2.73E-03	1.53E-03	8.27%	21.95%	20.46%	9.14E-04	3.32E-04	1.00E-03	1.27E-05	9.21%
3.00E-01	8.00E-03	3.10E-04	2.03E-03	7.27%	23.32%	31.59%	1.04E-03	1.43E-04	9.11E-04	1.55E-05	9.05%
4.50E-01	4.92E-03	9.04E-04	7.91E-04	8.20%	19.61%	23.13%	1.14E-03	1.51E-04	1.02E-03	2.05E-05	8.56%

Section 1iw (y=100mm)

X	SDu	SDv	SDw	REu	REv	REw	SDu'	SDv'	SDw'	SDk	REk
(m)	(m/s)	(m/s)	(m/s)	(%)	(%)	(%)	(m/s)	(m/s)	(m/s)	(m2/s2)	(%)
5.00E-02	4.42E-03	1.72E-02	1.21E-03	22.12%	24.90%	22.24%	2.19E-03	4.00E-04	3.77E-04	1.98E-05	13.55%
1.00E-01	4.72E-03	2.01E-02	2.42E-03	17.50%	22.57%	14.33%	1.06E-03	1.07E-03	1.11E-03	2.02E-05	11.40%
1.50E-01	3.42E-03	1.27E-02	3.32E-03	10.97%	32.36%	18.12%	1.21E-03	5.87E-04	6.75E-04	1.50E-05	9.49%
2.00E-01	2.83E-03	9.84E-04	2.44E-03	12.59%	15.14%	26.69%	9.78E-04	6.45E-04	4.55E-04	1.56E-05	9.14%
3.00E-01	2.41E-03	1.96E-04	9.40E-04	11.82%	21.45%	17.91%	8.51E-04	8.50E-04	9.71E-04	2.08E-05	7.61%
4.50E-01	1.42E-03	7.14E-04	9.82E-04	5.05%	29.15%	20.90%	7.68E-04	9.65E-04	1.09E-03	1.93E-05	8.20%

Section 2iw (y=208mm)

X	SDu	SDv	SDw	REu	REv	REw	SDu'	SDv'	SDw'	SDk	REk
(m)	(m/s)	(m/s)	(m/s)	(%)	(%)	(%)	(m/s)	(m/s)	(m/s)	(m2/s2)	(%)
5.00E-02	7.19E-03	8.64E-03	6.37E-04	22.47%	20.17%	17.97%	1.46E-03	8.77E-04	9.87E-04	2.61E-05	12.68%
1.00E-01	1.24E-02	1.07E-02	2.27E-03	19.93%	23.31%	34.61%	1.09E-03	6.32E-04	5.42E-04	1.73E-05	10.12%
1.50E-01	1.25E-02	4.69E-03	8.08E-04	11.38%	15.01%	21.00%	1.35E-03	2.42E-04	2.75E-04	1.92E-05	13.03%
2.00E-01	1.02E-02	2.45E-03	3.75E-04	12.62%	24.68%	24.41%	8.57E-04	2.15E-04	2.11E-04	1.35E-05	8.03%
3.00E-01	2.46E-03	4.05E-04	6.17E-06	7.18%	28.21%	38.86%	8.26E-04	3.15E-04	2.25E-04	1.18E-05	8.09%
4.50E-01	4.10E-03	2.65E-05	7.19E-05	4.92%	38.72%	33.86%	8.16E-04	4.05E-04	4.75E-04	1.16E-05	8.52%

Section 2c (y=248mm)

X	SDu	SDv	SDw	REu	REv	REw	SDu'	SDv'	SDw'	SDk	REk
(m)	(m/s)	(m/s)	(m/s)	(%)	(%)	(%)	(m/s)	(m/s)	(m/s)	(m2/s2)	(%)
5.00E-02	5.14E-03	5.42E-03	1.40E-03	19.76%	24.65%	31.16%	1.62E-03	3.66E-04	3.66E-04	2.44E-05	13.64%
1.00E-01	4.51E-03	6.01E-03	9.76E-04	8.81%	24.73%	17.12%	5.98E-04	6.51E-04	7.51E-04	1.04E-05	7.84%
1.50E-01	7.15E-03	4.51E-03	9.56E-04	10.07%	24.07%	14.71%	6.21E-04	8.69E-04	7.52E-04	1.04E-05	10.10%
2.00E-01	8.19E-03	2.02E-03	3.24E-04	9.59%	21.82%	17.05%	7.84E-04	4.49E-04	5.49E-04	9.43E-06	9.65%
3.00E-01	8.19E-03	4.12E-04	4.22E-05	10.56%	24.87%	21.12%	6.78E-04	5.05E-04	7.15E-04	7.82E-06	10.52%
4.50E-01	8.25E-03	1.72E-05	1.22E-04	11.29%	44.42%	39.48%	6.81E-04	6.49E-04	9.49E-04	1.02E-05	10.66%

Section 2ow (y=283mm)

X	SDu	SDv	SDw	REu	REv	REw	SDu'	SDv'	SDw'	SDk	REk
(m)	(m/s)	(m/s)	(m/s)	(%)	(%)	(%)	(m/s)	(m/s)	(m/s)	(m2/s2)	(%)
5.00E-02	5.50E-03	6.37E-04	3.66E-03	17.74%	26.97%	26.76%	2.40E-03	7.75E-04	8.75E-04	2.70E-05	22.15%
1.00E-01	6.50E-03	6.51E-04	2.66E-04	15.85%	27.64%	40.99%	1.43E-03	3.22E-04	4.22E-04	1.70E-05	12.08%
1.50E-01	7.50E-03	8.69E-04	8.75E-04	14.42%	42.70%	23.88%	1.33E-03	2.42E-04	7.54E-04	1.78E-05	11.33%
2.00E-01	7.85E-03	4.49E-04	7.55E-04	11.83%	14.06%	36.55%	2.04E-03	1.51E-04	1.05E-04	2.12E-05	16.56%
3.00E-01	4.21E-03	5.05E-05	1.71E-04	5.14%	21.43%	46.65%	1.13E-03	3.51E-04	2.51E-04	1.47E-05	9.72%
4.50E-01	7.50E-03	1.53E-05	3.19E-05	9.38%	35.43%	40.26%	1.03E-03	4.51E-04	4.54E-04	1.40E-05	9.32%

Table A4.3 Standard deviations and relative errors for the flowrate of 180l/min (nominal velocity of 0.1m/s) level 3 (z=100mm)

Section 1ow (y=25mm)

X	SDu	SDv	SDw	REu	REv	REw	SDu'	SDv'	SDw'	SDk	REk
(m)	(m/s)	(m/s)	(m/s)	(%)	(%)	(%)	(m/s)	(m/s)	(m/s)	(m2/s2)	(%)
5.00E-02	5.45E-03	5.31E-03	3.12E-03	18.08%	22.15%	18.84%	1.72E-03	1.48E-03	1.04E-03	2.53E-05	16.81%
1.00E-01	8.67E-03	6.67E-03	2.07E-03	11.59%	27.79%	31.55%	1.13E-03	1.00E-03	1.62E-03	2.08E-05	14.43%
1.50E-01	9.76E-03	1.16E-02	1.16E-03	8.69%	22.07%	32.28%	1.00E-03	2.46E-04	1.43E-03	1.70E-05	10.12%
2.00E-01	9.99E-03	1.52E-03	2.17E-03	7.67%	26.27%	33.59%	8.10E-04	1.02E-04	1.35E-03	1.59E-05	8.76%
3.00E-01	4.33E-03	8.56E-04	1.56E-03	3.23%	27.05%	31.50%	1.62E-03	1.32E-04	1.04E-03	2.69E-05	12.69%
4.50E-01	3.88E-03	1.29E-03	4.27E-04	3.14%	20.64%	23.72%	1.00E-03	1.10E-04	9.25E-04	1.91E-05	8.15%

Section 1c (y=60mm)

X	SDu	SDv	SDw	REu	REv	REw	SDu'	SDv'	SDw'	SDk	REk
(m)	(m/s)	(m/s)	(m/s)	(%)	(%)	(%)	(m/s)	(m/s)	(m/s)	(m2/s2)	(%)
5.00E-02	4.41E-03	1.03E-02	3.12E-03	16.13%	17.58%	27.26%	1.29E-03	1.31E-04	1.52E-03	1.85E-05	13.30%
1.00E-01	8.12E-03	1.21E-02	1.21E-03	12.29%	19.93%	23.88%	1.13E-03	1.42E-04	1.29E-03	1.50E-05	12.70%
1.50E-01	9.41E-03	6.41E-03	4.13E-03	9.54%	19.44%	28.91%	4.46E-04	2.96E-04	1.02E-03	9.67E-06	8.54%
2.00E-01	9.93E-03	3.03E-03	3.32E-03	9.33%	30.72%	21.56%	1.02E-04	3.32E-04	1.30E-03	1.10E-05	9.93%
3.00E-01	7.23E-03	1.02E-03	2.31E-03	6.80%	38.96%	21.05%	2.33E-04	1.33E-04	1.11E-03	9.88E-06	7.40%
4.50E-01	2.81E-03	9.41E-04	9.10E-04	2.87%	21.67%	21.25%	2.09E-04	1.08E-04	1.22E-03	1.32E-05	6.03%

Section 1iw (y=100mm)

X	SDu	SDv	SDw	REu	REv	REw	SDu'	SDv'	SDw'	SDk	REk
(m)	(m/s)	(m/s)	(m/s)	(%)	(%)	(%)	(m/s)	(m/s)	(m/s)	(m2/s2)	(%)
5.00E-02	1.24E-03	2.13E-02	1.25E-03	22.49%	27.17%	23.11%	1.11E-03	1.79E-03	1.43E-03	2.29E-05	16.66%
1.00E-01	3.24E-03	2.05E-02	2.16E-03	10.60%	23.02%	17.42%	7.94E-04	1.10E-03	1.61E-03	1.87E-05	14.31%
1.50E-01	3.52E-03	1.25E-02	3.18E-03	8.62%	38.08%	18.03%	9.74E-04	2.46E-04	1.04E-03	1.37E-05	10.63%
2.00E-01	2.41E-03	8.44E-04	4.42E-03	10.56%	20.54%	30.93%	7.94E-04	1.02E-04	1.03E-03	1.36E-05	9.04%
3.00E-01	2.54E-03	9.47E-04	3.95E-04	12.21%	22.53%	26.61%	7.36E-04	1.37E-04	1.10E-03	1.86E-05	6.42%
4.50E-01	2.77E-03	1.37E-03	9.82E-04	8.73%	34.02%	21.57%	7.56E-04	1.31E-04	9.49E-04	1.87E-05	5.43%

Section 2iw (y=208mm)

X	SDu	SDv	SDw	REu	REv	REw	SDu'	SDv'	SDw'	SDk	REk
(m)	(m/s)	(m/s)	(m/s)	(%)	(%)	(%)	(m/s)	(m/s)	(m/s)	(m2/s2)	(%)
5.00E-02	1.04E-02	1.10E-02	1.03E-03	22.28%	25.28%	22.87%	1.33E-03	1.93E-04	1.65E-03	2.17E-05	16.15%
1.00E-01	1.18E-02	1.12E-02	1.21E-04	15.78%	25.56%	20.66%	1.01E-03	1.74E-04	9.13E-04	1.19E-05	12.98%
1.50E-01	9.24E-03	6.74E-03	4.13E-04	9.90%	27.51%	27.35%	3.45E-04	2.30E-04	9.10E-04	6.11E-06	9.76%
2.00E-01	9.49E-03	3.20E-03	1.33E-04	9.97%	31.67%	37.77%	1.10E-04	4.33E-04	1.13E-03	6.67E-06	12.69%
3.00E-01	7.57E-03	5.71E-04	4.23E-05	8.20%	39.05%	27.61%	2.53E-04	3.13E-04	6.11E-04	4.19E-06	7.39%
4.50E-01	4.28E-03	1.64E-05	1.41E-04	4.69%	30.64%	33.10%	1.82E-04	1.06E-04	6.71E-04	3.99E-06	7.02%

Section 2c (y=248mm)

X	SDu	SDv	SDw	REu	REv	REw	SDu'	SDv'	SDw'	SDk	REk
(m)	(m/s)	(m/s)	(m/s)	(%)	(%)	(%)	(m/s)	(m/s)	(m/s)	(m2/s2)	(%)
5.00E-02	7.12E-03	7.10E-03	1.91E-03	16.42%	31.07%	29.06%	1.41E-03	1.48E-03	9.14E-04	2.26E-05	15.23%
1.00E-01	6.32E-03	5.21E-03	4.02E-04	9.46%	20.65%	34.64%	1.08E-03	1.41E-03	9.16E-04	1.71E-05	14.55%
1.50E-01	5.35E-03	6.12E-03	6.23E-05	6.46%	34.38%	29.47%	4.74E-04	2.25E-04	8.91E-04	7.66E-06	8.83%
2.00E-01	4.24E-03	2.84E-03	4.42E-05	4.77%	33.14%	25.00%	4.79E-04	9.10E-05	7.91E-04	6.24E-06	9.03%
3.00E-01	4.25E-03	4.47E-04	7.40E-05	4.65%	29.88%	36.60%	4.74E-05	1.54E-04	6.11E-04	3.67E-06	6.12%
4.50E-01	4.28E-03	1.37E-05	1.31E-04	4.67%	35.82%	31.50%	2.76E-04	1.31E-04	5.95E-04	4.04E-06	6.91%

Section 2ow (y=283mm)

X	SDu	SDv	SDw	REu	REv	REw	SDu'	SDv'	SDw'	SDk	REk
(m)	(m/s)	(m/s)	(m/s)	(%)	(%)	(%)	(m/s)	(m/s)	(m/s)	(m2/s2)	(%)
5.00E-02	8.10E-03	7.51E-04	2.10E-03	26.81%	31.96%	25.47%	1.73E-03	2.19E-04	1.07E-03	2.13E-05	15.89%
1.00E-01	6.12E-03	7.11E-04	1.21E-03	11.90%	29.31%	28.20%	1.30E-03	1.97E-04	1.11E-03	1.99E-05	11.78%
1.50E-01	6.92E-03	6.07E-04	6.41E-04	11.44%	29.85%	30.52%	7.34E-04	4.23E-04	6.49E-04	1.15E-05	7.29%
2.00E-01	4.95E-03	8.51E-04	7.13E-05	7.51%	26.85%	38.54%	6.11E-04	6.43E-04	7.11E-04	1.11E-05	7.45%
3.00E-01	6.76E-03	1.80E-04	7.42E-05	8.84%	34.20%	31.16%	4.25E-04	3.31E-04	6.61E-04	7.75E-06	5.54%
4.50E-01	5.43E-03	1.42E-04	1.02E-04	7.09%	34.34%	35.67%	4.18E-04	3.11E-04	6.71E-04	7.62E-06	5.48%

Table A4.4 Standard deviations and relative errors for the flowrate of 180l/min (nominal velocity of 0.1m/s) level 4 (z=140mm)

Section 1ow (y=25mm)

X	SDu	SDv	SDw	REu	REv	REw	SDu'	SDv'	SDw'	SDk	REk
(m)	(m/s)	(m/s)	(m/s)	(%)	(%)	(%)	(m/s)	(m/s)	(m/s)	(m2/s2)	(%)
5.00E-02	5.62E-03	5.64E-03	2.53E-03	20.59%	23.41%	37.02%	2.21E-03	1.79E-03	1.73E-04	2.78E-05	21.08%
1.00E-01	6.88E-03	7.15E-03	2.20E-03	9.08%	29.58%	41.07%	1.31E-03	1.03E-03	1.12E-04	1.54E-05	13.38%
1.50E-01	6.32E-03	6.18E-03	4.57E-04	5.70%	26.79%	43.50%	1.21E-03	2.46E-04	1.26E-04	1.36E-05	9.52%
2.00E-01	9.88E-03	1.96E-03	1.26E-03	7.71%	34.31%	28.90%	1.03E-03	1.24E-04	1.12E-04	1.36E-05	8.10%
3.00E-01	5.32E-03	3.47E-04	1.01E-03	4.04%	28.09%	27.39%	2.10E-03	1.32E-04	9.12E-05	3.12E-05	16.02%
4.50E-01	8.80E-03	7.24E-04	4.21E-04	7.12%	22.45%	31.38%	1.03E-03	1.02E-04	1.03E-05	1.64E-05	7.63%

Section 1c (y=60mm)

X	SDu	SDv	SDw	REu	REv	REw	SDu'	SDv'	SDw'	SDk	REk
(m)	(m/s)	(m/s)	(m/s)	(%)	(%)	(%)	(m/s)	(m/s)	(m/s)	(m2/s2)	(%)
5.00E-02	3.23E-03	6.31E-03	5.61E-04	20.97%	10.45%	33.97%	1.70E-03	1.91E-03	1.31E-04	2.53E-05	18.42%
1.00E-01	3.32E-03	1.35E-02	1.45E-03	4.32%	23.61%	34.52%	1.61E-03	1.31E-03	1.20E-04	1.90E-05	17.22%
1.50E-01	4.23E-03	2.02E-02	1.71E-03	3.85%	31.23%	27.90%	1.40E-03	4.62E-04	2.55E-04	1.35E-05	11.59%
2.00E-01	5.46E-03	2.99E-03	1.71E-03	5.37%	25.74%	22.12%	1.10E-03	2.36E-04	2.31E-04	6.03E-06	7.63%
3.00E-01	4.43E-03	2.94E-03	1.61E-03	3.72%	23.70%	19.64%	1.00E-03	2.44E-04	1.23E-04	5.63E-06	7.04%
4.50E-01	4.13E-03	2.29E-03	9.85E-04	4.04%	29.11%	18.44%	1.10E-03	2.04E-04	1.03E-04	1.44E-05	10.60%

Section 1iw (y=100mm)

X	SDu	SDv	SDw	REu	REv	REw	SDu'	SDv'	SDw'	SDk	REk
(m)	(m/s)	(m/s)	(m/s)	(%)	(%)	(%)	(m/s)	(m/s)	(m/s)	(m2/s2)	(%)
5.00E-02	1.06E-03	1.26E-02	1.25E-03	21.63%	19.30%	28.46%	7.16E-04	2.44E-04	1.13E-03	8.93E-06	15.69%
1.00E-01	2.21E-03	2.05E-02	1.56E-03	11.05%	28.82%	34.46%	1.09E-03	1.21E-03	6.10E-04	1.45E-05	13.87%
1.50E-01	2.16E-03	1.48E-02	1.83E-03	10.80%	41.94%	21.73%	4.60E-04	1.05E-03	4.51E-04	1.03E-05	8.86%
2.00E-01	2.41E-03	4.36E-03	2.06E-03	7.77%	33.29%	19.27%	9.80E-04	4.82E-04	3.50E-04	6.91E-06	9.14%
3.00E-01	1.86E-03	3.35E-03	3.51E-04	4.21%	27.00%	24.06%	6.00E-04	5.48E-04	4.75E-04	9.10E-06	6.33%
4.50E-01	2.41E-03	3.37E-03	9.21E-04	4.20%	32.43%	26.93%	9.00E-04	4.35E-04	2.51E-04	1.40E-05	6.22%

Section 2iw (y=208mm)

X	SDu	SDv	SDw	REu	REv	REw	SDu'	SDv'	SDw'	SDk	REk
(m)	(m/s)	(m/s)	(m/s)	(%)	(%)	(%)	(m/s)	(m/s)	(m/s)	(m2/s2)	(%)
5.00E-02	1.00E-02	1.24E-02	1.00E-03	19.23%	17.73%	24.69%	2.48E-03	2.44E-03	1.30E-03	3.39E-05	29.13%
1.00E-01	6.70E-03	7.62E-03	5.00E-04	8.36%	9.13%	21.60%	1.29E-03	2.14E-03	1.03E-03	2.06E-05	19.35%
1.50E-01	8.41E-03	4.12E-03	4.10E-04	8.59%	26.21%	25.81%	1.36E-03	1.53E-03	5.10E-04	2.19E-05	16.08%
2.00E-01	1.40E-02	1.70E-03	2.24E-04	13.73%	44.53%	50.77%	8.30E-04	8.17E-04	5.03E-04	1.33E-05	9.79%
3.00E-01	1.14E-02	7.52E-05	1.22E-04	10.46%	37.53%	46.60%	7.83E-04	4.82E-04	4.50E-04	1.19E-05	8.95%
4.50E-01	6.14E-03	1.27E-04	2.24E-04	8.77%	41.13%	43.12%	6.68E-04	3.48E-04	5.10E-04	1.20E-05	6.76%

Section 2c (y=248mm)

X	SDu	SDv	SDw	REu	REv	REw	SDu'	SDv'	SDw'	SDk	REk
(m)	(m/s)	(m/s)	(m/s)	(%)	(%)	(%)	(m/s)	(m/s)	(m/s)	(m2/s2)	(%)
5.00E-02	8.30E-04	3.12E-03	6.05E-04	16.94%	50.28%	55.00%	1.63E-03	2.06E-03	3.08E-04	2.44E-05	18.82%
1.00E-01	6.50E-03	1.53E-02	1.50E-03	8.33%	17.56%	40.54%	1.02E-03	2.10E-03	2.00E-04	1.92E-05	18.64%
1.50E-01	6.06E-03	2.24E-02	1.10E-03	6.73%	29.09%	34.98%	8.30E-04	6.18E-04	5.50E-04	6.67E-06	12.34%
2.00E-01	6.00E-03	2.86E-03	7.13E-04	5.50%	36.52%	32.42%	2.48E-04	3.61E-04	3.13E-04	3.43E-06	5.38%
3.00E-01	5.60E-03	1.72E-03	3.63E-04	4.34%	38.31%	47.78%	4.25E-04	4.36E-04	2.31E-04	3.53E-06	8.11%
4.50E-01	7.60E-03	2.79E-03	4.93E-04	7.45%	55.73%	44.83%	3.25E-04	2.36E-04	1.31E-04	2.10E-06	6.57%

Section 2ow (y=283mm)

X	SDu	SDv	SDw	REu	REv	REw	SDu'	SDv'	SDw'	SDk	REk
(m)	(m/s)	(m/s)	(m/s)	(%)	(%)	(%)	(m/s)	(m/s)	(m/s)	(m2/s2)	(%)
5.00E-02	3.71E-03	6.42E-04	5.31E-04	24.03%	27.38%	35.74%	2.10E-03	2.13E-03	3.11E-04	1.79E-05	25.33%
1.00E-01	1.10E-02	5.21E-04	2.20E-03	19.58%	21.21%	28.48%	1.11E-03	2.41E-03	2.70E-04	2.42E-05	17.60%
1.50E-01	1.03E-02	6.18E-04	1.26E-03	17.36%	26.00%	20.50%	1.34E-03	7.62E-04	6.55E-04	2.02E-05	11.68%
2.00E-01	1.02E-02	6.36E-04	6.31E-04	12.32%	19.92%	39.18%	1.51E-03	5.36E-04	3.31E-04	1.93E-05	13.59%
3.00E-01	1.10E-02	7.44E-05	1.23E-04	9.24%	31.70%	32.84%	1.03E-03	4.04E-04	2.63E-04	1.33E-05	9.62%
4.50E-01	1.00E-02	7.24E-06	2.13E-04	13.44%	45.82%	29.31%	9.40E-04	2.14E-04	1.23E-04	1.18E-05	8.55%

Table A4.5 Standard deviations and relative errors for the flowrate of 180l/min (nominal velocity of 0.1m/s) level 5 (z=180mm)

Section 1ow (y=25mm)

X	SDu	SDv	SDw	REu	REv	REw	SDu'	SDv'	SDw'	SDk	REk
(m)	(m/s)	(m/s)	(m/s)	(%)	(%)	(%)	(m/s)	(m/s)	(m/s)	(m2/s2)	(%)
5.00E-02	6.14E-03	8.18E-03	4.10E-04	23.34%	34.92%	17.06%	1.11E-03	2.03E-04	5.24E-04	5.55E-06	21.47%
1.00E-01	6.45E-03	1.26E-02	4.79E-04	8.29%	31.78%	32.49%	7.96E-04	2.36E-04	5.89E-04	4.08E-06	18.50%
1.50E-01	9.71E-03	8.03E-03	1.23E-04	8.77%	28.78%	34.15%	6.11E-04	7.93E-05	3.24E-04	3.03E-06	12.19%
2.00E-01	9.43E-03	2.21E-03	4.60E-04	7.20%	33.93%	32.28%	2.14E-04	1.02E-04	1.09E-03	4.53E-06	16.88%
3.00E-01	9.58E-03	2.71E-04	4.12E-04	7.01%	24.67%	30.45%	1.47E-04	6.39E-05	7.32E-04	2.87E-06	10.93%
4.50E-01	9.55E-03	1.02E-03	2.25E-04	7.22%	43.17%	46.91%	1.14E-04	2.39E-05	6.82E-04	2.79E-06	9.50%

Section 1c (y=60mm)

X	SDu	SDv	SDw	REu	REv	REw	SDu'	SDv'	SDw'	SDk	REk
(m)	(m/s)	(m/s)	(m/s)	(%)	(%)	(%)	(m/s)	(m/s)	(m/s)	(m2/s2)	(%)
5.00E-02	2.14E-03	1.49E-02	8.87E-04	13.07%	26.89%	27.30%	9.97E-04	2.50E-04	4.10E-04	6.31E-06	19.88%
1.00E-01	9.61E-03	7.35E-03	1.60E-04	13.73%	11.62%	30.13%	4.58E-04	1.02E-04	1.06E-03	4.57E-06	17.89%
1.50E-01	1.34E-02	1.45E-02	3.07E-04	14.58%	37.28%	13.18%	4.51E-04	3.55E-04	4.64E-04	3.55E-06	10.54%
2.00E-01	7.83E-03	2.35E-03	5.13E-04	8.15%	33.04%	13.50%	3.71E-05	4.35E-04	2.24E-04	2.25E-06	5.91%
3.00E-01	5.98E-03	9.51E-04	6.31E-04	5.75%	23.47%	19.43%	5.71E-05	2.23E-04	4.14E-04	2.33E-06	6.24%
4.50E-01	5.58E-03	8.25E-04	5.18E-04	5.47%	19.97%	34.38%	2.14E-05	2.20E-04	3.44E-04	2.05E-06	5.27%

Section 1iw (y=100mm)

X	SDu	SDv	SDw	REu	REv	REw	SDu'	SDv'	SDw'	SDk	REk
(m)	(m/s)	(m/s)	(m/s)	(%)	(%)	(%)	(m/s)	(m/s)	(m/s)	(m2/s2)	(%)
5.00E-02	6.42E-03	1.78E-02	8.12E-04	21.39%	21.31%	34.56%	1.09E-03	2.25E-04	1.84E-03	1.11E-05	24.20%
1.00E-01	4.51E-03	2.65E-02	5.13E-05	10.74%	28.04%	36.65%	7.60E-04	3.59E-04	6.06E-04	5.13E-06	15.82%
1.50E-01	7.10E-03	8.34E-03	7.15E-04	12.46%	24.30%	23.37%	1.10E-03	7.93E-05	8.21E-04	9.21E-06	17.74%
2.00E-01	4.34E-03	2.05E-03	1.20E-03	8.87%	38.76%	27.54%	3.67E-04	2.50E-04	9.00E-04	5.93E-06	9.90%
3.00E-01	5.78E-03	2.71E-03	3.12E-04	10.93%	31.96%	48.81%	2.47E-04	3.93E-05	7.90E-04	4.74E-06	10.75%
4.50E-01	5.48E-03	2.13E-03	5.12E-04	9.55%	46.00%	41.28%	3.64E-04	8.93E-05	4.90E-04	3.17E-06	8.17%

Section 2iw (y=208mm)

X	SDu	SDv	SDw	REu	REv	REw	SDu'	SDv'	SDw'	SDk	REk
(m)	(m/s)	(m/s)	(m/s)	(%)	(%)	(%)	(m/s)	(m/s)	(m/s)	(m2/s2)	(%)
5.00E-02	6.14E-03	8.52E-03	5.03E-04	19.82%	19.70%	30.70%	7.01E-04	5.03E-04	3.66E-04	3.86E-06	16.57%
1.00E-01	6.09E-03	3.54E-03	3.66E-04	7.55%	6.52%	24.07%	6.13E-04	2.12E-04	3.08E-04	3.15E-06	13.76%
1.50E-01	1.41E-02	1.47E-02	2.22E-04	17.45%	44.81%	21.85%	5.14E-04	4.94E-04	3.31E-04	3.18E-06	13.98%
2.00E-01	8.27E-03	5.28E-03	1.52E-04	8.11%	43.74%	40.29%	7.12E-05	3.45E-04	3.08E-04	1.69E-06	7.19%
3.00E-01	9.83E-03	5.15E-04	5.22E-05	16.68%	37.24%	40.57%	5.71E-05	2.35E-04	4.08E-04	1.84E-06	4.73%
4.50E-01	5.83E-03	2.53E-04	1.25E-04	10.15%	39.53%	52.61%	3.71E-05	2.03E-04	3.91E-04	1.69E-06	4.30%

Section 2c (y=248mm)

X	SDu	SDv	SDw	REu	REv	REw	SDu'	SDv'	SDw'	SDk	REk
(m)	(m/s)	(m/s)	(m/s)	(%)	(%)	(%)	(m/s)	(m/s)	(m/s)	(m2/s2)	(%)
5.00E-02	6.17E-03	1.68E-03	2.24E-04	20.57%	27.02%	19.87%	9.26E-04	2.51E-04	5.00E-04	6.90E-06	16.31%
1.00E-01	5.12E-03	2.49E-03	5.87E-04	10.24%	30.14%	20.49%	5.96E-04	5.94E-04	3.24E-04	3.44E-06	15.93%
1.50E-01	1.05E-02	3.38E-03	2.24E-04	11.79%	43.08%	12.59%	9.58E-04	9.27E-05	2.24E-05	5.09E-06	17.76%
2.00E-01	8.11E-03	2.54E-03	2.06E-04	8.45%	51.87%	25.76%	6.72E-04	4.96E-04	5.62E-05	4.40E-06	14.30%
3.00E-01	7.81E-03	1.34E-03	8.21E-05	8.32%	29.73%	33.28%	4.72E-04	9.27E-05	2.24E-05	1.59E-06	10.22%
4.50E-01	5.81E-03	2.25E-03	9.72E-05	5.70%	43.35%	35.53%	3.37E-04	9.27E-05	2.24E-05	1.25E-06	7.60%

Section 2ow (y=283mm)

X	SDu	SDv	SDw	REu	REv	REw	SDu'	SDv'	SDw'	SDk	REk
(m)	(m/s)	(m/s)	(m/s)	(%)	(%)	(%)	(m/s)	(m/s)	(m/s)	(m2/s2)	(%)
5.00E-02	6.41E-03	4.52E-04	1.05E-03	19.92%	28.33%	19.48%	1.07E-03	7.50E-04	6.37E-04	8.87E-06	16.93%
1.00E-01	4.61E-03	1.54E-03	7.37E-04	12.73%	36.72%	19.43%	8.61E-04	4.21E-04	6.31E-04	5.65E-06	17.47%
1.50E-01	7.14E-03	1.47E-03	8.22E-04	11.52%	30.40%	25.64%	1.11E-03	9.49E-04	7.33E-04	7.87E-06	24.05%
2.00E-01	7.83E-03	6.53E-04	3.15E-04	18.64%	26.98%	27.95%	9.71E-05	7.35E-04	6.31E-04	4.32E-06	12.72%
3.00E-01	7.98E-03	2.51E-04	5.22E-05	10.94%	36.22%	34.10%	8.57E-05	4.42E-04	6.41E-04	3.38E-06	9.58%
4.50E-01	8.10E-03	1.13E-04	1.25E-04	13.78%	33.49%	29.63%	6.10E-04	1.62E-04	7.39E-04	4.73E-06	12.90%

Appendix B

Table B1 Results of flocculation efficiency for test groups 1, 4, 7, 10, 13 and 16 (See Table 5.1)

Flow rate (l/minute)	Nominal velocity (m/s)	Volume weighted kinetic energy(m^2/s^2)	n_o/n_i (group 1)	n_o/n_i (group 4)	n_o/n_i (group 7)	n_o/n_i (group 10)	n_o/n_i (group 13)	n_o/n_i (group 16)
56.4	0.100	3.08E-4	6.85	11.20	15.70	6.41	6.00	15.60
42.3	0.075	1.94E-4	10.50	15.90	22.70	8.03	13.50	19.80
36.7	0.065	1.61E-4	8.88	16.40	25.60	8.12	11.90	22.00
33.8	0.060	1.45E-4	8.67	17.10	29.30	8.33	12.40	24.50
28.2	0.050	1.26E-4	7.46	20.30	33.40	6.98	11.50	26.40
19.7	0.035	8.97E-5	5.20	16.50	21.70	3.30	7.49	12.40

Table B2 Results of flocculation efficiency for test groups 2, 5, 8, 11, 14 and 17 (See Table 5.1)

Flow rate (l/minute)	Nominal velocity (m/s)	Volume weighted kinetic energy(m^2/s^2)	n_o/n_i (group 2)	n_o/n_i (group 5)	n_o/n_i (group 8)	n_o/n_i (group 11)	n_o/n_i (group 14)	n_o/n_i (group 17)
56.4	0.100	3.40E-4	5.40	8.98	13.60	5.40	5.66	10.30
42.3	0.075	2.39E-4	6.20	11.10	13.30	4.20	5.88	13.50
36.7	0.065	2.01E-4	5.33	11.00	12.90	3.33	5.03	10.20
33.8	0.060	1.84E-4	5.12	10.80	13.80	3.12	5.12	11.30
28.2	0.050	1.56E-4	3.47	8.94	13.20	3.37	3.97	10.20
19.7	0.035	1.14E-4	2.86	4.75	6.85	2.76	3.10	5.89

Table B3 Results of flocculation efficiency for test groups of 3, 6, 9, 12, 15 and 18 (See Table 5.1)

Flow rate (l/minute)	Nominal velocity (m/s)	Volume weighted kinetic energy(m^2/s^2)	n_o/n_1 (group 3)	n_o/n_1 (group 6)	n_o/n_1 (group 9)	n_o/n_1 (group 12)	n_o/n_1 (group 15)	n_o/n_1 (group 18)
56.4	0.100	3.58E-4	3.22	5.32	7.82	2.22	3.48	5.88
42.3	0.075	2.67E-4	3.01	5.24	5.33	2.30	2.54	5.01
36.7	0.065	2.29E-4	2.78	4.33	4.80	2.18	2.35	4.23
33.8	0.060	2.12E-4	2.50	3.98	4.50	2.15	2.33	4.01
28.2	0.050	1.79E-4	2.20	4.11	4.10	2.12	2.22	5.21
19.7	0.035	1.25E-4	1.45	2.43	3.33	1.65	1.88	3.33

Table B 4 Results of flocculation efficiency for test groups 19, 20, 21 and 22 (See Table 5.1)

Flow rate (l/minute)	Nominal velocity (m/s)	n_o/n_1 (group 19)	n_o/n_1 (group 20)	n_o/n_1 (group 21)	Flow rate (l/minute)	Nominal velocity (m/s)	Volume weighted kinetic energy(m^2/s^2)	n_o/n_1 (group 22)
56.4	0.100	10.31	14.93	11.30	180	0.100	1.57E-04	4.27
42.3	0.075	11.02	22.36	14.60	135	0.075	1.15E-04	4.02
36.7	0.065	13.60	24.80	15.28	117	0.065	9.96E-05	3.88
33.8	0.060	15.20	26.13	16.36	108	0.060	9.22E-05	2.37
28.2	0.050	16.06	27.83	19.34	90	0.050	7.66E-05	2.28
19.7	0.035	21.80	30.75	12.81	63	0.035	5.32E-05	2.01